DESIGN OF A NOVEL ROTARY COMPACT POWER PACK FOR THE SERIES HYBRID ELECTRIC VEHICLE

Design and Simulation of a Compact Power Pack Consisting of a Novel Rotary Engine and Outer Rotor Induction Machine for the Series Hybrid Electric Vehicle Powertrain

Hossein AMIRIAN

Submitted for the Degree of Doctor of Philosophy

School of Engineering, Design and Technology

University of Bradford

2010

Design of a Novel Rotary Compact Power Pack for the Series Hybrid Electric Vehicle

H. Amirian

Abstract

Keywords: Hybrid Electric Vehicle, Compact Power Pack, Novel Rotary Engine, Outer Rotor Generator

Hybrid electric vehicles significantly reduce exhaust emissions and increase fuel economy. Power packs are the most fundamental components in a series powertrain configuration of a hybrid vehicle, which produce the necessary power to run the vehicle. The aim of this project is to design a compact power pack for a series hybrid vehicle, using virtual prototyping. The hybrid electric vehicle characteristics and configurations are analysed, followed by an explanation of the principles of induction machines. A new type of rotary induction machine with an outer rotor construction is designed to be coupled with the novel rotary internal combustion engine with rotating crankcase in order to form the compact power unit for the hybrid vehicle. The starting and generation performance of the designed machine is analysed by an electric machine simulator, called JMAG. ADVISOR software is studied and utilised to simulate the overall vehicle performance, employing different categories of power packs in the powertrain. Results show that the proposed compact power pack has the best performance in terms of fuel economy, emissions and battery charging compared to the existing power unit options. Over the city cycle, fuel economy is increased by up to 47 % with emission reduced by up to 36 % and over the highway cycle, fuel economy is increased by up to 69 % with emission reduced by up to 42 %.

Acknowledgements

I would like to thank all of those who contributed their knowledge and time to make this work complete. I express my first and sincere appreciation to my academic supervisor, Professor Kambiz Ebrahimi for his valuable support, advice and encouragement to accomplish this thesis. Additionally I acknowledge the constructive comments and suggestions given to me by Dr. Byron Mason, Dr. Antonios Pezouvanis, Dr. Abolfath Nikranjbar and Mr. Antosh Lewalski in the Hybrid Powertrain Engineering Research Centre (HYPERC), University of Bradford. Finally my especial thanks go to my parents for their patience and spiritual supports during this research.

Table of Contents

List of Figures

List of Tables

Nomenclature

A	Specific stator current load (A/m)
a	Vehicle initial acceleration (m/s^2)
A_b	Rotor slot area (mm^2)
a_{eff}	Effective turns ratio of a transformer
A_{er}	End ring cross section area(m^2)
a_{er}	The longer side of the end ring cross section (mm)
A_{frame}	Total area of frame including finns (m^2)
A_{ls}	Stator slot lateral area (m^2)
A_{su}	Slot useful area (mm^2)
A_{vf}	Vehicle frontal area (m^2)
A_w	Magnetic wire cross section (mm^2)
B_{cr}	Rotor back core flux density (T)
B_{cs}	Stator back core flux density (T)
b_{er}	The shorter side of the end ring cross section (mm)
B_g	Airgap flux density (T)
b_{or}	Rotor slot opening width (mm)
b_{os}	Stator slot opening width (mm)
B_{pr}	Rotor tooth flux density pulsation
B_{ps}	Stator tooth flux density pulsation
B_r	Rotor magnetic field density (T)
b_{r1}	Shorter side of the rotor slot (mm)
b_{r2}	Longer side of the rotor slot (mm)
B_s	Stator magnetic field density (T)
b_{s1}	Longer side of the stator slot (mm)

b_{s2}	Shorter side of the stator slot (mm)
b_{tr}	Rotor tooth width (mm)
B_{tr}	Rotor tooth flux density (T)
B_{ts}	Stator tooth magnetic flux density (T)
b_{ts}	Stator tooth width (mm)
C	Celsius
C_0	Esson's constant (J/m^3)
C_{cr}	Average length of flux path in the rotor back core
C_{cs}	Average length of flux path in the stator back core
C_d	Coefficient of aerodynamic drag
C_m	A variable used in Equations (5.112) and (5.113) in order to compact the equations
$Cos\varphi_n$	Rated power factor
C_s	A variable used in Equation (5.74) in order to compact the equation
D_{er}	End ring diameter (m)
D_g	Airgap (mm)
D_{ir}	Rotor inner diameter (m)
D_{is}	Stator inner diameter (m)
D_{is}^2L	Output coefficient (m^3)
D_{or}	Outer diameter of the rotor (m)
D_{os}	Stator outer diameter (mm)
d_w	Bare wire diameter (mm)
E_g	Airgap electromotive force per phase (V)
E_{lr}	Induced rotor voltage at locked-rotor condition (V)
E_r	Actual value of rotor voltage (V)
$E`_r$	Value of rotor voltage referred to stator (V)

f	Supply frequency (Hz)
f_0	Fundamental frequency (= 50 Hz, rated frequency)
F_{ar}	Aerodynamic drag force (N)
F_d	Drive force (N)
f_e	Electrical frequency (Hz)
F_{hr}	Hill climbing resistance force (N)
F_m	Magnetisation mmf (Aturns)
f_m	Mechanical frequency of magnetic field (Hz)
F_{mcr}	Rotor back core mmf (Aturns)
F_{mcs}	Stator back core mmf (Aturns)
F_{mg}	Airgap mmf (Aturns)
F_{mtr}	Rotor tooth mmf (Aturns)
F_{mts}	Stator tooth mmf (Aturns)
f_r	Frequency of the induced voltage in the rotor (HZ)
f_{rc}	Coefficient of tire rolling resistance
F_{rr}	Rolling resistance force (N)
g	Gravity acceleration constant (m/s^2)
G_t	Stator tooth weight (Kg)
G_{tr}	Rotor teeth weight (Kg)
G_y	Yoke weight (Kg)
h_{cr}	Rotor back core height (mm)
h_{cs}	Stator back iron height (mm)
h_{ins}	Total insulation thickness from slot middle to teeth wall (m)
h_{or}	Rotor slot opening height (mm)
h_{os}	Stator slot opening height (mm)
h_r	Rotor slot height (mm)

h_s	Stator slot useful height (mm)
H_{tr}	Rotor tooth magnetic field strength (A/m)
H_{ts}	Stator tooth magnetic field strength (A/m)
h_w	Wedge height (mm)
I_{ac_nl}	No-load active current (A)
I_b	Rated current of the rotor bar (A)
I_{er}	End ring current (A)
I_n	Rated current (A)
I_r	Actual value of rotor current (A)
$I`_r$	Rotor current referred to stator (A)
$\left\|I`_r\right\|$	Magnitude of the rotor current referred to stator (A)
I_s	Starting current (A)
I_μ	Magnetisation current (A)
i_μ	Magnetisation current per unit (actual value / base value)
J_b	Rotor bar current density (A/mm^2)
J_{cu}	Current density (A/mm^2)
J_{er}	End ring current density (A/mm^2)
K	Ratio of rotor mmf to stator mmf
K_c	Total Carter coefficient
K_{cs}	Stator carter coefficient
K_{cr}	Rotor carter coefficient
K_E	emf coefficient
K_f	Form factor
K_{Fe}	Coefficient of influence of lamination insulation thickness
K_{fill}	Slot fill factor

K_{fin}	Coefficient of cooling fins
K_{pr}	A variable used in Equation (5.103) in order to compact the equation
K_{ps}	A variable used in Equation (5.103) in order to compact the equation
K_q	Zone factor
K_R	Skin effect resistance coefficient for the bar
K_{r1}	A variable used in Equation (5.79) in order to compact the equation
K_{r2}	A variable used in Equation (5.79) in order to compact the equation
K_s	Total saturation factor
K_{skew}	Coefficient of skewing effect for the magnetising reactance
$1+ k_{st}$	Tooth saturation factor
K_t	Coefficient of core loss augmentation
K_w	Stator winding factor
K_x	Coefficient of skin effect for the leakage reactance
K_y	Chording factor
K_y	Coefficient of mechanical machining
L	Stack length of the machine (m)
l_c	Coil length (m)
l_{end}	End connection length (m)
L_{er}	End ring length (m)
l_{er}	End ring segment length (m)
l_g	Airgap length (m)
$\sum losses$	Total machine loss
m	Vehicle mass (Kg)
n	Number of rotor bars in JMAG
n_m	Mechanical speed of the stator magnetic field (rpm)
n_{ph}	Number of phases

N_r	Number of rotor slots
n_r	Rotor speed (rpm)
N_s	Number of stator slots
n_s	Number of conductors per slot
n_{sync}	Synchronous speed (rpm)
P	Number of poles
P_{ag}	Air-gap power (KW)
P_{Al}	Rotor cage losses (W)
P_{Cu}	Stator winding copper losses (W)
P_{conv}	Converted power (KW)
P_d	Drive power (KW)
P_{dm}	Power of drive motor (KW)
P_G	Generator rated power (KW)
P_{Gout}	Generator output power (KW)
P_{iron}	Core losses (W)
P_{iron}^f	Fundamental iron loss (W)
P_{iron}^h	Harmonic iron loss (W)
P_{mv}	Mechanical/ventilation losses (W)
P_n	Rated power (KW)
P_{rcl}	Rotor copper losses (KW)
p_{sl}	Specific losses at 1.0 T and 50 Hz (W/Kg)
P_{stray}	Stray losses (W)
P_t	Stator teeth fundamental loss (W)
P_y	Stator yoke (back iron) fundamental loss (W)
q	Number of stator slots per pole
rad	radians

R_{be}	Rotor bar /end ring segment equivalent resistance (Ω)
R_{be180}	Rotor bar /end ring segment equivalent resistance at 180 °C (Ω)
$R_{be180°}^{S=1}$	Rotor bar /end ring segment equivalent resistance at S=1 and 180 °C (Ω)
$R_{be180°}^{S=S_n}$	Rotor bar /end ring segment equivalent resistance at S_n and 180 °C (Ω)
R_c	core losses resistance (Ω)
R_{er}	Resistance of the end ring between bars (Ω)
R_r	Rotor resistance (Ω)
$R`_r$	Rotor resistance referred to the stator (Ω)
$(R`_r)_{S=1}$	Rotor resistance referred to the stator at S=1 (Ω)
$(R`_r)_{S=Sn}$	Rotor resistance referred to the stator at rated slip (Ω)
R_s	Stator resistance (Ω)
S	Slip
S_{500}	Slip at 500 rpm
S_{airgap}	Airgap apparent power (KVA)
S_{bk}	Breakdown slip
$(S_{bk})_f$	Breakdown slip at frequency of f
$SD1_{st}$	Stator outside diameter in JMAG (mm)
$SD2_{ro}$	Outside diameters of rotor coil in JMAG (mm)
$SD2_{st}$	Outside diameter of stator coil in JMAG (mm)
$SD3_{ro}$	Inside diameters of rotor coil in JMAG (mm)
$SD3_{st}$	Inside diameter of stator coil in JMAG (mm)
$SD4_{ro}$	Rotor inside diameter in JMAG (mm)
Sec.	Second(s)
S_n	Rated slip
T	Tesla
T_{bk}	Breakdown torque (Nm)

$(T_{bk})_f$	Breakdown torque at frequency of f (Nm)
T_{ind}	Induced torque (Nm)
T_n	Rated electromagnetic torque (Nm)
T_s	Starting torque (Nm)
V	Vehicle velocity (m/s)
v	Velocity of a bar relative to the magnetic field (m/s)
V_{DCavg}	Average value of DC voltage (V)
V_{LL}	Line to line voltage (V)
V_{max}	Maximum value of phase voltage (V)
V_{ph}	Phase voltage (V)
$(V_s)_f$	Stator phase voltage at frequency of f (V)
V_{Th}	Thevenin voltage (V)
V_w	Head-wind velocity (m/s)
W	Number of turns per phase
X_{be}	Equivalent rotor bar leakage reactance (Ω)
X_{lr}	Locked-rotor rotor reactance (Ω)
X_m	Magnetising reactance (Ω)
$X_{m\ skew}$	Magnetisation reactance for the skewed rotor slots (Ω)
X_{rl}	Rotor leakage reactance (Ω)
$X`_{rl}$	Rotor leakage reactance referred to stator (Ω)
$X`_{rl\ skew}$	Rotor leakage reactance referred to stator for the skewed rotor slots (Ω)
$(X`_{rl})^{S=1}_{sat}$	Rotor leakage reactance referred to stator at S=1 and condition of leakage flux path saturation
$(X`_{rl})^{S=1}_{skew}$	Rotor leakage reactance referred to stator for the skewed rotor slots at S=1(Ω)

$(X`_{rl})_{skew}^{S=S_n}$	Rotor leakage reactance referred to stator for the skewed rotor slots at rated slip (Ω)
X_{sl}	Stator leakage reactance (Ω)
$(X_{sl})_{sat}^{S=1}$	Stator leakage reactance at S=1 and condition of leakage flux path saturation
X_{Th}	Thevenin reactance (Ω)
y	Coil span (mm)
$\frac{y}{\tau}$	Chording factor $(\frac{y}{\tau}=\beta=\frac{\text{coil span}}{\text{pole pitch}})$
Z_r	Rotor impedance (Ω)
$Z`_r$	Rotor impedance referred to stator (Ω)
Z_{Th}	Thevenin impedance (Ω)
α	Road angle (in degrees)
α_{cond}	Lumped coefficient of slot insulation conductivity and thickness (W/m^2K)
α_{conv}	Frame thermal convection (W/m^2K)
α_{ec}	Electrical angle between emfs in neighbouring slots (rad)
α_f	Firing angle (rad)
α_i	Flux density shape factor
α_i	Pole spanning coefficient
α_{rcr}	Ratio of rotor bar current density at the starting point of the starter machine to the bar current density of the generator at steady state
α_{rlr}	Ratio of the steady state value of rotor cage losses of the starter machine to the rotor cage losses of the generator at the steady state
α_{scr}	Ratio of stator current density at the starting point of the starter machine to the stator current density of the generator at the steady state

α_{slr} Ratio of stator coil losses of the starter machine to the stator coil loses of the generator

β Chording factor ($\beta = \frac{\text{coil span}}{\text{pole pitch}} = \frac{y}{\tau}$)

β_s Reverse of the field penetration depth in Aluminium (m^{-1})

γ_s A variable used in Equation (5.52) in order to compact the equation

γ_r A variable used in Equation (5.53) in order to compact the equation

γ_{dr} The ratio between the rotor differential leakage and the main inductance

γ_{ds} The ratio between the stator differential leakage and the main inductance

γ_{Fe} Iron specific weight (Kg/m^3)

ΔS Difference between rated slip and breakdown slip

ΔT Difference between rated torque and breakdown torque (Nm)

$\Delta\theta_{Cu}$ Temperature differential between slot wall and the slots conductors (°C)

$\Delta\theta_{frame}$ Frame temperature (°C)

ξ A variable used in Equation (5.69) in order to compact the equation

η Output efficiency

η_{dm} Efficiency of drive motor (%)

η_n Rated efficiency

η_t Efficiency of transmission (%)

θ Temperature in Celsius (°C)

θ_{amb} Ambient temperature (°C)

θ_{Cu} Stator winding temperature (°C)

λ Stack length to pole pitch ratio

λ_{dr} Coefficient of rotor differential leakage permeance

λ_{ds} Coefficient of stator differential leakage permeance

λ_{ec} Coefficient of the end connection specific geometric permeance

λ_{er}	Coefficient of end ring permeance
λ_{ins}	Slot insulation thermal conductivity (W/m°K)
λ_r	Coefficient of the rotor slot geometric specific permeance
λ_s	Coefficient of the stator slot geometric specific permeance
μ_o	Air permeability (H/m)
ρ	Air density (Kg/m^3)
ρ_{Al}	Resistivity of the cast Aluminium (Ωm)
$(\rho_{Al})_\theta$	Resistivity of the cast Aluminium at θ °C (Ωm)
ρ_{Cu}	Copper resistivity (Ωm)
$(\rho_{Cu})_\theta$	Copper resistivity at θ °C (Ωm)
σ	Rotor bars electric conductivity (1/ Ωm)
τ	Pole pitch (mm)
τ_r	Rotor slot pitch (mm)
τ_s	Stator slot pitch
φ_1	A variable used in Equation (5.76) in order to compact the equation
ω_r	Mechanical speed of rotor (rad/s)
ω_{sync}	Synchronous speed (rad/s)
Φ	Airgap pole flux (Wb)

Abbreviations

AC	Alternative Current
ADVISOR	Advanced Vehicle Simulator
C5C	Cylindrical five-stroke Cycle
CAD	Computer Aided Design
CAE	Computer Aided Engineering
CC	City Cycle
CI	Compression Ignition
CO	Carbon Monoxide
DC	Direct Current
DI	Direct Injection
EC	European Commission
EEC	European Economic Community
emf	electromotive force
EU	European Union
EV	Electric Vehicle
FEM	Finite Element Method
g/km	Grams/ kilo metre
GE	General Electric
Genset	Generator Set
GUI	Graphical User Interface
HC	HydroCarbons
HEV	Hybrid Electric Vehicle
HW	HighWay
HWFET	HighWay Fuel Economy Test

Hz	Hertz
ICE	Internal Combustion Engine
IDI	InDirect Injection
IEE	Institution of Electrical Engineers
IEEE	Institute of Electrical and Electronics Engineers
IM	Induction Machine
ISG	Integrated Starter-Generator
KJ	Kilo Joule
Km/h	Kilometre per hour
L/100Km	Litre per 100 Kilometres
LL	Line to Line
mmf	magneto motive force
mpg	miles per gallon
mph	mile per hour
NE	Novel Engine
NEMA	National Electrical Manufacturers Association
NiMH	Nickel Metal Hybrid
Nm	Newton metre
NMHC	Non-Methane HydroCarbon
NOx	Nitrogen Oxides
OBD	OnBoard Diagnostic
ORIM	Outer Rotor Induction Machine
ORTP	Outer Rotor Trapezoidal
PM	Particular Matter
PM	Permanent Magnet
rms	root mean square

rpm	revolutions per minute
SI	Spark Ignition
SOC	State Of Charge
Tr	Trip
UDDS	Urban Dynamometer Driving Schedule
V	Volt
Wh	Watt-hour

Chapter 1 Introduction

In recent years, all the main automotive manufacturers have paid resolute attention to Hybrid Electric Vehicle (HEV) technology to reduce exhaust emissions, increase fuel economy (the distance travelled per unit of fuel used) and improve the performance parameters. HEV technology combines an internal combustion engine, battery pack and electric machine to satisfy the lower emissions as required by legislation.

The Power unit consisting of an Internal Combustion Engine (ICE) and generator plays an essential role in this subject as heart of the HEV power system with series configuration. In the series configuration of the HEVs, engine drives the generator in order to charge the batteries and then the battery pack feeds an electric traction motor for running the vehicle wheels [1].

In most electric and hybrid electric cars, the power demand in vehicles has been increased and more engine driven systems have been replaced with electrical system. Advanced power electronics technology is utilised to supply and control the electrical loads including lights, air-conditioning, electric motors for different tasks, vehicle dynamics controllers and other electrical accessories [2].

Also, some loads such as anti-lock braking, rear-wheel steering and ride-height adjustment will be driven by electric systems in the future [3]. In fact, electrical systems may need a lower power but a higher efficiency engine to drive the generator. In addition engine can be used when required, which results in optimum fuel economy and performance [4 , 5].

The improving performance demand in HEVs has resulted in a requirement for a higher onboard generation capacity at higher voltage. The higher voltage decreases the weight and volume of the wiring harness. With the high generation need, the torque characteristics of the generator and starter motor (an electric machine utilised to start up the engine) get closer to each other. Therefore, the integration of the starter and generator machines into a single machine would be technically practicable and economically beneficial [1 , 4].

In addition, the power unit losses directly reflect on the HEV overall efficiency and therefore impact the fuel economy. Such demands in the HEV power system efficiency bring an important challenge in terms of the more compact power unit design solution [1 , 6].

In this project a compact power pack (Genset) consisting of a novel rotary engine and new type of Induction Machine (IM) with an Outer Rotor construction was designed. The designed power pack was simulated and compared with the existing power packs used in hybrid vehicles. The advanced vehicle simulator (ADVISOR) [7] was utilised to carry out the comparison and analysis. The developed induction machine also acts as an Integrated Starter-Generator (ISG).

The simulation results show that the developed system meets the high power requirements of the battery pack in a typical small HEV. This would result in greater fuel economy, lower emissions and higher performance of the vehicle equipped with the Genset. Figure 1.1 shows the schematic representation of the overall system. It basically consists of an internal combustion engine and the induction machine which act as both generator and starter motor for the ICE.

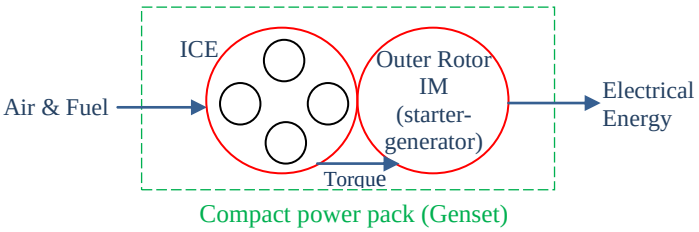

Figure 1.1 Schematic representation of the proposed power pack

1.1 Starters, Generators and ISGs

Starter motors are utilised to crank the engines in vehicles. Since 1910 when the first starter motor was developed, its technology has been upgraded in terms of the weight and size reduction, input voltage level, gear reduction, reliability and performance improvements. There are different techniques to start the engine and each method has its own advantages and disadvantages. The characteristics of each methods are introduced as follows [1 , 8 , 9].

The first method of cranking an ICE involves using a single starter motor, which is gear coupled to the crankshaft and is able to deliver the torque up to 150 Nm. This motor brings the engine speed up to 150-200 rpm and then the fuel is injected and ignited. Then, the starter motor is stopped and the engine climbs up to the idle speed by itself. Using of this method results in the high usage of fuel and high hydrocarbons emissions. Also, utilised coupling gears in this method causes high acoustic noises.

A second technique involves using the high speed starter motor which can crank the ICE to its idle speed of about 600-800 rpm over the internal of 1-1.5 sec. The fuel is then injected to the engine for combustion. This technique provides the smooth and fast start-up but combustion is not stabilised at such high speed.

A third method of starting up the engine is utilising two starter motors. The first starter motor cranks the engine up to 400 rpm and then disengaged. At this point the second starter motor is engaged to increases the crankshaft speed further to 600-800 rpm. Then, fuel is injected and the support of the second starter motor is withdrawn simultaneously. The first starter motor should have high power to overcome the high inertia while the second is required to increase the crankshaft speed. The advantages of this method is providing a reliable and efficient cold starting whilst additional cost and higher space requirements due to the second motor are drawbacks of the this method.

The generators are used in vehicles to supply the required electrical powers. The electrical loads of the conventional vehicle are powered by Lundell generator, which is a claw pole synchronous machine. The generated AC voltage from the machine is rectified and regulated to 12V DC voltage [8 , 10].

The efficiency of Lundell generators is very low because of producing the high losses in the machine windage and rotor. The output power density of these types of generators is also very low due to the high permeability of the claw poles [10].

The automotive power requirements have been raised over the decades because of ever increasing number of electrical loads. Performance loads such as windshield defrosters, electric steering, incandescent lights and heated seats imposing a higher demand of electric power. With the high power demands, there is a need to switch over the conventional 14V DC power systems to higher voltage of 42V DC systems. Therefore the conventional generators are not able to provide such high power requirements efficiently [1 , 11 , 12].

The advanced Integrated Starter-Generator (ISG) technology can fulfil the high power requirements efficiently. ISGs would perform the combined starting and generating functions by providing more than 150 Nm starting torque and delivering at least 4 KW electric power at 42V. The ISG is connected to the crankshaft and can cancel out the engine vibration by producing torque pulsations which results in a smoother vehicle drive [1 , 13 , 14].

The ISGs are coupled to the engines in two ways: by offset or by direct coupling configurations. In the offset option, there is little modification required near the engine and it can be incorporated without difficulties. The offset coupling is performed by gear, chain or belt [1 , 9].

Both the gear and chain drive couplings require the ISG to be positioned near to the transmission. A major issue with the gear coupling is that the high speed level causes the gear teeth scoring which results in damaging the gears. This problem can be reduced by using high grade materials but it would increase the manufacturing costs.

The advantage of the chain drive is that the chains used in this drive have smaller width than when a belt is utilised, because of strength, durability and longer life. The disadvantage of the chain coupling is its high level of noise, which can be reduced by utilising silent chains, but this would increases the cost.

The belt drive option is low cost and gives silent operation. Also unlike the chain and gear configurations it does not need any lubrication. When the belt coupling is used the proper selection of accessories such as locking nuts to fasten pulleys, torque tensioner

becomes very important. Also, there would be a need for dampening materials because of higher inertia in the ISG.

The direct coupling of the ISG provides quiet start, higher power at lower speed of the generator. In the direct coupling, ISG would have a larger diameter, typically 2.5 times greater than the offset coupled ISG, which provides the possibility of higher electric loading [1 , 15].

As shown in Figure 1.2, in the series configuration of the HEVs, the power packs are utilised in order to process the traction power, required by the wheels as well as powering the accessory loads. This would demand high power with high efficiency. In the series configuration, the ICE is turned on by the starter motor and then operates at constant speed and torque to drive the generator whenever the battery pack requires considerable recharging power [16].

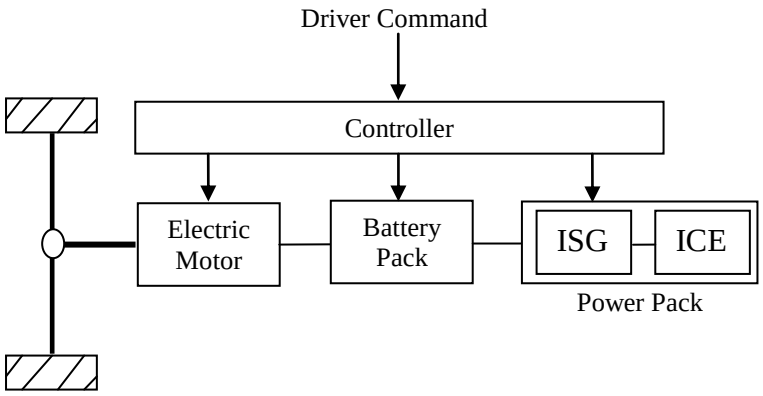

Figure 1.2 Schematic representation of the series HEV powertrain system

1.2 Compact Power Pack (Genset) for Series HEVs

Figure 1.3 shows the proposed compact power pack system. This system is similar to the conventional power unit systems used in the series configuration of the HEVs. In

both systems, ICE drives the generator and then the produced AC voltage is converted to required DC voltage for charging the battery pack.

The difference between the former power packs and Genset is that the engine utilised in Genset is a novel engine in terms of having a cylindrical dynamic crankshaft. Also, the integrated starter-generator of the Genset is a new type in terms of the rotor construction. The positions of the rotor and stator in this machine are exchanged and so it is called outer rotor IM (starter-generator) in Figure 1.1.

The specific construction of the novel engine and outer rotor machine, as shown in Figure 1.4 provides the possibility of coupling the novel engine directly with the electric machine. Therefore the pulley, tensioners and belt can be removed from the drivetrain. The function of the flywheel is served by the outer rotor of the electric machine. Direct coupled configuration could also result in vibration damping of the engine.

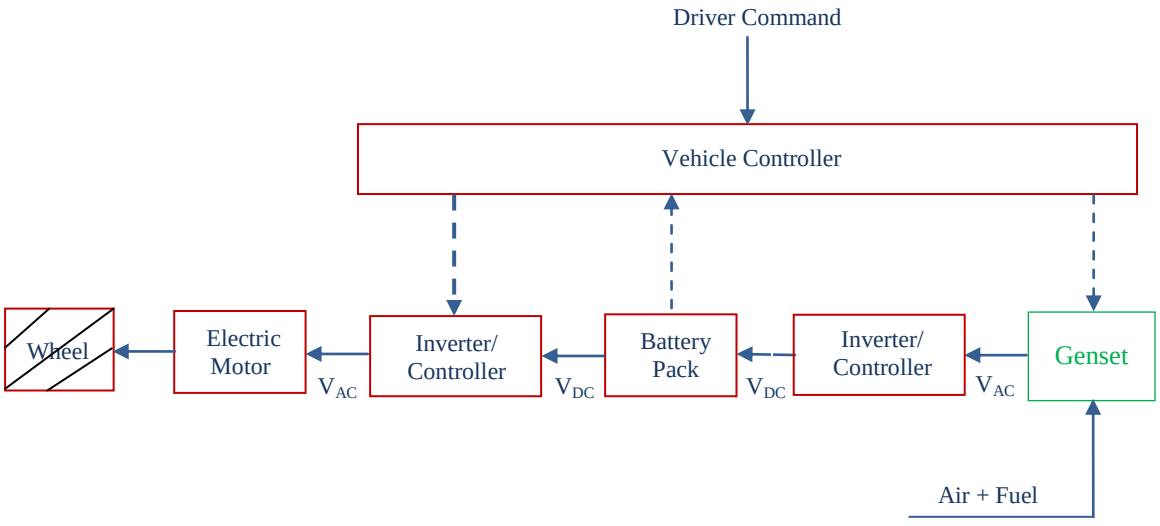

Figure 1.3 The Genset system principle

Under the direct coupled configuration shown in Figure 1.4, the compact power pack is placed in a 1:1 speed ratio for starting and generating. Presently, coupling speed is

increased with typical ratio of 2.5 [1]. Therefore the new ISG has to be a larger and heavier machine to provide the required starting torque.

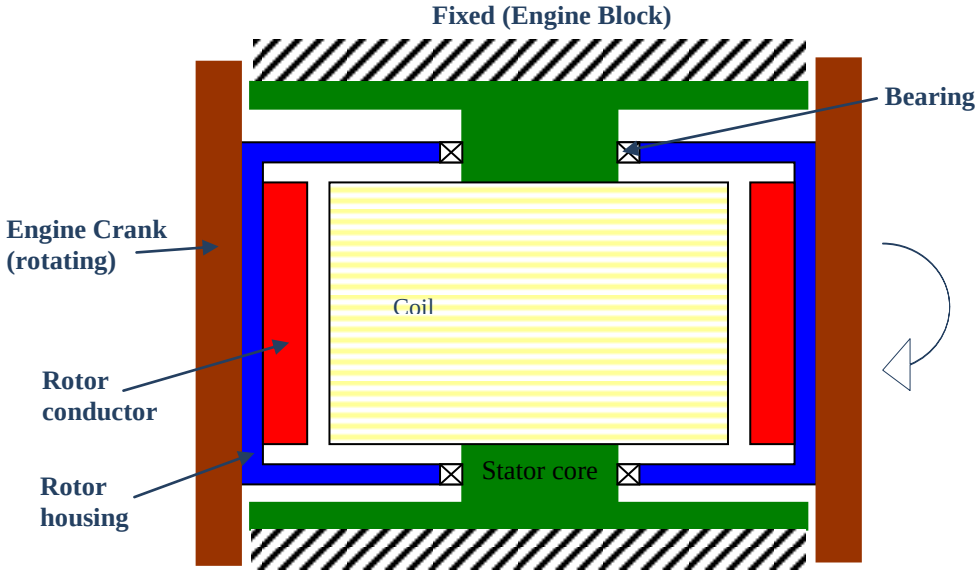

Figure 1.4 Compact power pack construction

1.3 Novel Internal combustion Engine (C5C)

A novel cylindrical internal combustion engine based on the five-stroke Atkinson cycle (C5C), which is a variant of the four-stroke cycle is being developed in the University of Bradford [17]. Normally the four cycles are intake, compression, expansion, and exhaust. As shown in Figure 1.5, the fifth stroke added is the combustion which is distinguished from the very fast expansion stroke. Engines running on this five-stroke cycle are claimed to be up to 30 percent more efficient than equivalent four-stroke engines [17].

The C5C engine is a cylindrical crank rotor internal combustion engine which is a hollow rotating crank shaft engine is a type of reciprocating engine that replaces the common crankshaft with a hollow cylindrical crank rotor. Pistons press down on the cylindrical crank rotor in sequence, forcing it to rotate around its centre.

The key advantage of the design is that the cylinders are arranged in a circular orientation around the cylinder and parallel to the crankshaft rotation axis. The cylinders are aligned with the output shaft (crankshaft) as shown in Figure 1.6. This results in a very compact, cylindrical engine, for which reason the design is also known as a barrel engine. The engine is operating by having the cylindrical crankshaft revolve in one circle while the pistons are firing in sequence one after another.

In the power pack designed in this project the electric machine is acting as the flywheel which increases the rotational inertia to smooth out the power pulses. The C5C engine rotates the electric machine to provide electric enery to be stored in the HEV battery pack while the engine speed remains constant.

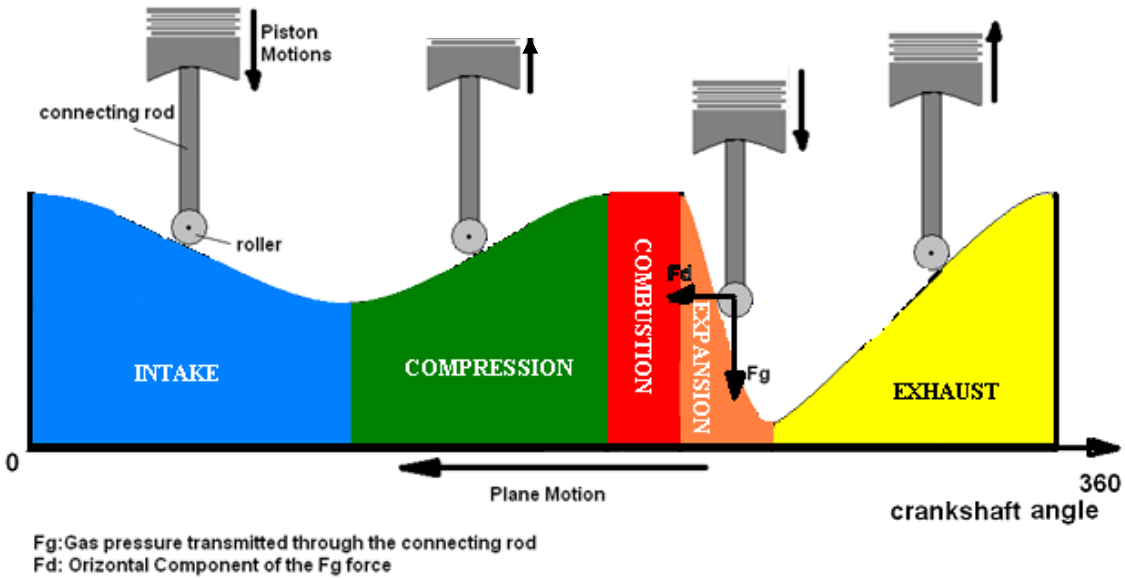

Figure 1.5 Working principle of the C5C engine [17]

The C5C engine shown in Figure 1.6 weights approximately 100 Kg and is calibrated to rotate at speed of 1550 rpm. This engine can be started by 200 Nm force with speed of 500 rpm over the interval of 0.6 sec. provided by the starter motor. The average diameter of the rotating crankcase is approximately 0.32 m [17].

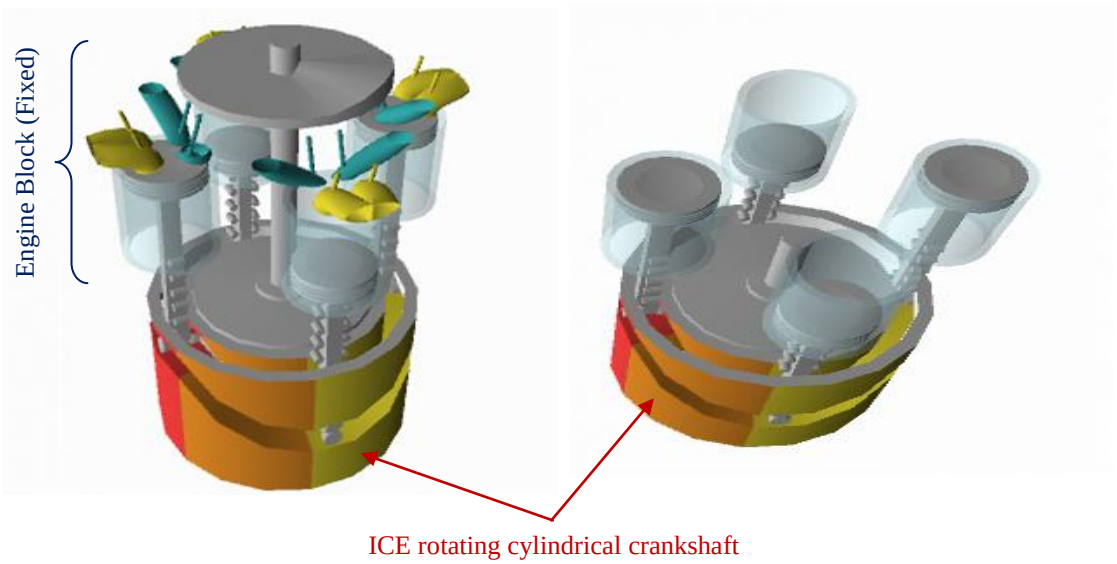

Figure 1.6 The novel rotary engine construction [17]

1.4 Aims and Objectives

The purpose of the project is to design a new type of induction machine with outer rotor construction that can interact with the novel rotary engine in order to form a compact power pack for HEVs. The main objective of the thesis can be classified into the following sub-aims.

- Sizing the components of a series HEV, particularly the power pack elements.
- Designing a new type of induction machine as an integrated starter-generator that can satisfy the main requirements of a compact power pack for the HEV.
- Applying an advanced vehicle simulator to analyse the performance parameters of the HEV equipped with the compact power pack (Genset)
- Comparing the HEV performance parameters when utilising Genset or existing power packs

1.5 Structure of the Thesis

The thesis is organised into the following chapters. Figure 1.7 shows the schematic diagram of the thesis layout.

- Chapter 1: This chapter contains a brief introduction of the thesis. The reasons behind the demands for more compact power packs are explained and the idea which is proposed to solve this problem is explained. The construction of the targeted compact power pack consisting of a novel engine and new starter/generator are explained as well as declaring the specifications of the novel engine. The objectives of the project and organization of the thesis are then presented in this chapter.
- Chapter 2: The second chapter gives a background of the HEVs technology, explaining their prospects and characteristics. The features of different configurations of the HEVs drivetrain are also investigated. The powertain components of the HEV, including its power pack elements are sized in this chapter.
- Chapter 3: Third chapter explains the induction machine construction and operation principles in both modes of motoring and generation. The equivalent circuit of induction machines is analysed and then the torque-speed characteristics of the machine is derived using this circuit.
- Chapter 4: This chapter explains the major factors and features of induction machine design, highlighting the specifications of different design classes. The procedure of induction machine design is shown by a flowchart. Then, the equations for calculating the main dimensions of induction machines are presented.

- Chapter 5: The specifications of the targeted outer rotor electric machine are determined in this chapter. Then, an Outer Rotor Induction Machine (ORIM) which is proposed to work as an integrated starter-generator for the small HEV is designed. The equivalent circuit elements of this machine are calculated in order to determining its operation characteristics including efficiency and power factor. The determined values are used to confirm if the designed machine meets the specified targets. This requires several iterations in the design process but only the last procedure is reported.
- Chapter 6: This chapter introduces a finite element package as electric machines simulator, explaining its structure and approach. The proposed induction machine is then simulated to analyse its motoring and generation characteristics. The main performance parameters of the machine are quantified to investigate that the designed machine meets the specified requirements of the proposed starter/generator.
- Chapter 7: In this chapter, the operation performance of the compact power pack when it is used in a small HEV is simulated by an advanced vehicle simulator. The simulation results are presented in the case of the HEV with Genset or conventional power packs options. Then, the results of the analysis are studied and compared to distinguish between the characteristics of the proposed compact power pack and the conventional ones.
- Chapter 8: The last chapter of the thesis contains the discussion of the work, summary of the results, conclusions and recommendations for further work.

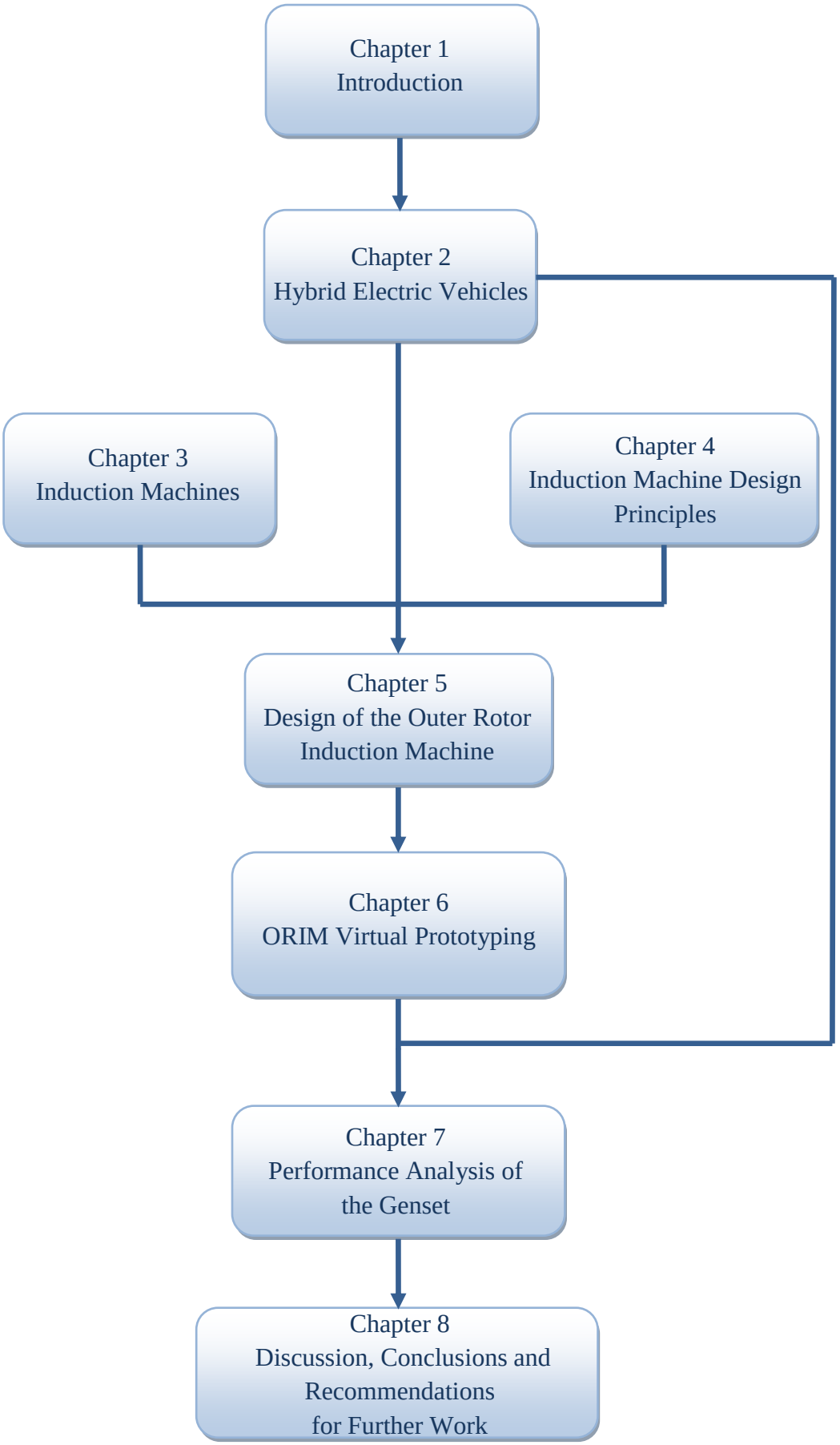

Figure 1.7 Schematic diagram of the thesis layout

Chapter 2 Hybrid Electric Vehicles

Electric vehicles have been in use since the 19th century. In 1834, Thomas Davenport in the USA built the first electric road car powered by a primary battery [18]. This was achieved after inventors derived the operative electric motors using the Volta pile on basis of Faraday phenomenon.

The developments of electric vehicles were continued by invention of secondary cell and battery and construction the first DC electric motor of more than one horsepower. In 1881, G. Trouvé made the first electric vehicle to be fed by a secondary battery [18].

After all of these major events, Carl Benz built the first internal combustion engine vehicle in 1885. In 1899 Ferdinand Porsche designed the first electric/internal combustion hybrid vehicle. In this vehicle, front-wheel electric motors were powered by the batteries which were charged by a generator. The generator was driven by a gasoline engine. By 1912, while range of gasoline fuelled internal combustion engine vehicles increased in Europe and the USA, the electric and HEVs were also being expanded. The Century Electric Roadster of 1912 shows the advances of HEVs typically [18].

During 1925 to 1960 was a dark age for electric vehicle industry because the gasoline powered combustion engines improved rapidly and HEVs were more expensive versus conventional and even pure electric vehicles.

After 1960, electric vehicles appeared again because of air pollution caused by gasoline powered vehicles. Important advances in power electronics have helped to make powertrains with good performance. The forthcoming shortage of gasoline products and

their costs were other significant factors which overcame the shortcomings of the earlier dark age for the electric vehicles [18 , 19].

2.1 The outlooks for Hybrid Electric Vehicles

In the following Subsections, the position of the HEVs in the early days and in the future are stated. Most of the vehicle manufacturers have considered the importance of the HEVs in their vehicle development programs to satisfy the emission regulations and improve the fuel economy. They are challenging to achieve the more benefits of the hybrid vehicles using the advanced technologies.

2.1.1 Year 2000 Status

In the last quarter of the 20^{th} century car manufacturers turned their attention to hybrid and electric vehicles seriously when emission regulations made constricted. In 1997, the Toyota hybrid system Prius was released. Two years later, new types of HEVs were presented by the Japanese manufacturers such as Honda, Mitsubishi, Nissan and Toyota. In January 2000 at the North American international Auto Show, the world's major manufacturers: BMW, General Motors, Toyota and Daimler Chrysler introduced twenty three HEVs [20 , 21].

2.1.2 The Present Status of Hybrid Electric Vehicles

Fuel prices and emissions play important roles in the automobile industry nowadays. Environmental issues are pushing Auto-manufacturers to pay attention to make vehicles with lower emissions and high fuel efficiency. Customers would like to have a good fuel economy for their vehicles as well [22]. Therefore hybrid and electric vehicles are still suitable to obtain this aim with their cleaner power sources.

Electric vehicles are still extremely limited by their range per battery pack charge with their current technologies. As gasoline engines are doing very well at steady speed operation and electric motors give more acceleration, so by combining both of these devices as hybrid electric technology both benefits can be achieved. In this case, HEVs satisfy customer needs with greater fuel economy compared to conventional cars. Also the car can be used for long period without recharging. On the other hand HEV technology also takes an enormous step forward to limit greenhouse gas emissions [20].

2.1.3 The Future of Hybrid Electric Vehicles

HEV technology is an advanced technology to achieve the lower emissions and greater fuel economy in the vehicles when they are provided to have the battery-only range [23].

In 2020 the fuel cell will be the best HEV power source. However gasoline and methanol will be used. In addition, HEVs fuel economy range will be 1.7 to 2.6 times the conventional cars.

The future aim of the HEVs manufacturers is to reduce the nitrogen oxides and particulate matter emissions considerably with comparison to conventional cars emissions. Also, the higher cost of hybrid electric vehicles will decrease from 66% to 33% more than a 20,000 USD conventional vehicle by 2020 [23].

2.2 Hybrid Electric Vehicle Definition and its Components

Any vehicle is called hybrid when it combines two or more power supplies. HEVs are equipped with internal combustion engines, battery and electric motors [18 , 24].

The International Electrotechnical Commission's (IEC) definition for a hybrid vehicle is that a vehicle which its propulsion power supply can be obtained from two or more kinds of energy sources during particular operations and one of these sources must be on-board. If at least one of the energy sources can provide electric energy, the hybrid vehicle is called a hybrid electric vehicle [22].

The Hybrid electric vehicle components and their brief characteristics are shown in Figure 2.1 and listed as follows.

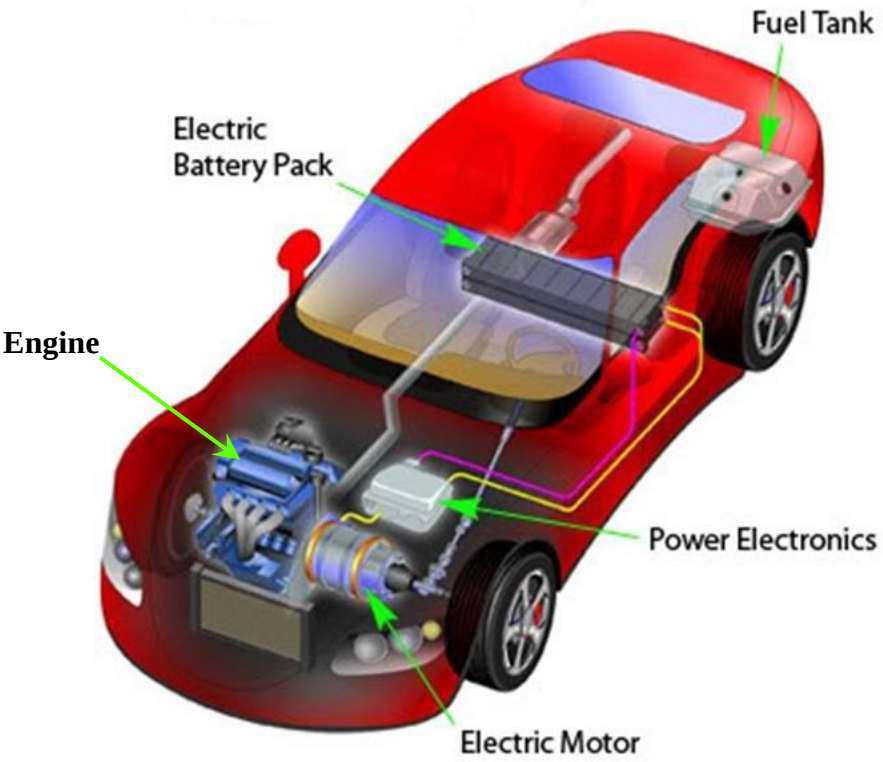

Figure 2.1 Hybrid electric vehicle components [25]

Fuel Tank – Fuel tank contains gasoline or diesel to supply the conventional engine.

Engine – Internal combustion engine in HEV works the same as in any conventional vehicle. Continuous explosions in ICEs produces power that press down pistons

connected to a rotating crankshaft. Finally this rotating force which is called torque is transmitted to the car wheels.

The engine of HEV is smaller than that in conventional engine in size. It is made using advanced technologies to have high efficiency and low emissions. Two common types of engines are Spark Ignition (SI) and Compression Ignition (CI) engines which are called as gasoline and diesel engines respectively. It has been predicted that HEVs will use a fuel cell power source by 2020 instead [23].

Batteries – Batteries are input power supplies for electric motors used in HEVs. The batteries used in HEVs should have high specific energy, high power with high-peak and pulse-specific power, high charge acceptance and long calendar and cycle life [25]. The mean battery-only range was 49 km in 2005. It is expected this range to be 70 km and 92 km in 2010 and 2020 respectively [23].

The main types of batteries considered for hybrid electric and pure electric vehicles are lead–acid, nickel-cadmium, nickel metal hybrid (NiMH), lithium ion, lithium polymer [25 , 26].

Electric Motor – The electric motor is a fundamental component in driving the hybrid electric vehicle. The electric motor is powered by a battery pack to convert the electrical energy to the mechanical energy. This function is performed in power mode, whilst in the regenerative mode; the kinetic energy of a vehicle can be recovered by the electric machine during deceleration to recharge the batteries. In the regenerative mode, electric motor operates as a generator to charge the batteries using advanced power electronics.

The electric motors are able to deliver high torque at low speed and also they can operate in a wide range of speed with constant power characteristics. Therefore electric drivers can accelerate the car from stop or in highway and overcome the high torque requirements such as hill climbing. These characteristics of electric motors lead to this fact that HEVs do not require complex transmission systems.

Until 1960s, the DC motors were always utilised in the electric vehicles powertrains. Because theses motors can be supplied by battery unit directly and also have an easy control system and low weight. DC motors up to 20 KW will probably continue to be used in small cars [18 , 27].

With advanced power electronic technology, in the early days and after 1960s, AC machines have been used in the electric vehicles. These power electronic devices are able to operate in the high current applications and convert the direct current to alternative current with variable amplitude and frequency, therefore it has been possible to control the AC motors in variable speed which is necessary for hybrid vehicle propulsion systems [18 , 28].

Suitable categories of AC motors for hybrid electric vehicle applications are induction, synchronous permanent magnet and switched reluctance motors. These types of AC motors are more efficient than DC motors over a wide range of operation. In addition, they have more advantages of reliability, size, cost and weight. However the application and utility of the switched reluctance motors as an electric driver in the vehicles are under investigation because of their complicated control [18 , 28].

The induction motors benefit from their mature technology as the most commonly used electric motors in industry. They are famous for their good starting torque and high torque features. Some other advantages of induction machines are their high reliability, low cost and low maintenance [1].

Cage induction motors have been accepted as the best choice for the electric vehicle applications due to their ruggedness and reliability. They fulfil the main requirements of the HEVs propulsion better than the other options. Also, their low cost makes them more attractive to be selected between the other electric propulsion drives. However competition of permanent magnet electric motors with induction motors remains hard [29].

Induction machines are particularly popular for electric vehicles and series HEVs where a high power machine is required. Unlike permanent magnet machines, IMs can be rated for high power levels and unlike switched reluctance machines, IMs have lower acoustic noise. The output power of the permanent magnet machine is limited by the size of the magnets, which are utilised to provide excitation for the machine. The cost of the magnets greatly influences the cost of the machine and so limits the size of the machine [30].

Generator – Generators are mostly utilised in HEVs with series configuration. They are powered by ICE and produce electrical energy in order to charge the batteries. As explained in Chapter 1, high generation capacity requirement makes the torque characteristics of the generator and starter motor to get closer to each other and so they can be integrated. The integrated starter-generator is an advanced technology that fulfils

the increasing power demands of the conventional or hybrid vehicles. ISGs perform the both functions of engine starting and power generation.

Three strong candidate electric machines for the ISG application are induction, permanent magnet (PM) and switched reluctance machines. Induction machines have good starting torque, high reliability and low maintenance and cost. The noise level and torque ripples of IMs are lower than those of the other machines. [1].

PM machines utilise permanent magnets on their rotor to produce the magnetic field and so they can operate at high speeds up to 24,580 rpm without failure but on the other hand presence of magnets brings demagnetisation problems at high temperatures [31 , 32].

Switched reluctance machines do not have magnets or coils on their rotor and so they can benefit from the rugged structure to have better performance at high speed and temperatures [33]. The drawback of switched reluctance machines is that they suffer from high torque ripples due required non-sinusoidal voltage in input circuit. This feature also results in high noise levels [8 , 34].

Though the PM machines have a higher efficiency but they are more expensive. The quick magnetic field changes in the switched reluctance machines also cause a higher noise. The induction machine typed is selected in this project to be used as ISG for the HEV powertrain. The induction machine offers a wide range of speed and operates in harsh environment with lower maintenance and cost. In addition, it can be fully deenergised in the case of a short circuit in windings and so provides a better failure mode [35].

Transmission–The basic function of transmissions in both of the hybrid and conventional vehicles are the same. Different types of HEV transmission systems have been presented as manual, automated shifted manual, continuously variable and usual automatic transmission with torque converter [25].

2.3. Advantages of Hybrid Electric Vehicles

The electric vehicles rely to batteries as their only sources of power, and these batteries have limitation in range and long recharge time. By combining electric drive and engine in HEVs, these limitations can be removed. In HEVs emissions and fuel consumptions of conventional engine is reduced because of increasing the engine efficiency by the use of different methods of combining of engine and electric motor and applying advanced control strategies to optimise their relations. Electric motors can provide better power curve than internal combustion engines in variable speeds and also can give greater torque at low speeds. They also increase the acceleration performance of vehicle [18].

As hybrid electric cars have an alternative power source other than petrol or diesel engine which is electric motor and batteries, so the engine can be switched off in stationary periods, such as stop times behind the red light.

2.3.1 Lower Weight of Vehicle

The hybrid electric vehicles are lighter and roomier than pure electric vehicles in the same size and power. The reason for this fact is that the HEVs need fewer batteries as required energy. These batteries are recharged by the generator continuously. The same function of engine which drives alternator in conventional vehicle [24].

2.3.2 Smaller Internal Combustion Engine

The size of internal combustion engines in HEVs can be designed to be a little above of required average power instead of maximum power demand. Therefore the size of them can be reduced and so they will be lighter and more efficient [25]. The reason is that big engine is heavier and has bigger cylinder displacement and heavier piston which leads to using more energy by the car even when the vehicle is not moving. Emissions and fuel consumption would be reduced by increasing the average engine efficiency which is the aim of the manufacturing of the electric and HEVs.

2.3.3. Regenerating the Braking Energy

One of the main advantages of hybrid electric vehicles is its possibility for recovering the braking energy. In conventional vehicles the kinetic energy is wasted as heat during deceleration in the brakes. Accounting amount of braking energy in urban cycle which is 40 % to 45 % of the energy consumption of the vehicle, the importance of this issue will be clearer considering reduction of CO2 as well.

Regenerative braking systems in HEVs detain and save a part of the braking energy which is wasted in conventional vehicles during braking and so it leads to increasing the vehicle efficiency. The amount of captured energy from regenerative braking can be used for initial acceleration using ultra capacitors. In this case, the life of the batteries will be extended [24 , 36].

2.4 Different Configurations of Hybrid Electric Vehicles

Different types of HEV propulsion systems are distinguished by how the internal combustion engine and electric motor are connected and how they work together. Two basic configuration of hybrid drive system are series and parallel. Most hybrid cars use

parallel technology and most of the hybrid trains, trucks and transit buses use series type. Series hybrids are helpful in driving cycles that include many stops and starts, such as for delivery vehicles as well.

HEVs also can be manufactured in series-parallel configuration. In this case, the series configuration can be applied when car is driven in low speeds and parallel configuration is used for highway and acceleration [24 , 36]. The Prius' series-parallel power train uses this technology where generator charges the batteries to power the electric motor (series configuration) and also the motor and internal combustion engine is combined to drive the car directly (parallel configuration) [22].

Future hybrid electric vehicles have predicted to run with series drive technology [23]. The reason is that the fuel cell is the forward running of HEV's power plant as it was mentioned in Subsection 2.1.3 and fuel cell car must have series configuration and so the share of series hybrid vehicles has risen as fuel cell share has increased. In addition, the share of the series drive is more expected to increase as the all-electric range rises because the size of electric components would be more appropriate [23].

2.4.1 Series Configuration

In the HEVs which have series power drive, the internal combustion engine is used to drive the generator. The converted electrical energy in output of the generator charges the batteries which drives the electric motor to move the wheels. The engine-generator part and batteries can supply electric energy simultaneously when the huge amount of power is needed.

In the series systems there is no mechanical connection between the hybrid power part and wheels whereas in parallel configuration this direct mechanical connection is necessary. This means in the series HEVs, power is converted from chemical energy to mechanical energy then to electrical energy and it is converted back to mechanical one again to move the wheels. Figure 2.2 shows a series configuration of a hybrid electric vehicle [24].

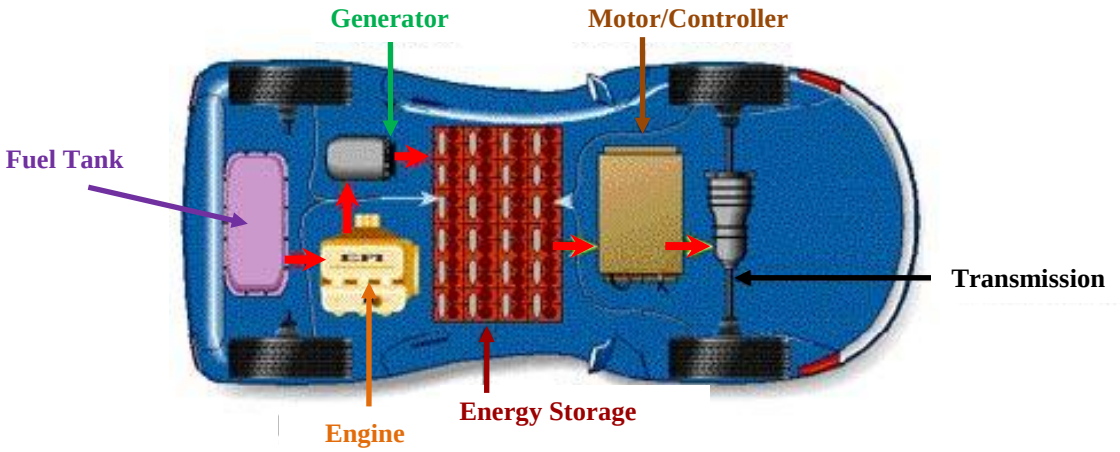

Figure 2.2 Series configuration of a hybrid electric vehicle [24]

2.4.1.1 Advantages of Series Configuration in Hybrid Electric Vehicles

The HEVs which use series configuration do not need a complex transmission because electrical motors are able to move the vehicle within a wide range of speeds efficiently. Also the engine function can be adjusted continuously to its most efficient speed if it is required. Furthermore in this system engine never stops which result to lower emission. Engine makes the generator to work at best possible performance as well.

Since there is not any mechanical connection between the internal combustion engine and the wheels, position of the engine will be very flexible and its location can be chosen outside of the passenger section [18 , 24].

In some types of series HEVs small electric motors are named as in-wheel motors that are mounted at each wheel which is easier to control the powertrain drive and so makes the simpler traction control and allows the possibility of all wheels drive. For example, the U.S. army hybrid RST-V vehicle has used four 50 KW electric motors, one at each wheel [37].

2.4.1.2 Disadvantages of Series Hybrid Configuration

The HEVs with series powertrain need a separate generator to charge the battery pack which needs hard operation of engine to drive the generator. Also its battery pack is larger and so heavier than parallel cars. In addition, the efficiency of the vehicle is decreased because of two times conversion of mechanical to electrical energy in power drive [18 , 24].

2.4.2 Parallel Configuration

In parallel drive systems, fuel converter and electric motor are connected to the mechanical transmission directly. They can be sub-classified depending upon how much drive power each part delivers. In some types, the internal combustion engine is the main drive power whereas the electric motor provides additional power when it is needed such as in hill climbing and acceleration periods. In some other types of parallel HEVs, the electric motor can be a drive power alone. Figure 2.3 shows a parallel configuration of a hybrid electric vehicle [24].

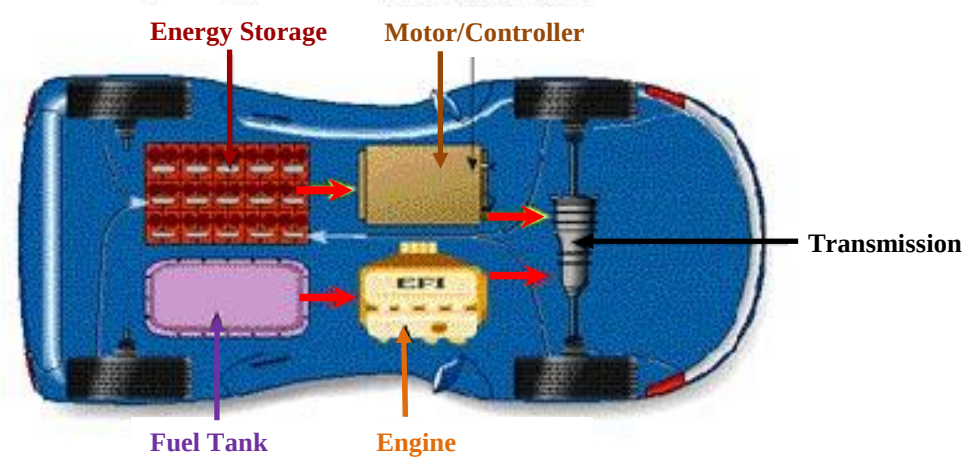

Figure 2.3 Parallel configuration of a hybrid electric vehicle [24]

2.4.2.1 Advantages of Parallel Configuration in Hybrid Electric Vehicles

Most parallel cars do not need an extra generator for recharging the batteries. This can be done by the electric motor which regenerates the brake energy during deceleration. Electric motor is often placed in the location of the flywheel between the transmission and internal combustion engine [24]. The removal of the generator including rectifier decreases the cost and weight considering the elimination of the additional gearboxes and clutches as well.

In parallel systems compared to series one, there is only one conversion process between mechanical and electrical energy, so the efficiency is higher than series one which needs two conversion. Also it is not required to transmit the power via batteries and this gives further efficiency. More efficiency will result to better fuel economy.

In HEVs which have used the parallel system, the engine should only work whenever the vehicle is moving unless battery is not charged enough, and in that case it is required to use the engine to drive the motor directly to act as a generator and regenerate the braking energy. This leads to reducing the engine noise [18 , 24].

2.4.2.2 Disadvantages of Parallel Hybrid Configuration

The downside of parallel configuration is its higher emission. The reason is that there are a few well-defined positions for installing the engine in the mechanical coupled powertrains and as the engine speed need to be changed more than series configuration it will be hard to get low emission [18].

Parallel vehicle is more complex and both of the power drives must be connected to the transmission system mechanically. In this case, controller needs to calculate amounts of required power for drivetrain and also value of power which each individual component will supply.

2.5 Sizing of the Powertrain Components of the Series HEV

In this section, the electrical powertrain components of the series HEV are sized. These components include engine, generator, batteries and electric drive motor. The estimated value of the generator power is used in Chapter 5 as a design parameter to design the generator for the specified hybrid electric vehicle. This value and the estimated values for the battery and dive motor sizes are used in the Chapter 7 for simulation of the hybrid electric vehicle.

In series hybrid electric vehicles, an electric motor provides the required traction torque. The behaviour of the traction motor in the HEV is the same as an electric drive motor in the pure electric vehicle. Therefore the size of the drive machine for an EV and series HEV is almost equal. The difference between EV and series HEV is that the later one has a generator to charge the batteries. Subsequently, batteries save the energy to spend it over the drive cycles.

2.5.1 Vehicle Data and Vehicle Performance Specification

The power required from the propulsion system depends on the desired specification of a vehicle and vehicle physical data. The vehicle which is proposed to utilise the compact power pack in this project is supposed to have the following specifications.

Acceleration: 0-100 Km/h (0-27.77 m/s) in 15 seconds.

Vehicle maximum speed: 110 Km/h (30.55 m/s)

Vehicle frontal area: 2 m^2

Vehicle mass including passengers: 1250 Kg

Gradibility: Grade of 30 % at 45 Km/h (12.5 m/s)

2.5.2 Electric Drive Motor Size Estimation:

Electric drive motor in a vehicle drivetrain needs to provide a sufficient power to accelerate the vehicle and move it at the rated speed. In fact, this power should overcome the road load resistances which are rolling, aerodynamic and climbing resistances [26 , 38].

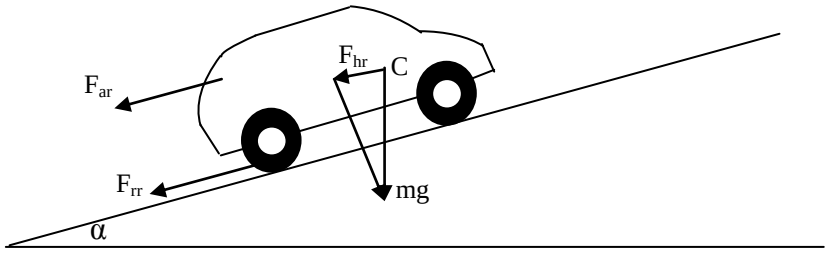

Figure 2.4 Resistance forces on a vehicle along a slope

Figure 2.4 shows forces vectors on a vehicle where C is the centre point of gravity of a vehicle. The rolling resistance force is presented by F_{rr} and is produced by the tire deformation on the constant roadway surface. The value of this resistance depends on the vehicle mass and road angle as shown in the following equation.

$$F_{rr} = f_{rc}.m.g.\cos\alpha \quad (2.1)$$

where f_{rc} presents the tire rolling resistance coefficient and α is the road angle. f_{rc} is almost constant and it hardly changes with vehicle speed. Typical value of f_{rc} is 0.015 but it has been reduced to 0.005 by the developed special tyres of electric vehicles [39]. m is the vehicle mass and g indicates the gravity acceleration constant (9.8 m/s^2).

F_{ar} shows the aerodynamic drag force in the Figure 2.4. This resistance is made by the air acting upon the car and its value depends on the vehicle frontal area, vehicle speed and head-wind speed as presented in the following equation,

$$F_{ar} = 0.5.\rho.C_d.\ A_{vf}.(V+V_w)^2 \quad (2.2)$$

where ρ presents the air density, C_d is the aerodynamic drag coefficient, A_{vf} is vehicle frontal area and V and V_w present the vehicle and head-wind velocities respectively. Air density varies with humidity, altitude and temperature but in most cases it has a typical value of 1.25 Kg/m^3.

The typical value of C_d is 0.3 but in electric vehicles it can be reduced to 0.2 because main components of the electric vehicle can be located more flexible than conventional one, and it needs less cooling air ducting and under-vehicle pipe-work [39]. The average value for the wind velocity can be taken as 5 m/s(11.18 mph) according to the Beaufort scale [40 , 41].

F_{hr} shows the hill climbing resistance force in the Figure 2.4. The value of this force is a function of road angle as it is shown in the following equation.

$$F_{hr} = m.g.\sin(\alpha) \quad (2.3)$$

where α is the road angle in degrees.

Power required from the drive motor to overcome the road load resistances is changed for different positions of the vehicle. In the following subsection the drive power for different positions of the vehicle is calculated.

2.5.2.1 Required Drive Power for Initial Acceleration

In this section the value of the power needed to accelerate the vehicle from the stop point is calculated based on the desired specification given in Subsection 2.5.1.

Based on the discussion in Subsection 2.5.2 and from the Newton's second law of motion:

$$F_d = m.a + F_{rr} + F_{ar} \quad (2.4)$$

where F_d is the drive force and a presents the vehicle initial acceleration. It is assumed vehicle is on a level road. Applying Equations (2.1) and (2.2) results in:

$$F_d = m.a + f_{rc}.m.g + 0.5.\rho.C_d.\ A_{vf}.(V+V_w)^2 \quad (2.5)$$

By substituting the values of the parameters according to Subsections 2.5.1 and 2.5.2 the drive force is calculated as follows.

$$F_d = 1250 \times \frac{27.77}{15} + (0.005 \times 1250 \times 9.8) + (0.5 \times 1.25 \times 0.2 \times 2 \times (27.77 + 5))^2$$

$$F_d = 2.643 \text{ KN}$$

The required drive power from the drive motor can be calculated using the following equation.

$$P_d = F_d.V \tag{2.6}$$

which gives the value of the drive power as:

$$P_d = 2.643 \times 27.77 = 73.39 \text{ KW}$$

2.5.2.2 Required Drive Power for Cruising at Maximum Velocity

In this section, the value of the power needed to cruise the hybrid vehicle at maximum speed is calculated. The vehicle is mostly has this position when it runs on a highway. If it is supposed that the vehicle moves at a constant maximum velocity, the Equation (2.4) can be written as:

$$F_d = f_{rc}.m.g + 0.5.\rho.C_d.\ A_{vf}.(V+V_w)^2 \tag{2.7}$$

Substituting the parameters in the equation above mentioned in Subsections 2.5.1 and 2.5.2 gives the value of drive force as:

$$F_d = \{(0.005 \times 1250 \times 9.8) + (0.5 \times 1.25 \times 0.2 \times 2 \times (30.55 + 5)^2)\}$$

$$F_d = 377.20 \text{ N}$$

Now, the required drive power can be calculated using the Equation (2.6) as:

$$P_d = 377.20 \times 30.55 = 11.523 \text{ KW}.$$

2.5.2.3 Hill Climbing Drive Power

As it was mentioned in Subsection 2.5.1 the hybrid electric vehicle needs to cruise a hill with grade of 30 % with constant velocity of 12.5 m/s. When a vehicle climbs a hill with a constant speed it requires overcoming the hill climbing resistance as well as fraction and aerodynamic resistances. Therefore the Equation (2.7) becomes as follows.

$$F_d = f_{rc}.m.g.\cos(\alpha) + 0.5.\rho.C_d.A_{vf}.(V+V_w)^2 + m.g.\sin(\alpha) \quad (2.8)$$

Grade of 30 % equals an angle of 27 degrees. By substituting the vales of parameters in the Equation (2.8) the drive force can be calculated as:

$$F_d = \{(0.005 \times 1250 \times 9.8 \times \cos 27^\circ) + (0.5 \times 1.25 \times 0.2 \times 2 \times (12.5+5)^2) + (1250 \times 9.8 \times \sin 27^\circ)\}$$

F_d = 5692.51 N

Now, the required drive power for the desired gradibility can be calculated using the Equation (2.6) as:

$$P_d = 5692.51 \times 12.5 = 71.156 \text{ KW}$$

Electric drive motor should able to provide the maximum value of the calculated required powers for different positions of the hybrid vehicle. If the calculated values of required drive powers in Subsection 2.5.2 are reviewed it can be seen that the acceleration mode requires the highest power. But this demand is only for the short periods of time and electric motor does not need to provide this power at all the time.

The second highest value for the required drive power refers to the hill climbing situation. The drive motor needs to provide this power in a longer period compared to the acceleration mode. Drive power has been calculated as 71.156 KW in Subsection 2.5.2.3 for the climbing position of the hybrid vehicle.

The power demand for vehicle electrical loads such as head lamps, engine cooling fan and heated windshield should be added to the calculated drive power. The average value for the electrical loads is about 3 KW [1 , 42]. Therefore the required power for driving the hybrid vehicle based on the desired operation is determined as follows.

$$P_d = 71.156 + 3 = 74.156 \text{ KW}$$

It is important to consider the drive motor and transmission efficiencies when sizing the drive motor for the hybrid electric vehicle. Electric drive motors often have a high efficiency and it is about 91 % for induction motors at low and high speeds [1]. Transmission efficiency is about 95 % typically [26] and therefore the electric drive motor power should be as follows.

$$P_{dm} = \frac{P_d}{\eta_{dm} \times \eta_t} \tag{2.9}$$

P_{dm} represents the power of drive motor and η_{dm} and η_t are the efficiencies of drive motor and transmission respectively. Therefore drive motor's power can be calculated as:

$$P_{dm} = \frac{74.156}{0.91 \times 0.95}$$

$$P_{dm} = 85.78 \text{ KW}$$

It is decided to select the induction motor option between the other types of traction motors to drive the vehicle, according to the discussion made in Section 2.2. The nearest size of a standard induction motor to the calculated drive power is 90 KW [43]. Therefore a 90 KW three phase induction motor can be selected for the desired HEV propulsion system.

2.5.3 Battery Pack Size Estimation

Different battery types such as lead-acid, NiCd, Li-ion have be used in the electric and hybrid electric vehicles. Nickel metal hybrid is one of the most advanced batteries which has been used in a range of HEVs including Ford Escape, Toyota Prius, Honda insight and Volvo ECC [18 , 39]. In this project, Ovonic 12HEV20 NiMH battery is chosen because of its high power density and rapidly charge capabilities. The specifications of this battery is summarised in Table 2.1.

Table 2.1 12HEV20 Ovonic battery specifications [44]

Nominal Voltage (V)	12
Nominal capacity (Ah)	20
Dimensions:	
Length (mm)	340
Height (mm)	91
Width (mm)	75
Weight (kg)	5.4
Volume (L)	2.3
Nominal Energy* (Wh)	250
Specific Energy (Wh/kg)	46
Energy Density (Wh/L)	110

Peak Power* (KW)	3.0
Specific Power (W/kg)	550
Power Density (W/L)	190

* Capacity and Energy measurements at charge rate C/3 and power measurements from 10 sec. pulses at 50 % DOD (Depth of Discharge) at 35°C battery temperature

A 90 KW electric drive motor, sized in Subsection 2.5.2 requires 164 Kg of battery, which is almost 31 battery cells because specific power of the 12HEV20 cell is 550 W/Kg. This gives a nominal voltage rating of 372 volts. The similar voltage range has been used by some electric and hybrid electric vehicles such as General Motors EV1, Nissan Altra EV, Mitsubishi HEV, and General Motors Precept HEV [18].

To charge a 12 volt battery pack, a 14V DC system voltage is required, which is called 14V system. Similarly, 42V systems are used to charge the 36 volt battery packs in the vehicular systems [34]. The 144 volt and 288 volt battery packs, which are used in mild hybrid and full hybrid vehicles, utilise 150V DC and 330V DC systems respectively [1]. Using Mirosoft Excell 2007extrapolation, it is estimated that the electrical system for the 372 volt battery pack should be approximately 420 VDC, as shown in Figure 2.5.

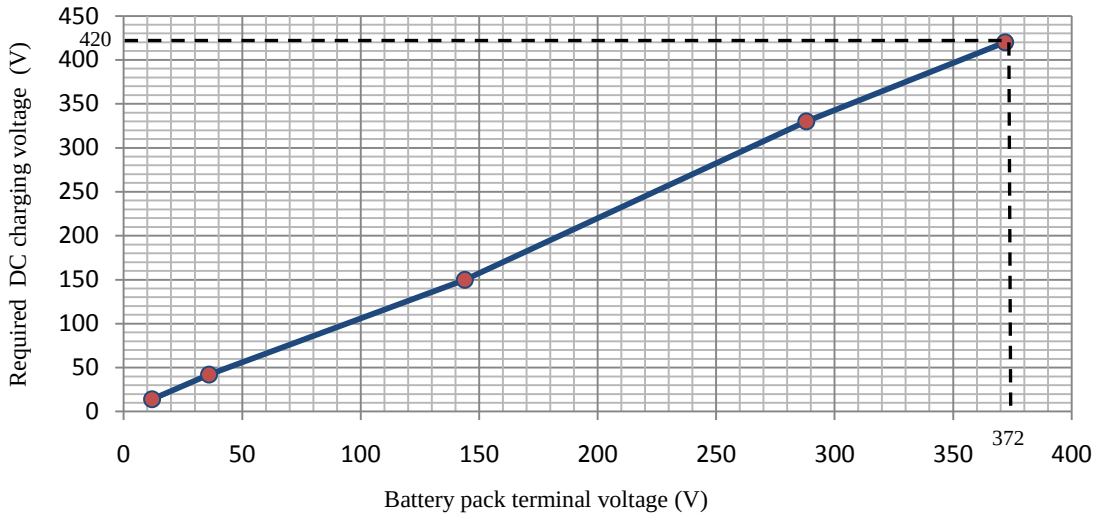

Figure 2.5 Battery charging voltages for vehicular systems

2.5.4 Generator Sizing

The estimation of the generator size can be done by calculating the energy capacity requirements of the desired vehicle. To achieve a charge sustainable series hybrid vehicle, battery pack needs to maintain the same state of charge at the end of the drive cycle as in the starting of the drive cycle. In other words, generator should feed the exact amount of energy that has been consumed by the battery pack to drive an electric motor over a drive cycle.

Table 2.1 shows that the value of a stored energy in a 12HEV20 battery pack is 250Wh. Therefore the total stored energy for the 31 battery pack will be as follows.

$$\text{Total Stored Battery Energy} = 250 \times 31 = 7750 \text{ Wh}$$

$$= 27.89 \text{ MJ}$$

NiMH batteries can be recharged very quickly and nominal rapid charge time is approximately 15 minutes. The battery charge efficiency is very close to 100 % between 20 % and 80 % of charge, but in the last 20 % state of charge, the charge efficiency falls off greatly [39 , 45]. Therefore, battery charging starts at 20 % of charge up to 80 % of full charge. Therefore the energy requirements from the generator can be calculated as follows.

$$\text{Energy required from the Generator} = 27.89 \text{ MJ} \times (80 - 20)\ \% = 16.734 \text{ MJ}$$

Generator is required to provide the value of energy calculated above in about 15 minutes in ultra fast charging mode. In this case, the generator output power is calculated as:

$$P_{Gout} = \frac{16.734}{15 \times 60} = 18.59\,KW$$

Assuming an efficiency of 90 % for a generator the size of the generator should be:

$$P_G = \frac{18.59}{0.9} = 20.65\,KW$$

The nearest standard size to the calculated size of electric machine is 22 KW [43]. Therefore the generator which is supposed to be used in the desired HEV powertrain should be having a rated power of 22 KW.

The worst case of operation for the generator is when it works continuously to charge the batteries for a long time. This happens when the drive motor runs the vehicle on a highway at maximum speed. The delivered power from the batteries to the drive motor is recovered by the generator in the batteries. The power required to drive the vehicle by an electric motor is calculated for the desired series HEV in a high way. This calculation is performed to ensure that the calculated size for the generator is large enough to overcome the worst case power requirements.

The drive power for the situation that the desired vehicle runs in a high way with the maximum speed calculated in Subsection 2.5.2.2 which is 11.523 KW. If the efficiency of the generator, battery recharging and rectifier is assumed 90 % each, then the generator rated power is calculated as:

$$P_G = \frac{11.523}{0.9 \times 0.9 \times 0.9} = 15.81 KW$$

The calculated power is within the calculated size of 22 KW for the generator, and so this ensures that the chosen size for the generator is large enough to charge the batteries in a worst case of operation of the vehicle.

The output voltage of the generator should be converted to DC to charge a battery pack. A three phase controlled rectifier as shown in Figure 2.6 is used to rectify the AC voltage of the generator [1].

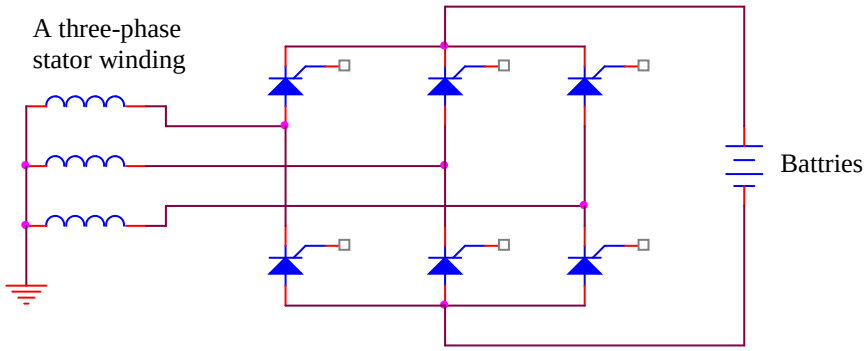

Figure 2.6 Three-phase single level controlled rectifier

For 42V DC and 14V DC systems the minimum generated line to line voltage is 27V AC and 9V AC in rms respectively if a three phase induction machine with synchronised rectifier controller is used [34]. Therefore, for the 420V DC system, it is estimated that a minimum line to line voltage of 270V AC in rms should be used for the proposed HEV's generator. The Equation (2.10) is used to calculate a range of output voltage of the rectifier of Figure 2.6 where α_f is the firing angle of the switches [46]. The specified range of α ensures a continuous DC voltage in the output of the rectifier.

$$V_{DCavg} = \frac{3}{\pi}\sqrt{2}V_{LL}\cos\alpha_f \qquad 0 < \alpha_f < \frac{\pi}{3} \tag{2.10}$$

If a standard value of 415V AC is selected for the line to line voltage (V_{LL}) of the generator, the average value of DC voltage will be between the following values.

$$280.22V < V_{DCavg} < 560.44V \qquad 0 < \alpha_f < \frac{\pi}{3}$$

The desired DC value of approximately 420V is between the calculated values, and so the selected value of 415V AC can be selected as line to line voltage of the generator.

2.5.5 Internal Combustion Engine Sizing

The same size for the internal combustion engine as generator should be considered. It is assumed that the novel engine has a high efficiency about 45 %. Therefore the actual size of engine is computed as 48.88 KW.

2.6 Summary

This chapter started by looking at the prospects of HEVs, followed by an investigation into the advantages of hybrid technology. The characteristics of different configurations of the HEVs drivetrain were studied. It is expected that the future HEVs will meet the considerable reduction of NOx and particulate matter aim. It was found that the cage rotor induction machine is the best candidate for the HEV applications because of its high ruggedness and reliability and low maintenance and cost characteristics. The sizes of powertrain components of a HEV with series configuration were estimated. The calculated values are used in designing process of the proposed induction machine as well as the HEV analysis in the later chapters. The next chapter explains the induction machine principles and characteristics.

Chapter 3 Induction Machines

Induction machine is one of the most suitable AC machines that could be used in the HEVs. Induction machines are widely used and most frequently in industries as they have simple and rugged constructions, low cost, high reliability and efficiency [47].

Induction machines have two main drawbacks of high starting current and low power factor at light loads. [48].

The speed of an induction machine is constant and therefore induction machines are mainly utilised in the applications that need constant speed operation. In the recent years Induction machines have been used in various variable speed applications and this has been possible with advanced power electronic controllers.

In this chapter, a literature review of induction machines including their operation principles and torque-speed characteristics for motoring and generation modes are analysed.

3.1 Induction Machine Construction

The notable feature of induction machines construction is that they do not require field current supply compared to synchronous machines. Induction machines magnetic field is generated by induced voltage in the rotor rather than being produced by an external field supply. This is the reason they are called induction machines which is referred to the induction phenomenon happens in the rotor of the machine [49]. Figure 3.1 shows a

cutaway diagram of an induction machine. Two main components of induction machines are stators and rotors.

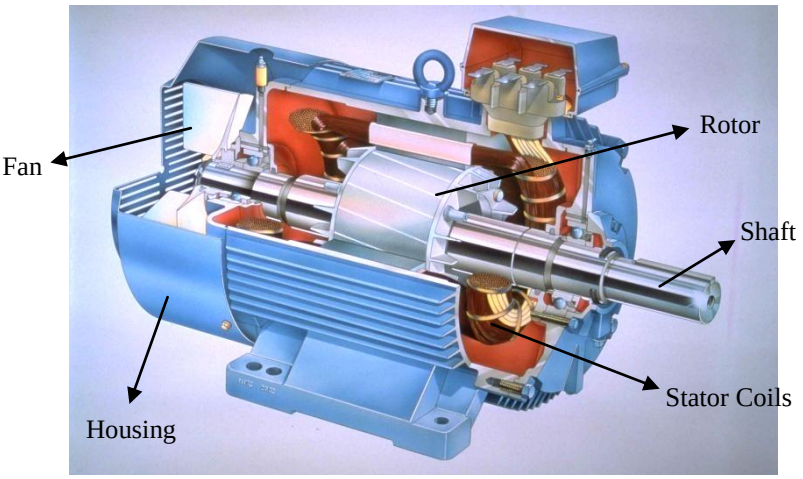

Figure 3.1 An industrial induction machine [50]

A stator is the stationary part of the AC machine, while a rotor is the revolving part of it. The stator of an induction machine has the same construction as the stator of a synchronous machine. The stator consists of a hollow space supported by a steel frame and slotted laminations which make up a cylindrical core. As Figure 3.2 shows the stator slots are punched out of the inner circumference of the laminations to provide the space for the stator windings [47 , 49]. The laminations are riveted or welded together after assembling into a core pack and pressing them [48].

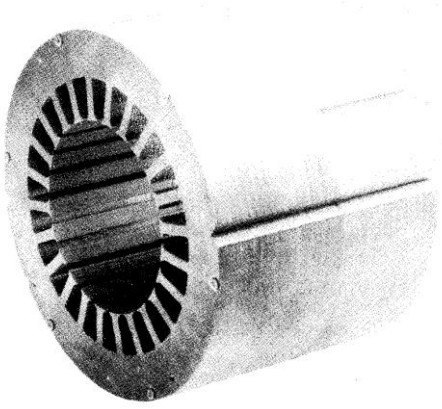

Figure 3.2 A riveted stator of an induction machine [48]

Induction machines of having an outer diameter of stator less than one metre have one piece core laminations. For small machines, i.e. power rating up to 37 KW, partially closed slots are utilised in the stator core assembly. As Figure 3.3 shows, the teeth have parallel sides while slots are tapered [48].

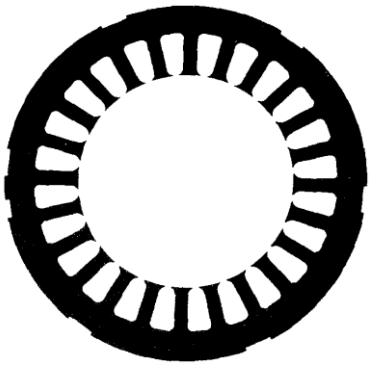

Figure 3.3 Small induction machines stator slots [48]

The rotors in induction machines are constructed differently from synchronous machines. Induction machines rotors are in two types of squirrel cage and wound rotors.

As Figure 3.4 shows, the cage rotor of an induction machine is constructed by a series of conductor bars shorted by two end-rings at each end of conductors. This type of rotor is referred to as a squirrel cage because these bars are similar to the exercise wheels that are run by squirrels [49].

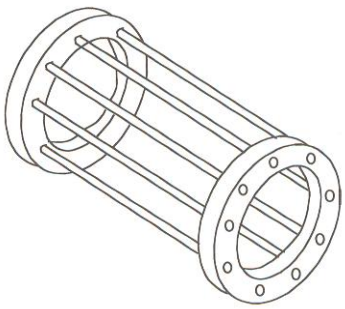

Figure 3.4 A squirrel cage rotor of an Induction Motor [26]

In the case of squirrel cage rotors, end-rings, the rotor conductors and fans are cast simultaneously by stacking the laminations in a core mould into which molten aluminium is forced. Some induction machines use rectangular or round copper bars cut as their rotor slots have the same shape. The bars are driven into slots and their both ends are welded, brazed or soldered to the end-rings. If this process of manufacturing is replaced by die-casting it will cost much less but it will require a much higher temperature for copper cage casting [48].

Wound rotor induction machines have three phase Y-connected windings on the rotor. This set of windings is mirror images of the stator windings and the ends of them are tied to slip rings on the rotor shaft. Some carbon brushes ridded on the slip rings short the end of the wires set [49]. Figure 3.5 shows a rotor of a wound rotor induction machine.

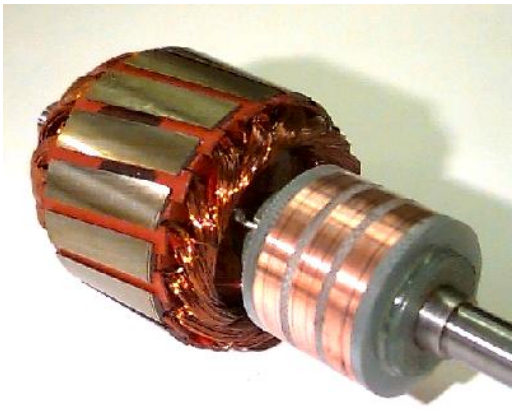

Figure 3.5 A wound rotor of a three-phase induction machine [51]

Slip ring brushes make a possibility of inserting external resistances into the rotor which can be used to modify the torque-speed and starting characteristics of the machine [48 , 49].

The application of the squirrel cage induction motors in industries has been spread as they have low cost and strong construction. The wound rotor types of induction machines require much more maintenance that cage rotor ones due to their brushes and slip rings [49]. Therefore in this project only the squirrel cage induction machine has been investigated as they are more desirable in HEV applications too.

3.2 Principles of Induction Machine Operation

Induction machines are motors that convert the electrical energy to the mechanical energy and generators that convert the mechanical energy to the electrical energy. The basic principle for all type of AC machines is based on the rotating magnetic field concept. Therefore the rotating magnetic field principle is reviewed in this section to find out how an induction machine operates.

3.2.1 The Rotating Magnetic Field

If a three-phase current, each of equal magnitudes and phase difference by 120 degree are flowed in a three-phase set winding on the stator of an AC machine, then a rotating magnetic field is produced. The magnetic field rotation is in an anticlockwise direction with a constant magnitude [49].

Figure 3.6 illustrates the simple case of a three-phase stator windings, a-a`, b-b`, and c-c` which are 120° apart. It is supposed that the three-phase current, each of equal magnitude and phase difference by 120° flows in the coils. Cross signs show that the direction of the current flows into the page, while dot signs show the direction of the current is out of the page in each coil.

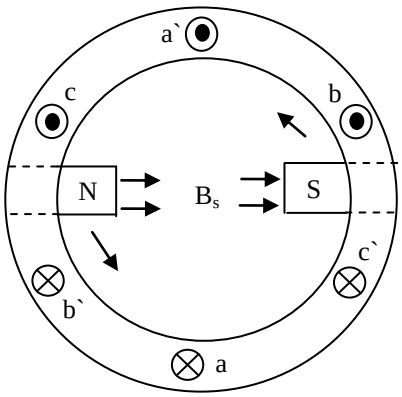

Figure 3.6 The stator rotating magnetic field vectors

This arrangement of stator coils produces a two-pole rotating magnetic field which is represented as north (N) and south (S) poles. B_s represents the stator magnetic flux density which rotates in the anticlockwise direction as shown in Figure 3.6. Two poles rotate one mechanical turn for each cycle of the applied electric current. Therefore the magnetic field rotation speed in revolutions per minute is equal to the applied electric current frequency in Hz.

To understand the relationship between the mechanical speed of the magnetic field and electrical frequency, the stator winding pattern (a-c`-b-a`-c-b`) is repeated twice within the stator. This is shown in Figure 3.7 by winding order of:

a-c`-b-a`-c-b`- a-c`-b-a`-c-b`

which is the previous winding pattern repeated twice.

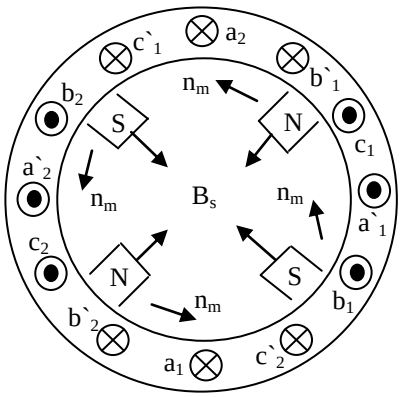

Figure 3.7 The stator four-pole rotating magnetic field

If the same current set as the two-pole stator current set is applied to the stator coils, then four magnetic poles are produced and rotate anticlockwise with a mechanical speed of n_m.

In this winding pattern, each pole rotates only halfway around the stator in each electrical cycle. As each electrical cycle is completed in 360 electrical degrees and the mechanical circling is 180 degrees, therefore the relationship between the electrical and mechanical frequencies can be presented by the following equation for four-pole stators.

$$f_e = 2f_m \tag{3.1}$$

where f_e is the electrical frequency of the current and f_m is the mechanical frequency of poles.

In general, the relationship between the mechanical frequency of the magnetic field and electrical frequency in AC machines is:

$$f_e = \frac{P}{2} f_m \tag{3.2}$$

where P represents the pole numbers.

Equation (3.2) can be replaced by the following equation if f_m is replaced by revolutions per minute n_m, noting that $f_m = n_m/60$.

$$f_e = \frac{P}{120} n_m \tag{3.3}$$

In induction machines, n_m is replaced by n_{sync} and it is derived by the following equation:

$$n_{sync} = \frac{120 f_e}{P} \tag{3.4}$$

where n_{sync}, f_e, and P represent the synchronous speed of magnetic field in revolutions per minute, electrical frequency in Hertz and magnetic pole numbers respectively [49].

3.2.2 Induced Torque in an Induction Motor

If a three phase-voltage, each of equal magnitude and phase difference by 120 degree is applied to the stator of an induction machine it will act as a motor. The produced stator rotating magnetic field passes over the rotor conductors and induces voltage in rotor bars. This is because of the relative speed of the bars compared to the rotating magnetic field (Faraday's Law). The induced voltage in each rotor conductor bar can be expressed by the following equation,

$$E_r = (v \times B_s) \bullet l_g \tag{3.5}$$

where v is the velocity of a bar relative to the magnetic field. B_s and l_g represent the stator magnetic flux density vector and airgap length respectively. Vector l points along the direction of the bar towards the end making the angle with respect to the vector $v \times B_s$. The positive end of the induced voltage would be in the direction of the vector $v \times B_s$.

The speed of induction motors rotor never reaches the synchronous speed. The difference between rotor speed of an induction machine represented by n_r and magnetic field synchronous speed represented by n_{sync} is defined as rotor slip represented by term of S in the following equation.

$$S = \frac{n_{sync} - n_r}{n_{sync}} \tag{3.6}$$

Generally, the magnitude and frequency of the induced voltage in the rotor depends on the relative motion between n_r and n_{sync}. If there is no relative motion between magnetic field synchronous speed and rotor speed, i.e. S is equal to zero; there is no induced voltage in the rotor.

The maximum relative motion happens when rotor does not turn, called locked-rotor state. In this condition, S is equal to unity and the maximum voltage magnitude and frequency is induced in the rotor.

According to the discussion above, the magnitude and frequency of the induced voltage in the rotor depends on the slip (S) and are given by the following equations:

$$E_r = SE_{lr} \tag{3.7}$$

$$f_r = Sf_e \tag{3.8}$$

where E_{lr} represents the induced voltage at locked-rotor condition and f_e is electrical frequency of the applied voltage.

Figure 3.8 shows the stator and rotor magnetic field vectors which rotate in an anticlockwise direction. The positive end of the induced voltage in a bar would be in the direction of the resulting vector of $v \times B$ according to Equation (3.5).

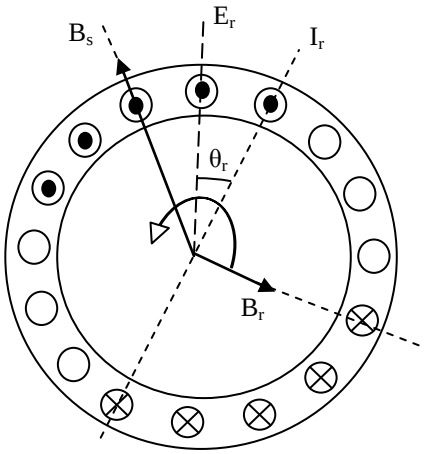

Figure 3.8 The stator and rotor rotating magnetic field vectors

As Figure 3.8 shows by cross signs, the induced voltage in the lower bars is into the page, because the relative motion of the lower bars compared to the stator magnetic field is to the left. The upper bars relative motion to the stator magnetic field is to the right, so the induced voltage is out of the page. This is shown by dot signs for the upper

bars in Figure 3.8. Therefore the direction of the current flow for the upper bars is out of the page and for the lower bars is in the opposite direction.

The induced voltages in the rotor conductors produce the rotor bar currents. Since the rotor bars have an inductive assembly, a rotor bar current lags its induced voltage. The rotor bars currents produce the rotor magnetic field which is shown by B_r in Figure 3.8.

Torque is generated in an induction motor because of the interaction of stator magnetic field with rotor magnetic field. This principal is called Lorentz force principle which is the basic principle of AC and DC machines operation. Induced torque is a vector given by:

$$T_{ind} = kB_r \times B_s \tag{3.9}$$

where B_r and B_s are the rotor and stator magnetic field density vectors and k depends on the construction of the machine and magnetic permeability [26 , 49].

The induced torque is anticlockwise and so rotor turns in the anticlockwise direction. The speed of the rotor depends on the load but never reaches to the synchronous speed according to Faraday's Law shown in Equation (3.5).

3.2.3 Induction Generator Operation Principle

If an external torque is applied to an induction machine shaft to turn the rotor with a speed higher than the synchronous speed, machine act as a generator. The output torque and slip of the machine are negative in the generating mode.

Since induction machines do not have a magnetic field supply, an external reactive source should be connected to the stator to maintain its magnetic field at all times. This external power system also controls the generated voltage as there is no field current in induction machine to control the output terminals voltage.

It is also possible to run a rotor of an induction machine to act as a generator without having an external source. The required reactive power can be provided by three capacitors connected to the machine stator as shown in the following figure.

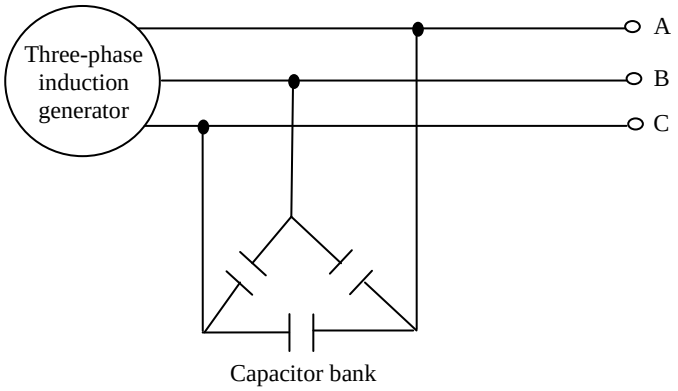

Figure 3.9 Self excited induction generator with capacitor bank [49]

At the start of running an induction generator, the residual magnetism in the rotor generates a small voltage. That produced voltage makes capacitor currents flow, which in turn increases the voltage. Higher voltage increases the capacitors currents and this process is done continuously to build up the full voltage. If there is no residual magnetism at the start point, the rotor can be magnetized by running it as an electric motor for a moment to provide the residual magnetism [49].

3.3 Equivalent Circuit of an Induction Machine

The induction machines operation is based on the induction of voltage in the rotor conductors from the stator coils. The voltage induction action is the same phenomenon

that happens in the transformers and so the equivalent circuit of an induction machines is very similar to a transformer equivalent circuit with a shorted output.

The transformer model of an induction motor is shown in Figure 3.10. R_s and R_r represent the stator and rotor resistances, while X_{sl} and X_{rl} represent the stator and rotor leakage reactances respectively. X_m is the magnetising reactance and R_c represents the core losses.

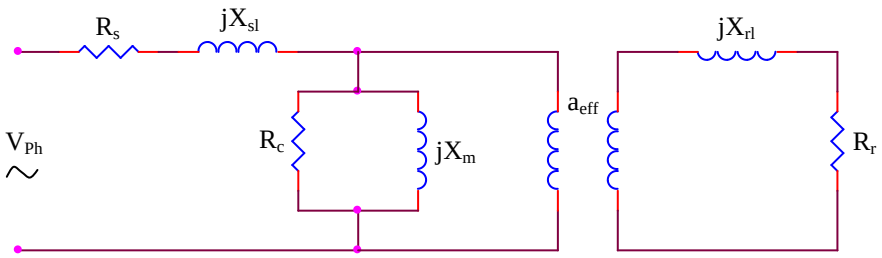

Figure 3.10 The transformer per-phase model of an induction machine [49]

In fact, R_s and R_r represent the stator and rotor copper losses respectively which are the resistive heating losses of the windings. The stator and rotor leakage fluxes represented by X_{sl} and X_{rl} are the fluxes in the stator and rotor which escape the cores and do not participate in magnetic interaction between stator and rotor cores.

Core losses of the machine include eddy current and hysteresis losses. Eddy current losses are resistive heating losses in the stator and rotor cores caused by induced voltage in the cores which results in circulating current in the cores. Hysteresis losses are related to the energy needed to rearrange the core magnetic domains in each half-cycle [49].

The rotor core losses of an induction machine are very smaller than stator core losses and so all the core losses are shown at the stator side. The reason for rotor core losses to be tiny is that an induction machine normally operates at the speed close to synchronous

speed which means that the relative motion of magnetic fields on the rotor surface is very slow [49].

The transformer in Figure 3.10 is an ideal transformer with an effective turns ratio of a_{eff}. The value of a_{eff} for wound rotor induction machines is the ratio of stator conductors per phase to the rotor conductors per phase modified by winding factor differences [49]. As there are no distinct rotor windings in the cage induction machines, therefore determining the a_{eff} in this case is difficult. However it can be calculated rather precisely by utilising the finite element method [52].

Rotor circuit elements in the secondary side of the transformer can be referred to the primary side by means of the transformer turns ratio. The value of the referred voltage is a_{eff} times the value of the rotor voltage, while the referred current value is the value of the rotor current divided by a_{eff}. The following equations show the relationship between the referred and actual values of the rotor voltage and current phasors.

$$E`_r = a_{eff} E_r \tag{3.10}$$

$$I`_r = \frac{I_r}{a_{eff}} \tag{3.11}$$

Consequently, the referred rotor impedance is a^2_{eff} times the rotor impedance as shown in the following equation.

$$Z`_r = a^2_{eff} Z_r \tag{3.12}$$

The difference between a transformer and induction machine equivalent circuits is that the frequency of the induced voltage in the rotor of an induction machine is a variable of slip. The rotor frequency is shown by Equation (3.8) and it can be stated that the varying rotor frequency affects the rotor impedances and voltage.

To obtain a final equivalent circuit of an induction machine, first, the rotor impedance is found by the following equation.

$$Z_r = \frac{E_r}{I_r} \tag{3.13}$$

If Equations (3.7) and (3.8) are utilised, the rotor current can be presented by the following equation:

$$I_r = \frac{SE_{lr}}{R_r + jSX_{lr}} \tag{3.14}$$

where X_{lr} is the locked-rotor rotor reactance.

Equation (3.14) can be written as the following equation.

$$I_r = \frac{E_{lr}}{\frac{R_r}{S} + jX_{lr}} \tag{3.15}$$

From this point of view, the rotor impedance is:

$$Z_r = \frac{R_r}{S} + jX_{lr} \tag{3.16}$$

Equations (3.12) and (3.16) are used to find the referred resistance and reactance of the rotor as given in the following equation.

$$R`_r = a^2_{eff} R_r \tag{3.17}$$

$$X`_{rl} = a^2_{eff} X_{lr} \tag{3.18}$$

where $R`_r$ and $X`_{rl}$ represent the values of the rotor resistance and rotor reactance referred to the stator.

Figure 3.11 shows the final per-phase equivalent circuit of an induction machine. The rotor circuit elements have been referred to the stator side. This circuit is used in Chapter 6 to simulate the performance of the machine after being designed in Chapter 5.

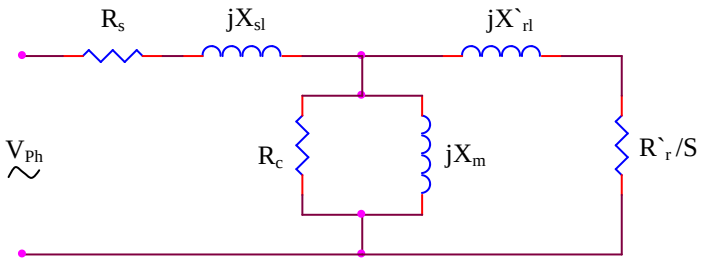

Figure 3.11 An induction machine per-phase equivalent circuit referred to the Stator

3.4 Torque-speed Characteristics of an Induction Machine

In this section, the relationship between the torque and rotor speed of an induction machine is analysed. This studies results in finding the torque-speed curve which shows how the torque of an induction machine changes as the load varies.

First, the induced torque of an induction motor is determined based on the following equation.

$$T_{ind} = \frac{P_{conv}}{\omega_r} \tag{3.19}$$

In Equation (3.19), P_{conv} represents the converted power and ω_r represents the mechanical speed of the rotor of an induction machine in radian per second. To obtain the converted power of an induction motor, power losses should be subtracted from the electrical power available in input of the motor. The remaining power is converted to mechanical power in rotor of the induction motor.

As an induction machine equivalent circuit in Figure 3.11 shows, the first losses in the machine is the stator windings copper loss represented by the stator resistance R_s. Then, some power is dissipated in cores as hysteresis and eddy current losses as explained in Section 3.3. The remaining power which is transferred to the rotor across the airgap called the airgap power. After this transformation is completed, some of the transferred power is lost in rotor as the rotor copper loss and the rest is converted to the mechanical energy.

According to the explanation above, the converted power available in the output of an induction machine can be shown by the following equation where P_{ag} and P_{rcl} represent the airgap power and rotor copper losses respectively.

$$P_{conv} = P_{ag} - P_{rcl} \tag{3.20}$$

Since the only element in the rotor circuit which can consume the airgap power is the resistor $R`_r/S$, the airgap power can be found using the following equation where $|I`_r|$ represents the magnitude of the rotor current refereed to stator.

$$P_{ag} = 3|I`_r|^2 \frac{R`_r}{S} \tag{3.21}$$

The rotor copper loss is given by the following equation.

$$P_{rcl} = 3|I`_r|^2 R`_r \tag{3.22}$$

By substituting Equations (3.21) and (3.22) into Equation (3.20), the converted power is derived finally as:

$$P_{conv} = 3|I`_r|^2 R`_r\left(\frac{1-S}{S}\right) \tag{3.23}$$

From Equations (3.21) and (3.23), it is concluded that:

$$P_{conv} = (1\text{-}S)\, P_{ag} \tag{3.24}$$

Therefore, Equation (3.19) can be modified by utilizing Equation (3.24) as shown in the following equation.

$$T_{ind} = \frac{(1-S)P_{ag}}{\omega_r} \tag{3.25}$$

Rotor speed in revolutions per minute is derived from Equation (3.6) as:

$$n_r = (1\text{-}S)\, n_{sync} \tag{3.26}$$

In Equation (3.27), the rotor speed and magnetic field synchronous speed in the previous equation are expressed in term of ω_r and ω_{sync} where ω_r and ω_{sync} are the rotor and synchronous angular velocities respectively, both in radian per second.

$$\omega_r = (1\text{-}S)\, \omega_{sync} \tag{3.27}$$

Substituting Equation (3.27) into Equation (3.25) yields:

$$T_{ind} = \frac{P_{ag}}{\omega_{sync}} \tag{3.28}$$

Airgap power P_{ag} can be known by determining the referred rotor current in Equation (3.21). To determine the referred rotor current, Thevenin equivalent circuit of the stator side of the equivalent circuit shown in Figure 3.11 is found first. According to Thevenin's theorem, any linear circuit that can be separated by two terminals from the whole system, can be replaced by the Thevenin voltage source in series with the Thevenin impedance [49].

The Thevenin voltage of the stator side of the induction machine equivalent circuit is calculated by opening the circuit terminals at the $X`_{rl}$ and finding the voltage present at open terminals. Figure 3.12 shows the Thevenin voltage terminals and is used to find the Thevenin voltage at open terminals.

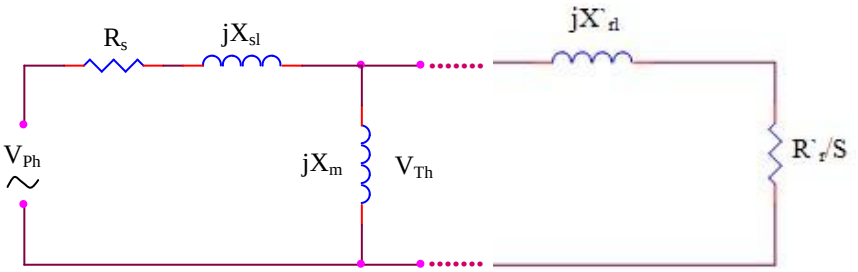

Figure 3.12 The Thevenin equivalent circuit of the stator side of an induction machine

Equation (3.29) expresses the open-circuit voltage present at open terminals.

$$V_{Th} = \frac{jX_m}{R_s + jX_{sl} + jX_m} V_{ph} \tag{3.29}$$

To calculate the Thevenin impedance of the stator side of the induction machine equivalent circuit, the phase voltage V_{ph} is shorted and then the Thevenin impedance is seen by looking into terminals. Therefore the Thevenin impedance is reactance X_m parallel with stator impedance as shown in the following equation.

$$Z_{Th} = R_{Th} + jX_{Th} = \frac{jX_m(R_s + jX_{sl})}{R_s + j(X_{sl} + X_m)} \tag{3.30}$$

The rotor current referred to stator can be calculated from the resulting equivalent circuit shown in Figure 3.13.

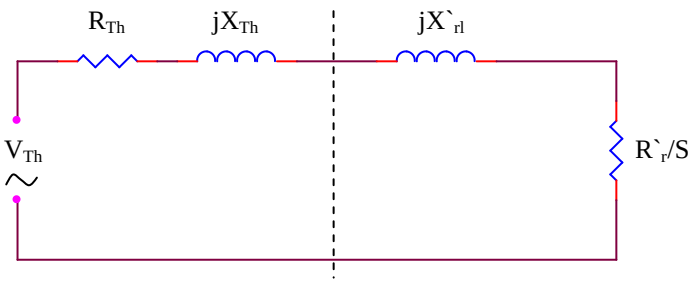

Figure 3.13 The Thevenin equivalent circuit of an induction machine

In the circuit shown in Figure 3.13, the magnitude of the rotor current referred to stator is given by:

$$\left|I`_r\right| = \frac{V_{Th}}{\sqrt{(R_{Th} + R`_r/S)^2 + (X_{Th} + X`_{rl})^2}} \tag{3.31}$$

Then, the airgap power is found by substituting Equation (3.31) into Equation (3.21), resulting in:

$$P_{ag} = \frac{3V^2_{Th} R`_r/S}{(R_{Th} + R`_r/S)^2 + (X_{Th} + X`_{rl})^2} \tag{3.32}$$

Therefore, the induced torque in the rotor is calculated by utilizing Equation (3.28) and it is given by the following equation.

$$T_{ind} = \frac{3V^2_{Th} R`_r/S}{\omega_{sync}(R_{Th} + R`_r/S)^2 + (X_{Th} + X`_{rl})^2} \tag{3.33}$$

The graphical relationship between the torque and rotor speed of an induction machine is shown in Figure 3.14. The diagram is divided into two regions, where the first region is called motoring region and the second one is named generating region.

Equation (3.6) shows that in the motoring region, slip (S) is between zero and one, while in the generating region slip is negative.

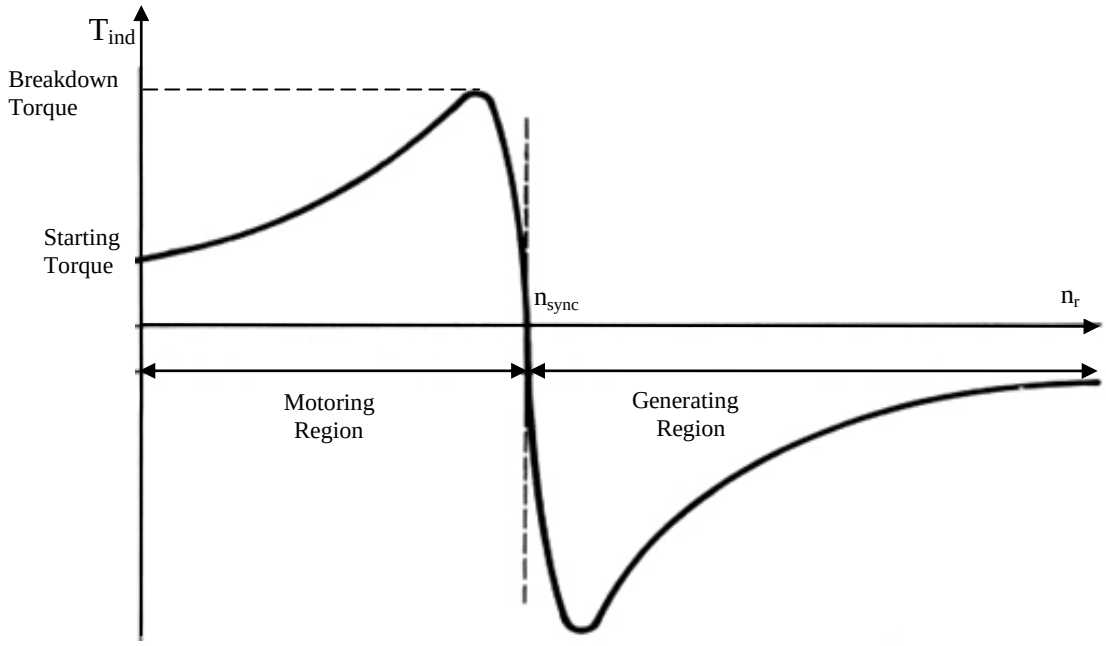

Figure 3.14 The torque-speed diagram of an induction machine [49]

Equation (3.33) confirms that the induced torque is zero at synchronous speed which slip S=0 as discussed in Subsection 3.2.2. Induction machine always works in a speed slightly different from the synchronous speed. In this case, where the slip is small, the relationship between load and machine speed is linear.

The Breakdown torque shown in Figure 3.14 is the maximum possible torque which is 2 to 3 times the rated torque. At this point, for an incremental increase in load, the rotor current increscent is balanced by the power factor decrement [49].

3.5 Summary

In this chapter, the induction machine construction was explained first. It was followed by an investigation into the three-phase AC machines operation principle and reviewing the rotating magnetic field principle. Then, the induced torque in induction motors and induced voltage in induction generators were studied. The electrical equivalent circuit per-phase of an induction machine was executed based on the transformer model of the

machine. Finally, the torque-speed diagram of the induction machine was derived from its equivalent circuit for motoring and generating modes of the machine operation.

Chapter 4 Induction Machine Design Principles

Induction machines are used in different applications in industry for various power and speed ranges. Induction machines can be divided into constant and variable speed machines, for which the design specifications are different. However, design principles are similar for both the variable and constant speed machines. Also, at some point in time a constant speed machine may be supplied from a variable voltage and frequency power supply in order to provide variable speed [53].

In this chapter, the design principles of induction machines for constant voltage and frequency with an output power of less than 100 KW are presented. The target induction machine is designed in the next chapter.

4.1 Induction Machine Design Factors

There are some main factors that should be considered in the induction machine design process. The design factors which are explained in the following subsections influence the design procedure.

4.1.1 Materials

The main materials utilised in fabricating of induction machines are magnetic-steel for laminations, aluminium and copper for windings.

Materials characteristics play an important role in induction motor design. Magnetic materials specify flux density and losses. Thermal conductivity of insulations and conductors current density are also key factors in this concept.

Advanced magnetic and insulation materials improves the performance of the machine and eliminates the manufacturing cost. Induction machines geometry is also affected by new improved materials.

4.1.2 Standards

Induction machines performance specifications such as efficiency, power factor and breakdown torque are identified in the national and international standards. The electric machine standards presented by IEC, IEEE and NEMA globalise using induction machines for various applications and also provide widely accepted solutions [53]. However the induction machine standards limit the alternatives for designers.

4.1.3 Specific Factors

It is possible to have some special factors for induction machines in special applications. For example, in transportation applications, high efficiency and ease of maintenance become important whereas water pumps need to be low noise and reliable.

4.1.4 Cost

Cost is the predominant factor for many of induction machines manufacturers. The manufacturing cost includes expenses of materials, fabrication and maintenance. Cost issue also become important when a decision is made about replacing an old machine with a new one. New machine has higher efficiency but its cost is higher than the repairing cost of the old one [53].

4.2 Induction Machine Design Features

In this section, the main issues involved in induction machine design, highlighted in [53 , 54] are presented by dividing them into five areas of Electrical, Magnetic, Dielectric, Thermal and Mechanical.

4.2.1 Electrical Design

Induction machine power supply specifications including magnitude of voltage, frequency and number of phases are specified. These data, targeted efficiency and power factor values are utilised to determine the phase connection type, number of slots, pole numbers and winding factors. Stator and rotor current densities are imposed.

4.2.2 Magnetic Design

Rotor diameter, type of cooling, power and speed of the machine are calculated from the output coefficients. Then, with a specific airgap flux density and current loading, the length of stack can be calculated.

Based on the fixed flux densities in different parts of the magnetic circuit with known current density and slot mmfs, the values of core height, outer diameter of stator and the slot sizes are calculated. In this point, the initial current density can be secured by modifying the stack length [53].

4.2.3 Insulation Design

According the voltage insulation class and application of the induction machine, the insulations of core and conductors, end connection and terminal leads are specified.

4.2.4 Thermal Design

Heat is caused by losses in induction machines like the other type of electric machines. Temperature must be calculated for the induction machine components including core, windings and frame to make sure that the components temperature is kept in safe boundaries. Selecting a suitable cooling type is very important depends on the level of power and the environment in which induction machine operates. In some high speed application of induction machines stator water cooling is used instead of air cooling systems.

4.2.5 Mechanical Design

Issues like noise, vibration, maximum allowable speed, rotor bearing design, mechanical stress of shaft and inertia represent the mechanical design of the induction machines.

4.3 Induction Machine Design Classes

Various torque-speed curves can be achieved by changing the characteristics of the rotor of an induction machine. For example, an induction machine that has a high resistance rotor has a higher starting torque and rated slip. NEMA in the US and IEC in Europe have defined and standardise the design classes for induction machines to assist the industry in choosing appropriate machine for different applications.

The specifications of different design classes are explained in the following subsections according to [49]. Fig. 4.1 shows rotor bar cross sections for various design classes of induction machine.

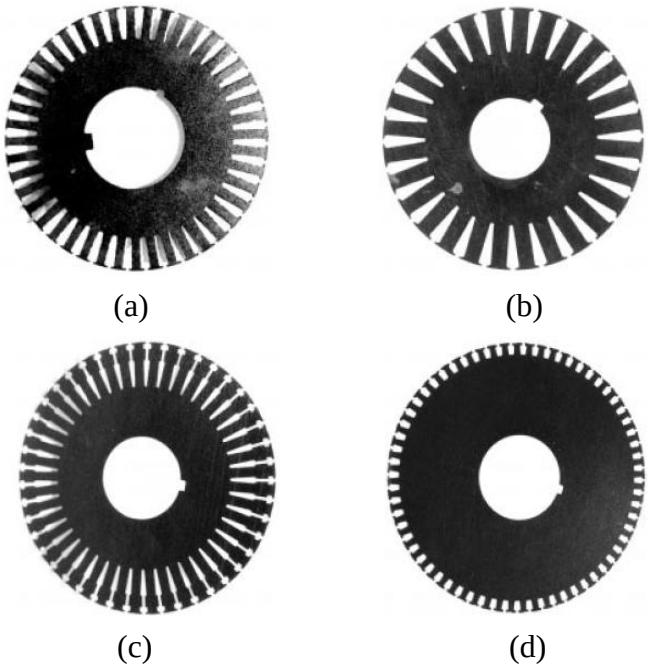

Figure 4.1 (a) Design class A- large bars close the surface; (b) Class B- deep rotor bars; (c) Class C- double cage rotor; (d) Class D- small bars close the surface [49].

4.3.1 Design Class A

Class A designed induction machines have a normal starting toque and current with low slip. The breakdown torque of a class A machine is two to three times bigger than its rated torque and it occurs at a slip lower than 0.2.The main problem of this type of design is high inrush current of the machine on starting. In recent years, the class A designed machines have been replaced by class B machines. Some applications of these machines are driving blowers, fans, generator sets and machine tools.

4.3.2 Design Class B

Class B induction machines have a low slip and starting current with normal starting torque. Rotor reactance is increased in this class and so the breakdown torque is less than that of the class A machine. Class B designed have the same application as class A induction machines. Because of lower starting current of Class B designs, they replaced class A induction machines.

4.3.3 Design Class C

Class C designed induction machines have a low rated slip and starting current with high starting torque. These types of machines have double cage rotors, so their cost becomes higher than other classes. This type of induction machines are applied in pumps conveys and compressors where high starting torque are required.

4.3.4 Design Class D

Starting torque in this type of induction machines is very high. Their starting current is low but they have a high rated slip. In this type of machines, rotor bars are smaller with high resistance materials which shift the maximum torque to a very low speed. Because of the high rotor resistance, the rated slip is high for class D designed machines and its value can be up to 0.17. A typical application of these machines is in punch presses where a very high inertia load is required to be accelerated.

Fig.4.2 shows torque-speed characteristics in motoring mode for different design classes of induction machines.

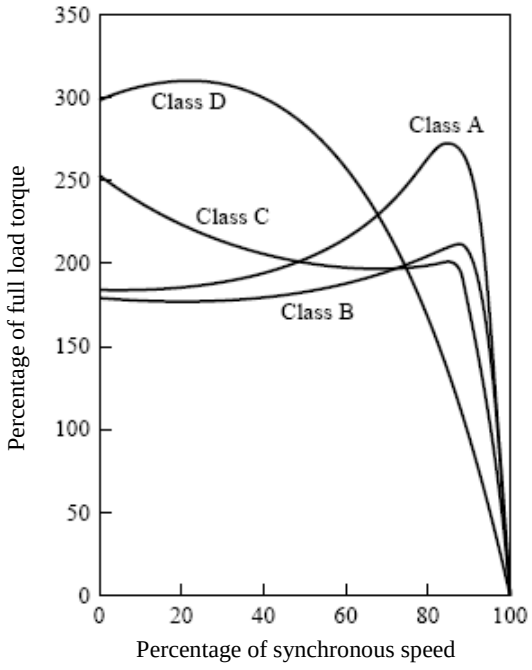

Figure 4.2 Torque-speed curves for different motor design classes [49]

4.4 Induction Machine Design Algorithm

The process of induction machine design starts with design specifications and assigned quantities of current and flux densities. This is followed by calculation of the stator internal diameter, core length, stator slots and stator external diameter after finding the stator and rotor currents. The design process is continued by calculating the rotor slots and cage sizing. The values like stator external diameter and wire gauges should be adjusted to standardised values. The actual quantities of the current and flux densities are then verified [48 , 53].

As shown in Figure 4.3, if the stator and rotor teeth magnetic saturation coefficients are not equal to allocated values, the design is restarted by adjusting the tooth flux densities until enough convergence is gained in teeth saturation coefficient.

In the next step, the magnetisation current and equivalent circuit electric parameters are calculated and then losses, efficiency and rated slip are determined. The design algorithm is then continued by computing the machine performance parameters such as breakdown torque, power factor and temperature rise.

Finally, the performance of the designed induction machine is checked and if it is not satisfactory, the design procedure is restarted with the new initial values of current or flux densities.

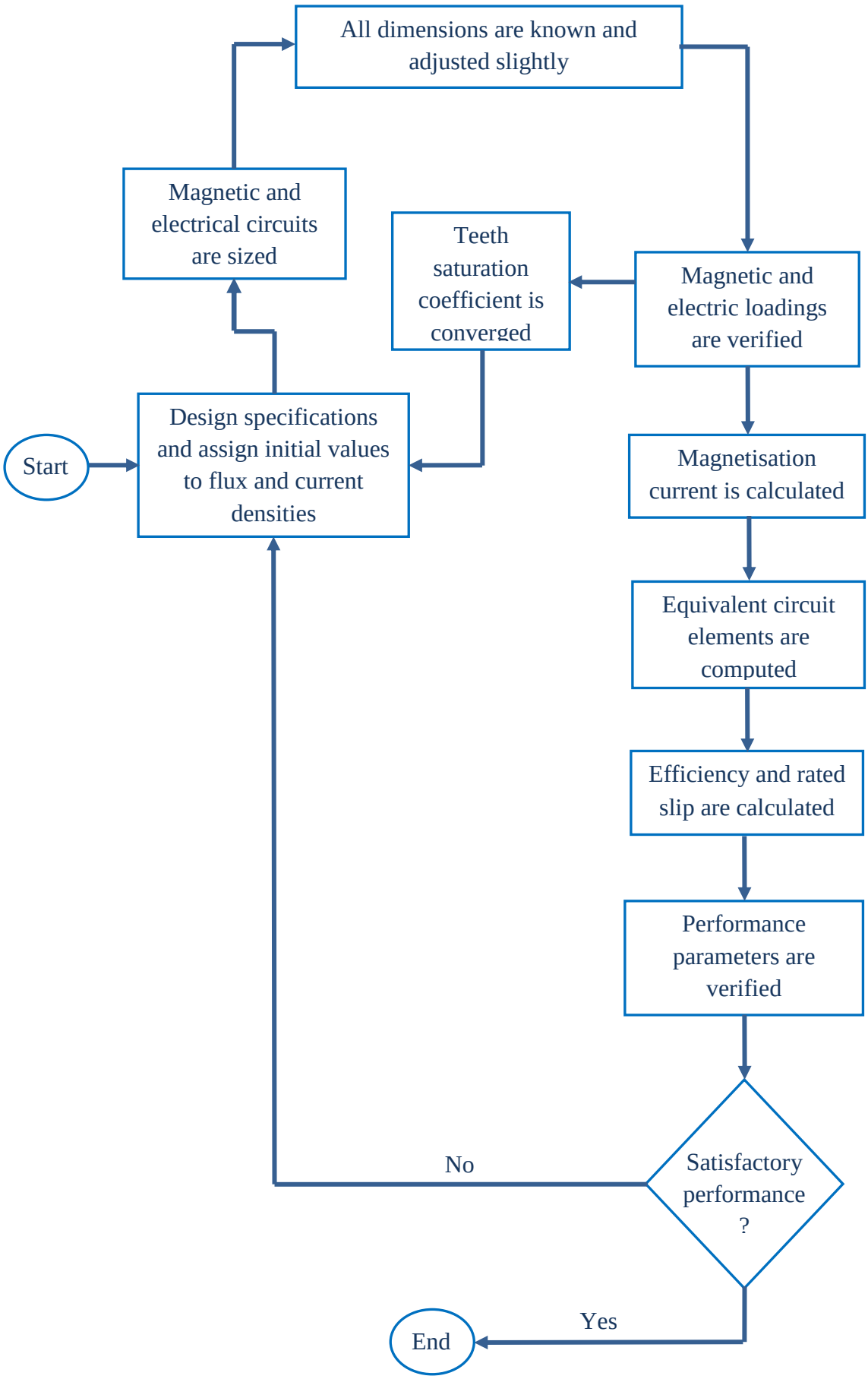

Figure 4.3 The induction machine design flowchart

4.5 Output Coefficient Design Concept

Basically, to design an induction machine, the machine is sized for given specifications including input power and load. The widespread accepted design concept of the output coefficient as an established theoretical approach to stator bore diameter is determined by $D_{is}^2.L$, where D_{is} is the stator inner diameter and L represents the stack length of the machine.

The calculation of the relationship between $D_{is}^2.L$ and machine performance and power is started by computing the apparent power of the airgap as follows. E_g and I_n represent the airgap electromotive force (emf) per phase and rated current respectively.

$$S_{airgap} = 3E_g.I_n \tag{4.1}$$

To calculate the sizing equation $D_{is}^2.L$ for main dimensions of an induction machine under design, the airgap emf per phase E_g may be written as a function of airgap pole flux Φ,

$$E_g = 4f.K_f.W.K_w.\phi \tag{4.2}$$

where f represents the frequency and K_f is the form factor that depends on teeth saturation. W and K_w also represent the turns per phase and winding factor respectively [53].

The airgap pole flux Φ in the equation above can be expressed as follows according to [53 , 54]. α_i is the flux density shape factor that depends on the teeth magnetic saturation coefficient and B_g represents the airgap flux density.

$$\phi = \alpha_i . \tau . L . B_g \tag{4.3}$$

In the equation above τ is the pole pitch and it is found by the following equation where P represents the number of poles.

$$\tau = \frac{\pi . D_{is}}{P} \tag{4.4}$$

The rated current I_n in Equation (4.1) can be expressed as follows where A is the specific stator current load in A/m [53].

$$I_n = \frac{A . \pi . D_{is}}{6W} \tag{4.5}$$

At last, airgap apparent power presented by Equation (4.1) can be calculated by using Equations (4.1) to (4.5). Equation (3.4) in the previous chapter is also used to replace the $\frac{f}{P}$ by $\frac{n_{sync}}{120}$ and so the airgap apparent power is calculated as follows.

$$S_{airgap} = K_f . \alpha_i . K_w . \pi^2 . D_{is}^{\ 2} . L . \frac{n_{sync}}{60} . A . B_g \tag{4.6}$$

The term of $K_f.\alpha_i.K_w.\pi^2.A.B_g$ in the equation above is known as the machine volume utilisation factor or Esson's constant and it is shown by C_0 [48 , 53]. Therefore, the output coefficient D_{is}^2L can be shown as follows.

$$D_{is}^2 L = \frac{1}{C_0}\frac{60}{n_{sync}} S_{airgap} \tag{4.7}$$

Typical values of C_0 which is dependent on the airgap apparent power and number of pole pairs can be found by prepared graphs for low power induction machine design purposes.

In standard design of an induction machine, a value is assigned to the stack length to pole pitch ratio and it is shown by term λ [48 , 53]. λ can be written as follows by using Equation (4.4).

$$\lambda = \frac{L}{\tau} = \frac{LP}{\pi D_{is}} \tag{4.8}$$

Now, the stator inner diameter can be derived from Equation (4.7) with Equation (4.8) and replacing $\frac{60}{n_{sync}}$ by $\frac{P}{2f}$ as follows.

$$D_{is} = \sqrt[3]{\frac{P}{\pi\lambda}\frac{1}{C_0}\frac{P}{2f} S_{airgap}} \tag{4.9}$$

The stator outer diameter is found by the standard table of the outer to inner stator diameter ratios data. This data determines the outer diameter of the stator of the machine for a variety of pole numbers.

In the further step, with specified stator current density, the flux densities of stator teeth and back core is calculated. This process is followed by approaching the stator and rotor slots sizing, stator wire gauge and machine performance parameters.

4.6 Summary

In this chapter, the main factors and features of induction machine design were explained. This was followed by describing IM different design classes and their specifications. Then, the design algorithm for induction machines was presented to show the procedure of the machine design. Finally, the output coefficient of induction machines was calculated as well as separation of the main dimensions equations. In the next chapter, the desired ORIM is designed based on the design principles explained in this chapter.

Chapter 5 Design of the Outer Rotor Induction Machine (ORIM)

In this chapter, an ORIM is designed based on the electric machine design principles explained in the previous chapter. The targeted machine is supposed to be integrated with the novel engine, presented in Chapter 1 and operate together as a power pack. This power unit produces electric power to charge the batteries of the hybrid electric vehicle.

In the design process of an electric machine, the main dimensions of stator and rotor including the shape of slots, winding parameters and slot numbers are determined. Equations used in this chapter are those widely accepted and used in standard design of induction machines presented in the related text books and academic papers [53, 55, 56, 57]. Due to the new construction method of the ORIM in terms of the rotor construction, some of the equations require modification and where applicable are stated in the chapter.

After the design process is completed, the elements of the induction machine equivalent circuit shown in Figure 3.11 are derived for simulation purposes and reported in the next chapter. Also, some of the performance parameters of the designed induction machine are obtained by using the given equations. The calculated machine operation characteristics can be compared with the simulation results in the next chapter.

The temperature rise in the machine is the other part of design process. This part needs to be validated to check that it fulfils the machine thermal requirements based on the insulation class defined for the electric machine.

5.1 Outer rotor Induction Machine Specifications

As it was explained in Chapters 2 and 3, the required induction machine for the power pack of the HEV is an outer rotor type with the following specifications.

- Rated power: P_n = 22 KW
- Rated efficiency: η_n = 90 %
- Rated power factor: $Cos\varphi_n$ = 0.9
- Rated line to line voltage: V_{LL} = 415V
- Synchronous speed: n_{sync} = 1500 rpm
- Outer rotor diameter: D_{or} = 0.3276 m
- Number of phases: n_{ph} = 3
- Stator phases connection mode: Star

In the selection of the number of poles, two facts have to be taken into account. First, it should be considered that a low number of poles increase the noise, weight and volume of the machine. Having a large pole numbers, for limited speed and frequency, also increases the losses. The optimum number of poles, P = 4 is recommended in [58].

The electric frequency of the machine can be determined by Equation (3.4). With a synchronous speed of 1500 rpm and 4 poles, the electric frequency of the machine is calculated as follows.

$$f = \frac{n_{sync} \times P}{120} = \frac{1500 \times 4}{120} = 50\,Hz$$

The thermal class for electric machines used in the hybrid electric applications is class H whose maximum allowable temperature is 180°C [54 , 59].

5.2 Stator Main Dimensions

In this section, the main dimensions of the proposed electric machine are designed based on the widely accepted $D_{is}^2 L$ output constant concept explained in Chapter 4.

The stator inner diameter D_{is} is calculated as follows where C_0 is Esson's constant. λ and S_{airgap} represent the stack ratio and airgap apparent power respectively. P is the number of poles.

$$D_{is} = \sqrt[3]{\frac{P}{\pi\lambda}\frac{P}{2f}\frac{S_{airgap}}{C_0}} \tag{5.1}$$

As Figure 5.1 shows, the value of paremeter C_0 depends on the airgap apparent power and pole numbers. Therefore the airgap apparent power is calculated first, as shown in Equation (5.2).

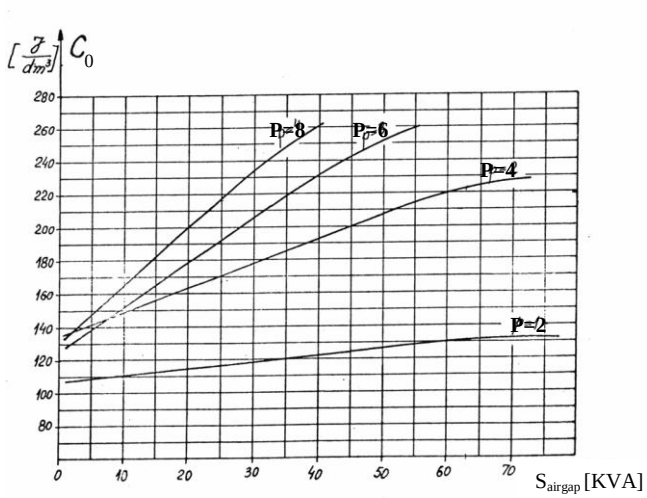

Figure 5.1 Esson's constant C_0 – S_{airgap} diagram [53]

$$S_{airgap} = \frac{K_E P_n}{\eta_n C os \varphi_n} \tag{5.2}$$

In the equation above, K_E is emf coefficient which represents the ratio of the airgap emf over rated current. The value of K_E is determined using the following equation.

$$K_E = 0.98 - 0.005\frac{P}{2} \tag{5.3}$$

So, for the ORIM under design, K_E is equal to:

$$K_E = 0.98 - 0.005 \times 2 = 0.97$$

The airgap apparent power S_{airgap} can be now determined as:

$$S_{airgap} = \frac{0.97 \times 22000}{0.9 \times 0.9} = 26345.68\,VA = 26.34568\,KVA$$

C_0 is extracted from Figure 5.1 for the calculated airgap apparent power, C_0 = 172000 J/m^3.

The standard assign values of stack ratio λ for different pole numbers are given in Table 5.1. The initial value of λ is chosen as 1.5.

Table 5.1 Stack aspect ratio [53]

P	2	4	6	8
λ	0.6 – 1.0	1.2 – 1.8	1.6 – 2.2	2 - 3

All the parameters are now known to calculate the inner diameter of the stator core using Equation (5.1).

$$D_{is} = \sqrt[3]{\frac{4}{\pi \times 1.5}\frac{4}{2 \times 50}\frac{26345.68}{172000}} = 0.1732\,\text{m}$$

The stack length is calculated as follows.

$$L = \frac{\lambda \pi D_{is}}{P} \tag{5.4}$$

$$L = \frac{1.5 \times \pi \times 0.1732}{4} = 0.204\,\text{m}$$

The pole pitch can be calculated at this stage as follows.

$$\tau = \frac{L}{\lambda} \tag{5.5}$$

$$\tau = \frac{0.204}{1.5} = 0.136\,\text{m}$$

When the number of stator slots is being selected, two factors must be taken into account. A large number of stator slots result in narrow stator teeth, increased stator losses, teeth saturation and increased leakage inductance. On the other hand, a small number of stator slots cause vibration and abnormal noise. The optimum number of the stator slots per pole, q is recommended to be equal to two in [58 , 60]. For q = 2 the slot pitch is determined using the follows equation.

$$\tau_s = \frac{\tau}{3q} \tag{5.6}$$

$$\tau_s = \frac{0.136}{3\times 2} = 22.6\times 10^{-3}\,\text{m}$$

Optimum ratios of the inner to outer stator diameter for the induction machines below 100 KW are given in the following table.

Table 5.2 Internal/external stator diameter ratio [53]

P	2	4	6	8
$\frac{D_{is}}{D_{os}}$	0.54 – 0.58	0.61- 0.63	0.68 – 0.71	0.72 – 0.74

The value of $\frac{D_{is}}{D_{os}} = 0.62$ is chosen for the proposed four-pole induction machine and thus:

$$D_{os} = \frac{0.1732}{0.62} = 0.2793\,\text{m}$$

The large airgap reduces the efficiency and power factor while a small airgap increases space airgap field harmonics. For P > 2, airgap is introduced as:

$$D_g = (0.1 + 0.012\sqrt[3]{P_n}).10^{-3}\,\text{m} \tag{5.7}$$

Therefore, in this design, the airgap is determined as follows.

$$D_g = (0.1 + 0.012.\sqrt[3]{22000}).10^{-3} = 0.436 \times 10^{-3}\,\text{m} \approx 0.44 \times 10^{-3}\,\text{m}$$

5.3 The Stator Winding

As shown in Sub-section 3.2.1, the slots of the stator and rotor cores are filled with electric conductors and connected in such a way that they produce the required number of poles, and form the windings in induction machines. The stator conductors are insulated from the cores.

In this section, the three-phase stator winding is designed by assigning coils in the slots to different phases, establishing coil connections per phase and finally determining the size of the conductor and the number of turns for coils.

The number of stator slots is determined by the following equation where n_{ph} represents the number of phases in the stator and q is the number of the stator slots per pole per phase.

$$N_s = (P)\ (q)\ (n_{ph}) \tag{5.8}$$

The number of stator slots per pole per phase has to be low to have robust teeth and smallest shaft diameter for preventing the mechanical stress and vibration [58 , 60].

Therefore q is selected as q=2 and so for the proposed three phase machine, the number of stator slots is $N_s = 4 \times 2 \times 3 = 24$.

Double layer winding allows chorded coils such that coils end connections are shortened and so copper loss is reduced. Therefore it is preferred to have a two-layer stator winding to get a better sinusoidal form of the flux. This leads to a smaller magnetising current and current waveform harmonics as well as higher power factor. In addition, cooling and ventilation are improved which is very important in hybrid electric vehicle applications due to the harsh environment of electric machines [53 , 58].

In a two-layer winding the number of coils and slots are equal, so the number of coils per phase in this design is $N_s/m = 24/3 = 8$. Each phase occupies 8 slots in each layer where current direction in 4 slots is inward and in another 4 slots is outward. Each phase should produce four poles with each layer. For example, phase A in the first layer includes slots 1, 2, 7', 8', 13, 14, 19', 20'. The superscript prime refers to an outward current direction in the coils.

The pole pitch in terms of slot pitches is $\tau = N_s/P = 24/4 = 6$. Two-layer windings allow the possibility of chorded coils (fractional pitch) such that coil span (y) is smaller than pole pitch (τ).

In this design, coil span (y) is selected such that $y/\tau = 5/6$, so called chorded coils or fractional pitch where $y < \tau$. Chorded coils would decrease the coil end connection length and also reduce the fifth and seventh order of the stator mmf space harmonic with their rotor core surfaces and cage losses. Less mmf harmonics results in removal of

parasitic torque, radial forces, extra winding and core losses, noise and vibration [53 , 61].

The distribution of phases in slots is shown in Figure 5.2 for a two-layer stator winding. The superscript primes in phases A`, B` and C` refers to an outward current direction in coils. The second layer is displaced by $\tau - y = 6 - 5 = 1$ slot to the left as shown for phase B in Figure 5.2.

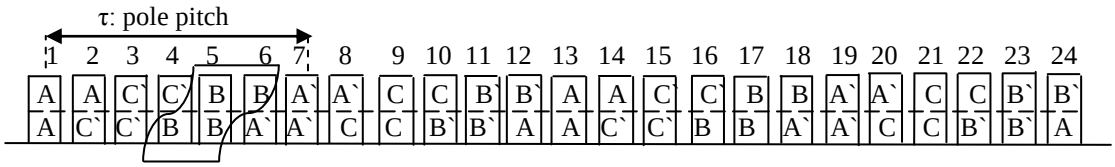

Figure 5.2 Slot/phase allocation

The electrical angle between emfs in neighbouring slots is calculated as follows.

$$\alpha_{ec} = \frac{\pi P}{N_s} \tag{5.9}$$

$$\text{So, } \alpha_{ec} = \frac{\pi \times 4}{24} = \frac{\pi}{6}$$

The largest common divisor of number of slots and pole pairs (24,2) is 2 and so the number of stator slot emfs is 24/2 =12. Emf phasors has 12 arrows as shown in Figure 5.3 for one layer.

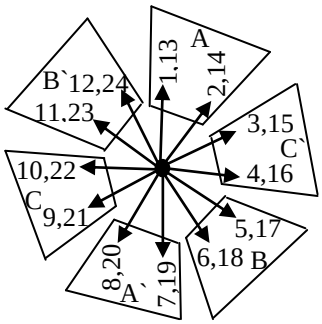

Figure 5.3 Star of emf phasors

Chording factor is defined as follows:

$$K_y = \sin\frac{\pi}{2}\frac{y}{\tau} \tag{5.10}$$

So, $K_y = \sin(\frac{\pi}{2}\times\frac{5}{6}) = 0.9659$

The zone factor is found by the following equation.

$$K_q = \frac{\sin\frac{\pi}{6}}{q\sin\left(\frac{\pi}{6q}\right)} \tag{5.11}$$

$$K_q = \frac{0.5}{2\sin\left(\frac{\pi}{6\times 2}\right)} = 0.9659$$

Therefore, the stator winding factor which is defined as follows can be determined.

$$K_w = K_q K_y \tag{5.12}$$

$$K_w = 0.9659 \times 0.9659 = 0.9329$$

The pole flux is known by the following equation:

$$\Phi = \alpha_i \tau L B_g \tag{5.13}$$

where B_g represents the airgap flux density and α_i is pole spanning coefficient.

Airgap flux density for P = 4 poles induction machines is recommended as B_g = (0.65 – 0.78)T. Pole spanning coefficient α_i depends on the tooth saturation factor 1+ k_{st} as shown in Figure 5.4 [53]. With the initial value for $1+k_{st}$ = 1.3 the pole spanning coefficient α_i = 0.71 and form factor K_f = 1.09. Form factor is used in Equation (5.14) to find the number of turns per phase.

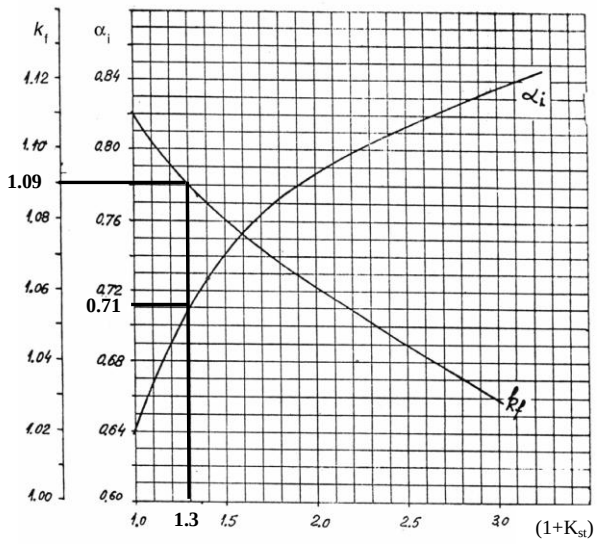

Figure 5.4 teeth saturation factor versus pole spanning coefficient [53]

By substituting the known values in Equation (5.13), the pole flux is calculated as:

$$\phi = 0.71 \times 0.136 \times 0.204 \times 0.7 = 13.789 \times 10^{-3}\ \text{Wb}$$

Now, the number of turns per phase can be determined using the following equation.

$$W = \frac{K_E V_{ph}}{4 K_f K_w f \phi} \tag{5.14}$$

So, the number of turns per phase is:

$$W = \frac{0.97 \times \left(\frac{415}{\sqrt{3}}\right)}{4 \times 1.09 \times 0.9329 \times 50 \times 13.789 \times 10^{-3}} = 82.89\ \text{turns / phase}$$

The number of conductors per slot is:

$$n_s = \frac{W}{\frac{P}{2} q} \tag{5.15}$$

$$n_s = \frac{82.89}{2 \times 2} = 20.72$$

As two-layer windings are performed for stator slots, there will be two distinct coils per slot which requires an even number for n_s. The number of conductors per slot is selected as $n_s = 20$. With the chosen n_s, the number of turns per slot per phase has to be corrected from Equation (5.15) which results in W = 80 turns/phase.

Consequently, the actual airgap flux density is recalculated as follows.

$$B_g = 0.7 \times \frac{82.89}{80} = 0.725T$$

The rated line current is given as:

$$I_n = \frac{P_n}{\eta_n C os \varphi_n \sqrt{3} V_{LL}} \tag{5.16}$$

So, $I_n = \frac{22000}{0.9 \times 0.9 \times \sqrt{3} \times 415} = 37.786\,A$

Current density for high efficiency induction machines is recommended as follows [53].

$$\begin{aligned} J_{cu} &= 4 - 7\ A/mm^2 \text{ for } P = 2,4 \\ J_{cu} &= 5 - 8\ A/mm^2 \text{ for } P = 6,8 \end{aligned} \tag{5.17}$$

Magnetic wire cross section is:

$$A_w = \frac{I_n}{J_{cu} a} \tag{5.18}$$

So, with $J_{cu} = 4.5\ A/mm^2$, $A_w = \frac{37.786}{4.5 \times 1} = 8.39689\,mm^2$

The bare wire diameter is calculated as follows.

$$d_w = \sqrt{\frac{4A_w}{\pi}} \tag{5.19}$$

$$d_w = \sqrt{\frac{4 \times 8.39689}{\pi}} = 3.270\,\text{mm}$$

The nearest standard bare wire diameter is 3.350 mm according to the Wire Table presented for small electrical machines design shown in Table 5.3.

Table 5.3 Wire diameter table [48]

Bare Wire[mm]	Insulated[mm]
3.150	3.294
3.200	3.444
3.350	3.498
3.400	3.584
3.550	3.702
3.600	3.748

5.4 Stator Slot Sizing

Useful slot area is calculated by the following equation where K_{fill} represents the slot fill factor.

$$A_{su} = \frac{\pi d^2_w n_s}{4K_{fill}} \tag{5.20}$$

For round wires used in electric machines above 10 KW, a slot fill factor is selected such that K_{fill} = 0.4 – 0.44. With K_{fill} = 0.4, the slot useful area is calculated as:

$$A_{su} = \frac{\pi \times 3.350^2 \times 20}{4 \times 0.4} = 440.71 \text{mm}^2$$

For small motors with size of less than 37 KW semiclosed slots with parallel teeth (trapezoidal slots), shown in Figure 3.3 are used. The stator slots of induction machines used as starter/alternator for HEV applications is recommended to be semiclosed rectangular or trapezoidal shape to limit the skin effects [48 , 61]. Therefore the trapezoidal stator slots as shown in Figure 5.5 are selected in this design.

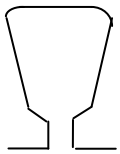

Figure 5.5 Stator slot shape

As explained in Section 1.3, ORIM has a different construction, comparing with conventional induction machines in terms of the stator and rotor positions. The stator of the ORIM under design is placed inside the rotor of the machine, therefore the stator slots have to be created on the outer side of the stator and the rotor slots have to be created on the inner side of the rotor. This new construction of stator and rotor slots for the ORIM contrasts with that of the conventional induction machines.

Figure 5.6 shows the stator slots and teeth geometry. Slot opening width b_{os}, wedge height h_w and slot opening height h_{os} are assigned values of 2 to 3mm $\leq 8D_g$ (where D_g equals airgap, (equation 5.7)), 1 to 4 mm and 0.5 to 1.0 mm respectively from past experiences achieved by [53]. All variables shown in Figure 5.6 are introduced and their values are determined in this section.

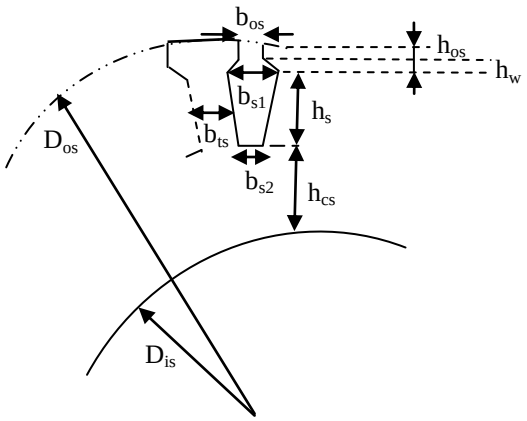

Figure 5.6 Stator slot geometry

It is supposed that all the airgap flux passes through the stator teeth and so:

$$B_g \tau_s L \approx B_{ts} b_{ts} L K_{Fe} \tag{5.21}$$

In Equation (5.21), b_{ts} represents the tooth width, shown in Figure 5.6 and B_{ts} is the tooth magnetic flux density with assigned value between 1.5 T and 1.65 T. K_{Fe} is the influence of lamination insulation thickness coefficient. The value of K_{Fe} is almost equal to 0.96 for 0.5 mm thick lamination [53].

The stator tooth width can be derived from equation (5.21) as:

$$b_{ts} = \frac{B_g \tau_s}{B_{ts} K_{Fe}} \tag{5.22}$$

With B_{ts} = 1.55 T and K_{Fe} = 0.96, the stator tooth width is:

$$b_{ts} = \frac{0.725 \times 22.6 \times 10^{-3}}{1.55 \times 0.96} = 11.01 \text{mm}$$

The longer side of the stator slot b_{s1}, shown in Figure 5.6 can be calculated by the following equation where D_{os} is the stator outer diameter determined in Section 5.2 by using Table 5.2.

$$b_{s1} = \frac{\pi(D_{os} - 2\times h_{os} - 2h_w)}{N_s} - b_{ts} \tag{5.23}$$

With b_{os} = 2.2 mm, h_{os} = 1 mm, h_w = 1.5 mm:

$$b_{s1} = \frac{\pi(279.3 - 2\times 1 - 2\times 1.5)\times 10^{-3}}{24} - 11.01\times 10^{-3} = 24.89\,\text{mm}$$

As the slot has trapezoidal shape, the slot useful area and the shorter side of the stator slot b_{s2}, shown in Figure 5.6 can be shown by the following equations:

$$A_{su} = h_s \frac{(b_{s1} + b_{s2})}{2} \tag{5.24}$$

$$b_{s2} \approx b_{s1} + 2h_s \tan\frac{\pi}{N_s} \tag{5.25}$$

From the equations above, b_{s2} can be derived as:

$$b_{s2} = \sqrt{b^2_{s1} - 4A_{su}\tan\frac{\pi}{N_s}} \tag{5.26}$$

By substituting the known values of parameters in the equation above, b_{s2} is known as:

$$b_{s2} = \sqrt{(24.89\times10^{-3})^2 - 4\times440.71\times10^{-6}\times\tan\frac{\pi}{24}} = 19.68\,\text{mm}$$

The stator slot useful height h_s shown in Figure 5.6 is determined From Equation (5.24) as follows.

$$h_s = \frac{2\times440.71\times10^{-6}}{(24.89+19.68)\times10^{-6}} = 19.78\,\text{mm}$$

The design is proceed by finding the tooth saturation factor $1+K_{st}$ with the assumption that the stator and rotor has the same effect in this respect. F_{mts} and F_{mtr} represent the stator and rotor tooth mmf respectively and F_{mg} is airgap mmf in the following equation.

$$1+K_{st} = 1+\frac{(F_{mts}+F_{mtr})}{F_{mg}} \tag{5.27}$$

The airgap mmf is:

$$F_{mg} \approx K_c D_g \frac{B_g}{\mu_0} \tag{5.28}$$

where K_c and μ_o represent the Carter coefficient and air permeability respectively. K_c is defined for opened slots as the ratio of the fundamental airgap flux density to the amplitude of the sinusoidal airgap flux density which occurs in the absence of slot and stator mmf harmonics.

From past experience [53], Kc is assigned an initial value of 1.2 but the precise value, calculated in Section 5.6 after sizing the rotor slots, is expected to be close to this initial value. Therefore the airgap flux mmf is calculated as follows.

$$F_{mg} = 1.2 \times 0.44 \times 10^{-3} \times \frac{0.725}{1.256 \times 10^{-6}} = 304.78 \text{ Aturns}$$

From the magnetisation data, shown in Table 5.4, the stator tooth magnetic field strength is found as H_{ts} = 1760 A/m for B_{ts} = 1.55 T.

Table 5.4 Lamination magnetisation data [53]

B[T]	H[A/m]
1.45	1050
1.5	1340
1.55	1760
1.6	2460
1.65	3460
1.7	4800

As a result, the stator tooth mmf can be determined by the following equation.

$$F_{mts} = H_{ts} (h_s + h_{os} + h_w) \quad (5.29)$$

$$F_{mts} = 1760 \ (19.78 + 1 + 1.5).10^{-3} = 39.213 \text{ Aturns.}$$

Assuming the initial value of 1.3 for tooth saturation factor $1+K_{st}$, the value of rotor tooth mmf F_{mtr} is calculated from Equation (5.27) as follows.

$$F_{mtr} = K_{st} F_{mg} - F_{mts} \tag{5.30}$$

Hence, rotor tooth mmf is:

$$F_{mtr} = 0.3 \times 304.78 - 39.213 = 52.22 \text{ Aturns}$$

As there is no significant difference between calculated rotor tooth mmf and stator tooth mmf values, the design process is acceptable to this point and it can be continued.

If rotor tooth mmf is very smaller than stator tooth mmf or opposite, for selected tooth saturation factor $1+K_{st}$, a smaller value of airgap flux density B_g should be chosen. Then, the design process has to be repeated from Equation (5.13) and the iterative procedure is stopped when $F_{mts} \approx F_{mtr}$.

The stator back iron height can be calculated from the following equation.

$$h_{cs} = \frac{D_{os} - (D_{is} + 2(h_{os} + h_w + h_s)}{2} \tag{5.31}$$

$$h_{cs} = \frac{279.3 - (173.2 + 2(1 + 1.5 + 19.78))}{2} = 30.77 \text{ mm}$$

The back core flux density is determined by the following equation.

$$B_{cs} = \frac{\phi}{2Lh_{cs}} \tag{5.32}$$

$$B_{cs} = \frac{13.789 \times 10^{-3}}{2 \times 0.204 \times 30.77 \times 10^{-3}} = 1.10\,T$$

The back core flux density B_{cs} should have a value between 1.4 to 1.7 T but the resultant B_{cs} is smaller than the desired one.

There are three ways to increase the stator back core flux density. The simplest way is to decrease the stator outer diameter until B_{cs} reaches the range of 1.4 to 1.7 T. The second solution is to select a smaller stack aspect ratio in Equation (5.1) which results in a bigger stator inner diameter, a shorter back iron height h_{cs} and hence a higher B_{cs}. The final way to increase the stator back core flux density consists in decreasing current density and thus increasing slot height h_s.

Selecting a smaller stack aspect ratio (in the second way) leads to a bigger stack length L which is not desired. The third solution is also not a good way to increase the stator back core flux density because the high efficiency induction machine is desired, and so the simplest way is chosen by decreasing the stator outer diameter.

The stator outer diameter is decreased to D_{os} = 0.2665 m. Consequently the design process has to be brought back to Equation (5.23).

The longer side of the stator slot b_{s1} is recalculated with the new stator outer diameter utilising Equation (5.23) as follows.

$$b_{s1} = \frac{\pi(266.5 - 2\times1 - 2\times1.5)\times10^{-3}}{24} - 11.01\times10^{-3} = 23.22\,\text{mm}$$

The shorter side of the stator slot b_{s2} is determined by Equation (5.26) as:

$$b_{s2} = \sqrt{(23.22\times10^{-3})^2 - 4\times440.71\times10^{-6}\times\tan\frac{\pi}{24}} = 17.52\,\text{mm}$$

From Equation (5.24):

$$h_s = \frac{2\times440.71\times10^{-6}}{(23.22+17.52)\times10^{-6}} = 21.63\,\text{mm}$$

As a result, the stator tooth mmf is:

F_{mts} = 1760 (21.63 + 1+ 1.5).10^{-3} = 42.47 Aturns.

From Equation (5.30):

$$F_{mtr} = 0.3\times304.78 - 42.47 = 48.96\,\text{Aturns}$$

The stator back iron height is calculated from the Equation (5.31).

$$h_{cs} = \frac{266.5 - (173.2 + 2(1+1.5+21.63))}{2} = 22.52\,\text{mm}$$

The back core flux density with new stator back iron height is determined by Equation (5.32).

$$B_{cs} = \frac{13.789 \times 10^{-3}}{2 \times 0.204 \times 22.52 \times 10^{-3}} = 1.50\,T$$

This is an acceptable value which is between the desired range of 1.4 to 1.7 T.

5.5 Rotor Slot Sizing

The correspondence between the number of stator and rotor slots has to be selected carefully to decrease additional losses, vibration, noise and parasitic torque [53].

As discussed in Section 3.2, the theory behind an induction machine operation and induction of current and torque in the rotor are based on the assumptions that the rotating mmf is sinusoidally distributed over the poles and similarly, the rotor mmf is distributed over the induced poles.

In practice, the airgap flux frequency has a number of harmonics because of the mmf concentration in a number of slots. This results in winding harmonics of the order n, given by $n = 6N \pm 1$ where N is an integer. The other reason for flux harmonics is the stator and rotor slot openings, which results in slot harmonics caused by the airgap ripple. In addition, saturation and irregularity in the airgap length may cause harmonics in mmf [48].

The flux harmonics produces extra poles rotating at sub-synchronous speed, either in the same direction of fundamental field or opposing. The induction machine rotor reacts to each harmonic flux and so produces a parasitic torque-speed characteristic which consequently makes the torque-speed characteristic irregular. This may stop the machine working at standstill, or produces excessive noise [48].

Slot harmonics or tooth ripples appear because of the reactance variations when the slotted rotor turns around the slotted stator. Therefore the proper combination of stator and rotor slots has to be considered to avoid having the same order of stator and rotor harmonics with coincident speeds. One of the possibilities that may cause this problem is that the stator and rotor have the same number of slots.

The discussion above leads to some rules in selecting the rotor slots number. The number of rotor slots should never be equal to the number of stator slots but should be 15 to 30 % different. Also, subtract of the rotor slots number from the stator slots number should not be equal to:

$$\pm P, \pm 2P, \pm 3P, \pm 5P, \pm 1, \pm 2, \pm (P \pm 1), \pm (P \pm 2)$$

where P is the number of poles, to avoid synchronous cusps, magnetic locking, noise and vibration[48].

The most satisfactory of rotor slot numbers for the 4 pole induction machine which has 24 stator slots is given as follows [53].

16, 18, 20, 30, 33, 34, 35, 36

For the induction motor under design, the number of rotor slots is considered as $N_r = 34$. The rotor slots of traction motors and starter/generators used in HEV applications are manufactured with trapezoidal shape that results in teeth with sides parallel to one another, as shown in Figure 5.7. These slot shapes provides maximum bar cross section area giving minimum resistance to harmonics [54 , 61 , 62 , 63 , 64].

Closed rotor slots reduces starting current, noise, vibration and friction losses though the breakdown and starting torque are smaller as well as rated power factor [53].

Figure 5.7 Rotor slot shape

To start sizing the rotor slots, the rated current of the rotor bar is calculated by the following equation where K is the ratio of rotor mmf to stator mmf.

$$I_b = K\frac{2n_{ph}WK_w}{N_r}I_n \tag{5.33}$$

In fact, rotor mmf is slightly smaller than stator mmf and their ratio K is defined as follows where $Cos\varphi_n$ represents the rated power factor of the designed machine.

$$K = 0.8Cos\varphi_n + 0.2 \tag{5.34}$$

By substituting the value of power factor in Equation (5.34) above,

$$K = 0.8\times 0.9 + 0.2 = 0.92$$

Now, rated rotor bar current is calculated by using Equation (5.33).

$$I_b = 0.92\times\frac{2\times 3\times 80\times 0.9329}{34}\times 37.786 = 457.84\,A$$

For high efficiency applications, rotor bar current density is selected equal to J_b = 3.42 A/mm^2 [53]. The rotor slot area is determined as follows.

$$A_b = \frac{I_b}{J_b} \tag{5.35}$$

With chosen rotor bar current density, the rotor slot area is:

$$A_b = \frac{457.84}{3.42} = 133.87\,\text{mm}^2$$

The end ring current is calculated by the following equation.

$$I_{er} = \frac{I_b}{2\sin\frac{\pi P}{2N_r}} \tag{5.36}$$

By substituting the values in the equation above, the end ring current is:

$$I_{er} = \frac{457.84}{2\sin\frac{\pi \times 4}{2 \times 34}} = 1245.82\,\text{A}$$

The end ring current density J_{er} is selected such that J_{er} = (0.75 – 0.8) J_b [53]. With J_{er} = 0.75 J_b :

$$J_{er} = 0.75 \times 3.42 \times 10^6 = 2.565 \times 10^6\ \text{A/m}^2$$

The end ring cross section can be known by the following equation.

$$A_{er} = \frac{I_{er}}{J_{er}} \tag{5.37}$$

Hence, the end ring cross section area is:

$$A_{er} = \frac{1245.82}{2.565 \times 10^{6}} = 485.70 \times 10^{-6}\ \text{m}^2$$

As discussed in Section 5.4, due to the new construction of the ORIM in terms of the rotor position, the rotor slots of the machine under design have to be created on the inner side of the rotor.

Figure 5.8 shows the rotor slots and teeth geometry with all variables shown on it. The rotor slot opening width b_{or} and slot opening height h_{or} are assigned values of b_{or} = 1.5 mm and h_{or} = 0.5 mm [53].

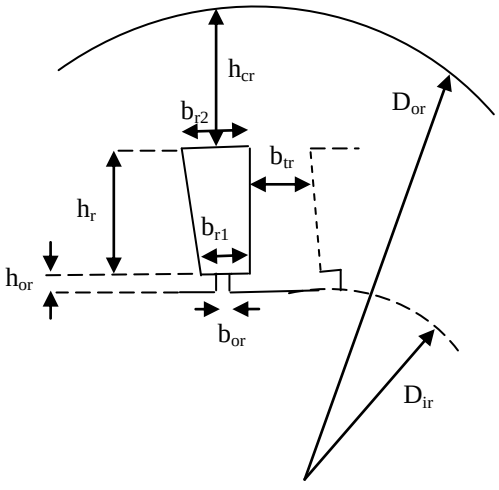

Figure 5.8 Rotor slot geometry

Rotor slot pitch can be calculated by the following equation:

$$\tau_r = \frac{\pi(D_{os} + 2D_g)}{N_r} \tag{5.38}$$

So, the rotor slot pitch is:

$$\tau_r = \frac{\pi(266.5 + 2 \times 0.44) \times 10^{-3}}{34} = 24.70\,\text{mm}$$

The rotor tooth width b_{tr} is calculated as follows.

$$b_{tr} \approx \frac{B_g}{K_{Fe} B_{tr}} \tau_r \tag{5.39}$$

With the rotor tooth flux density B_{tr} = 1.7 T,

$$b_{tr} = \frac{0.725}{0.96 \times 1.7} \times 24.70 \times 10^{-3} = 10.97\,\text{mm}$$

The shorter side of the rotor slot b_{r1} shown in Figure 5.8 is calculated by the following equation.

$$b_{r1} = \frac{\pi(D_{os} + 2D_g + 2h_{or})}{N_r} - b_{tr} \tag{5.40}$$

By substituting the values of variables in Equation (5.40),

$$b_{r1} = \frac{\pi(266.5 + 2\times 0.44 + 2\times 0.5)\times 10^{-3}}{34} - 10.97\times 10^{-3} = 13.83\,\text{mm}$$

As the rotor slot has a trapezoidal shape, the longer side of the rotor slot b_{r2} shown in Figure 5.8 is found using the following equation.

$$b_{r2} = \sqrt{b^2_{r1} + 4A_b \tan\frac{\pi}{N_r}} \tag{5.41}$$

So, $b_{r2} = \sqrt{13.83^2 + 4\times 133.87\times \tan\frac{\pi}{34}} = 15.52\,\text{mm}$

To complete the process of designing rotor slot geometry, rotor slot height is found using the following equation.

$$h_r = \frac{2A_b}{b_{r1} + b_{r2}} \tag{5.42}$$

So, $h_r = \frac{2\times 133.87}{13.83 + 15.48} = 9.13\,\text{mm}$

Now, the rotor tooth mmf can be calculated as follows.

$$F_{mtr} = H_{tr} (h_r + h_{or}) \tag{5.43}$$

From Table 5.4 H_{tr} is equal to 4800 A/m and so with B_{tr} = 1.7 A/m, the rotor tooth mmf is equal to:

$$F_{mtr} = 4800 \times (9.13 + 0.5) \times 10^{-3} = 46.22 \,\text{Aturns}$$

This F_{mtr} is close to the F_{mtr} calculated using Equation (5.30) in Section 5.4 which confirms the validity of design up to this stage.

When F_{mtr} is very large, the rotor flux density may be increased and design is re-calculated from Equation (5.39) to have a smaller rotor tooth width which results in a smaller rotor slot height and finally smaller F_{mtr}.

If F_{mtr} had been too small, the rotor tooth flux density may have been decreased and the design recalculated from Equation (5.39) until an acceptable value for F_{mtr} is found. Increased rotor tooth width leads to a larger bar current density which could decrease the efficiency. To avoid this problem in designing a high efficiency machine, the alternative method can be taken by increasing the tooth saturation factor 1+ K_{st} and return the design to Equation (5.13).

The rotor back core height is calculated with back core flux density of B_{cr} = 1.4 – 1.7 T using the following equation.

$$h_{cr} = \frac{\phi}{2}\frac{1}{L.B_{cr}} \tag{5.44}$$

B_{cr} is chosen as B_{cr} = 1.65 T and so:

$$h_{cr} = \frac{13.789\times10^{-3}}{2}\times\frac{1}{0.204\times1.65} = 20.48\,\text{mm}$$

The rotor inner diameter is found as follows.

$$D_{ir} = D_{os} + 2D_g \tag{5.45}$$

So, $D_{ir} = 0.2665 + 2\times0.44\times10^{-3} = 0.2674\,\text{m}$

The outer diameter of the rotor can be calculated as:

$$D_{or} = D_{os} + 2D_g + 2(h_{or} + h_r + h_{cr}) \tag{5.46}$$

Hence the rotor outer diameter is:

$$D_{or} = 0.2665 + 2\times0.44\times10^{-3} + 2\times(0.5 + 9.13 + 20.48)\times10^{-3} = 0.3276\,\text{m}$$

The cross section of the end ring for the outer rotor induction machine under design is shown in Figure 5.9.

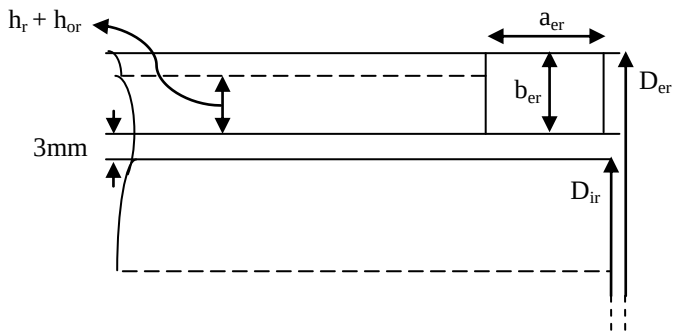

Figure 5.9 End ring cross section

The shorter side of the end ring cross section b_{er} is calculated by the following equation:

$$b_{er} = (1.0 – 1.2).(h_r + h_{or}) \tag{5.47}$$

In this design,

$$b_{er} = 1.0\ (9.13+0.5) = 9.63\ \text{mm}$$

The longer side of the end ring cross section a_{er} can be now determined as follows.

$$a_{er} = \frac{A_{er}}{b_{er}} \tag{5.48}$$

$$\text{So, } a_{er} = \frac{485.70\times10^{-6}}{9.63\times10^{-3}} = 50.44\,\text{mm}$$

Generally, for the conventional inner rotor induction machines there is 3mm - 4 mm difference between rotor outer diameter and end ring outer diameter [53]. But, for the ORIM under design, the stator and rotor are transposed, and thus the position of the

rotor slots, as shown in Figure 5.8. Therefore this 3mm is added to D_{ir} and b_{er} to obtain the end ring outer diameter, as shown in the following equation.

$$D_{er} = D_{ir} + b_{er} + 3\times10^{-3} \tag{5.49}$$

By substituting the known values in the equation above, the end ring diameter is found.

$$D_{er} = 0.2674 + 9.63\times10^{-3} + 3\times10^{-3} = 0.280\,\text{m}$$

5.6 The magnetisation Current

The magnetisation mmf is calculated using the following equation,

$$F_m = 2\left(K_c D_g \frac{B_g}{\mu_0} + F_{mts} + F_{mtr} + F_{mcs} + F_{mcr} \right) \tag{5.50}$$

where K_c is Carter coefficient and F_{mcs} and F_{mcr} represent stator and rotor back core mmfs respectively. F_{mts} and F_{mtr} are stator and rotor tooth mmfs which have been determined prevoiusly.

Carter coefficient K_c was shown to be 1.2 in Equation (5.28) but it can be calculated precisely at this stage because all of the required variables are known to find K_c. The total Carter coefficient K_c is calculated as follows,

$$K_c = K_{cs}K_{cr} \tag{5.51}$$

where K_{cs} is the stator carter coefficient and is calculated as:

$$K_{cs} = \frac{\tau_s}{\tau_s - \gamma_s} \tag{5.52}$$

and K_{cr} is the rotor carter coefficient and it is determined as follows.

$$K_{cr} = \frac{\tau_r}{\tau_r - \gamma_r} \tag{5.53}$$

Variable γ_s in equation (5.52) is calculated as:

$$\gamma_s = \frac{b_{os}^{\ 2}}{5D_g + b_{os}} \tag{5.54}$$

By substituting the known values from previous sections in the equation above,

$$\gamma_s = \frac{(2.2\times10^{-3})^2}{(5\times0.44+2.2)\times10^{-3}} = 1.1\times10^{-3}$$

and variable γ_r in equation (5.53) is calculated as:

$$\gamma_r = \frac{b_{or}^{\ 2}}{5D_g + b_{or}} \tag{5.55}$$

So, $\gamma_r = \frac{(1.5\times10^{-3})^2}{(5\times0.44+1.5)\times10^{-3}} = 0.61\times10^{-3}$

From Equation (5.52) and (5.53),

$$K_{cs} = \frac{22.6\times10^{-3}}{(22.6-1.1)\times10^{-3}} = 1.05$$

and

$$K_{cr} = \frac{24.70\times10^{-3}}{(24.70-0.61)\times10^{-3}} = 1.02$$

Consequently, K_c is

$$K_c = 1.05\times1.02 = 1.1$$

The calculated value is close to the assigned value in Equation (5.28) which was equal to 1.2, so the design holds.

The stator back core mmf is:

$$F_{mcs} = C_{cs}\frac{\pi(D_{is}+h_{cs})}{P}H_{cs}(B_{cs}) \qquad (5.56)$$

C_{cs} is an empirical coefficient which represents an average length of flux path in the stator back core and its value is approximately equal to $C_{cs} \approx 0.88.e^{-0.4B_{cs}^{2}}$.

With B_{cs} =1.50 T, from Table 5.4, H_{cs} = 1340 A/m

$$F_{mcs} = 0.88 \times e^{-0.4 \times 1.50^2} \times \frac{\pi(0.1732 + 0.02252)}{4} \times 1340 = 73.69 \text{ Aturns}$$

The rotor back core mmf is:

$$F_{mcr} = C_{cr} \frac{\pi(D_{or} - h_{cr})}{P} H_{cr}(B_{cr}) \tag{5.57}$$

where $C_{cr} \approx 0.88e^{-0.4B_{cr}^2}$ is an empirical coefficient which represents an average length of flux path in the rotor back core.

With B_{cr} =1.65 T, from Table 5.4 H_{cr} = 3460 A/m, the rotor back core mmf is:

$$F_{mcr} = 0.88 \times e^{-0.4 \times 1.65^2} \frac{\pi(0.3276 - 0.02048)}{4} \times 3460 = 247.18 \text{ Aturns}$$

Now, magnetisation mmf can be determined by Equation (5.50) as follows.

$$F_m = 2 \times (1.2 \times 0.44 \times \frac{0.725 \times 10^{-3}}{1.256 \times 10^{-6}} + 42.47 + 46.22 + 73.69 + 247.18) = 1428.67 \text{ Aturns}$$

The total saturation factor K_s is calculated by the following equation.

$$K_s = \frac{F_m}{2F_{mg}} - 1 \tag{5.58}$$

So, $K_s = \frac{1428.67}{2 \times 304.78} - 1 = 1.344$

The magnetisation current produces the revolving flux in the stator linked to the rotor of the machine. The same phenomenon happens in transformers by the exciting current which creates a mutual flux in the transformer. The value of magnetisation current for induction machines lies between 30 % and 50 % of stator rated current [47].

The magnetisation current in an induction machine may be calculated from,

$$I_{\mu} = \frac{\pi P(\frac{F_m}{2})}{6\sqrt{2}WK_w} \tag{5.59}$$

hence, $I_{\mu} = \frac{\pi \times 4 \times (\frac{1428.67}{2})}{6\sqrt{2} \times 80 \times 0.9329} = 14.17\,\text{A}$

To calculate the per unit value of I_{μ} (shown by i_{μ}), the value of I_{μ} (magnetisation current) is divided by base current (rated current) value as follows.

$$i_{\mu} = \frac{I_{\mu}}{I_n} \ \% \tag{5.60}$$

By substituting the values in the equation above:

$$i_{\mu} = \frac{14.17}{37.786} = 37.5\ \% = 0.375\ \text{Per unit}$$

5.7 Resistances and Reactances

The stator resistance shown in Figure 3.11, Chapter 3 which represents the stator copper losses is calculated using the following equation,

$$R_s = \rho_{Cu} \frac{l_c W}{A_{Cu}} \tag{5.61}$$

where ρ_{co} is copper resistivity and l_c represents the coil length calculated as follows.

$$l_c = 2(L + l_{end}) \tag{5.62}$$

where l_{end} represents the end connection length and it comes from:

$$l_{end} = 2y - 0.02 \quad \text{for P = 4} \tag{5.63}$$

y/τ is called chording factor and the value of 5/6 was assigned for the stator winding in Section 5.3. Generally y/τ is between unity and 2/3 [53].

Hence, y (coil span) is derived as:

$$y = \frac{5}{6}\tau \tag{5.64}$$

So, $y = \frac{5}{6} \times 0.136 = 0.11333$ m

and

$$l_{end} = 2 \times 0.11333 - 0.02 = 0.20666 \text{ m}$$

The stator rated temperature is not known yet but as it was stated in Section 5.1, for hybrid electric vehicle applications the thermal class H is selected. The maximum allowable temperature in this class is 180°C.

The copper resistivity at θ°C is:

$$(\rho_{Cu})_{\theta} = (\rho_{Cu})_{20°C}\left(1 + \frac{1}{273}(\theta - 20)\right) \tag{5.65}$$

The resistivity of copper at 20 °C is $(\rho_{Cu})_{20°C} = 1.78 \times 10^{-8} \Omega m$ [53] and so:

$$(\rho_{Cu})_{180°C} = (\rho_{Cu})_{20°C}\left(1 + \frac{1}{273}(180 - 20)\right) = 2.82 \times 10^{-8}\ \Omega m$$

From (5.61) and (5.62), the stator resistance is

$$R_s = 2.82 \times 10^{-8} \times \frac{2 \times (0.204 + 0.20666) \times 80}{8.39689 \times 10^{-6}} = 0.2207\,\Omega$$

To calculate the rotor resistance referred to stator, shown in Figure 3.11, the rotor bar /end ring segment equivalent resistance is calculated first by the following equation.

$$R_{be} = \rho_{Al}\left[\frac{L}{A_b}K_R + \frac{l_{er}}{2A_{er}\sin^2\left(\frac{\pi P}{2N_r}\right)}\right] \tag{5.66}$$

where K_R is the skin effect resistance coefficient for the bar.

The resistivity of the cast aluminium at 20°C is $(\rho_{Al})_{20°C} = 3.1\times10^{-8}\Omega m$ [53] and the end ring segment length is:

$$l_{er} = \frac{\pi(D_{er} - b_{er})}{N_r} \tag{5.67}$$

So, $l_{er} = \frac{\pi(0.2800 - 9.63\times10^{-3})}{34} = 24.98\times10^{-3}$ m

Bar skin effect resistance coefficient for rectangular slots, but traditionally adopted for related shapes is:

$$K_R = \xi\frac{(\sinh 2\xi + \sin 2\xi)}{(\cosh 2\xi - \cos 2\xi)} \approx \xi \tag{5.68}$$

where

$$\xi = \beta_s h_r\sqrt{S} \tag{5.69}$$

β_s is the reverse of the field penetration depth in aluminium and is determined as:

$$\beta_s = \sqrt{\frac{2\pi f \mu_0}{2\rho_{Al}}} \tag{5.70}$$

By substituting the known values in the equation above:

$$\beta_s = \sqrt{\frac{2\times\pi\times 50\times 1.256\times 10^{-6}}{2\times 3.1\times 10^{-8}}} = 79.776\,\mathrm{m}^{-1}$$

With S =1,

$$\xi = 79.776\times 9.13\times 10^{-3}\times\sqrt{1} = 0.728$$

From Equation (5.68)

$$K_R \approx 0.728$$

Now, the rotor bar/end ring segment equivalent resistance at S=1 and at 180 °C can be determined as follows.

$$R_{be\,180^\circ}^{S=1} = 3.1\times 10^{-8}\left(1+\frac{1}{273}(180-20)\right)\left[\frac{0.204}{133.87\times 10^{-6}}\times 0.728 + \frac{24.98\times 10^{-3}}{2\times 485.70\times 10^{-6}\sin^2\left(\frac{\pi\times 4}{2\times 34}\right)}\right]$$

$$R_{be\,180^\circ}^{S=1} = 9.199\times 10^{-5}\,\Omega$$

Now, the rotor resistance referred to the stator at S=1 can be calculated using the following equation.

$$(R`_r)_{S=1} = \frac{4n_{ph}}{N_r}(WK_w)^2 R_{be180°} \tag{5.71}$$

By substituting the determined values in the equation above:

$$(R`_r)_{S=1} = \frac{4\times 3}{34}(80\times 0.9329)^2 \times 9.199\times 10^{-5} = 0.1808\,\Omega$$

The stator leakage reactance per phase shown in Figure 3.11 is:

$$X_{sl} = 4\mu_0 2\pi fL\frac{W^2}{Pq}(\lambda_s + \lambda_{ds} + \lambda_{ec}) \tag{5.72}$$

where λ_s, λ_{ds}, λ_{ec} are the coefficients of the stator slot geometric specific permeance, stator differential leakage permeance and the end connection specific geometric permeance respectively.

The stator slot coefficient is calculated using the following equation.

$$\lambda_s = \left[\frac{2}{3}\frac{h_s}{(b_{s1}+b_{s2})} + \frac{2h_w}{(b_{os}+b_{s1})} + \frac{h_{os}}{b_{os}}\right]\left(\frac{1+3\beta}{4}\right) \tag{5.73}$$

where β is the chording factor ($\beta = \frac{y}{\tau}$).

$$\lambda_s = \left[\frac{2}{3}\times\frac{21.63\times 10^{-3}}{(23.22+17.52)\times 10^{-3}} + \frac{2\times 1.5\times 10^{-3}}{(2.2+23.22)\times 10^{-3}} + \frac{1\times 10^{-3}}{2.2\times 10^{-3}}\right]\left(\frac{1+3\times\frac{5}{6}}{4}\right) = 0.811$$

Stator differential coefficient is:

$$\lambda_{ds} \approx \frac{0.9\tau_s q^2 K_w{}^2 C_s \gamma_{ds}}{K_c g(1+K_{st})} \tag{5.74}$$

where

$$C_s = 1 - 0.033\frac{b_{os}{}^2}{g\tau_s} \tag{5.75}$$

and

$$\gamma_{ds} = (0.25\sin\varphi_1 + 2.6)\times 10^{-2}; \quad \text{for } q = 2$$
$$\varphi_1 = \pi(6\beta - 5.5) \tag{5.76}$$

So, $\gamma_{ds} = (0.25\sin\left(\pi(6\times\frac{5}{6} - 5.5)\right) + 2.6)\times 10^{-2} = 2.35\times 10^{-2}$

From (5.75):

$$C_s = 1 - 0.033\times\frac{(2.2\times 10^{-3})^2}{0.44\times 10^{-3}\times 22.6\times 10^{-3}} = 0.984$$

Consequently, from Equation (5.74):

$$\lambda_{ds} = \frac{0.9\times 22.6\times 10^{-3}\times 2^2\times 0.9329^2\times 0.984\times 2.35\times 10^{-2}}{1.1\times 0.44\times 10^{-3}(1+0.3)} = 2.60$$

The end connection coefficient for two-layer windings is calculated using the following equation.

$$\lambda_{ec} = 0.34\frac{q}{L}(l_{end} - 0.64\times\beta\times\tau) \tag{5.77}$$

So, $\lambda_{ec} = 0.34\times\frac{2}{0.204}(0.20666 - 0.64\times\frac{5}{6}\times 0.136) = 0.4471$

From (5.72), the stator phase reactance is:

$$X_{sl} = 4\times 1.256\times 10^{-6}\times 2\pi\times 50\times 0.204\times\frac{80^2}{4\times 2}(0.811 + 2.60 + 0.4471) = 0.994\,\Omega$$

To calculate the rotor leakage reactance referred to stator, shown in Figure 3.11, the equivalent rotor bar leakage reactance is calculated first, using the following equation.

$$X_{be} = 2\pi f\mu_0 L(\lambda_r K_x + \lambda_{dr} + \lambda_{er}) \tag{5.78}$$

where λ_r, λ_{dr} and λ_{er} are the rotor slot geometric specific, rotor differential leakage permeance and end ring permeance coefficient.

For trapezoidal slots of Figure 5.8:

$$\begin{aligned}
\lambda_r &\approx \frac{2h_r K_{r1}}{3(b_{r1} + b_{r2})} + \frac{h_{or}}{b_{or}}K_{r2} \\
K_{r1} &\approx \frac{1}{4} + \frac{3}{4}K_{r2} \\
K_{r2} &\approx \frac{1+3\beta}{4}
\end{aligned} \tag{5.79}$$

By substituting the values in the equations above:

$$K_{r2} = \frac{1+3\times\frac{5}{6}}{4} = 0.87$$

and

$$K_{r1} = \frac{1}{4} + \frac{3}{4}\times 0.87 = 0.90$$

As a result,

$$\lambda_r = \frac{2\times 9.13\times 10^{-3}\times 0.9}{3(13.83+15.52)\times 10^{-3}} + \frac{0.5\times 10^{-3}}{1.5\times 10^{-3}}\times 0.87 = 0.477$$

Rotor differential coefficient is:

$$\lambda_{dr} = \frac{0.9\tau_r\gamma_{dr}}{K_c D_g}\left(\frac{N_r}{3P}\right)^2 \tag{5.80}$$

where

$$\gamma_{dr} = 9\left(\frac{3P}{N_r}\right)^2 10^{-2} \tag{5.81}$$

$$\text{So, } \gamma_{dr} = 9\times\left(\frac{3\times 4}{34}\right)^2 10^{-2} = 1.121\times 10^{-2}$$

and

$$\lambda_{dr} = \frac{0.9\times 24.70\times 10^{-3}\times 1.121\times 10^{-2}}{1.1\times 0.44\times 10^{-3}}\left(\frac{34}{3\times 4}\right)^2 = 4.133$$

The end ring permeance coefficient comes from:

$$\lambda_{er} = \frac{2.3\times(D_{er}-b_{er})}{N_r\times L\times 4\sin^2\left(\frac{\pi P}{2\times N_r}\right)}\log\frac{4.7\times(D_{er}-b_{er})}{b_{er}+2a_{er}} \tag{5.82}$$

So, $\lambda_{er} = \frac{2.3\times(280-9.63)\times 10^{-3}}{34\times 0.204\times 4\sin^2\left(\frac{\pi\times 4}{2\times 34}\right)}\log\frac{4.7\times(280-9.63)\times 10^{-3}}{(9.63+2\times 50.44)\times 10^{-3}} = 0.7041$

The skin effect coefficient for the leakage reactance is calculated by the following equation.

$$K_x \approx \frac{3}{2\xi}\frac{(\sin(2\xi)-\sin(2\xi))}{(\cosh(2\xi)-\cos(2\xi))} \approx \frac{3}{2\xi} \tag{5.83}$$

For $\xi = 0.709$ determined in Equation (5.69), $K_x = \frac{3}{2\times 0.728} = 2.06$

From (5.78), the equivalent rotor bar leakage reactance is:

$$X_{be} = 2\pi\times 50\times 1.256\times 10^{-6}\times 0.204\times(0.477\times 2.06+4.133+0.7041)$$

$$X_{be} = 4.6846\times 10^{-4}\,\Omega$$

Now, the rotor leakage reactance referred to stator can be calculated by the following equation.

$$X`_{rl} = 4n_{ph}\frac{(WK_w)^2}{N_r}X_{be} \tag{5.84}$$

By substituting the known values in the equation above,

$$X`_{rl} = 4\times 3\frac{(80\times 0.9329)^2}{34}\times 4.6846\times 10^{-4} = 0.9209\,\Omega$$

The stator and rotor leakage reactances at standstill (S = 1) are reduced by a value between 0.7 and 0.8 for stator and 0.6 and 0.7 for rotor. This is because of the leakage flux path saturation. In this design average values are used.

$$\begin{aligned}(X_{sl})_{sat}^{S=1} &= X_{sl}\times(\frac{0.7+0.8}{2})\\ (X`_{rl})_{sat}^{S=1} &= X`_{rl}\times(\frac{0.6+0.7}{2})\end{aligned} \tag{5.85}$$

$$(X_{sl})_{sat}^{S=1} = 0.994\times 0.75 = 0.745\,\Omega$$

$$(X`_{rl})_{sat}^{S=1} = 0.9209\times 0.65 = 0.5986\,\Omega$$

Skin and leakage saturation effects have to be reduced for rated slip (S_n), i.e $K_R = K_x = 1$.

The rotor bar/end ring segment equivalent resistance is determined from Equation (5.66) for $K_R = 1$ as follows.

$$R_{be\,180^\circ}^{S=S_n} = 3.1\times10^{-8}\left(1+\frac{1}{273}(180-20)\right)\left[\frac{0.204}{133.87\times10^{-6}}\times1+\frac{24.98\times10^{-3}}{2\times485.70\times10^{-6}\sin^2\left(\frac{\pi\times4}{2\times34}\right)}\right]$$

$$R_{be\,180^\circ}^{S=S_n} = 1.124\times10^{-4}\,\Omega$$

Now, the rotor resistance at rated slip can be calculated as follows.

$$(R`_r)_{S_n} = (R`_r)_{S=1}\frac{R_{be\,180^\circ}^{S=S_n}}{R_{be\,180^\circ}^{S=1}} \tag{5.86}$$

$$(R`_r)_{S_n} = 0.1808\times\frac{1.124\times10^{-4}}{9.199\times10^{-5}} = 0.221\Omega$$

Also, the equivalent rotor bar leakage reactance at rated slip is calculated from Equation (5.78) for K_x =1 as follows,

$$(X_{be})_{S_n} = 2\pi\times50\times1.256\times10^{-6}\times0.204\times(0.477\times1+4.133+0.7041) = 4.2776\times10^{-4}\,\Omega$$

and so the rotor leakage reactance at rated slip is determined as:

$$(X`_{rl})_{S=S_n} = (X`_{rl})_{S=1}\frac{X_{be\,180^\circ}^{S=S_n}}{X_{be\,180^\circ}^{S=1}} = 0.9209\times\frac{4.2776\times10^{-4}}{4.6846\times10^{-4}} = 0.8409\,\Omega$$

The magnetisation X_m is:

$$X_m = \sqrt{\left(\frac{V_{ph}}{I_\mu}\right)^2 - R_s^{\,2}} - X_{sl} \tag{5.87}$$

$$X_m = \sqrt{\left(\frac{415}{14.17\sqrt{3}}\right)^2 - 0.2207^{\,2}} - 0.994 = 15.91\Omega$$

Generally, rotor slots are skewed to decrease the first slot harmonic torque and keep the rotor surface and tooth flux pulsation core losses under control [53]. Typically, a skewing C is equal to one stator slot pitch τ_s.

The magnetisation X_m for the skewed rotor slots is calculated by the following equation.

$$X_{mskew} \approx X_m K_{skew} \tag{5.88}$$

where

$$K_{skew} = \frac{\sin\frac{\pi}{2}\frac{\tau_s}{\tau}}{\frac{\pi}{2}\frac{\tau_s}{\tau}} \tag{5.89}$$

Substituting Equation (5.6) in the equation above gives,

$$K_{skew} = \frac{\sin\frac{\pi}{2}\frac{1}{3q}}{\frac{\pi}{2}\frac{1}{3q}} = \frac{\sin\frac{\pi}{12}}{\frac{\pi}{12}} = 0.9886$$

Now, with (5.87) and (5.88):

$$X_{mskew} = 15.91 \times 0.9886 = 15.7286\,\Omega$$

Also, rotor leakage reactance is decreased by a new term $X`_{rlskew}$.

$$X`_{rlskew} = X_m (1 - K_{skew}{}^2) \tag{5.90}$$

$$X`_{rlskew} = 15.91 \times (1 - 0.9886^2) = 0.3607\,\Omega$$

Therefore, the final values of rotor leakage reactance at S = 1 and S = S_n are determined by two following equations.

$$(X`_{rl})_{skew}^{S=1} = (X`_{rl})_{sat}^{S=1} + X`_{rlskew} \tag{5.91}$$

So, $(X'_{rl})_{skew}^{S=1} = 0.5986 + 0.3607 = 0.9593\,\Omega$

and

$$(X`_{rl})_{skew}^{S=S_n} = X`_{rl} + X`_{rlskew} \tag{5.92}$$

So, $(X`_{rl})_{skew}^{S=S_n} = 0.9209 + 0.3607 = 1.2816\,\Omega$

5.8 Losses and Efficiency

The output efficiency of electric machines is defined as follows.

$$\eta = \frac{P_{out}}{P_{in} + \sum \text{losses}} \tag{5.93}$$

The total machine loss is calculated as follows.

$$\sum \text{losses} = P_{Cu} + P_{Al} + P_{iron} + P_{mv} + P_{stray} \tag{5.94}$$

where P_{Cu}, P_{Al}, P_{iron}, P_{mv} and P_{stray} represent the stator winding copper losses, rotor cage losses (at $S = S_n$), core losses, mechanical/ventilation losses and stray losses respectively.

Stator winding or copper losses P_{Cu} is calculated by the following equation:

$$P_{Cu} = 3R_s I_n^{\,2} \tag{5.95}$$

So, $P_{Cu} = 3 \times 0.2207 \times 37.786^2 = 945.334\,\text{W}$

Rotor cage losses at $S = S_n$ is calculated by the following equation.

$$P_{Al} = 3(R`_r)_{S_n} I_m^{\,2} = 3(R`_r)_{S_n} K^2 I_n^{\,2} \tag{5.96}$$

By substituting the known values $(R`_r)_{Sn}$ and K determined by Equations (5.86) and (5.34),

$$P_{Al} = 3 \times 0.221 \times 0.92^2 \times 37.786^2 = 801.219\,\text{W}$$

The core loss consists of fundamental and harmonic iron loss shown by P^{f}_{iron} and P^{h}_{iron} respectively in the following equation.

$$P_{iron} = P^{f}_{iron} + P^{h}_{iron} \tag{5.97}$$

The fundamental core losses arise only in the teeth and yoke (back iron) of the stator because the frequency of the rotor is low. The harmonic iron loss which is also called the tooth flux pulsation core loss is produced by the stator and rotor slotting which cause variation in the distribution of the airgap flux density.

The fundamental iron loss is calculated as follows where P_t and P_y are the stator teeth and stator yoke fundamental losses.

$$P^{f}_{iron} = P_t + P_y \tag{5.98}$$

The stator teeth fundamental loss is calculated using the following equation.

$$P_t \approx K_t p_{sl} \left(\frac{f}{50} \right)^{1.3} B_{ts}{}^{1.7} G_t \tag{5.99}$$

where p_{sl} is the specific losses in W/Kg at 50 Hz and 1.0 Tesla and has a value between 2 and 3 W/Kg according to lamination manufacture data. Coefficient K_t represents the core loss augmentation because of mechanical machining such as sharpening of the cutting tools and stamping value which depends on the material and cutting tools quality. Its value is also between 1.6 and 1.8 [53]. G_t also represents the stator tooth weight and it is given as follows where γ_{iron} is iron specific weight.

$$G_t = \gamma_{Fe} N_s b_{ts} (h_s + h_w + h_{os}) L K_{Fe} \quad (5.100)$$

By substituting the known values in the equation above,

$$G_t = 7800 \times 24 \times 11.01 \times 10^{-3} (21.63 + 1.5 + 1) \times 10^{-3} \times 0.204 \times 0.96 = 9.74\,\text{Kg}$$

With B_{ts} = 1.55, f = f_0 = 50 Hz, K_t = 1.7 and P_{sl} = 2, from Equation (5.99) the stator teeth fundamental losses is:

$$P_t = 1.7 \times 2 \times \left(\frac{50}{50}\right)^{1.3} 1.55^{1.7} \times 9.74 = 69.76\,\text{W}$$

The stator yoke (back iron) fundamental loss is calculated by the following equation [53].

$$P_y = K_y p_{sl} \left(\frac{f}{50}\right)^{1.3} B_{cs}{}^{1.7} G_y \quad (5.101)$$

Again a value between 1.6 – 1.9 is assigned for K_y which accounts for mechanical machining, and the yoke weight, represented by G_y comes from:

$$G_y = \gamma_{Fe} \frac{\pi}{4} \left[D_{os}{}^2 - (D_{os} - 2h_{cs})^2 \right] L K_{Fe} \quad (5.102)$$

So,

$$G_y = 7800 \times \frac{\pi}{4} \times \left[0.2665^{\,2} - (0.2665 - 2 \times 22.52 \times 10^{-3})^2 \right] \times 0.204 \times 0.96 = 26.367\,\text{Kg}$$

With K_y = 1.6, B_{cs} = 1.50 from Equation (5.101), the stator yoke (back iron) fundamental losses is:

$$P_y = 1.6 \times 2\left(\frac{50}{50}\right)^{1.3} 1.50^{1.7} \times 26.367 = 168.10\,\text{W}$$

As a result, the fundamental iron losses P^f_{iron} from Equation (5.98) is:

$$P^f_{iron} = P_t + P_y = 69.76 + 168.10 = 237.86\ \text{W}.$$

The harmonic iron loss shown in Equation (5.97) is calculated using the following equation.

$$P^h_{iron} = 0.5 \times 10^{-4}\left[\left(N_r \frac{2f}{P} K_{ps} B_{ps}\right)^2 G_{ts} + \left(N_s \frac{2f}{P} K_{pr} B_{pr}\right)^2 G_{tr}\right] \qquad (5.103)$$

where

$$K_{ps} \approx \frac{1}{2.2 - B_{ts}} \qquad (5.104)$$

So, $K_{ps} = \dfrac{1}{2.2 - 1.55} = 1.5385$

and

$$K_{pr} \approx \frac{1}{2.2 - B_{tr}} \tag{5.105}$$

So, $K_{pr} = \frac{1}{2.2 - 1.7} = 2$

B_{ps} and B_{pr} coefficients shown in Equation (5.103) are the stator and rotor tooth flux density pulsations and determined by two following equations.

$$B_{ps} \approx (K_{cr} - 1)B_g \tag{5.106}$$

So, $B_{ps} \approx (1.02 - 1) \times 0.725 = 0.0145\,T$

and

$$B_{pr} \approx (K_{cs} - 1)B_g \tag{5.107}$$

So, $B_{pr} \approx (1.05 - 1) \times 0.725 = 0.0362$

The rotor teeth weight G_{tr} represented in Equation (5.103) is:

$$G_{tr} = \gamma_{Fe} L K_{Fe} N_r (h_r + h_{or}) b_{tr} \tag{5.108}$$

So, $G_{tr} = 7800 \times 0.204 \times 0.96 \times 34 \times (9.13 + 0.5) \times 10^{-3} \times 10.97 \times 10^{-3} = 5.490\,Kg$

Now, the harmonic iron loss can be calculated by Equation (5.103) as:

$$P_{iron}^{h} = 0.5\times10^{-4}\left[\left(34\times\frac{2\times50}{4}\times1.5385\times0.0145\right)^{2}\times9.74+\left(24\times\frac{2\times50}{4}\times2\times0.0362\right)^{2}\times5.490\right]$$

$$P_{iron}^{h} = 0.69\,\text{W}$$

From Equation (5.97) the total core loss is:

$$P_{iron} = 237.86 + 0.69 = 238.55\ \text{W}$$

The mechanical/ventilation losses for P = 4 are considered as $P_{mv} = 0.012\ P_n$. The stray losses standard value is $P_{stray} = 0.01P_n$ [53].

So, from Equation (5.95) the total losses is

$$\sum \text{losses} = 945.334 + 801.219 + 238.55 + 0.012\times22000 + 0.01\times22000 = 2469.103\,\text{W}$$

From Equation (5.94), the output efficiency is calculated as follows.

$$\eta = \frac{22000}{22000 + 2469.103} = 0.899 = 89.9\ \%$$

which is nearly equal to the target efficiency (90%), specified in Section 5.1, so the design holds. Otherwise, the design procedure had to be performed again using a larger stator inner diameter and then smaller current densities.

5.9 Operation Characteristics

The no-load active current is obtained by the no-load losses in the following equation.

$$I_{ac\_nl} = \frac{P_{iron} + P_{mv} + 3I_{\mu}{}^{2}R_{s}}{3V_{ph}} \tag{5.109}$$

So, $I_{ac\_nl} = \dfrac{238.55 + 0.012 \times 22000 + 3 \times 14.17^{2} \times 0.2207}{3 \times \dfrac{415}{\sqrt{3}}} = 0.884\,\text{A}$

The rated slip is calculated using the following equation.

$$S_{n} = \frac{P_{Al}}{P_{n} + P_{Al} + P_{mv} + P_{stray}} \tag{5.110}$$

Hence, $S_{n} = \dfrac{801.219}{22000 + 801.219 + 0.012 \times 22000 + 0.01 \times 22000} = 0.034$

The rated electromagnetic torque of an electric machine comes from:

$$T_{n} = \frac{P_{n}}{4\pi \dfrac{f}{P}(1 - S_{n})} \tag{5.111}$$

So, for the designed machine the rated torque is:

$$T_{n} = \frac{22000}{4\pi \dfrac{50}{4}(1 - 0.034)} = 144.98\,\text{Nm}$$

The torque-slip approximate relationship is given using the following equation:

$$T_{ind} = \frac{3P}{4\pi f} \frac{V_{ph}{}^2 \frac{R`_r}{S}}{\left(R_s + C_m \frac{R`_r}{S}\right)^2 + \left(X_{sl} + C_m (X`_{rl})_{skew}\right)^2} \quad (5.112)$$

where, $C_m \approx 1 + \frac{X_{sl}}{X_m}$.

The breakdown torque can be calculated by equation above for $\frac{d_{Tind}}{ds} = 0$ which determines the breakdown slip as $S_{bk} = \frac{C_m R`_r}{\sqrt{R_s{}^2 + (X_{sl} + C_m X`_{rl})^2}}$.

By substituting the breakdown slip in Equation (5.112), breakdown torque is calculated as follows.

$$T_{bk} = \frac{3P}{4C_m} \frac{1}{2\pi f} \frac{V_{ph}{}^2}{R_s + \sqrt{R_s{}^2 + \left(X_{sl} + C_m (X`_{rl})_{skew}\right)^2}} \quad (5.113)$$

As mentioned above, $C_m = 1 + \frac{X_{sl}}{X_m}$ and so $C_m = 1 + \frac{0.994}{15.7286} = 1.06$.By substituting the known values in equation (5.113),

$$T_{bk} = \frac{3 \times 4}{4 \times 1.06} \frac{1}{2\pi \times 50} \frac{\left(\frac{415}{\sqrt{3}}\right)^2}{0.2207 + \sqrt{0.2207^2 + \left(0.994 + 1.06 \times 1.2816\right)^2}} = 200.18\,\text{Nm}$$

The starting current is calculated using the following equation.

$$I_s = \frac{V_{ph}}{\sqrt{\left(R_s + R`_r^{S=1}\right)^2 + \left(X_{sl}^{S=1} + (X`_{rl})_{skew}^{S=1}\right)^2}} \tag{5.114}$$

$$\text{So, } I_s = \frac{\frac{415}{\sqrt{3}}}{\sqrt{\left(0.2207 + 0.1808\right)^2 + \left(0.745 + 0.9593\right)^2}} = 136.84\,\text{A}$$

Also, the starting torque can be computed as follows.

$$T_s = \frac{3(R`_r)_{S=1} I_s^{\,2} P}{4\pi \times f} \tag{5.115}$$

$$\text{So, } T_s = \frac{3 \times 0.1808 \times 136.84^2 \times 4}{4\pi \times 50} = 64.66\,\text{Nm}$$

The rated power factor can be determined using the following equation.

$$\text{Cos}\,\phi_n = \frac{P_n}{3 V_{ph} I_n \eta_n} \tag{5.116}$$

$$\text{Hence, } \text{Cos}\,\varphi_n = \frac{22000}{3 \times \frac{415}{\sqrt{3}} \times 37.786 \times 0.899} = 0.9$$

which is equal to the target value of the power factor, specified in Section 5.1.

It should be mentioned that several iterations in the design process such as selecting rotor slot number have been performed to design the induction machine with the desired characteristics such as efficiency and power factor but only the final design procedure has been reported.

5.10 Temperature Rise in the Designed Machine

As it was mentioned in Section 5.7, the thermal Class H is selected for electric machines in HEV applications which enables electric machine to operate in a temperature of 180°C. This is because of the harsh environment of an electric machine placed in a vehicle.

To validate the design thermally, the stator winding temperature in an induction machine is determined using the following equation.

$$\theta_{Cu} = \theta_{amb} + \Delta\theta_{Cu} + \Delta\theta_{frame} \tag{5.117}$$

where θ_{amb} is the ambient temperature and $\Delta\theta_{Cu}$ is the temperature differential between the slot wall and the slot conductors. $\Delta\theta_{frame}$ represents the frame temperature increase with respect to ambient.

The temperature differential between the slot wall and the slot conductors is computed as follows.

$$\Delta\theta_{Cu} = \frac{P_{Cu}}{\alpha_{cond} A_{ls}} \tag{5.118}$$

where α_{cond} represents both slot insulation thickness and insulation conductivity characteristics and it is calculated as follows.

$$\alpha_{cond} = \frac{\lambda_{ins}}{h_{ins}} \tag{5.119}$$

where λ_{ins} represents the slot insulation thermal conductivity in W/m°K and h_{ins} is insulation thickness in millimetres from the slot centre to tooth wall. Typically for small machines:

λ_{ins} = 0.25 W/mK and h_{ins} = 0.3mm [53].

$$\alpha_{cond} = \frac{0.25}{0.3\times10^{-3}} = 833\,W/m^2K$$

A_{sl} in Equation (5.118) represents the stator slot lateral area which is calculated using the following equation.

$$A_{ls} \approx (2h_s + b_{s2})LN_s \tag{5.120}$$

Hence, the stator slot lateral area is:

$$A_{ls} = (2\times21.63+17.52)\times10^{-3}\times0.204\times24 = 0.2976\,m^2$$

By substituting the known values in Equation (5.118), the temperature differential between the slot wall and the slots conductors is calculated as follows.

$$\Delta\theta_{Cu} = \frac{945.334}{833 \times 0.2976} = 3.81°C$$

The frame temperature increase with respect to ambient is determined using the following equation

$$\Delta\theta_{frame} = \frac{\sum losses}{\alpha_{conv} A_{frame}} \tag{5.121}$$

where α_{conv} and A_{frame} represent the fame thermal convection and total frame area including the cooling fins area respectively.

For small induction motors below 100 KW with self ventilators which have 4 poles, α_{conv} = 50 W/m^{2}K [53].

The frame total area including is determined as follows.

$$A_{frame} = \pi D_{or} (L + \tau) K_{fin} \tag{5.122}$$

With typical value of 3 for cooling fins coefficient K_{fin} [53], the total frame area is

$$A_{frame} = \pi \times 0.3276 \times (0.204 + 0.136) \times 3 = 1.050\,m^2$$

So, from Equation (5.121), the frame temperature increase with respect to ambient is

$$\Delta\theta_{\text{frame}} = \frac{2469.103}{50 \times 1.050} = 47.03°\text{C}$$

The ambient temperature of the starter/generator in HEV applications for such a direct coupling is considered 110°C [61].

Finally from (5.117), the winding temperature is calculated to be:

$$\theta_{\text{Cu}} = 120°\text{C} + 3.81°\text{C} + 47.03°\text{C} = 170.84°\text{C}$$

which is smaller than 180°C, so the design holds.

5.11 Summary

In this chapter, the specifications of the targeted electric machine were determined based on the requirements specified in the previous chapters. According to these specifications, an ORIM was designed by applying the widely accepted equations for induction machine design and modifying them where required. The design process was started by determining the main dimensions of the stator core and followed by stator winding. Then, suitable shapes for the stator and rotor slots were selected and sized. The resistances and reactances of the equivalent circuit of the induction machine, presented in Chapter 3 were determined. According to the equivalent circuit, the operation characteristics of the designed machine including efficiency and power factor were calculated in order to confirm that the specified targets for the ORIM are met. Finally it

was also confirmed that the design is thermally valid. In the next chapter, the simulation results of the designed ORIM which were performed by a finite element software are reported.

Chapter 6 ORIM Virtual Prototyping

This chapter looks at the Outer Rotor Induction Machine (ORIM) modelling and simulation using analytical methods. The electric machine design process requires the solution of complex and interrelated problems including electromagnetic, thermal and mechanical problems. To reach a viable design and meet all specifications of an electric machine, several iterations should be taken in the design process. Therefore Computer-Aided Engineering (CAE) tools are best suited for developing an electric machine. CAE tools make use of the analytical models of electric machines.

Advanced approximation techniques such as the Finite Element Method (FEM) can be used to model the behaviour of electric machines accurately and alternate designs can be assessed in a short period of time. In this method, machine specifications including dimensions, components materials and construction type are provided by a user as input data for CAE package. The input data is utilised to calculate the machine performance characteristics. The results can be used by a designer to change the design based on his experience to meet the design requirements [48].

The reliability and effectiveness of FEM has been proved in design and research. Most of CAE packages that analyse electrical machines utilise this powerful method to analyse the electromagnetic problems, because it provides a numerical simulation of electric machines with different geometries and operating conditions and gives the accurate information about electric machines behaviour before building them physically [48 , 65 , 66 , 67].

Many electromagnetic analysis packages such as ANSYS Emag, SPEED and Flux have been tried by different research institutions and laboratories. In this project a software package called JMAG is used to simulate the designed outer rotor induction machine.

6.1 Finite Element Method

The history of the FEM shows that this method was first used in structural analysis and also to solve problems of fluid flow in the 1950s. The paper presented by Silvester and Chari in 1970 proposed a formulation capable of solving complex geometries and moving towards the problem of magnetic nonlinearity [68].

In FEM, the electromagnetic field problem domain is divided into a number of elements. Then, the distribution of potential for each element is approximated by a polynomial and then a numerical solution to the original field problem is derived regarding some optimal criterion. Poisson and Laplace equations can be gained from Maxwell equation and solved under specified boundary conditions and expressed in terms of potentials [69].

FEM performs detailed field analysis but doing these calculations in the transient times requires a considerable amount of computational time, especially for the asymmetry conditions of electric machines [70].

6.2 JMAG-Studio Environment

JMAG-Studio is a comprehensive electromagnetic FEM tool developed by JRI Solutions Limited. JMAG supports users in designing electronic and electric equipment such as electric machines, actuators and antennae by performing electric and magnetic field analytic functions.

To process an analysis of an electric machine in JMAG, the following steps that are explained in Subsection 6.2.1 to 6.2.7 have to be carried out [71 , 72]. These instructions are implemented for the designed ORIM to perform the simulation settings in order to simulate the machine. The ORIM simulation settings and results are presented in Sections 6.3 and 6.4 for the generation and starting modes separately.

6.2.1 Physical Model of the Machine

In the first step, a virtual prototype of the machine is created in JMAG based on the rotor/stator dimensions derived in a design process. JMAG is also capable of importing Computer-Aided Design (CAD) data created by any other software for generating the model of the machine.

Creating the shape of an electric machine can be also done by Motor Template Tool in JMAG which can create a desired shape easily. The designed machine geometry, materials and conditions are defined in Motor Template by parameters. The values of parameters that have been determined within the design process are entered and exported to JMAG to create the model.

JMAG Motor Template Tool contains templates for different types of DC and AC machines including brush, universal, permanent magnet and induction. The available template for the induction machine is inner rotor type. Therefore a new type of template for the designed ORIM was required to be created.

When Motor Template is initiated the following window is appeared.

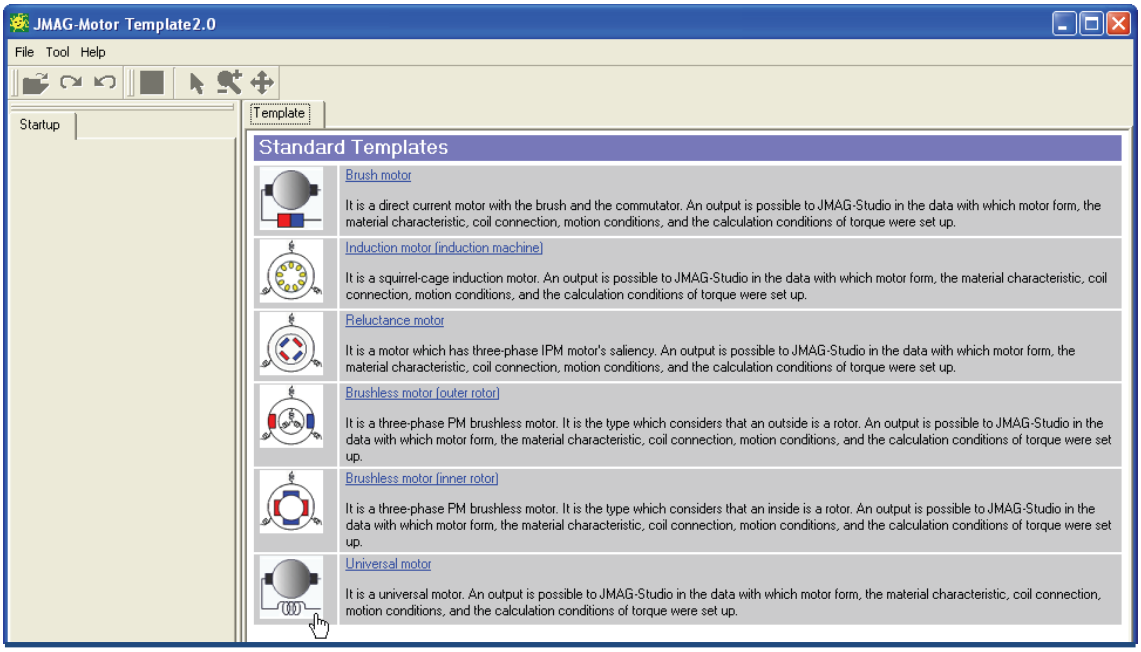

Figure 6.1 Motor template start-up window [71]

By clicking on the desired template icon, the main window appears as shown in Figure 6.2. In this figure ORTP is the name of the modified new template file for a trapezoidal ORIM. In the main window, main parameters of the stator and rotor dimensions are entered.

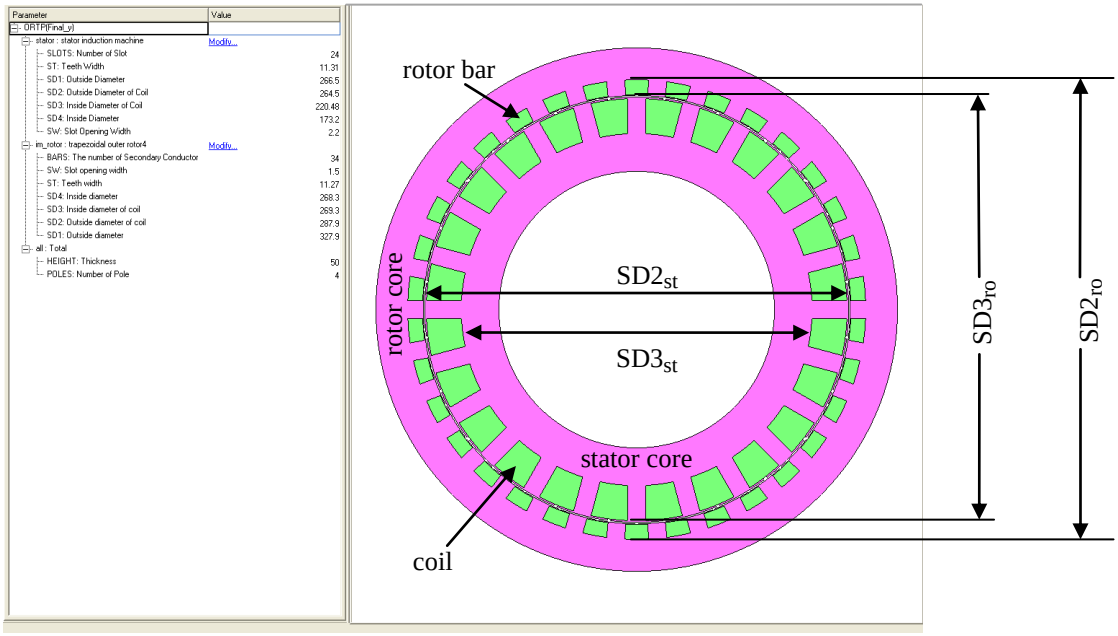

Figure 6.2 Dimensions window in JMA

The outside and inside diameter of stator coil named with terms $SD2_{st}$ and $SD3_{st}$ in the stator parameters list, shown in Figure 6.2 are calculated using the following equations respectively.

$$SD2_{st} = SD1_{st} - 2 \times h_{os} \tag{6.1}$$

$SD1_{st}$ is outside diameter of stator and h_{os} represents the stator slot opening height, shown in Figure 5.6, Chapter 5.

To determine the inside diameter of stator coil $SD3_{st}$, the following equation is used where h_s represents the stator slot height, shown in Figure 5.6, Chapter 5.

$$SD3_{st} = SD2_{st} - 2 \times h_s \tag{6.2}$$

Also, the inside and outside diameters of rotor coil named with $SD3_{ro}$ and $SD2_{ro}$, in the rotor parameters list, shown in Figure 6.2 are calculated using the following equations respectively. $SD4_{ro}$ is the rotor inside diameter and h_{or} represents the rotor slot opening height, shown in Figure 5.8, Chapter 5.

$$SD3_{ro} = SD4_{ro} + 2 \times h_{or} \tag{6.3}$$

And the outside diameter of rotor coil is determined as follows where h_r represents the rotor slot height, shown in Figure 5.8, Chapter 5.

$$SD2_{ro} = SD3_{ro} + 2 \times h_r \tag{6.4}$$

6.2.2 Material Properties Setting

In the Motor Template, the stator and rotor materials can be also set as shown in Figure 6.3. Different magnetic material properties are available in the Motor Template database and appropriate material is selected according to the design parameters. If it is necessary, a new database of materials can be added to Motor Template.

For the cage of an induction motor, copper or aluminium can be chosen as the material property. No set up is required for the coil and it is set as a non-magnetic material automatically in Motor Template.

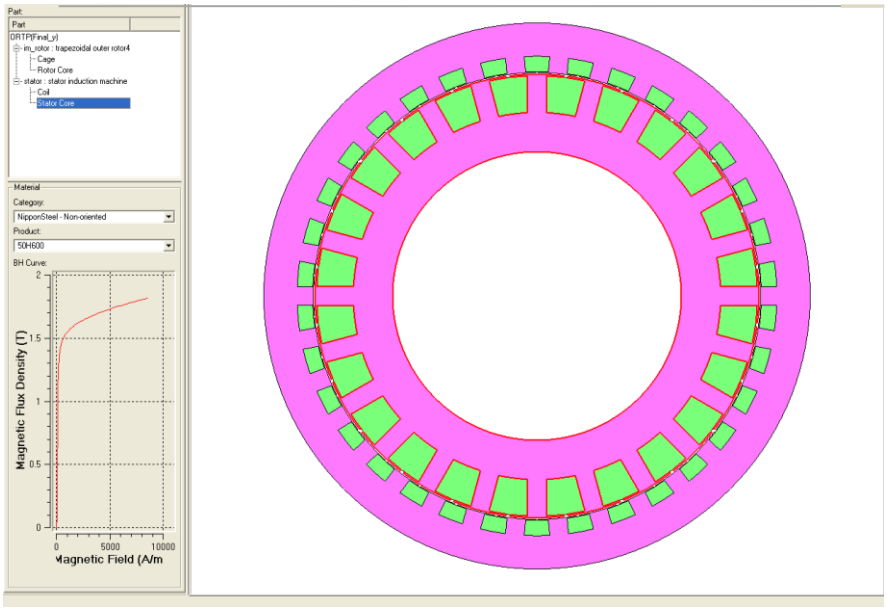

Figure 6.3 JMAG material window

6.2.3 Setting of stator winding

Motor Template has the facility of performing the stator winding for electric machines. The number of the layers of coils can be specified and also two methods of the automatic and manual windings are available in Motor Template. For an automatic winding, as shown in Figure 6.4 the coil pitch can also be defined to specify the number of slots spanned by one coil.

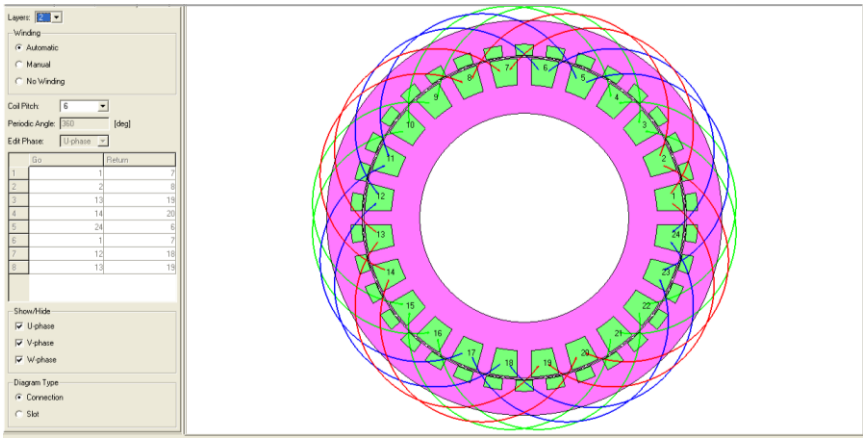

Figure 6.4 Winding window in JMAG

In the manual winding method, the windings are defined for each coil by specifying the slot numbers in the Go and Return columns in the tabular list shown in the figure above. In the slots allocated in Go column, current flows upward and current direction for slots in the Return column is downward.

6.2.4 Circuit setting

As Figure 6.5 shows, the data of the input circuit of the electric machines can be set in the circuit window as well as the number of turns of one phase and the rotation speed. Three phase current or voltage source power supplies can be selected and their specifications including phase connections type can be modified in this window.

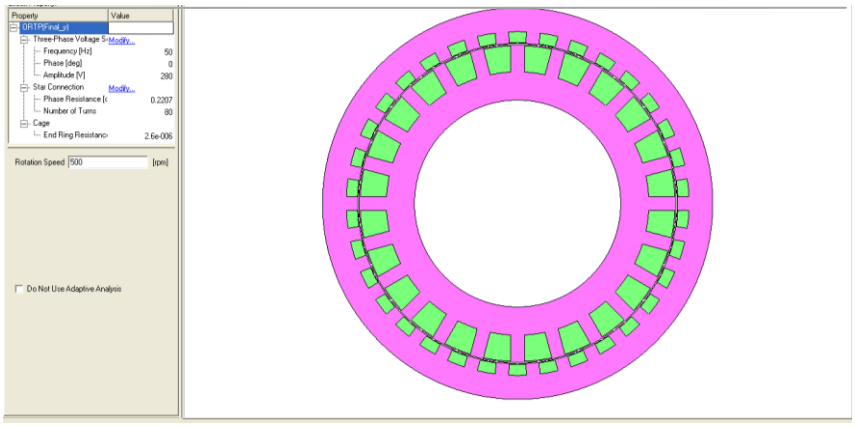

Figure 6.5 Circuit window in JMAG

The phase resistance shown in the window above is calculated within the design procedure. The end ring resistance component refers to the specification of the end ring used in the design process of the induction motor. For JMAG analysis, the resistance of the end ring between bars is calculated using the following equation [73].

$$R_{er} = \frac{1}{\sigma} \frac{L_{er}}{nA_{er}} \tag{6.5}$$

In the equation above, σ represents the rotor bars electric conductivity. L_{er} and A_{er} represent the end ring length and section area respectively. The number of rotor bars is shown by n.

With the "Do Not Use Adaptive Analysis" option off, the adaptive mesh control will be applied when the Data is exported to JMAG for simulation in the next step.

6.2.5 Exporting Template Data to JMAG

After all required settings that explained above are completed; the created electric machine in Motor Template is exported to JMAG to run the analysis of a designed machine.

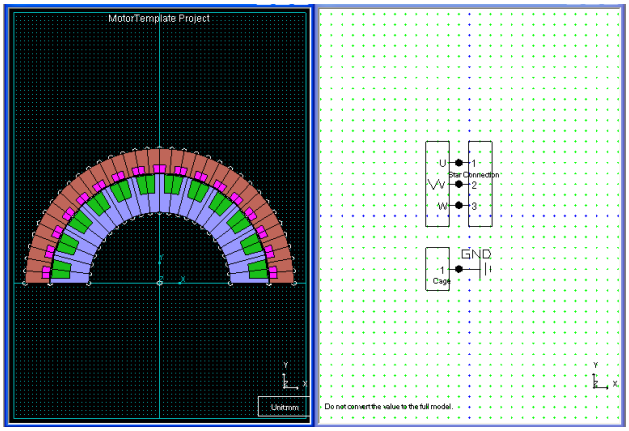

Figure 6.6 An exported template data to JMAG

The left window in Figure 6.6 represents the two-dimension analysis model while the right window is the circuit model which refers to a three phase power supply and three coils named u,v and w.

If the geometry and excitation of the analysis model in JMAG is symmetrical, then only a partial model is created in order to reduce the size of the model. For example, as Figure 6.6 shows, the whole analysis model has been made smaller to half model because the model geometry is symmetric. Consequently, data creation and calculation time is reduced [74].

6.2.6 Mesh Creating

JMAG performs the calculations and analysis based on the finite element method. The FEM divides the object as a finite number of elements and performs the calculations for each individual element. The object which is expressed as a finite number of elements appears as if meshes of a net are stretched and so this stage is called mesh creating. Mesh creating can be performed in two methods of manual or automatic creation. When the created shape in Motor Template is exported to JMAG, meshes are created automatically before the calculations are performed.

6.2.7 JMAG Data Analysis

After the procedures above are completed, JMAG is ready to conduct the simulation. If any errors during the calculations process occurs or the proper analysis conditions are not selected, the recalculations have to be performed. At the end, results are saved as a plot file.

The simulation results can be loaded as the output of analysis after the simulation process is completed. JMAG is facilitated with the vector and contour displays that show the magnetic flux and current densities for each node and element. Moreover, in the results plot file, output values can be displayed for each step of analysis.

In the following sections, the results of simulations performed in JMAG for the ORIM, designed in Chapter 5 are presented. Since it is supposed that ORIM operates in two different applications as the starter and generator machine, each application requires a different circuit setup in JMAG.

6.3 Analysis of ORIM as the Generator in JMAG

The following subsections show the setup steps that were performed in Motor Template before running the simulation for the designed ORIM when operates as the generator. The simulation results are shown in Section 6.3.3.

6.3.1 The Motor Template Settings for the Generator

To simulate the performance of the ORIM designed in Chapter 5 as a generator, the following settings explained in Subsections 6.2.1 to 6.2.4 should be applied to the ORTP Motor Template firstly.

The dimensions of the designed ORIM are summarised in Table 6.1. The Outside diameter of the stator coil in JMAG ($SD2_{st}$) is calculated using Equation (6.1) which gives:

$$SD2_{st} = 266.5 - 2 \times 1 = 264.5\,\text{mm}$$

The inside diameter of stator coil $SD3_{st}$ can be also known from Equation (6.2). Therefore,

$$SD3_{st} = 264.5 - 2 \times 21.63 = 221.24\,\text{mm}$$

Inside diameter of rotor coil in JMAG ($SD3_{ro}$) is calculated by Equation (6.3). So,

$$SD3_{ro} = 267.4 + 2 \times 0.5 = 268.4\,\text{mm}$$

Outside diameter of rotor coil $SD2_{ro}$ is also known from Equation (6.4) which gives:

$$SD2_{ro} = 268.4 + 2 \times 9.13 = 286.66\,\text{mm}$$

Table 6.1 Main dimensions of the ORIM

STATOR PART	(Dimensions in mm)
Number of slots: N_s	24
Tooth width: b_{ts}	11.01
Outside diameter: D_{os}	266.5
Outside diameter of coil: $SD2_{st}$	264.5
Inside diameter of coil: $SD3_{st}$	221.24
Inside diameter: D_{is}	173.2
Stator slot opening width: b_{os}	2.2
ROTOR PART	(Dimensions in mm)
Number of bars: N_r	34
Rotor slot opening width: b_{or}	1.5
Tooth width: b_{tr}	10.97

Inside diameter: D_{ir}	267.4
Inside diameter of coil: $SD3_{ro}$	268.4
Outside diameter of coil: $SD2_{ro}$	286.66
Outside diameter: D_{or}	327.6

The lamination thickness (50 mm) and the number of poles of the ORIM, determined in Chapter 5 are also entered in JMAG Dimensions Window, shown in Figure 6.2. The Motor Template setting procedure is now continued by the material properties setting explained in Subsection 6.2.2.

As Figure 6.7 shows, the magnetic material properties of both the ORIM stator and rotor cores, presented in Table 5.4 of Chapter 5 within the design procedure, are entered in Motor Template as the lamination magnetisation data.

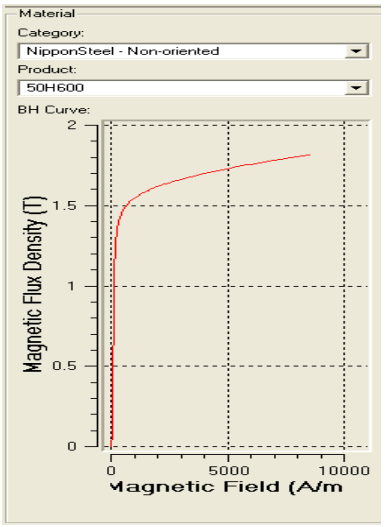

Figure 6.7 Magnetic properties of both stator and rotor cores

The material properties of the ORIM components which are set in JMAG are listed in Table 6.2.

Table 6.2 Material properties in JMAG

Part	Magnetising properties
Stator core	Magnetic material: Nippon steel 50H600
Rotor core	Magnetic material: Nippon steel 50H600
Cage	Aluminium
Coil winding	Non-magnetic material
Air region	Air

Two layer winding is performed for the Motor Template according to Figure 5.2 which represents the slot/phase allocation for the designed ORIM.

The resistance of the end ring between bars is calculated using Equation (6.5). In this equation, σ represents the rotor bars electric conductivity. The inverse of the rotor bars conductivity ($\frac{1}{\sigma}$) means resistivity (ρ). Since the cage of the ORIM is made of aluminium and the resistivity of the cast aluminium at 20°C is $(\rho_{Al})_{20°C} = 3.1\times10^{-8}\,\Omega m$ as discussed in Section 5.7, Chapter 5, therefore $\frac{1}{\sigma}$ or ρ_{Al} at the rated temperature of 180ºC is calculated as follows.

$$\frac{1}{\sigma} = \rho_{Al} = 3.1\times10^{-8}\times(1+\frac{1}{273}(180-20)) = 4.917\times10^{-8}\,\Omega m$$

The end ring length can be found using the following equation

$$L_{er} = \pi \times D_{er} \tag{6.6}$$

where D_{er} is the end ring diameter which was calculated by Equation (5.49) in the previous chapter. Therefore the end ring length is determined as follows.

$$L_{er} = \pi \times 0.28 = 879 \times 10^{-3}\,\text{m}$$

The end ring cross section area was also calculated in the previous chapter by Equation (5.37) as $A_{er} = 485.70 \times 10^{-6}\,\text{m}^2$. Therefore the end ring resistance between bars is calculated as follows by substituting the known values in Equation (6.5).

$$R_{er} = 4.917 \times 10^{-8} \times \frac{879 \times 10^{-3}}{34 \times 485 \times 10^{-6}} = 2.6 \times 10^{-6}\,\Omega$$

The input circuit parameters and the stator winding specifications that were obtained in Chapter 5 for the generator are summarised in Table 6.3. Since there is no voltage source connected to the stator coils of the machine, the first three rows of the following table are not applicable for the generator under analysis.

The generator rated speed is required to be calculated and set in JMAG. From Equation (5.110), it was determined that the rated slip is S_n = 0.034. As it was explained in Chapter 3, in the generating mode the rotor turns at a speed slightly higher than the synchronous speed but the absolute value of slip should be equal to the slip for the motoring mode [47]. Therefore the sign of the rated slip is negative for the generating mode. The generator rated speed is now derived from Equation (3.6) as follows.

$$n_m = (1 - S) n_{sync} \tag{6.7}$$

So, $n_m = (1-(-0.034)) \times 1500 = 1551 \text{rpm}$

Table 6.3 Input circuit parameters of the generator

Three phase voltage source	Not Applicable
Frequency	Not Applicable
Amplitude	Not Applicable
Stator phase resistance	0.2204 Ω
Number of turns per phase	80
End ring resistance	2.6×10^{-6} Ω
Rotation speed	1551 rpm

As it was explained in Subsection 3.2.3 induction generators require an external power source to maintain its magnetic field at all times as well as regulating the output voltage. Therefore, an current source is connected to the stator coils of the induction machine as shown in Figure 6.8. This current is induced into the short circuited rotor cage.

Three voltage probes are also connected between each phase terminals and ground to measure the generated voltage in the stator coils.

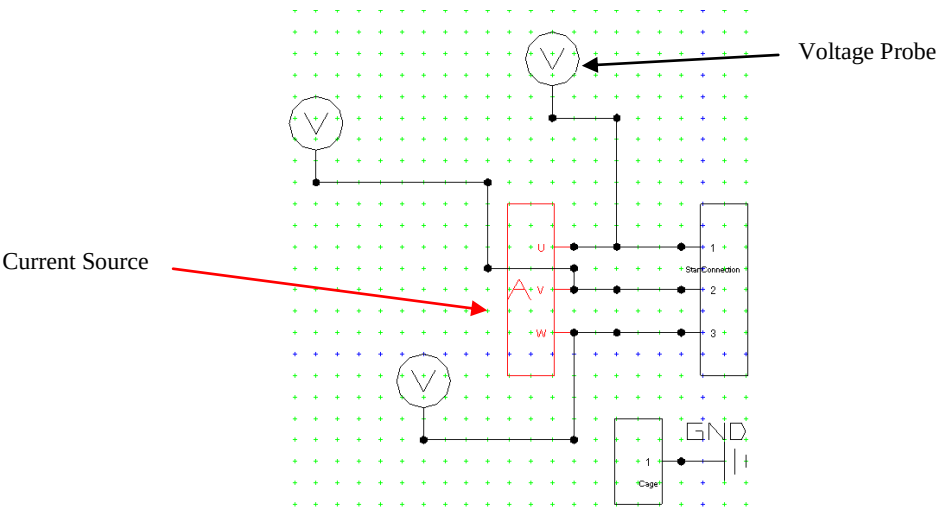

Figure 6.8 Generator circuit model

The magnetisation current is the magnetising component of the no-load current that produces the flux. The active component of the no-load current supplies the rotor friction and windage losses as well as stator iron losses. The stator current at no-load is about 0.3 to 0.5 of full –load current [47].

The magnetising current for the designed ORIM was calculated in Section 5.6 as i_{μ} = 14.17 A which is 37.5 % of the rated current. As Figure 6.9 shows, the amplitude of 20 A is set in JMAG for the designed outer rotor generator in this project to get the desired output voltage.

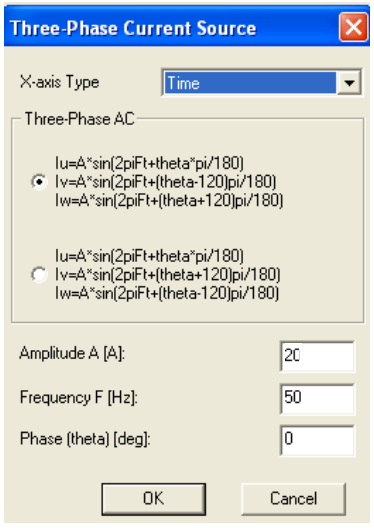

Figure 6.9 Current source setting

6.3.2 Simulation Conditions Setting

Few more conditions are required to be set in JMAG at this stage for the model under analysis in addition to the settings that were set in Motor Template. Stack length is one of the parameters that can be set in the analysis control window. For the model under design the stack length value is set to 0.204 m according to the calculations performed in Section 5.2 in the previous chapter.

Electromagnetic torque is set on the rotor core and bars to calculate the torque in the rotating parts and the default number of iterations is increased to 50 with a convergence tolerance of 0.001 for more precise calculations [73].

As it was mentioned in Subsection 6.2.6, the electromagnetic analysis in JMAG is performed based on the finite element method which needs the creation of meshes. If the physical model of the machine has been created using Motor Template rather than other CAD tools, the meshes are created automatically in JMAG before performing the calculations, as shown in the following figure.

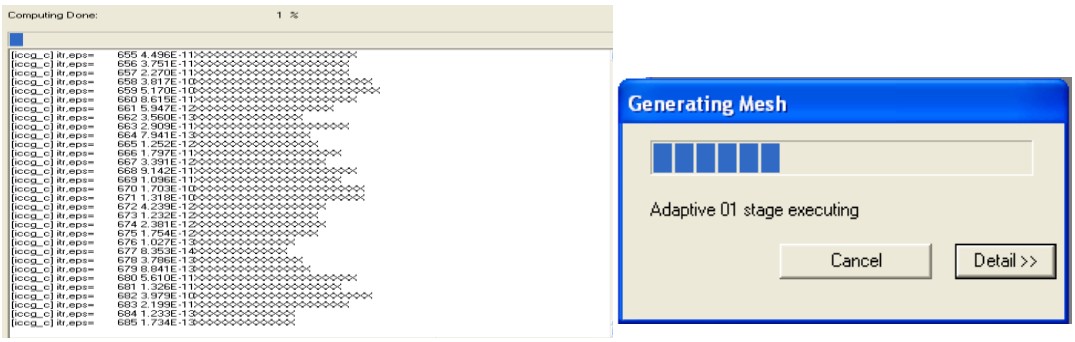

Figure 6.10 Mesh creating stage

6.3.3 Generator Simulation Results

After setting all required parameters in the Motor Template and JMAG, the model is ready to be analysed by JMAG. The simulation results are presented in this subsection to confirm the performance of the designed machine as generator.

6.3.3.1 Generated Voltage

Figure 6.11 shows the generated voltage in the output terminals of the stator coils. First five cycles (1×10^{-1} sec) is the ramping time. The generator voltage sub-transient and transient behaviour occurs before it reaches its steady state, after in about t = 2.6×10^{-1}

sec (260 ms). The rms value of each phase voltage at steady state is calculated using the following equation.

$$V_{ph} = \frac{V_{max}}{\sqrt{2}} \tag{6.8}$$

So, $V_{ph} = \frac{339}{\sqrt{2}} = 239.7\,V$

which is equivalent to 415V line to line (V_{LL}).

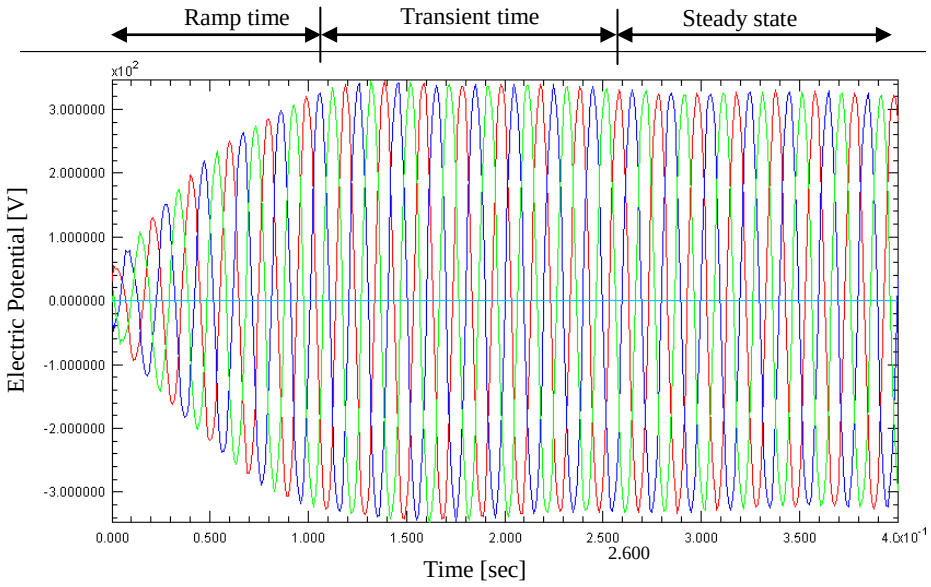

Figure 6.11 Generated output voltage

6.3.3.2 Magnetic Flux Density

Magnetic flux density of the generator components at a ramp and steady state are shown in Figures 6.12 and 6.13 respectively. Since over the ramp period voltage is not built completely, it is expected that flux densities at ramp times have smaller values than steady state.

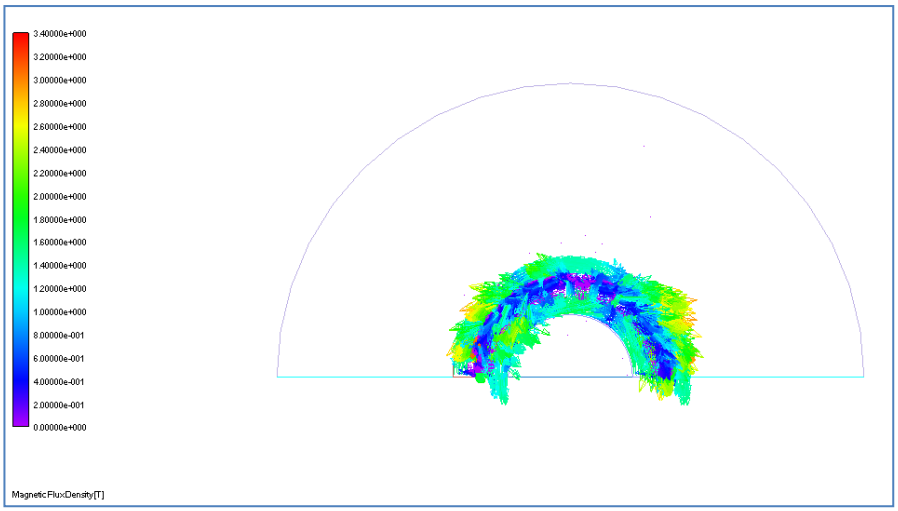

Figure 6.12 Magnetic flux densities at a ramp time[T]

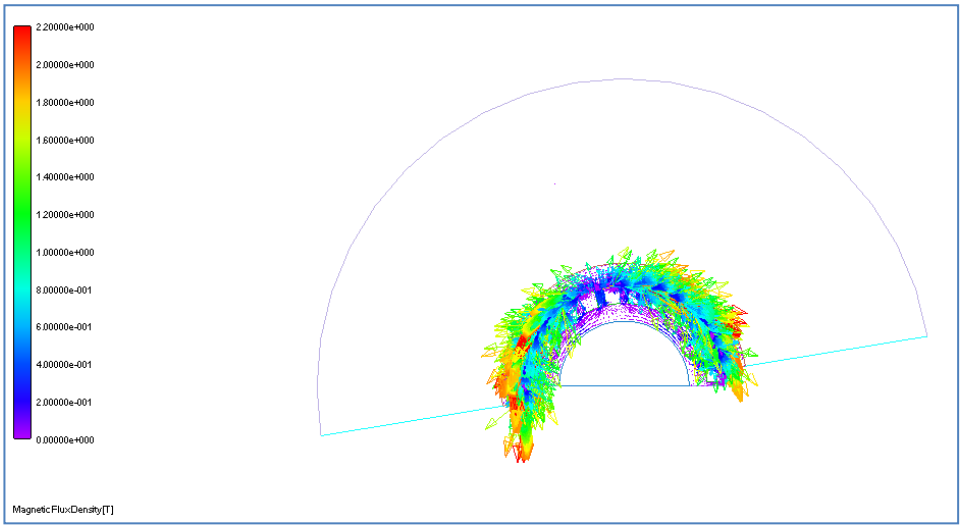

Figure 6.13 Magnetic flux densities at steady state [T]

The values of magnetic flux densities for the generator components calculated in Chapter 5 are summarised in Table 6.4. If these values are compared to the steady state values obtained by JMAG it can be seen that the generator components have smaller values of flux densities. This is because of that the simulated generator works at no-load condition and only magnetising current flows in the stator coils.

Table 6.4 Calculated flux densities of designed machine components

Component	Flux density [T]
Airgap	0.725
Stator tooth	1.55
Stator back core	1.50
Rotor tooth	1.70
Rotor back core	1.65

6.3.3.3 Current Densities

The current densities of the stator coil and rotor bars is shown in Figure 6.14 for the generator in steady state. It is expected that stator coils current density to be below the assigned values in Chapter 5, shown in Table 6.5. The reason is that just stator magnetising current flows in the coils in this simulation.

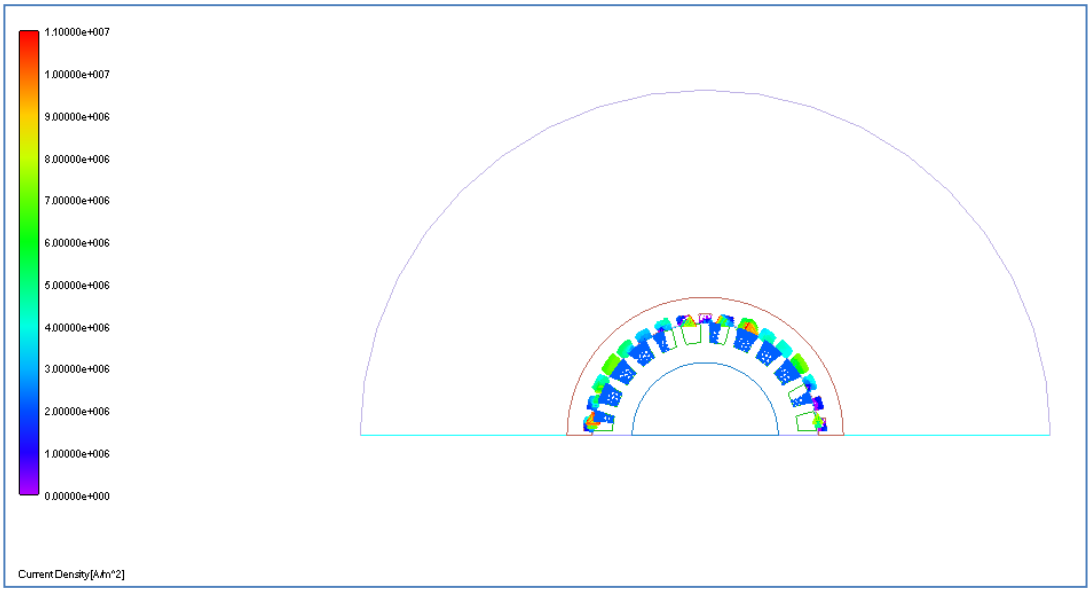

Figure 6.14 Current densities [A/mm^2]

Table 6.5 Allocated current densities of designed machine components

Component	Current density [A/mm^2]
Stator coil	4.5
Rotor bar	3.42

6.3.3.4 Losses

Figure 6.15 shows the generator components losses. The average cage loss at steady state is equal to 680W and the coil loss is equal to 130W. The coil loss can be calculated using Equation (5.95) for the applied current to stator coils with amplitude of 20A as mentioned in Subsection 6.3.1.

The rms value of this current is calculated as $\frac{20}{\sqrt{2}} = 14.14\,\mathrm{A}$, so:

$$P_{Cu} = 3 \times 0.2207 \times 14.14^2 = 132.38\,\mathrm{W}$$

The calculated value of stator copper loss has almost the same value as the simulated value, so the simulation accuracy can be proved in the loss analysis.

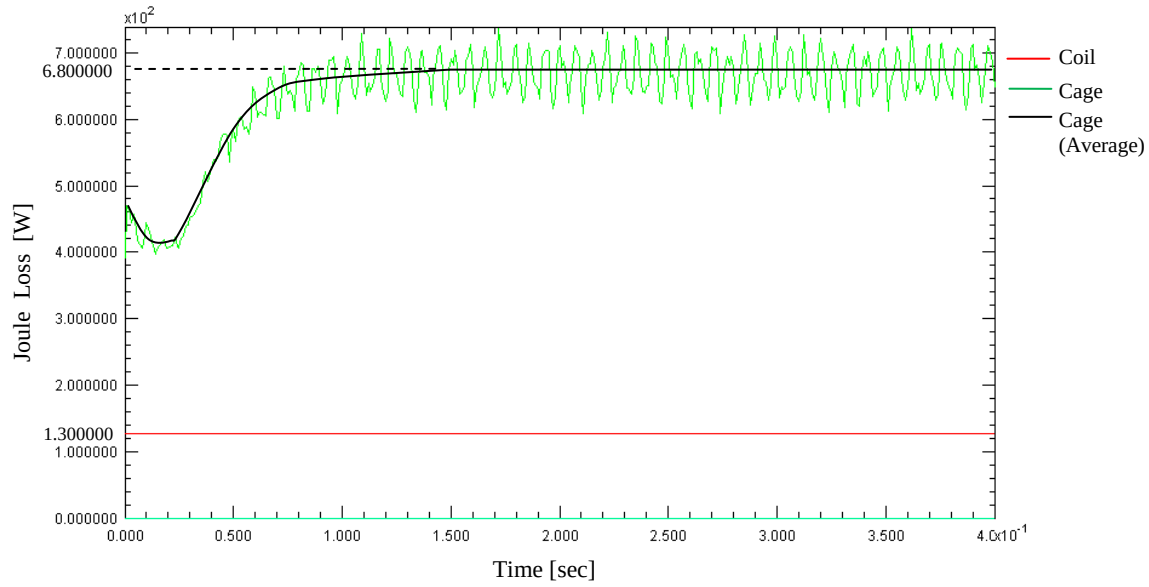

Figure 6.15 Generator components losses

6.4 Analysis of ORIM as the Starter Motor in JMAG

In this section, the machine input circuit is set to make the ORIM operate as the starter motor. Therefore, the input voltage source which was removed in JMAG for the generating mode, explained in Subsection 6.3.1 is required to be connected to the stator coils.

The specifications of the input voltage for the starter motor are determined in the following subsection. The other settings including machine dimensions and material properties remain the same as generator settings. The simulation results for starter motor are shown in Section 6.4.2.

6.4.1 Starter Motor Input Circuit Setting

As it was explained in Chapter 1, the desired speed for the starter motor to run the novel engine from the standstill is 500 rpm with a toque of about 200 Nm. To achieve the required torque at the lower speed than the rated speed of the machine, the voltage and frequency of the power supply have to be changed.

A simple and widely used method to control the mentioned characteristics of the starter motor is constant V/f scalar control. The V/f scalar control can change the torque-speed characteristics of an induction motor as shown in the following figure [53].

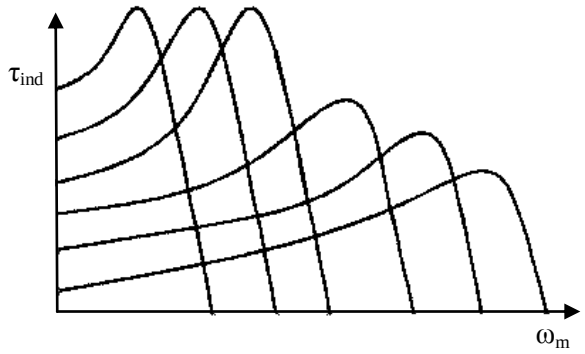

Figure 6.16 Induction motor torque-speed curves achievable by V/f control

To calculate the required frequency and voltage delivered by V/f scalar controller, the breakdown slip is calculated first for the designed motor. As it was explained in Section 5.9 in the previous chapter the breakdown slip can be calculated as:

$$S_{bk} = \frac{C_m R`_r}{\sqrt{R_s{}^2 + (X_{sl} + C_m X`_{rl})^2}} = \frac{1.06 \times 0.221}{\sqrt{0.2207^2 + (0.994 + 1.06 \times 1.2816)^2}} = 0.1$$

The difference between the rated slip S_n calculated in Chapter 5 and S_{bk} is defined as ΔS and its value is calculated as follows.

$$\Delta S = S_{bk} - S_n = 0.1 - 0.034 = 0.066$$

The rated slip for the starter motor is calculated as follows using Equation (3.6). As it is required for starter motor to run at 500rpm, therefore:

$$S_{500} = \frac{1500 - 500}{1500} = 0.67$$

It is supposed that V/f scalar controller does not change the value of ΔS for the starter motor. In this case, the breakdown slip at frequency of f Hz is:

$$(S_{bk})_f = \Delta S + S_{500} = 0.066 + 0.67 = 0.74$$

On the other hand the breakdown torque for the frequency of f Hz, neglecting the skin effect is calculated by the following equation [53] where f_0 represents the rated frequency (50 Hz).

$$(S_{bk})_f = \frac{R`_r}{\sqrt{R_s^{\,2} + (X_{sl} + X`_{rl})^2 \times (\frac{f}{f_0})^2}} \qquad (6.9)$$

To find the required frequency f, the known values are substituted in the equation above as follows.

$$0.74 = \frac{0.221}{\sqrt{0.2207^2 + (0.994 + 1.2816)^2 \times (\frac{f}{50})^2}}$$

which results in f = 4.42 Hz. The rms value of the stator phase voltage for the frequency of f Hz is calculated as follows [53].

$$(V_s)_f = \sqrt{\frac{4(T_{bk})_f \times 2\pi f \left(\sqrt{R_s{}^2 + \left((X_{sl} + X'_{rl}) \times \left(\frac{f}{f_0} \right) \right)^2} + R_s \right)}{3P}} \tag{6.10}$$

It is assumed that the difference between the rated torque and breakdown torque shown by ΔT for f = 4.42 Hz is the same as one for f_0 = 50 Hz. For the rated frequency of 50 Hz,

$$\Delta T = T_{bk} - T_n = 200.18 \text{ Nm} - 144.98 \text{ Nm} = 55.2 \text{ Nm}$$

Therefore the breakdown torque for f =4.42 Hz can be calculated as:

$$(T_{bk})_f = (T_n)_f + \Delta T = 200 \text{ Nm} + 55.2 \text{ Nm} = 255.2 \text{ Nm}$$

Therefore the stator phase voltage at the frequency of f is:

$$(V_s)_f = \sqrt{\frac{4 \times 255.2 \times 2 \times \pi \times 4.42 \times \left(\sqrt{0.2207^2 + \left((0.994 + 1.2816) \times \left(\frac{4.42}{50} \right) \right)^2} + 0.2207 \right)}{3 \times 4}}$$

which gives $(V_s)_f$ = 35.03V. This value is the rms value of the stator phase voltage and its amplitude can be calculated by Equation (6.8) as $30.78 \times \sqrt{2} = 49.54\,\text{V}$.

The amplitude of the input voltage is entered into the Motor Template circuit window as well as the calculated frequency for running the simulation in JMAG.

After several times of simulating the designed machine and viewing the results in JMAG, the required speed and torque was achieved with the amplitude of 50V and frequency of 5Hz for three-phase sinusoidal voltage source of the starter motor.

The input circuit parameters and the stator winding specifications obtained in Chapter 5 for the starter motor is summarised in Table 6.6. These data are required to be entered into the JMAG circuit window.

Table 6.6 Input circuit parameters of the starter motor

Three phase voltage source	Star connection
Frequency	5 HZ
Amplitude	50V
Stator phase resistance	0.2204 Ω
Number of turns per phase	80
End ring resistance	$2.6\times 10^{-6}\,\Omega$
Rotation speed	500 rpm

6.4.2 Starter Motor Simulation Results

In this subsection, the analysis results achieved by JMAG solver are presented to confirm the performance of the starter motor.

6.4.2.1 Torque

The electromagnetic torque generated by the starter motor is shown in Figure 6.17. As this figure shows, the average value of torque delivered by the designed motor is about 220 Nm that is able to start-up the engine from the stop-point according to Section 1.3 in Chapter 1.

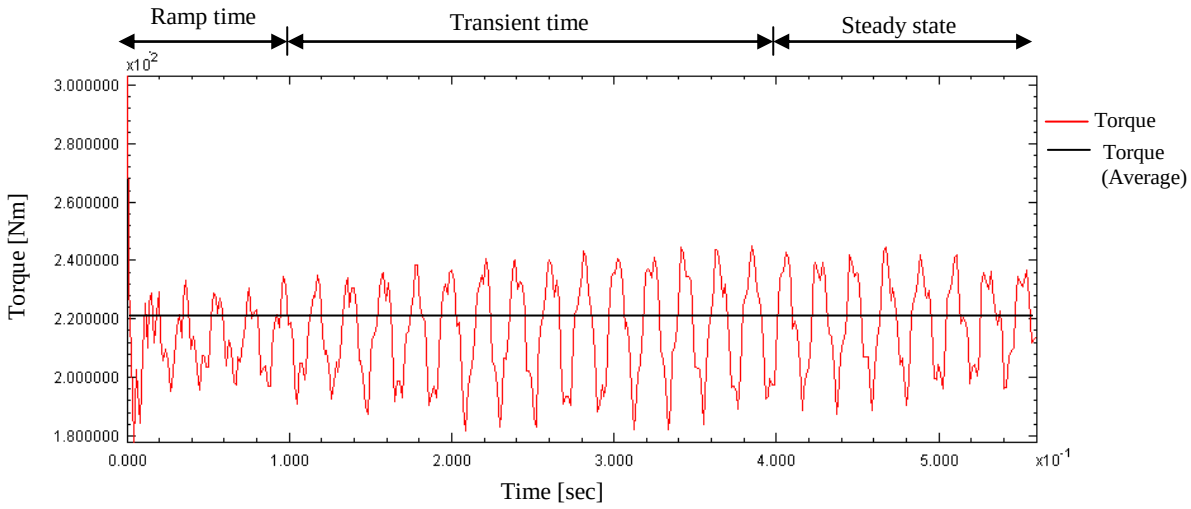

Figure 6.17 Generated torque of the starter motor

As explained in Section 1.3, Chapter 1, the small fluctuation of the torque from the average value (220 Nm), which is less than 10 %, can be damped by the engine while being started.

6.4.2.2 Current Density

The current density of stator coil and rotor bar is shown in Figure 6.18 at start point of the machine. Figure 6.19 shows the machine components current densities at a transient time. It is found out from the JMAG that the current densities decreases after motor started running. This happens because more current is drawn at start point than the steady state by the stator of an induction motor to generate the rotor flux.

As Figure 6.18 shows, stator coils and rotor bars current densities are equal to 2×10^7 A/m^2 (20 A/mm^2) and 6×10^7 A/m^2 (60 A/mm^2) respectively at the start point. These values are compared with the stator and rotor bar current densities of the generator, shown in Table 6.5.

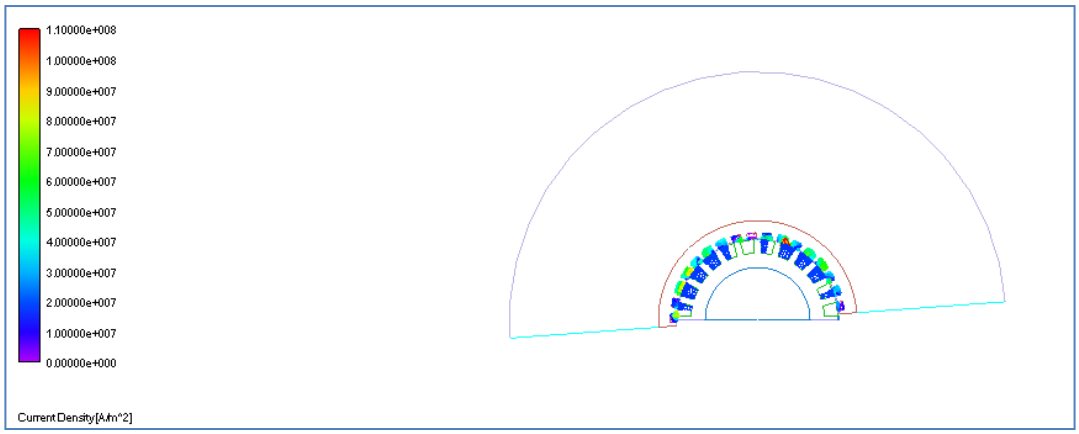

Figure 6.18 Current densities at start point [A/m^2]

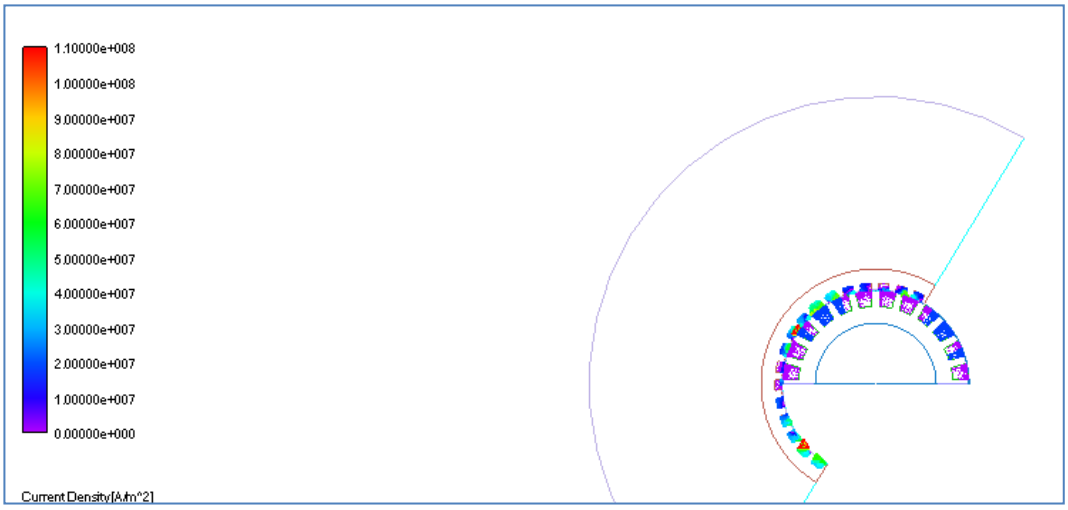

Figure 6.19 Current densities at a transient time[A/m^2]

α_{scr} shows the ratio of stator current density at the starting point of the starter machine to the stator current density of the generator at the steady state and α_{rcr} shows the ratio of rotor bar current density at the starting point of the starter machine to the rotor bar current density of the generator at steady state.

$$\alpha_{scr} = \frac{2\times10^{7}\,\mathrm{A/m^{2}}}{0.454\times10^{7}\,\mathrm{A/m^{2}}} = 4.40$$

and

$$\alpha_{rcr} = \frac{6\times10^{7}\,A/m^{2}}{0.342\times10^{7}\,A/m^{2}} = 17.54$$

It is concluded that the stator and rotor current densities of the starter machine have a magnitude of about 4 and 17 times larger than the generator stator and rotor current densities respectively. This fact occurs only within a fraction of a second for the ORIM and then the starter machine is disconnected from the V/f scalar controller while the engine is starting to rotate. After the engine is started, the ORIM is rotated by the engine and works as a generator.

6.4.2.3 Magnetic Flux Density

Figure 6.20 and 6.21 show the density of magnetic flux in the stator and rotor components of the starter motor in two different positions. The first figure shows the flux densities when the starter machine starts running, i.e. t = 0 sec and the second figure is within a transient state (t=0.06 sec).

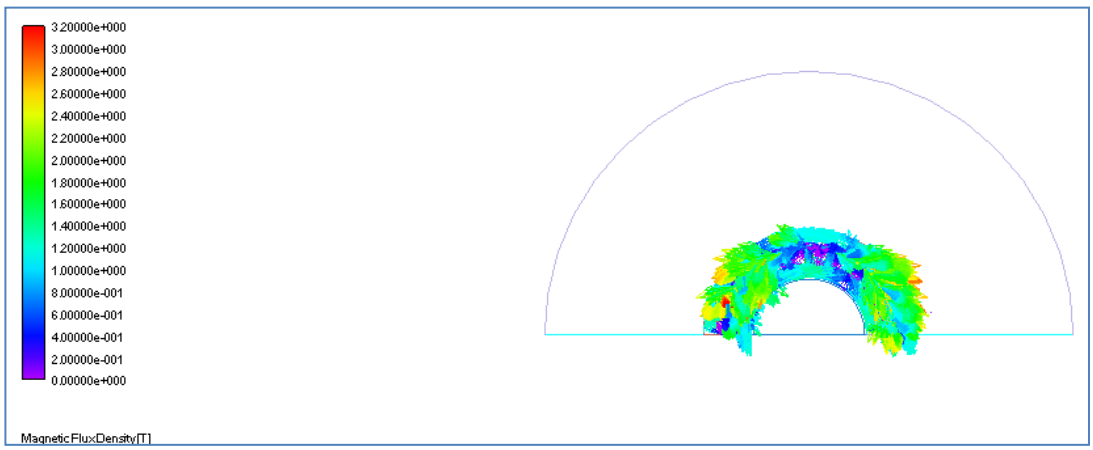

Figure 6.20 Magnetic flux density – start point [T]

As expected, the magnetic flux density in the transient state of the starter motor, as shown in Figure 6.21, is higher than the magnetic flux density tabulated in Table 6.4.

This is because of the higher current taken by the stator coils in the starting mode of the induction machine. The maximum calculated flux density by JMAG for the designed starter is equal to 3.2 T.

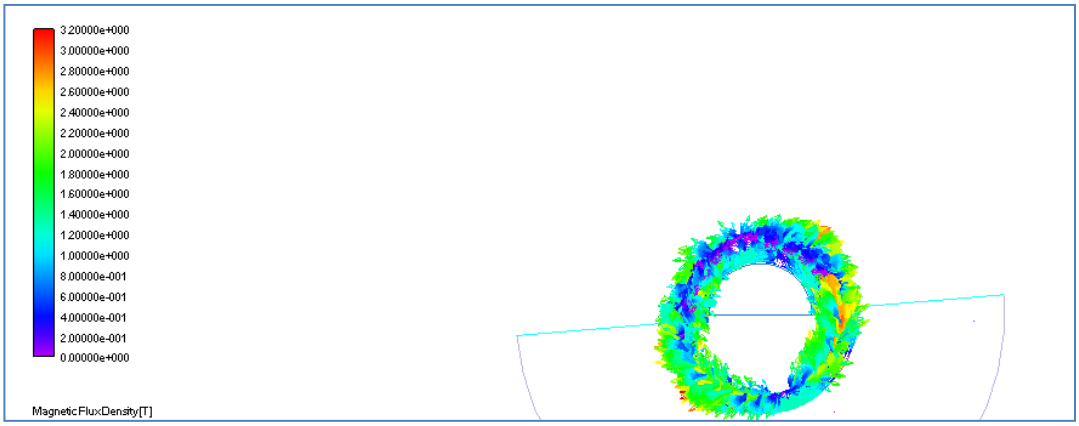

Figure 6.21 Magnetic flux density- a transient time [T]

6.4.2.4 Losses

The value of the power dissipated in the starter machine while it is trying to start-up the novel engine is shown in Figure 6.22.

The losses figure can be divided into transient and steady state parts. The transient period starts from t = 0.1 sec and continuous to t = 0.4 sec. and the steady state period starts from t = 0.4 sec.

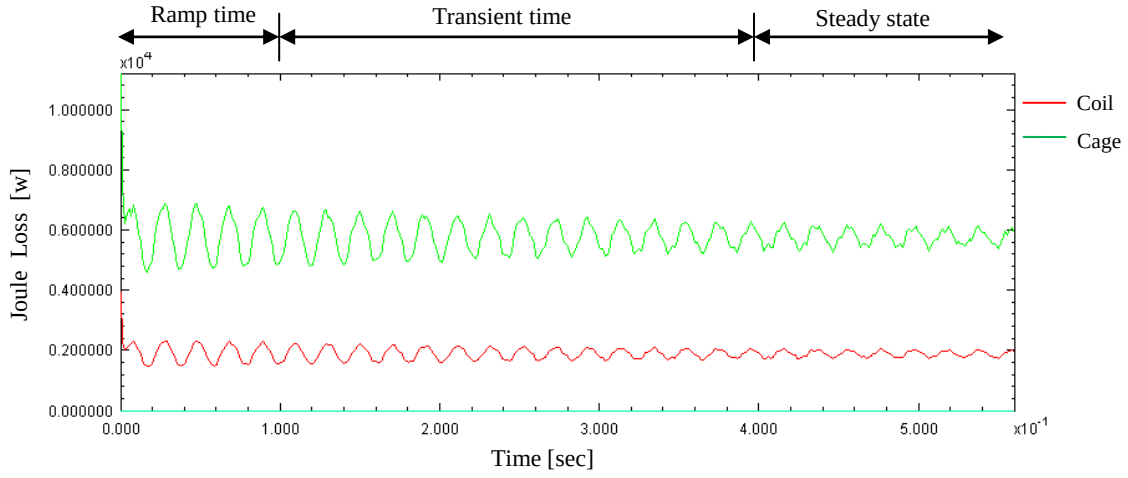

Figure 6.22 Starter machine losses

The average value of the rotor cage loss of the starter machine in the transient period is almost equal to the steady state value (0.6×10^4 W), as shown in Figure 6.22. The steady state value of rotor cage losses of the starter machine can be compared to the rotor cage losses of the generator at the steady state, calculated by Equation (5.96) in Section 5.8. The result is shown as follows where α_{rlr} represents the ratio of this comparison. The starter machine has 7.49 times larger rotor losses than the generator.

$$\alpha_{rlr} = \frac{0.6 \times 10^4 \text{W}}{801.219 \text{W}} = 7.49$$

The dissipated power in coil is equal to 0.2×10^4 W in both transient and steady states as shown in Figure 6.22. If this value is compared with the stator coil losses calculated in Section 5.8 for the steady state it is found that the starter coil dissipates 2.1 times higher power than the generator in steady state. This is shown by α_{slr} in the following division.

$$\alpha_{slr} = \frac{0.2 \times 10^4 \text{W}}{945.334 \text{W}} = 2.1$$

The stator coil and rotor cage high losses for the starter motor occurs only within a fraction of a second and then the starter machine is stopped by the V/f scalar controller after the engine is started. Then, the engine rotates the ORIM in order to operate as a generator.

6.5 Summary

In this chapter, the finite element software JMAG-Studio was introduced and used for analysis of the designed electric machine. The procedures of creating the shape of the

machine, material properties and circuit setting were explained. Finally, the operation performances of the designed induction machine were simulated for the starting and generating modes. The simulation results confirm that the designed machine meets the required specifications, determined in Chapters 1 and 2 and so is able to work as a starter motor or generator. In the next chapter the performance of the compact power pack is analysed.

Chapter 7 Performance Analysis of the Genset

In Chapter 2, the powertrain components of the series hybrid electric vehicle were sized and then, the proposed generator for this vehicle was designed and simulated in Chapters 5 and 6 respectively.

In this chapter, the performance of the Genset, which is supposed to operate as a power pack in the series HEV, is analysed. As it was explained in Chapter 1, the Genset is a power unit that includes the novel engine and ORIM providing the required energy to charge the batteries of the vehicle.

The performance of the power pack, designed in this project is compared to different types of power packs with the same size and for the same hybrid electric vehicle. Two main characteristics that form the operation performance of hybrid vehicles are their emissions and fuel consumption. The state of charge history of the battery pack can also show the capability of the designed generator.

ADVISOR is one of the most commonly used vehicle simulators and it is utilised in this project to analyse the HEV performance. This powerful simulator quantifies the main performance criteria of the HEV and the powertrain components. ADVISOR includes data, script files and models of the HEV components and works in the MATLAB/Simulink environment. More details about this program are given in Appendix A.

7.1 Procedure of the HEV Performance Analysis

Figure 7.1 shows the analysing procedure of the series hybrid vehicle equipped with ORIM or with different types of power packs available in ADVISOR.

One of the main specification data of the generator that is required is the generator efficiency map. This map is the efficiency data matrix of the electric machine and it has to be calculated for the designed ORIM and added into the corresponding MATLAB data file for the machine.

After calculating the efficiency map, the specification of the ORIM and the HEV, calculated in Chapter 2, are tabulated. These organised data are used in the associated MATLAB script files of the HEV components and entered via the input screen to perform the first step of simulation.

The HEV performance analysis is continued by simulating the HEV, equipped with Genset or with other types of power packs available in ADVISOR. Finally, the simulation results shown in the results screen are analysed and compared in order to distinguish between the operation characteristics of the Genset and the other power packs.

7.1.1 ORIM Efficiency Map

The efficiency map of the ORIM is a two-dimension lookup table indexed by output torque in column and rotor speed in row, containing the power losses of the generator. The lookup table executes two-dimension linear interpolation of the output torque and rotor speed values with generator input power map table. It also does extrapolation calculation for values which are out of the table.

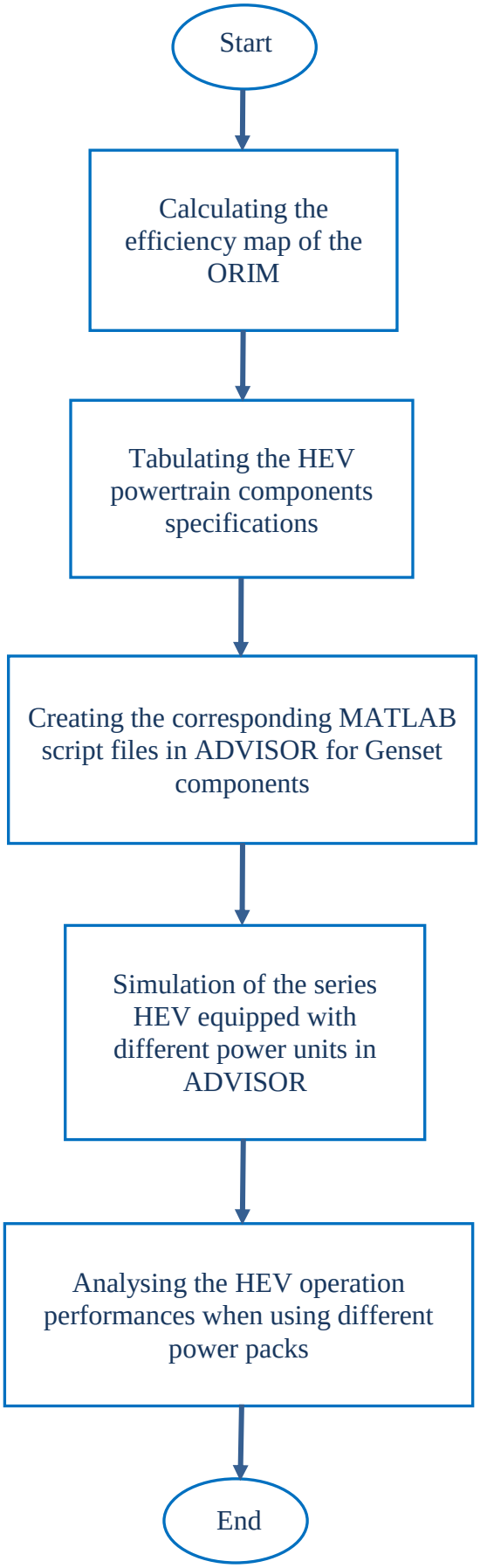

Figure 7.1 HEV analysis procedures

To compute the efficiency matrix or map of the designed machine, two vectors of the speed and torque of the machine are defined based on the designed machine characteristics achieved in Chapter 5. The toque and speed vectors correspond to the columns and rows of the efficiency map respectively.

Figure 7.2 shows the torque-speed characteristics of the designed ORIM which is similar to the expected torque-speed curve shown in Figure 3.14 in Chapter 3. In order to start the engine, the motoring characteristics (dashed curve) is changed to the starter motor curve by constant V/f scalar controller to provide the required 200 Nm at 500 rpm, as explained in Section 6.4.1 and shown in Figure 6.16.

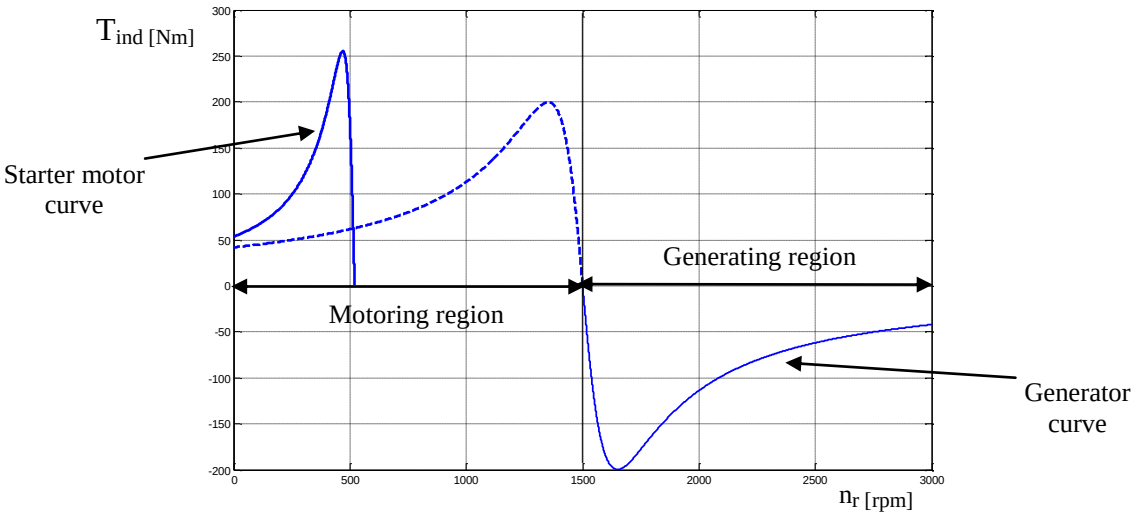

Figure 7.2 Torque-speed characteristics of the ORIM

The efficiency map of the designed ORIM is also provided by the MATLAB script file and shown in in Section B.2, Appendix B. It is assumed that efficiency at zero speed and torque are the same as nearest neighbours. The calculated efficiency map for ORIM is added into the corresponding MATLAB script file called GC_ORIM.m, presented in Appendix C. The GC_ORIM.m is the file that contains the designed generator specifications and interacts with the associated Simulink block diagram of the generator model in ADVISOR.

7.1.2 HEV and Genset Parameters

The powertrain components of the series hybrid electric vehicle sized in Chapter 2 are tabulated as follows.

Table 7.1 HEV powertrain components specifications

	Component	Type	Power [KW]	Efficiency [%]	Mass[Kg]
Genset	Fuel converter	Novel SI Engine	41	45	100
	Generator	ORIM	22	90	45
	Drive motor	Induction	90	91	119
	Battery pack	NiMH-Ovonic	No. of modules 31	Voltage 372	164

The specifications of the vehicle which utilise the ORIM as its auxiliary power unit are also shown in the following table.

Table 7.2 Hybrid vehicle specifications

Vehicle Specification	Value	Units
Configuration	____	Series
Mass	1250	Kg
Aerodynamic coefficient	0.2	____
Frontal area	2.0	m^2
Maximum speed	110	Km/h
Acceleration (0-100Km/h)	15	Sec.
Gradibility at 45Km/h	30	%

The MATLAB script file of the second component of the Genset, i.e novel engine, that contains its specifications, is named as FC_SI41_New and presented in Appendix C. The MATLAB script files of the other powertrain components of the HEV are also

presented in Appendix D. The MATLAB files of the HEV components interact with the related Simulink block diagrams of the components model during simulation.

7.1.3 HEV Performance Analysis

The procedure of the HEV Performance Analysis is continued by simulating the series hybrid vehicle using different types of power packs in ADVISOR. To run the simulation, the HEV components are selected in the input screen firstly. Then, the standard urban and highway drive cycles are chosen and the other simulation parameters are set too. The HEV includes a different type of power pack for each simulation. The simulation results are shown in the results screen.

The HEV analysis procedure ends with the studying and comparing the simulation results to recognise the characteristics and advantages of the novel Genset applied to the series HEV. The simulation results are presented in the following section.

7.2 HEV Simulations in ADVISOR

Three different types of power pack consisting of fuel converter and generator are applied separately to the vehicle. After quantifying the main performance criteria for the HEV equipped with the Genset or other types of power unit, the performance of the power packs are compared.

7.2.1 Input Parameters and Simulation Settings in ADVISOR

Figure 7.3 shows that a series configuration is selected for the analysis. The Genset components are added to the list boxes in the GUI input screen and the vehicle components, including Genset, can then be selected. The corresponding variables data are also entered into the text boxes in accordance with Tables 7.1 and 7.2.

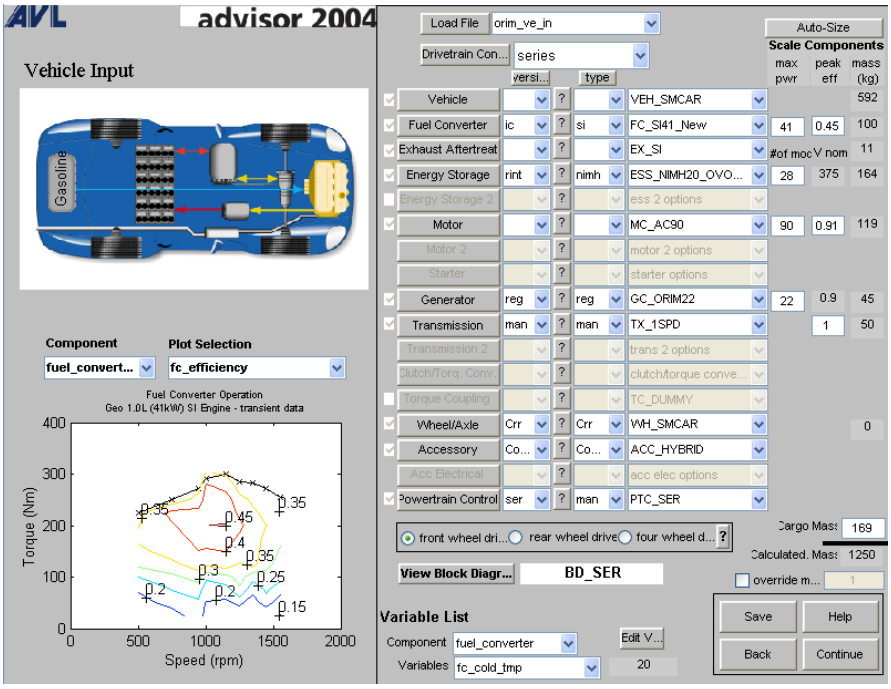

Figure 7.3 ADVISOR input GUI screen for the series HEV equipped with Genset

As it was explained in Subsection 2.5.3, Ovonic 12HEV20 nickel metal hybrid battery is chosen in this project for the series HEV.

One induction and one permanent magnet generator, available in ADVISOR have the closest, but a higher power value, than the author's designed 22 KW ORIM. These three machines have been selected for simulation and comparison of the results with each other. The novel engine, shown by SI_41_New in Figure 7.3, is selected with ORIM and the small SI engine is chosen with PM and IM generators in the corresponding GUI screens. Both engines are of the spark ignition type and have the same power values.

The size of the selected induction and permanent magnet generators are 25 KW and 32 KW respectively but their size can be scaled to 22 KW in the input GUI screen. The corresponding MATLAB files of these generators which are named as GC_IM22.m and GC_PM22.m are presented in Appendix D. The same weight is considered for the 22 KW ORIM as the 25 KW ordinary induction machine.

The specification of the vehicle components are listed in Table 7.3.

Table 7.3 The series HEV components specifications

Component	Description
Vehicle	Small car
Fuel Converter	41 KW SI novel engine (for ORIM) or 41 KW SI engine (for IM and PM)
Exhaust Aftertreat	Standard catalyst for SI engine
Energy Storage	Ovonic 20 Ah, 12V NiMH HEV battery module
Motor/Controller	GE 83 KW AC induction motor/inverter (scaled to 90 KW in ADVISOR)
Generator/Controller	(1) 22 KW ORIM Induction generator or (2) Unique Mobility 32 KW permanent magnet generator (scaled to 22 KW in ADVISOR) or (3) Solectria ACgtx 25 KW AC Induction generator (scaled to 22 KW in ADVISOR)
Transmission	1-speed transmission
Wheel/Axle	Wheel/axle assembly for small car
Accessory	700 W constant electric load
Powertrain Control	Series hybrid Powertrain control

As it was mentioned in Subsection 2.4.1.1, series hybrid electric vehicles do not need a complex transmission because electric machines can move the vehicle within a wide range of speeds efficiently. Since the selected traction motor for the vehicle is an AC electric machine, thus the single-speed transmission is selected for the vehicle. The selected wheel/axel and accessories are appropriate with the selected small car.

ADVISOR checks the compatibility of the selected components and if a component is not compatible with the others, the user is informed by the mismatched component warning box. In this case, user can allow ADVISOR to resize the component appropriately.

The standard city and high way drive cycles are set in simulation parameters screen for simulation of the HEV in ADVISOR. Figure 7.4 and 7.5 show the drive cycles that are utilised to test the HEV when it drives along them.

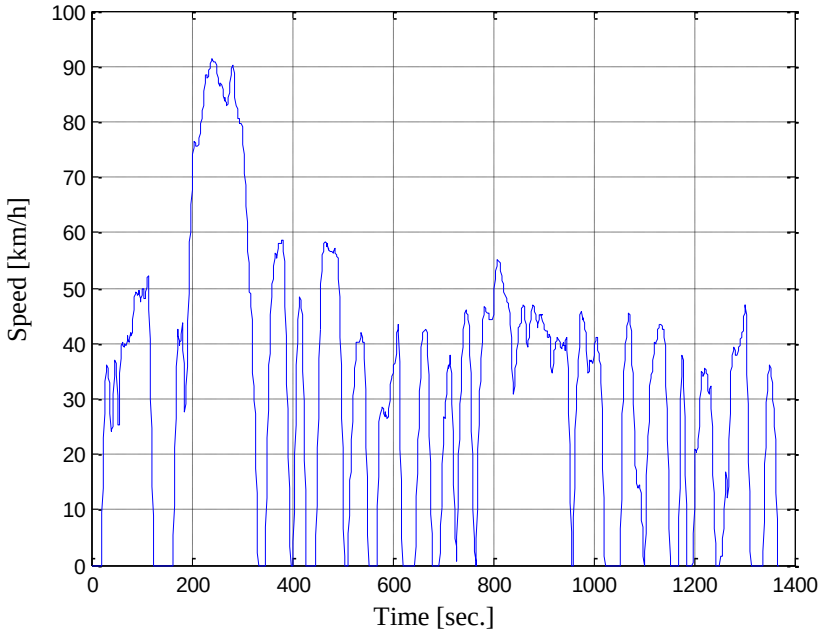

Figure 7.4 UDDS city drive cycle

The drive cycle shown in Figure 7.4 represents the Urban Dynamometer Driving Schedule (UDDS) which is the same as the first two bags of the Federal Test Procedure (FTP-75) and it is used for light duty vehicles.

The drive cycle shown in Figure 7.5 represents the Highway Fuel Economy Test (HWFET) driving cycle used by the United States Environmental Protection Agency (EPA) for Corporate Average Fuel Economy (CAFE) certification of passenger vehicles in the US.

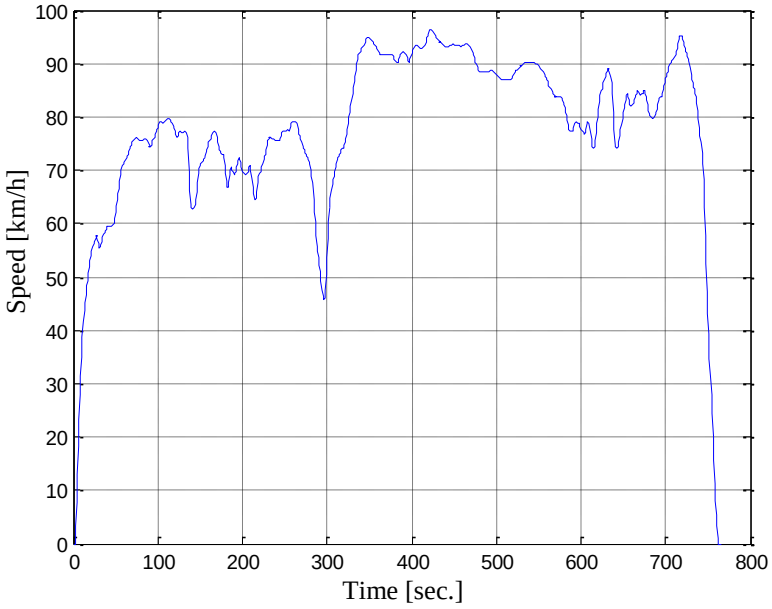

Figure 7.5 HWFET highway drive cycle

The performance of the HEV is also analysed for the combination of the city and highway drive cycles which is called trip drive cycle. Figure 7.6 shows the created trip drive cycle. MATLAB files of the all drive cycles explained above are presented in Appendix D.

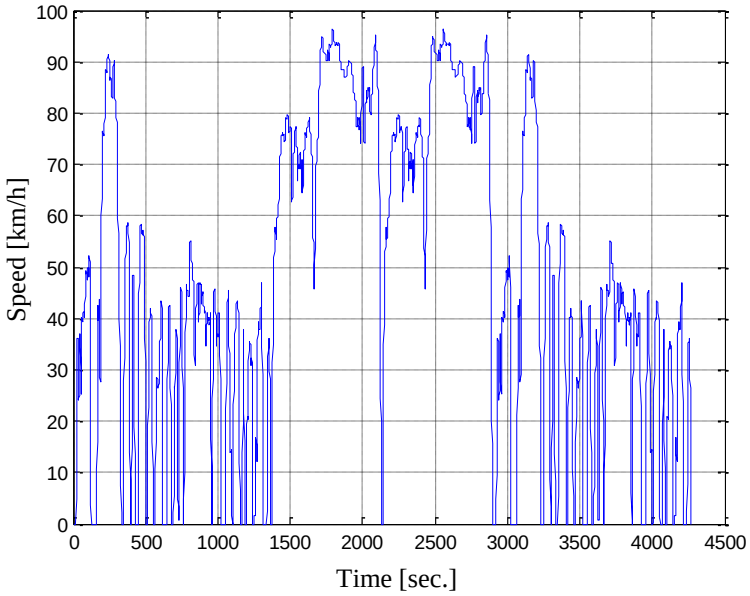

Figure 7.6 Trip drive cycle created in ADVISOR

Figure 7.7 shows the acceleration and gradibility tests parameters that are set before simulation. These settings are based on the information that is desired to be shown in the results screen.

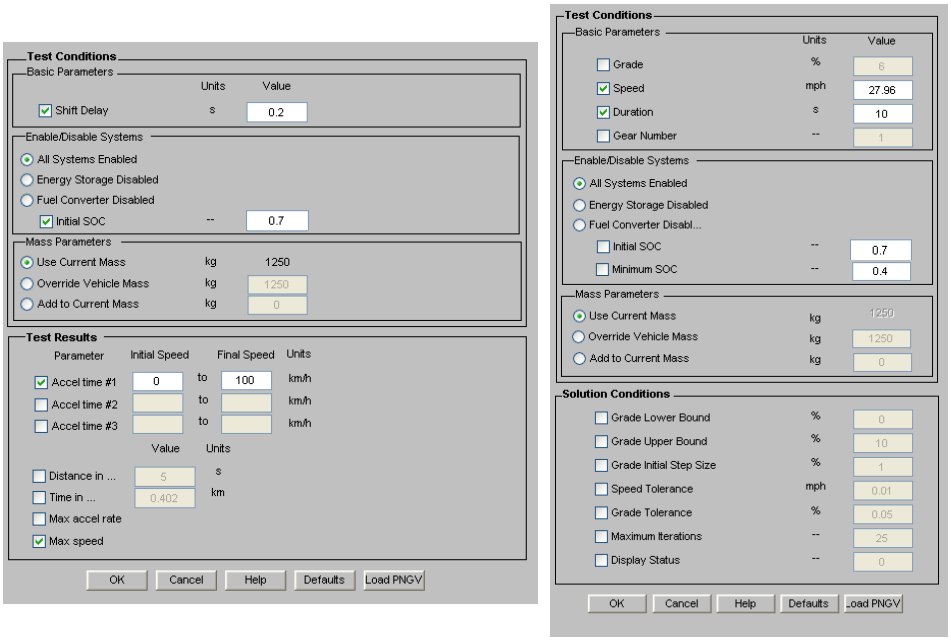

Figure 7.7 Simulation parameters setup in ADVISOR

To simulate the vehicle over city and highway cycle, 3.5 cycles of the UDDS and 5 cycles of the HWFET are applied to the vehicle to see the capability of the Power pack

over the long distance and also avoid zero emissions event. In the zero emissions occasion vehicle run all-electric and no fuel used.

7.2.2 HEV Simulation Results

In the following subsections, the HEV simulation results are shown. The HEV is simulated over various drive cycles including city, highway and a combined drive cycle, named trip. Simulations are performed when different types of power pack, including Genset (ORIM with the novel engine), PM generator with the small engine and finally IM generator with the small engine are applied to the HEV. The Specifications of the power packs and the other components of the vehicle are determined from Table 7.3 over the simulations.

7.2.2.1 City and Highway Simulation Results: ORIM

In this section the HEV utilising the ORIM generator and novel engine is simulated over the city and highway drive cycles. First, the HEV equipped with the designed Genset is simulated for the city cycle. Figure 7.8 shows the simulation results when 3.5 cycles of the UDDS city drive cycle is applied.

The first time-dependant plot from top shows the actual speed in Km/h achieved by the vehicle and confirms that there is no trace missed by the HEV. This means all the required speeds of the cycle, shown in Figure 7.4 were attained by the vehicle. The distance travelled through the cycles is 42.8 Km and the fuel consumption of the vehicle is 7.2 L/100Km which equals to the fuel economy of 32.5 mpg.

The vehicle can speed up from 0 - 100 Km/h in 7.9 seconds which is greater than the specified acceleration in Table 7.2. The maximum speed achieved by the vehicle is also

156.6 Km/h which is about 1.5 times greater than the specified value for the HEV. The calculated gradeability of the vehicle is also over the required value specified in Table 7.2.

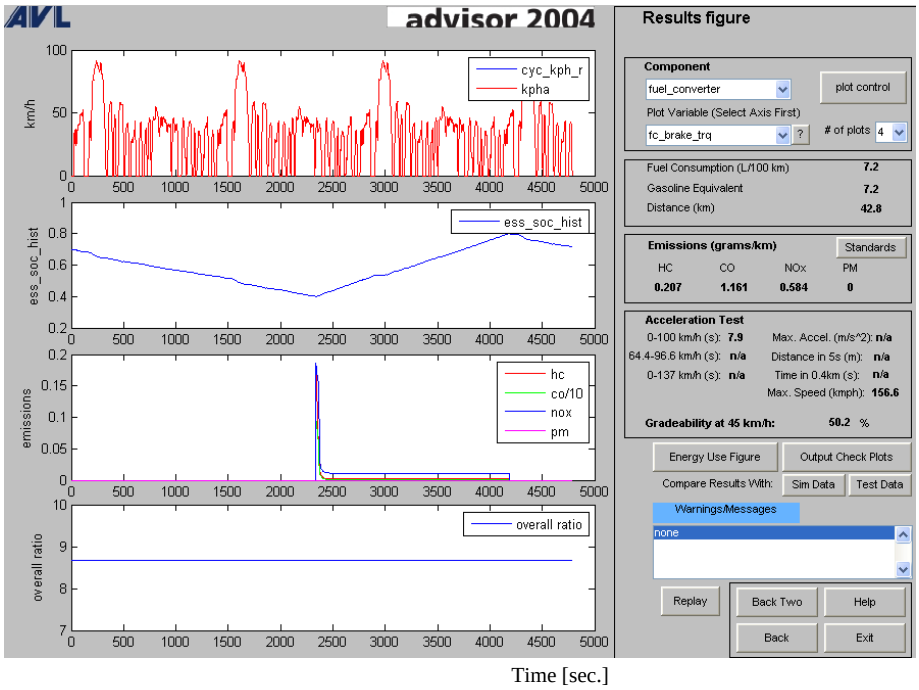

Figure 7.8 City cycle simulation results for the HEV equipped with the Genset

The second graph shows the state of charge history of the energy storage. The initial value of the SOC of the battery is 0.7 and the minimum and maximum states of charges are set to 0.4 and 0.8 respectively as ADVISOR default values. The result shows that the battery pack starts being charged by ORIM generator when it reaches its minimum state of charge at about t=2400 sec. The charging process continuous until battery reaches its maximum allowed state of charge.

The exhaust emissions including HydroCarbons (HC), Carbon Monxide (CO), Nitrogen Oxides (NOx) and Particular Matter (PM) emissions are displayed in ADVISOR simulation results screen. The emissions are calculated in grams/Km as shown in Figure 7.8. The results show that the values of emissions are acceptable according to the emission standards presented in Appendix E.

As the last plot in Figure 7.8 shows, the gear ratio has a constant value at different positions of the vehicle because the single speed transmission is used in the series HEVs as it was explained in Subsection 7.2.1.

Figure 7.9 shows the energy used by the components of the HEV in power and regenerative modes over the city cycle. The most of the energy is dissipated in the fuel converter compared to the other components. The energy stored in the battery pack at the end of the cycle is 147 KJ and the overall efficiency of the system is 7.2 %.

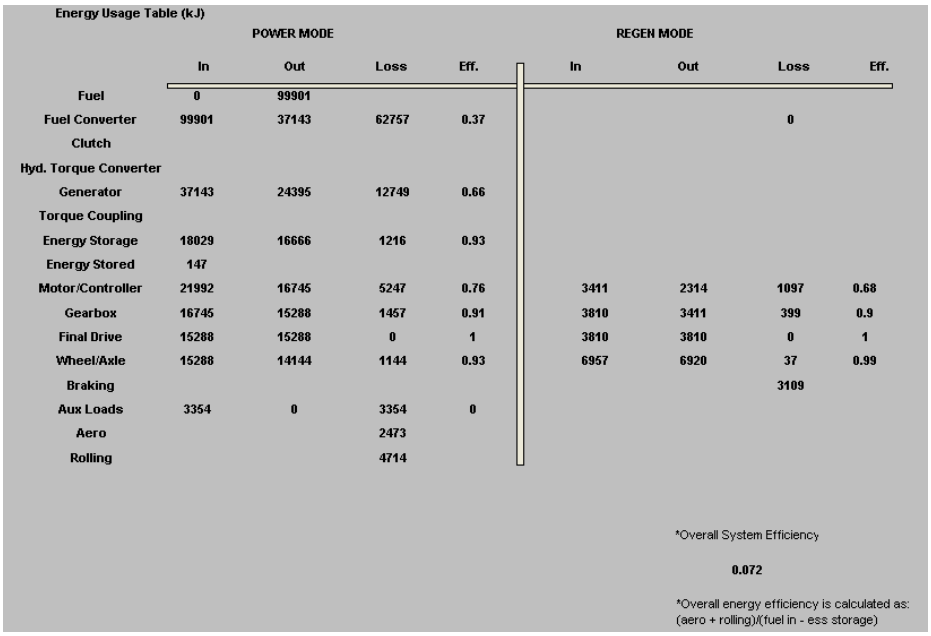

Energy Usage Table (kJ)

	POWER MODE				REGEN MODE			
	In	Out	Loss	Eff.	In	Out	Loss	Eff.
Fuel	0	99901						
Fuel Converter	99901	37143	62757	0.37			0	
Clutch								
Hyd. Torque Converter								
Generator	37143	24395	12749	0.66				
Torque Coupling								
Energy Storage	18029	16666	1216	0.93				
Energy Stored	147							
Motor/Controller	21992	16745	5247	0.76	3411	2314	1097	0.68
Gearbox	16745	15288	1457	0.91	3810	3411	399	0.9
Final Drive	15288	15288	0	1	3810	3810	0	1
Wheel/Axle	15288	14144	1144	0.93	6957	6920	37	0.99
Braking							3109	
Aux Loads	3354	0	3354	0				
Aero			2473					
Rolling			4714					

*Overall System Efficiency

0.072

*Overall energy efficiency is calculated as: (aero + rolling)/(fuel in - ess storage)

Figure 7.9 HEV components energy usage data over UDDS when using Genset

Figure 7.10 shows the simulation results for the HEV equipped with the Genset and when 5 cycles of the HWFET highway drive cycle, shown in Figure 7.5, are applied.

Since in the highway cycle, the vehicle travels longer distance with a higher speed in each sub-cycle and also the highway cycle has fewer stop points compared to the city cycle, the battery is discharged in a shorter time. The battery pack reaches its minimum allowed state of charge at about t=1200 sec. which is half of the discharge period for

the city cycle because city cycle gives batteries longer time of rest between discharge demands. Because of the same reasons mentioned above it also takes longer time for the battery to be charged over the highway mode.

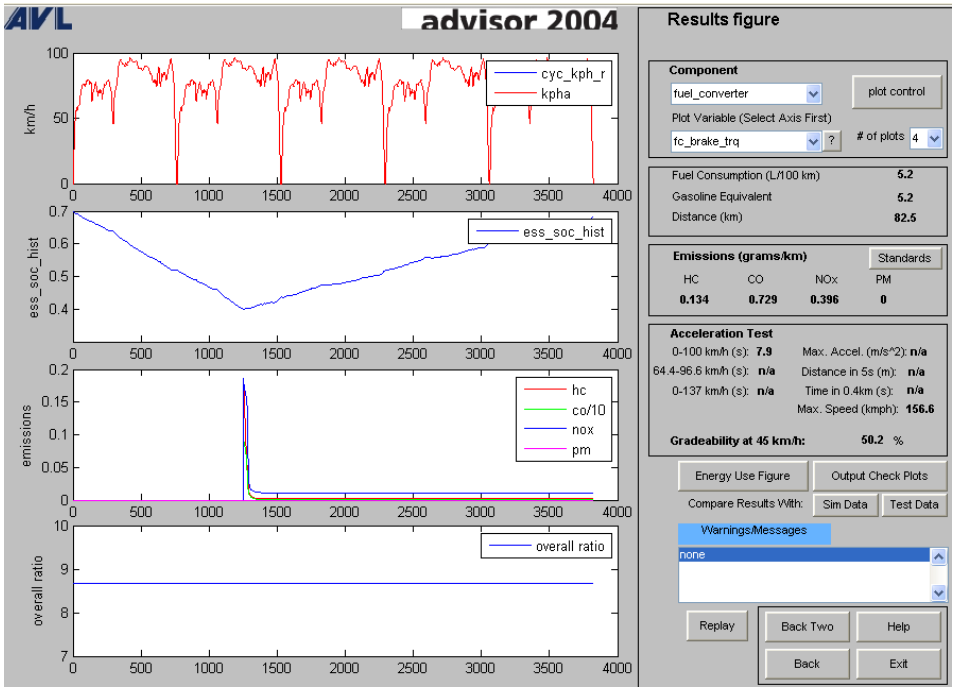

Figure 7.10 Highway cycle simulation results for the HEV equipped with Genset

Fuel consumptions and exhaust emissions for the highway cycle are calculated and the simulation results are shown in the figure above. As it was expected, vehicle consumes less fuel and has less exhaust emission in the highway than the city because of the fewer stop points over the highway cycles.

Figure 7.11 shows the energy used by the components of the HEV in power and regenerative modes in the highway cycle. The overall efficiency of the system is 14.4 %.

Energy Usage Table (kJ)

	POWER MODE				REGEN MODE			
	In	Out	Loss	Eff.	In	Out	Loss	Eff.
Fuel	0	136998						
Fuel Converter	136998	51022	85976	0.37			0	
Clutch								
Hyd. Torque Converter								
Generator	51022	33510	17512	0.66				
Torque Coupling								
Energy Storage	13150	12901	843	0.94				
Energy Stored	-595							
Motor/Controller	31962	28095	3867	0.88	1735	1377	357	0.79
Gearbox	28095	24855	3240	0.88	2017	1735	282	0.86
Final Drive	24855	24855	0	1	2017	2017	0	1
Wheel/Axle	24855	22867	1988	0.92	3097	3046	52	0.98
Braking							1029	
Aux Loads	2678	0	2678	0				
Aero			10671					
Rolling			9098					

*Overall System Efficiency

0.144

*Overall energy efficiency is calculated as: (aero + rolling)/(fuel in - ess storage)

Figure 7.11 HEV components energy usage data over HWFET when using Genset

7.2.2.2 City and Highway Simulation Results: PM Generator

In this section, the vehicle is simulated when it is equipped with a permanent magnet generator and ordinary fuel converter with the same powers as the Genset components.

As Figure 7.12 shows, the selected PM generator has less weight than the ORIM but fuel converter is heavier than the novel engine. If the rest of the components shown in Figure 7.3 are reviewed, it is seen that the other components of the HEV remain unchanged for this simulation.

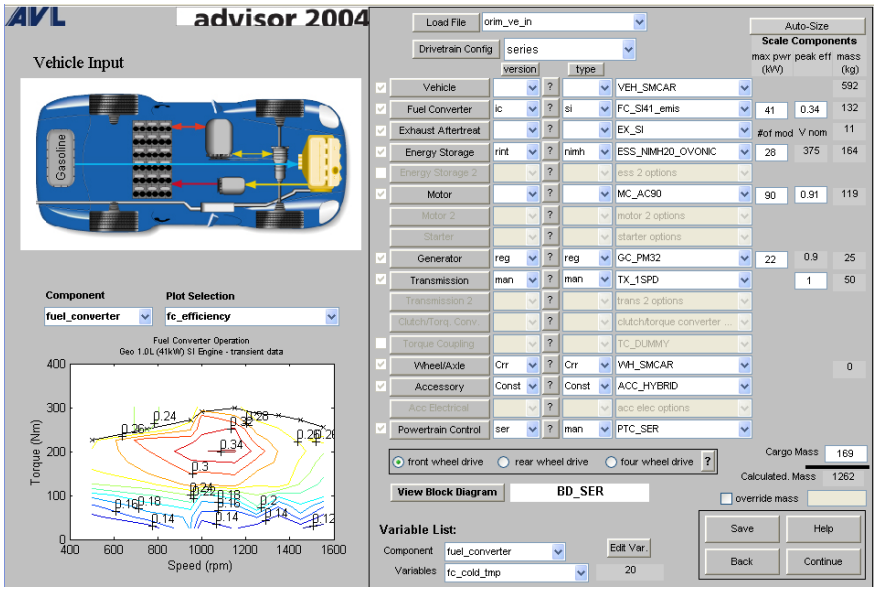

Figure 7.12 ADVISOR input GUI screen for the series HEV equipped with PM and SI_41

Figure 7.13 shows the simulation results for the HEV when it uses the permanent magnet generator over the city cycle.

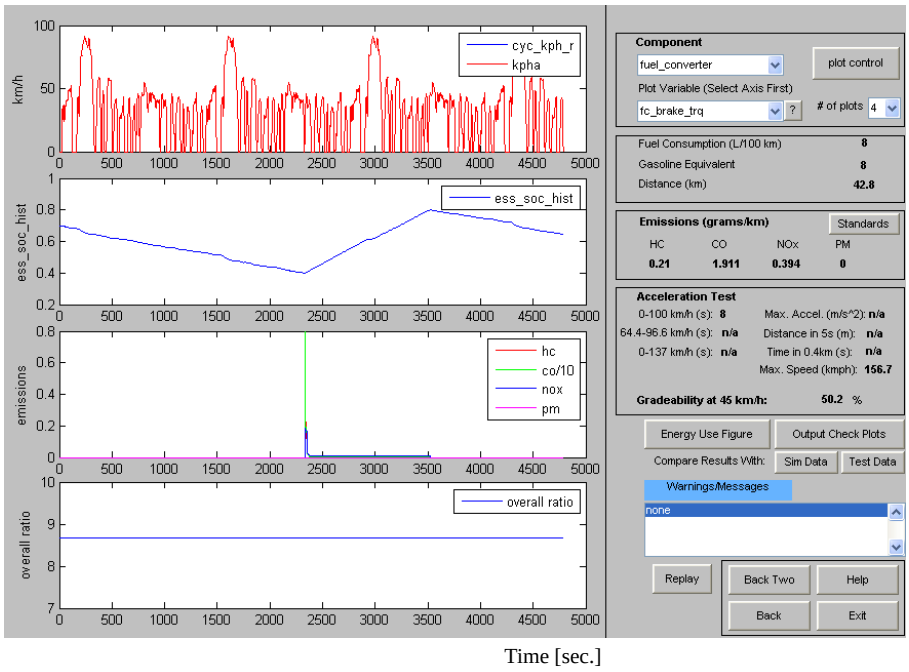

Figure 7.13 City cycle simulation results for the HEV equipped with PM and SI_41

If the simulation results shown above are compared with the results shown in Figure 7.8 for the Genset, it is concluded that the HEV equipped with ORIM and novel engine consumes less fuel and has lower missions over the city cycle.

The number of the charge and discharge cycles for the battery pack fed by PM charger shown in Figure 7.13 for the longer periods would be more than that for the battery pack fed by Genset. This means that the batteries fed by Genset will have a longer lifetime because in fact lifetime of the batteries is the number of discharge cycles obtainable in their lifetime [26].

The acceleration, maximum speed and gradeability capabilities of the HEV equipped with PM generator are the same as ones for the vehicle utilises Genset.

The efficiency achieved by the fuel converter as well as the overall efficiency of the system in the current simulation, shown in the following figure, is also lower than the one shown in Figure 7.9 for the HEV using the Genset.

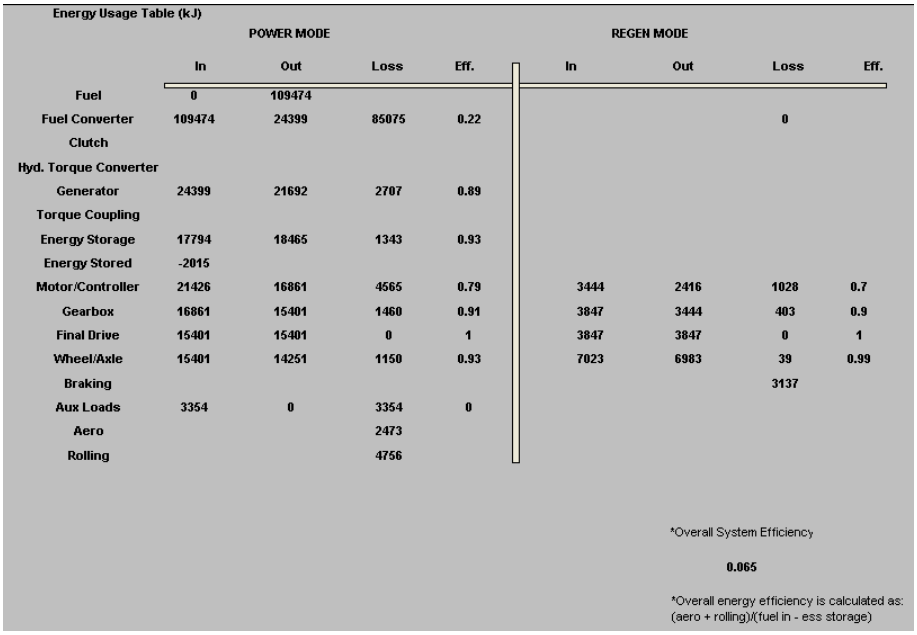

Energy Usage Table (kJ)

	POWER MODE				REGEN MODE			
	In	Out	Loss	Eff.	In	Out	Loss	Eff.
Fuel	0	109474						
Fuel Converter	109474	24399	85075	0.22			0	
Clutch								
Hyd. Torque Converter								
Generator	24399	21692	2707	0.89				
Torque Coupling								
Energy Storage	17794	18465	1343	0.93				
Energy Stored	-2015							
Motor/Controller	21426	16861	4565	0.79	3444	2416	1028	0.7
Gearbox	16861	15401	1460	0.91	3847	3444	403	0.9
Final Drive	15401	15401	0	1	3847	3847	0	1
Wheel/Axle	15401	14251	1150	0.93	7023	6983	39	0.99
Braking							3137	
Aux Loads	3354	0	3354	0				
Aero			2473					
Rolling			4756					

*Overall System Efficiency

0.065

*Overall energy efficiency is calculated as: (aero + rolling)/(fuel in - ess storage)

Figure 7.14 HEV components energy usage data over UDDS when using PM generator and SI-41

Now, the same HEV which utilises the PM generator as its power pack is simulated over the highway drive cycle. The simulation results are shown as follows.

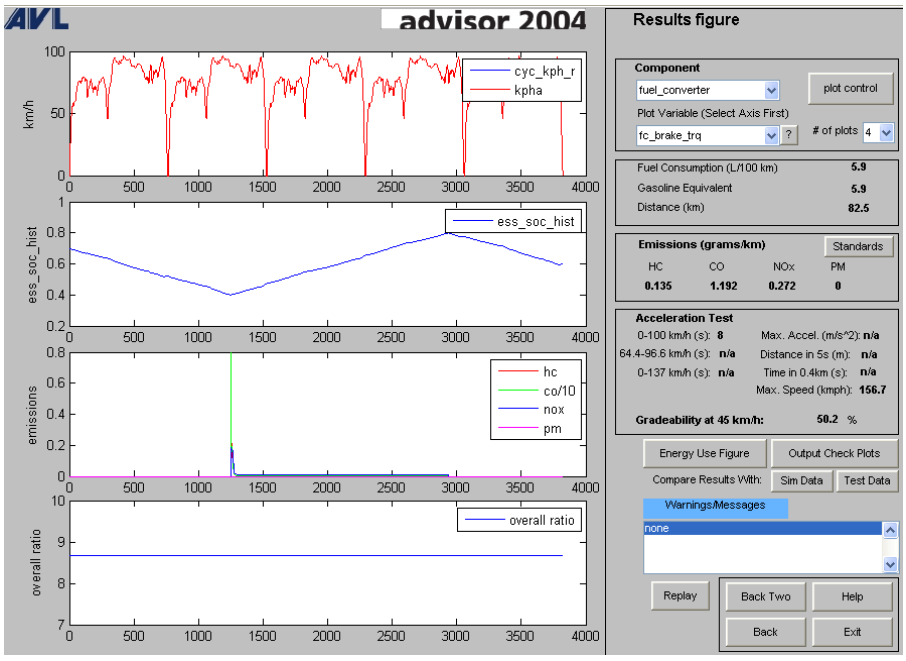

Figure 7.15 Highway cycle simulation results for the HEV equipped with PM and SI_41

If the simulation results shown in Figure 7.15 is compared with the ones shown in Figure 7.10 for the Genset it can be found out that the HEV equipped with PM generator has higher fuel consumption and total emissions over the highway drive cycle.

The batteries SOC results shows that the number of charge and discharge cycles for the longer distance will be bigger than the same batteries fed by ORIM generator in highway. Therefore the life of the battery pack would be shorter as this fact was also proved by the results of the batteries SOC over city cycle for the same HEV, explained in Subsection 7.2.2.2.

As shown in the following figure, the overall system efficiency achieved over the highway cycle by the vehicle utilising the PM generator is also lower than the one obtained by the HEV equipped with Genset as shown in Figure 7.11.

Energy Usage Table (kJ)

	POWER MODE				REGEN MODE			
	In	Out	Loss	Eff.	In	Out	Loss	Eff.
Fuel	0	155039						
Fuel Converter	155039	34610	120429	0.22			0	
Clutch								
Hyd. Torque Converter								
Generator	34610	30772	3838	0.89				
Torque Coupling								
Energy Storage	16875	19484	1255	0.93				
Energy Stored	-3864							
Motor/Controller	32098	28224	3873	0.88	1754	1395	360	0.79
Gearbox	28224	24981	3243	0.89	2029	1754	275	0.86
Final Drive	24981	24981	0	1	2029	2029	0	1
Wheel/Axle	24981	22982	1999	0.92	3132	3079	53	0.98
Braking							1049	
Aux Loads	2678	0	2678	0				
Aero			10671					
Rolling			9178					

*Overall System Efficiency

0.125

*Overall energy efficiency is calculated as: (aero + rolling)/(fuel in - ess storage)

Figure 7.16 HEV components energy usage data over HWFET when using PM generator and SI_41

7.2.2.3 City and Highway Simulation Results: IM Generator

Finally, the vehicle is simulated when it is equipped with an inner rotor induction generator and ordinary fuel converter with the same powers as the Genset components. As explained in Subsection 7.2.1, in fact the selected IM generator is 25 KW machine but its power is scaled to 22 KW in ADVISOR as it was done for the PM generator to have the same power as ORIM.

As Figure 7.17 shows, the selected fuel converter for IM is the same as one chosen for PM and the rest of the components of the HEV remain unchanged for this simulation.

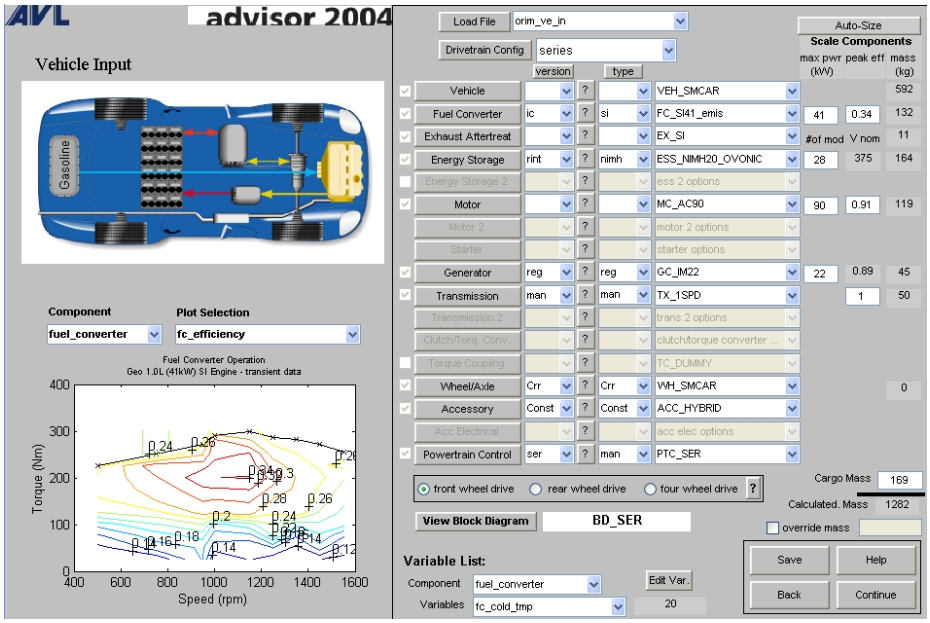

Figure 7.17 ADVISOR input GUI screen for the series HEV with IM and SI_41

Figure 7.18 shows the simulation results for the HEV equipped with IM generator and when 3.5 cycles of the UDDS city cycle, shown in Figure 7.5, are applied.

If the results shown in Figure 7.18 are compared with the ones were achieved when the HEV using Genset, shown in Figure 7.8, it is concluded that there is considerable difference in the fuel consumption and emission values. The HEV has better performance over the city cycle if it utilises the novel engine and the designed ORIM as its power pack.

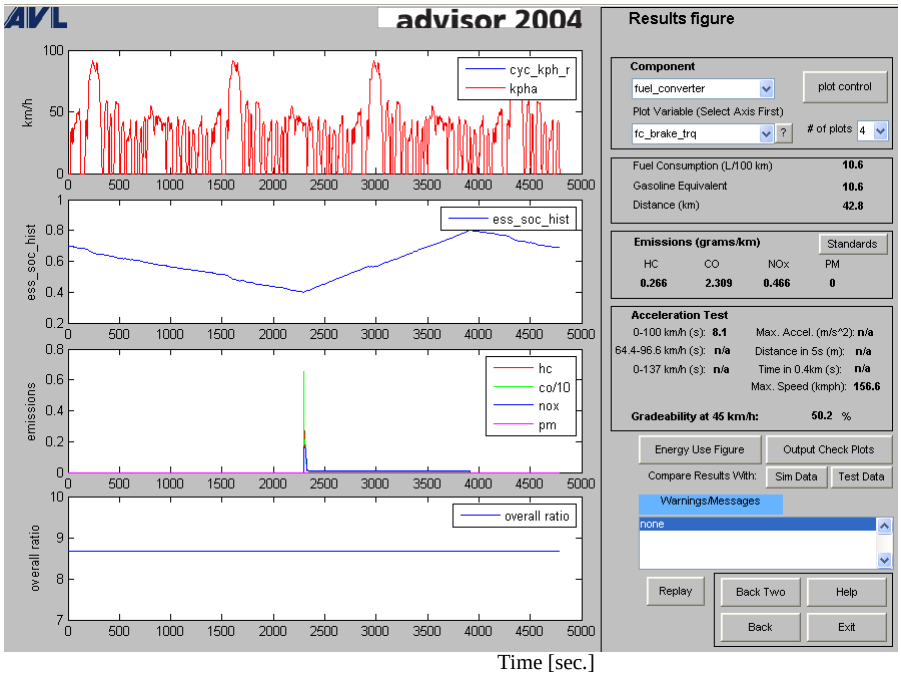

Figure 7.18 City cycle simulation results for the HEV equipped with IM and SI_41

The HEV equipped with the IM generator and SI_41engine has the same acceleration, maximum speed and gradeability capabilities as the vehicle utilises Genset.

The efficiency achieved by the fuel converter as well as the overall efficiency of the system in this configuration, shown in Figure 7.19, are also lower than the ones achieved by the HEV using the Genset, shown in Figure 7.9.

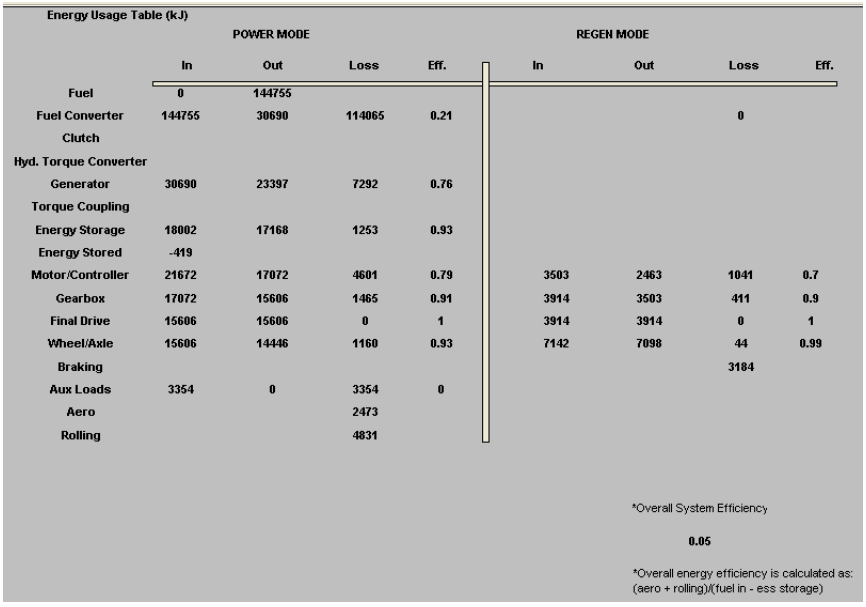

Figure 7.19 HEV components energy usage data over UDDS when using IM generator and SI_41

Figure 7.20 shows the simulation results for the HEV equipped with the IM and when 5 cycles of the HWFET highway drive cycle, shown in Figure 7.5, are applied.

The HEV simulation results for the Genset, shown in Figure 7.10 confirm that the performance of the vehicle over the highway cycle when it is powered by Genset is much better than that when the vehicle utilises IM generator and SI_41 engine as its power pack. This is because of that the later power unit consumes much more fuel and has higher exhaust emissions.

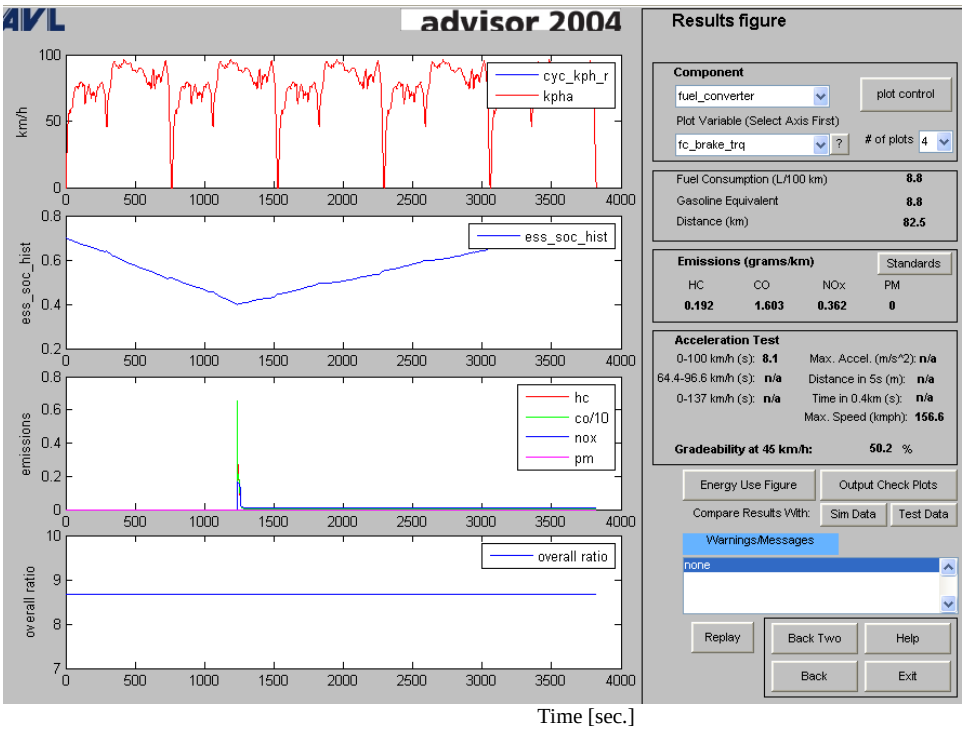

Figure 7.20 Highway cycle simulation results for the HEV equipped with IM and SI_41

The overall efficiency of the vehicle, over the highway, as shown in Figure 7.21, is also lower than the one achieved by the vehicle equipped with Genset.

All the simulations which were performed for the HEV utilising different types of power packs in each time of simulation showed that the HEV equipped with Genset has much better performance over the both city and highway cycles.

Energy Usage Table (kJ)

	POWER MODE				REGEN MODE			
	In	Out	Loss	Eff.	In	Out	Loss	Eff.
Fuel	0	230958						
Fuel Converter	230958	49049	181909	0.21			0	
Clutch								
Hyd. Torque Converter								
Generator	49049	37049	12000	0.76				
Torque Coupling								
Energy Storage	16031	12578	990	0.93				
Energy Stored	2464							
Motor/Controller	32344	28459	3885	0.88	1790	1426	364	0.8
Gearbox	28459	25211	3248	0.89	2075	1790	285	0.86
Final Drive	25211	25211	0	1	2075	2075	0	1
Wheel/Axle	25211	23191	2020	0.92	3195	3139	57	0.98
Braking							1063	
Aux Loads	2678	0	2678	0				
Aero			10671					
Rolling			9324					

*Overall System Efficiency

0.088

*Overall energy efficiency is calculated as: (aero + rolling)/(fuel in - ess storage)

Figure 7.21 HEV components energy usage data over HWFET when using IM generator and SI_41

7.2.2.4 Simulation Results for the HEV Over the Trip Cycle

In the further stage of the analysis, the HEV which is equipped with the components specified in Table 7.3 is simulated over the trip cycle, shown in Figure 7.6. The following figure shows the simulation results when the Genset is used in the vehicle as its power pack.

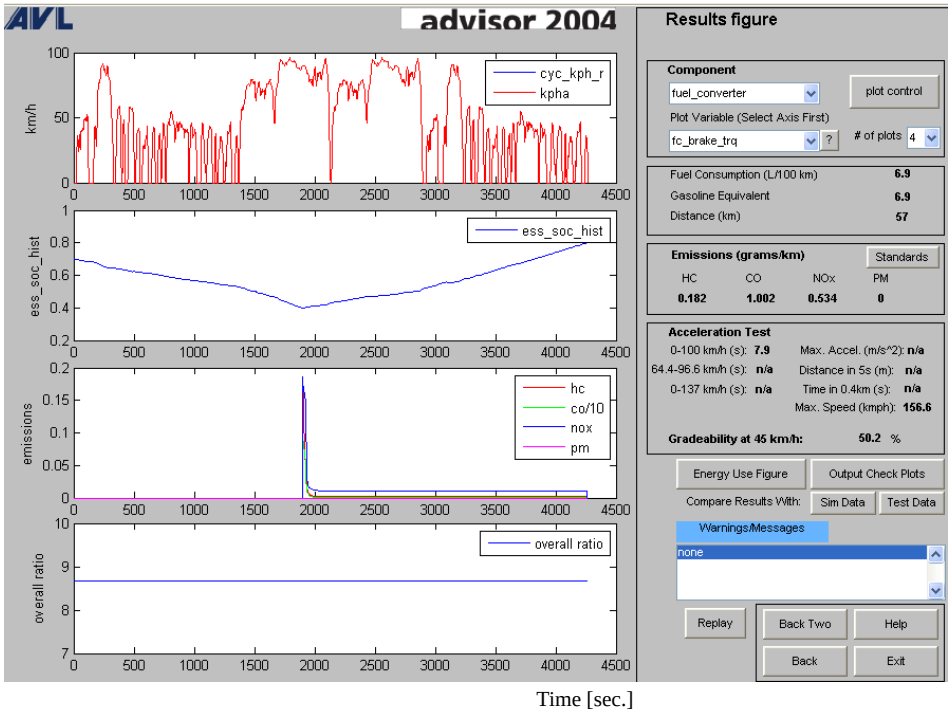

Figure 7.22 Trip drive cycle simulation results for the HEV equipped with Genset

The results shown in Figure 7.22 illustrates that the vehicle is capable to follow the required speed over the trip cycle while all tailpipe out emissions are lower than the standard values presented in Appendix E. The SOC history of the batteries shows that the Genset is able to recharge the battery pack when it reaches to the minimum allowed level of discharge.

Figure 7.23 shows the simulation results for the vehicle utilising PM generator and SI_41 engine over the trip cycle. These results illustrates that the fuel consumption and exhaust emission are higher than the ones achieved by the HEV equipped with Genset. The number of charge and discharge cycles of the battery pack fed by PM generator is also greater than that fed by Genset which results in a shorter lifetime for batteries.

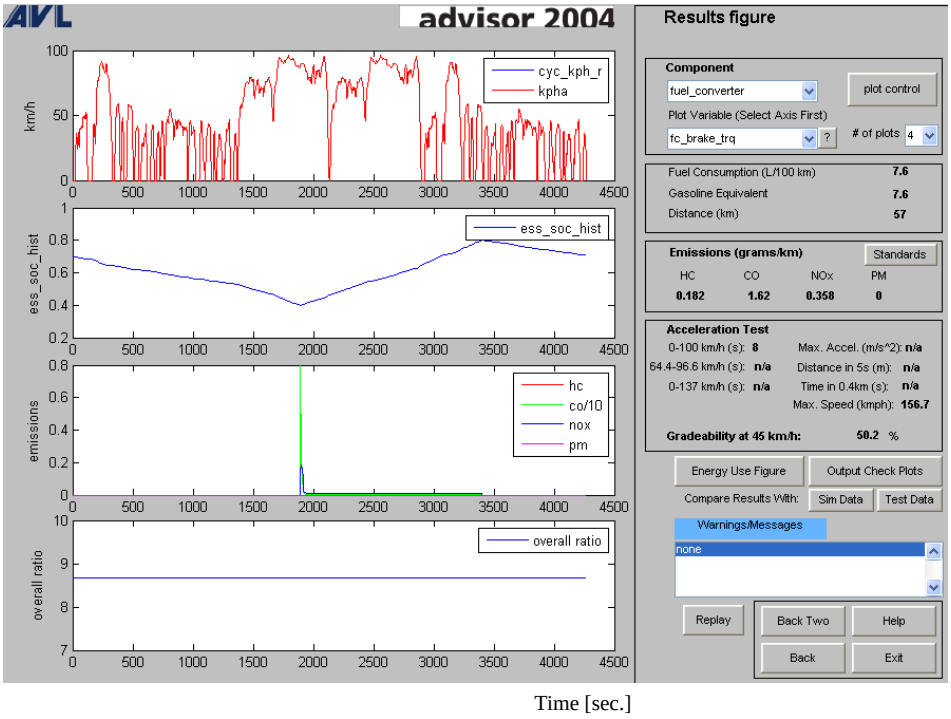

Figure 7.23 Trip drive cycle simulation results for the HEV equipped with PM and SI_41

Finally, the IM generator is replaced with the PM generator in the HEV and then the vehicle is simulated in ADVISOR. The simulation results are shown in Figure 7.24.

The results shown in Figure 7.24 in terms of the HEV fuel consumption and emissions, demonstrates that the Genset has much better performance than IM generator and SI_41 engine and is able to charge the battery pack with lower drawbacks of the power pack.

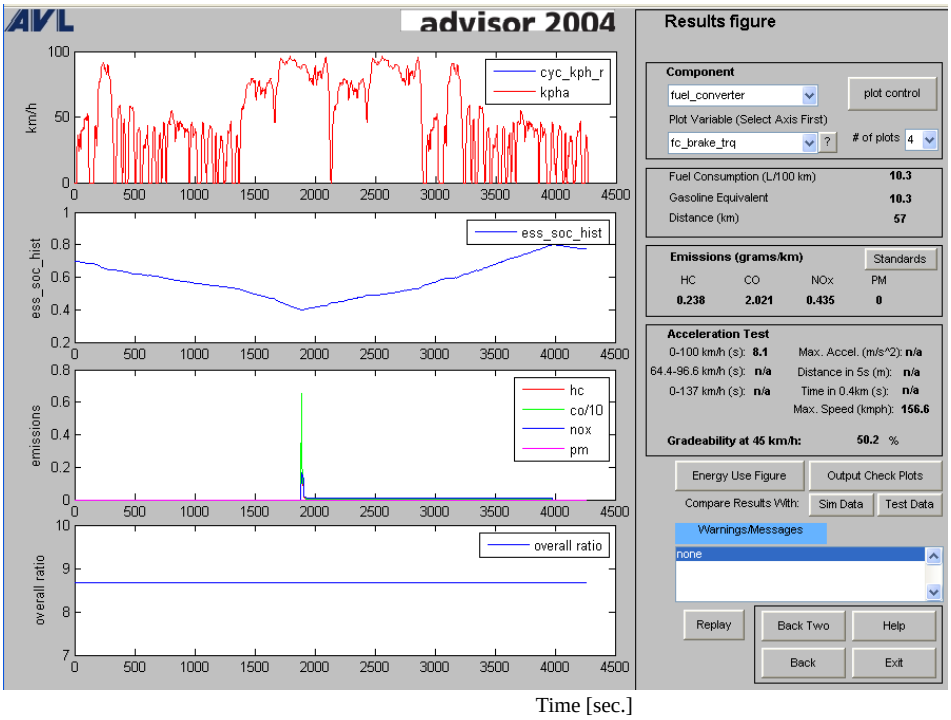

Figure 7.24 Trip drive cycle simulation results for the HEV equipped with IM and SI_41

7.3 Comparison of Results

By reviewing all simulation results shown in this chapter it is concluded that the HEV has better performance when it is equipped with the Genset to charge the battery pack over the different drive cycles. Table 7.4 summarises the fuel consumption, fuel economy and total emissions of the HEV utilising different power packs in each time of simulation.

The simulated data tabulated in Table 7.4 are presented by the bar chart in Figure 7.25 to illustrate the impact of different power packs on the HEV main performance parameters.

Table 7.4 HEV simulation results in summary over various drive cycles

	HEV Performance Parameters / Power Packs	Fuel consumption (L/100Km)	Fuel economy (mpg)	Emissions (g/Km) (HC+CO+NOX+PM)
City cycle	**ORIM + NE***	7.2	32.5	1.952
	PM + SI_41	8	29.3	2.515
	IM + SI_41	10.6	22.2	3.041
Highway cycle	**ORIM + NE***	5.2	45.2	1.259
	PM + SI_41	5.9	40	1.599
	IM + SI_41	8.8	26.8	2.157
Trip cycle	**ORIM + NE***	6.9	34	1.718
	PM + SI_41	7.6	30.9	2.16
	IM + SI_41	10.3	22.9	2.694

* NE: Novel Engine (C5C)

Table 7.4 shows an increase in fuel economy of approximately 11 % and 47 % over the city cycle in the case of the HEV with the Genset compared to the HEV with PM or IM generator options respectively. The exhaust emissions are also decreased by 23 % and 36 % when the Genset replaces the PM or IM generators coupled with the SI_41 engine.

Over the highway cycle, the fuel economy would be increased by approximately 13 % and 69 % for the HEV equipped with the Genset compared to PM or IM generators. The HEV emissions when utilising ORIM with novel engine is also lower than that of the HEV utilising PM or IM generators with small engine, by approximately 22 % and 42 % respectively.

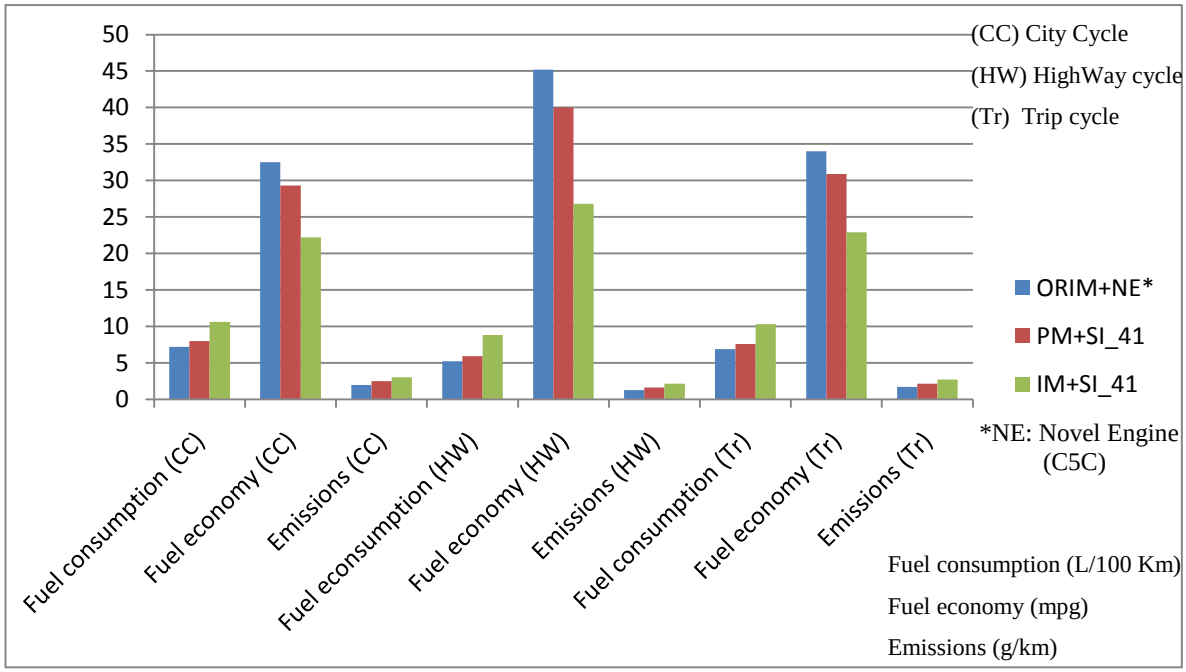

Figure 7.25 HEV performances for different configurations and over different drive cycles

7.3.1 Power Packs Performance

To find the capability limits of the different power packs, analysed in this chapter, the simulated results are compared to desired targets by spider plots. Table 7.5 shows the defined targets for the HEV as well as the centre values of the spider chart over the city cycle.

Table 7.5 Spider plot comparison values over UDDS for the HEV performance parameters

Parameter / Spider values	Fuel consumption (lp100Km)	Gasoline equivalent (lp100kmge)	HC emissions (g/Km)	CO emissions (g/Km)	NOx emissions (g/Km)	Grade (%)
Target: ring value (1)	7.5	7.5	0.22	1.3	0.97	50
Centre value (0)	15	15	0.4	2.8	3.4	0

Spider chart for the city cycle simulations is shown in Figure 7.26. The circle pointed by number 1 shows the band of value or target. Since the aim is to minimise the variables tabulated in Table 7.5, therefore the values inside the circle pointed by number 1 in the spider chart are greater than the outer values.

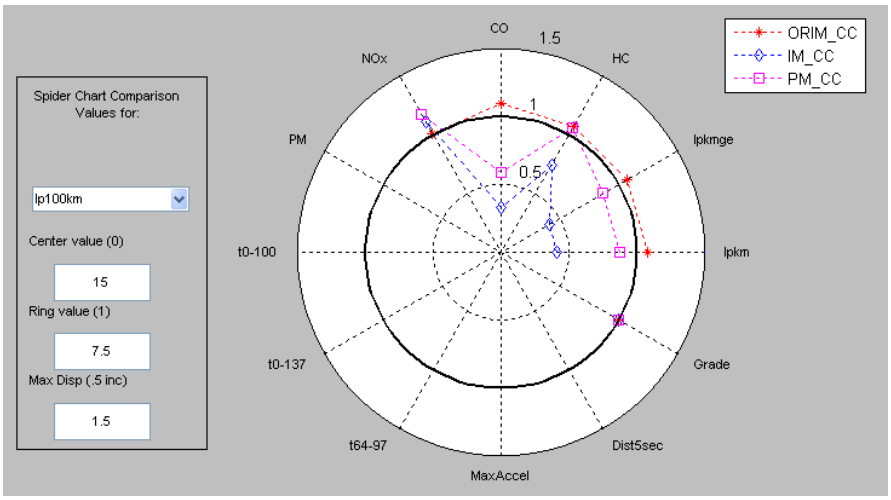

Figure 7.26 Comparison of the HEV city cycle simulation results with desired targets by spider chart

Spider plot shown in the Figure 7.26 demonstrates that the HEV equipped with ORIM generator and novel engine as its power pack, meets all the targets specified in Table 7.5. But the HEV using PM or IM generators and SI_41 engine is not able to meet some of the expected targets such as CO emission and fuel consumption over the city cycle.

Table 7.6 shows the defined targets for the HEV and the centre values of the spider chart over the highway cycle. This data are used to plot the spider chart in order to find and compare the capability limits of the different power packs.

Table 7.6 Spider plot comparison values over HWFET for the HEV performance parameters

Parameter / Spider values	Fuel consumption (lp100Km)	Gasoeline Equivalent (lp100kmge)	HC emissions (g/Km)	CO emissions (g/Km)	NOx emissions (g/Km)	Grade (%)
Target: ring value (1)	5.5	5.5	0.14	0.8	0.44	50
Centre value (0)	11	11	0.25	2	1.3	0

Figure 7.27 shows the increase in performance of the HEV utilising the ORIM and novel engine compared to using different types of power pack over the highway cycle. The performance parameters for the ORIM configuration meet the desired targets, whereas the parameters for the PM and IM configurations do not meet all the expected targets.

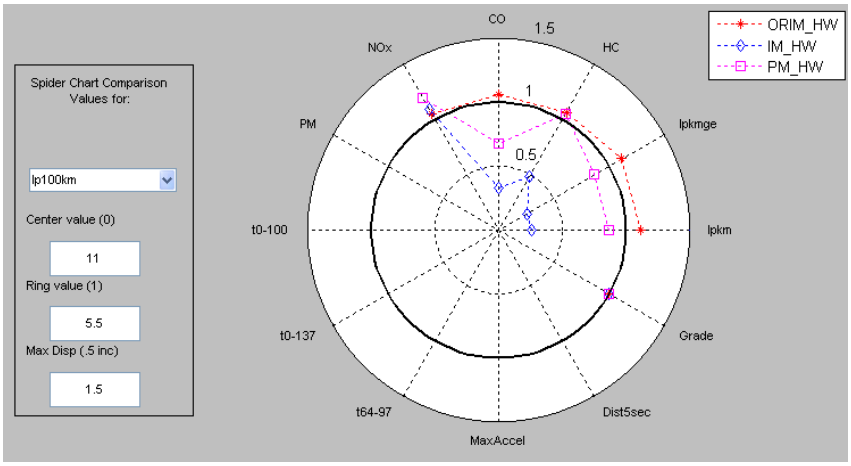

Figure 7.27 Comparison of the HEV highway simulation results with desired targets by spider chart

7.3.2 Effects of the Power Packs on the Battery Life

The important aim with batteries in the HEV application is how fast they are charged and discharged determining their ultimate lifetime. The fast charged batteries would have shorted lifetime as it was explained in Subsection 7.2.2.2 [75].

Figure 7.28 shows the charge and discharge rates of the batteries fed by different power packs over the different drive cycles.

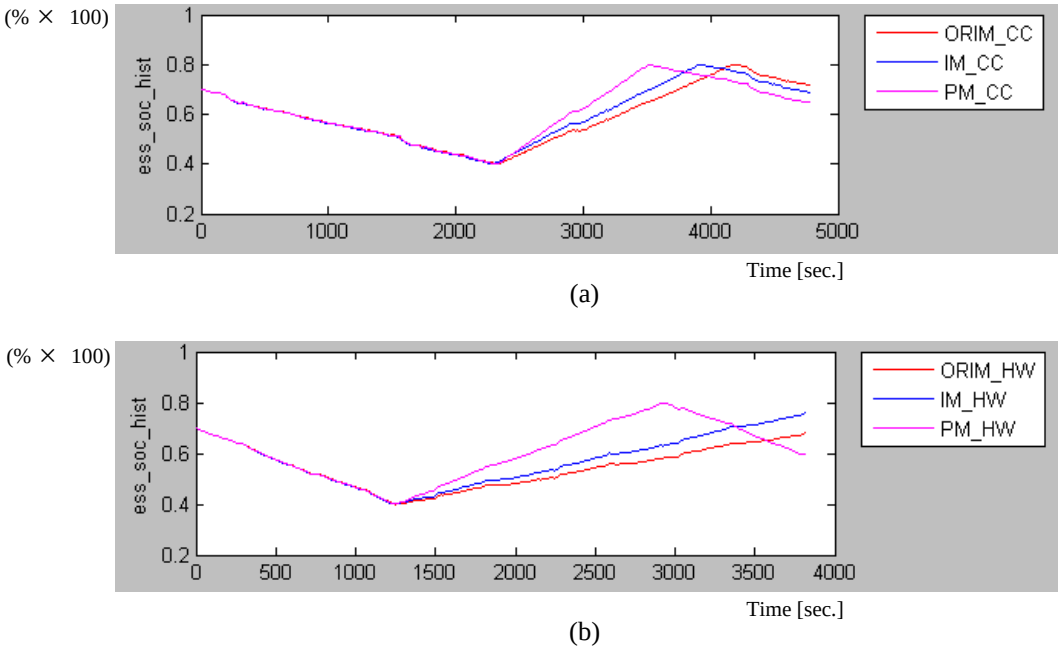

Figure 7.28 Comparison of the battery pack charging rates over; (a) city cycle and (b) highway cycle

All batteries have the same discharge rate but the battery pack powered by ORIM generator has the lowest charging rate over the both city and highway cycles. This results in a longer lifetime for the batteries fed by ORIM generator that is powered by the novel engine.

7.4 Summary

In this chapter, the series HEV, sized in Chapter 2 was simulated over different drive cycles in ADVISOR to study the new power unit performance characteristics. The analysis required to calculate the efficiency map of the ORIM, designed in Chapter 5. The corresponding MATLAB files of the HEV components, which interact with their Simulink models were also created or modified according to the components specifications. In each time of the simulations, the vehicle was equipped with different

types of power packs including the Genset which consists of the ORIM generator and novel engine. Simulation results shows that the new designed power pack has a better performance in terms of the fuel consumption, exhaust emissions and battery charging over the city, highway and trip drive cycles.

Chapter 8 Discussion, Conclusions and Recommendations for Further Work

Increasing global concerns regarding a more cleaner and energy efficient environment requires energy saving and a reduction in emissions. HEV technology is one solution for these emissions and energy conservation issues. The compact power pack presented in this thesis combines a hybrid power pack with new body construction features to meet an overall target of achieving higher fuel economy and lower emissions.

The objective of this project was to design a new type of induction machine with outer rotor construction that can interact with the novel rotary engine in order to form a compact power pack for HEVs.

Chapter one of this thesis began by looking at the increasing demands for more compact power units to increase the overall efficiency of HEVs in order to reduce fuel consumptions and emissions. The contribution of the project is introduced by presenting a novel engine and a new type of induction machine that form the compact power pack. The novelty of the engine comes from its dynamic crankcase which is coupled to the electric machine. The possibility of direct connection of the novel engine with rotating crankcase and the new type induction machine is because the rotor is positioned outside the stator (outer rotor electric machine). Due to the direct coupled configuration used in the compact power pack, the electric machine has to start the engine as well as generate the power. The integration of the starting and generating functions in this machine is possible because of its high generation capacity which makes the torque characteristics of the starter and generator machines to be close together.

8.1 Discussion

Chapter 2 starts with a literature search on the hybrid electric vehicle technology, its potential and advantages. It is expected that future HEVs will have considerably higher fuel economy and lower emissions than conventional vehicles. The advantages and disadvantages of different configurations of the HEV components were discussed. It was found that the cage rotor induction machine is the best candidate for the HEV applications because of its high reliability and ruggedness and low cost and maintenance features. There follows an explanation of sizing the power train components of a small HEV with series configuration that requires a three- phase 22KW generator in its power pack to satisfy the vehicle performance requirements.

As stated in the previous paragraph, the selected electric machine required to achieve the stated objective is the induction machine type. Chapter 3 continues to investigate the induction machine principles and construction. The equivalent circuit of induction machines was derived and then the torque-speed characteristics of an induction machine were analysed in the motoring and generation modes.

In Chapter 4, consideration of the main design principles and design factors of induction machines precede discussion of induction machine design issues, including electrical, magnetic and thermal design features. The relationship between rotor bars and behaviour of the induction machine was explained. The induction machines research was ended by presenting a flowchart showing the induction machine design algorithm. The equations used to design the main dimensions of the induction machine were also derived.

In Chapter 5, the outer rotor induction machine which is coupled directly to the novel engine was designed based on the calculated parameters for this machine. Since the rotor of the proposed induction machine is placed outside the stator, the position of the stator and rotor slots differ from those of the conventional machines. In the ORIM, stator slots are created on the outer side of the stator and rotor slots are created on the inner side of the rotor. This arrangement of slots resulted in the need to modify the standard design equations based on the new structure of the machine. Although only the final design procedure was reported in Chapter 5, several iterations of the ORIM design process was required in terms of specifying variables or parameters, such as slot numbers. The design was ended when the targets, including the machine efficiency and power factor, were met. Finally, the design was verified by calculating the target parameters, including efficiency and power factor, according to the equivalent circuit elements.

As explained in Chapter 6 JMAG, the simulation program, models the electric machines whilst quantifying the performance parameters accurately. The JMAG Motor Template Tool can be utilised to create the geometry of the ordinary machines. The ORIM is created as a new model and added to the simulation toolset. The magnetising current was injected to the ORIM and then its generation performance was analysed. The ORIM was found capable of providing the required power for the HEV. The calculated performance parameters of the ORIM by JMAG in the generation mode confirmed the design integrity. The frequency and voltage values required to run the ORIM as a starter motor were calculated when applying the constant V/f control technique. The simulation results proved the capability of the ORIM to start the engine at the required speed whilst satisfying the current and magnetic flux density limits. However, machine

losses, over the transient period of the starting mode are few times larger than that of the generation mode, but this occurs for a fraction of a second.

In Chapter 7, a HEV with series configuration employed one of the three machine alternatives, ORIM, IM or PM machines, sequentially as its generator and simulated by ADVISOR. The analysis was required to calculate the efficiency map of the ORIM in ADVISOR. The ORIM was coupled to the novel engine whereas the other electric machines, which have the same power values as ORIM, were coupled to a small ICE to form the HEV power pack options. The novel engine and small engine also have the same power values. The simulation results showed that the compact power pack utilising the ORIM and novel engine has the best performance in terms of the fuel consumption, emissions and battery charging.

8.2 Conclusions

The HEV simulation results presented in Chapter 7 confirms the capability of the Genset over different drive cycles. The high performance required by the HEV over the extended UDDS and HWFET drive cycles necessitates the enhanced efficiency of the power unit. This was achieved by employing the new construction of engine and generator and making possible direct coupling, which removes the conventional accessories such as gears and flywheel. Therefore the compact power pack results in lowering the system weight and increasing the efficiency.

When comparing the HEV with the Genset to the HEV with PM or IM generator options it is shown that an increase in fuel economy of approximately 11 % and 47 % and a decrease in exhaust emissions of 23 % and 36 % are achieved over the city cycle.

Over the highway cycle, fuel economy is increased by approximately 13 % and 69 % and emissions are decreased by approximately 22 % and 42 %.

The results shows that 32 Kg reduction in the vehicle weight and 11 % increment in power pack efficiency brings considerable achievements in terms of fuel consumption, emissions, overall efficiency and battery charging performances.

The HEV battery pack powered by generators have the same discharge rate but the battery pack powered by ORIM generator has the lowest charging rate over the both city and highway cycles. This results in a longer lifetime for the batteries fed by ORIM generator that is powered by the novel engine.

PM generator seems to have a better performance than an inner rotor IM, and so it is worth examining an outer rotor PM coupled with novel engine. However PM machines have their own difficulties such as cost and demagnetisation problem at high temperature.

8.3 Recommendations for Further Work

The work reported in this thesis can be developed by further research into the HEVs power units. The recommendations for further investigations are presented as follows.

- The performance of the HEV can be also simulated when equipped with a switched reluctance machine in the power unit. This research can be done for both modes of the inner rotor or outer rotor types of the machine. The overall system is simulated by ADVISOR. The results can be compared with the

achievements of this thesis. The characteristics of the switched reluctance machine such as cost, reliability and control should be also considered.

- Instead of the ORIM, an outer rotor PM electric machine, having the same power rating may be designed and coupled to the novel engine. The vehicle performances when utilising a PM can be compared to the results reported in the thesis for the ORIM generator.
- The capability of the compact power pack can be studied when it is used in a HEV with a kind of parallel configuration called power-assist or low storage hybrid. In this case, the electric machine operates as a generator during normal driving and also it assists the engine momentarily over acceleration times. In addition, the electric machine can capture the deceleration energy to regenerate it to electrical energy. Honda Insight has employed this configuration and achieved high performance parameters by employing an advanced lightweight PM machine and a new small engine technology to form a simple and compact powertrain [76]. This achievement may be compared to the proposed compact power pack capabilities when it is used in a vehicle with power-assist hybrid configuration.
- The compact power pack may be used in different applications rather than HEVs, such as portable generators. In this case, a new size and design specifications has to be determined for the compact power unit based on the desired application.

References

[1] A. Emadi, M. Ehsani, and J. M. Miller, *Vehicular Electric Power Systems: Land, See, Air, and Space Vehicles*. New York: Marcell Dekker, Inc, 2004.

[2] J. G. Kassakian, "The future of power electronics in advanced automotive electrical systems," in *Proc. of IEEE Power Electronics Specialist Conf.*, 1996, pp. 7-14.

[3] L. A. Khan, "Automotive electrical systems: Architecture and components," in *18th Digital Avionics Systems Conference on Air, Space, and Ground Vehicle Electronic Systems*, vol. 2. St. Louise, Missouri, Oct. 1999, pp. 8.C.5-1-8.C.5-10

[4] J. M. Miller and P. R. Nicastri, "The next generation automotive electrical power system architecture: Issues and challenges," in *17th Digital Avionics Systems Conference on Air, Space and Ground Vehicle Electronic Systems*, vol. 2. Bellevue, WA, Oct./Nov. 1998, pp. I15/1 - I15/8.

[5] S. Muller and X. Pfab, "Consideration for implementing a dual voltage power network," in *Convergence Transportation Electronics Association Congress*. Dearborn, MI, Oct. 1998.

[6] R. H. Johnston, "A history of automobile electrical systems," *SAE Automotive Engineering, Historical Series* vol. 104, pp. 53-66, Sep. 1996.

[7] ADVISOR 2004 – Virtual Vehicle Analysis. Available: http://www.avl.com/wo/webobsession.servlet.go/encoded/YXBwPWJjbXMmcGFnZT12aWV3Jm5vZGVpZD00MDAwMzA0NTk_3D.html

[8] C. P. Cho and D. R. Crecelius, "Vehicle alternator/generator trends towards next millennium," in *Proceedings of the IEEE International Vehicle Electronics Conference* vol. 1, Sep. 1999, pp. 433-438.

[9] R. R. Henry, B. Lequesne, S. Chen, J. J. Ronning, and Y. Xue, "Belt driven starter -generator for future 42-V systems," in *SAE Paper No. 2001 - 01-0728*, March 2001.

[10] D. J. Perreualt and V. Caliskan, "Automotive power generation and control," MIT, LEES Technical Report TR-00-003, May 2000.

[11] N. Traub, "Dual/higher voltage - A global opportunity," SAE Strategic Alliance Report, pp. 1-4, 1998.

[12] A. G. Williams, "The system approach and the impact of the design of higher voltage electrical power systems," *DIACS Colloquia Abstract*, pp. 1-4, May 2001.

[13] M. Ullrich, P. Thomas, Z. Klaus-Peter, G. Andreas, and H. Bernhard, "Starter/Generator for an internal combustion engine, especially an engine of a motor vehicle," US Patent No. 6,177,734, Jan. 2001.

[14] E. C. Lovelace, T. M. Jahns, J. L. K. Jr, and J. H. Lang, "An interior PM starter/alternator for automotive application ". Lab. for Electromagnetic and Electronic systems, MIT.

[15] M. E. Elbuluk and M. D. Kankam, "Potential starter/generator technologies for future aerospace applications," *IEEE Aerospace and Electronics Systems Magazine*, vol. 12, no. 5, pp. 24-31, May 1997.

[16] F. Crescimbini, A. D. Napoli, L. Solero, and F. Caricchi, "Compact permanent-magnet generator for hybrid vehicle applications," *IEEE Trans. Industry Applications*, vol. 41, No.5, pp. 1168-1177, September/October 2005.

[17] A. Pezouvanis and M. Ebrahimi, "C5C, cylindrical five-stroke cycle engine," HYPERC, School of Engineering, Design and Technology, University of Bradford, Pending Patent, July 2008.

[18] M. H. Westbrook, *The Electric Car: Developement and Future of Battery, Hybrid and Fuel-cell Cars (IEE Power and Energy Series 38)* : Co-published by Institutin of Electrical Engineers, London and Society of Automotive Engineers, Warrendale, PA, 2001.

[19] C. C. Chan, "An overview of electric vehicle technology," in *Proc. of the IEEE*, 1993, pp. 1202-1213.

[20] A. Campbell, A. Rengan, J. Steffey, and J. Ormiston. "The simulation of 42-volt hybrid electric vehicles," May 2001. Available: http://www.mth.msu.edu/Graduate/msim/MSIMProjectReports/MCP2.May.2001.report.pdf

[21] F. A. Wyczalek and F. W. Lilly, "Hybrid electric vehicles, year 2000 status," *IEEE AES Systems Magazine*, vol. 16, pp. 15-19, March 2001.

[22] D. Hermance and S. Sasaki, "Hybrid electric vehicles take to the streets," *IEEE Spectrum*, vol. 35, pp. 48-52, Nov. 1998.

[23] H. K. Ng, A. D. Vyas, and D. J. Santini. (Aug.1999). The Prospects for Hybrid Electric Vehicles, 2005-2020: Results of a Delphi Study. [Online]. Available: http://www.osti.gov/bridge/servlets/purl/11902-kmA5j/webviewable/11902.pdf

[24] National Renewable Energy Laboratory, "Hybrid Electric Vehicles," August 2008. Available: http://www.nrel.gov/vehiclesandfuels/hev/hevs.html

[25] Energy Efficiency and Renewable Energy, U.S. Depatment of Energy, "Hybrid Electric Vehicle Components," March 2009. Available: http://www.afdc.energy.gov/afdc/vehicles/hybrid_electric_components.html

[26] I. Husain, *Electric and Hybrid Vehicles Design Fundamentals*. Florida: CRC Press LLC, 2003.

[27] J. G. W. West, "DC, induction, reluctance and PM motors for electric vehicles," *Power Engineering Jornal*, vol. 8, pp. 77-88, Apr. 1994.

[28] Hybrid Electric Vehicle Team, College of Engineering, San Diego State University at San diego, "Electric Motor," October 1999. Available: http://www.engineering.sdsu.edu/~hev/motor.html

[29] M. Zeraoulia, M. E. H. Benbouzid, and D. Diallo, "Electric motor drive selection isues for HEV propulsion systems: A comparative study," *IEEE Trans. Vehicular Technology*, vol. 55, No. 6, November 2006.

[30] S. S. Williamson, S. M. Lukic, and A. Emadi, "Comprehensive drive train efficiency analysis of hybrid electric and fuel cell vehicles based on motor-controller efficiency modeling," *IEEE Trans. Power Electronics*, vol. 21, No. 3, pp. 730-740, May 2006.

[31] A. Jorg, K. Roland, M. Klaus, M. Martin, and W. Dittmar, "Starting device for an internal combustion engine and method for starting the internal combustion engine," US Patent No. 6,240,890, June 2001.

[32] F. B. Reiter, K. Rajashekara, and R. J. Krefta, "Salient pole generator for belt-driven automotive alternator application," in *36th Industry Application Conference*, vol. 1, Sep.-Oct. 2001, pp. 437-442.

[33] R. F. Wall and H. L. Hess, "Induction machines as an alternative for automotive electrical generation and starting systems," in *Proc. International Conference on Electric Machines and Drives*, May 1999, pp. 499-501.

[34] W. Cai, "Comparison and review of electric machines for integrated starter alternator applications," in *the 2004 IEEE Industry Applications*, 2004, pp. 386-393.

[35] H. Rahman. An integrated starter alternator and low cost, high performance drive for vehicular application. IEEE Trans. Vehicular Technology. [Online], Vol.57,No.3,pp.1454-1465.Available: http://ieeexplore.ieee.org/stamp/stamp.jsp?arnumber=04357460

[36] C. M. Jefferson and R. H. Barnard, *Hybrid Vehicle Propulsion*. Southampton, Boston: WIT Press, 2002.

[37] P. Faireley, "U.S. military goes for hybrid vehicles," *IEEE Spectrum*, vol. 41, pp. 24-25, Mar. 2004.

[38] M. Ehsani, K. M. Rahman, and H. A. Toliyat, "Propulsion system designof electric and hybrid vehciles," *IEEE Trans. Industrial Electronics*, pp. 19-27, 1997.

[39] J. Larminie and J. Lowry, *Electric Vehicle Technology Explained*. West Sussex: John Wiley and Sons, 2003.

[40] B. Gills. Understanding weather-Beaufort scale, Available: http://www.bbc.co.uk/weather/features/understanding/beaufort_scale.shtml

[41] S. Huler, *Defining the Wind : The Beaufort Scale, and How a 19th-Century Admiral Turned Science into Poetry*, : Crown, 2004.

[42] J. M. Miller, *Propulsion Systems for Hybrid Vehicles (IEE Power and Energy Series 45)*. London: The Institution of Electrical Engineering, 2004.

[43] International Electrotechnical Commission. "Rotating Electrical Machines. Part 1: Rating and Performance," IEC 60034-1:2004," 2004.

[44] D. Corrigan, I. Menjak, B. Cleto, S. Dhar, and S. Ovshinsky, "Nickel-Metal Hybrid Batteries For ZEV-Range Hybrid Electric Vehicles," in *17th International Electric Vehicle Symposium* Motreal, Canada, 2000.

[45] M. Fetcenko. (1999, May). Advanced materials for next generation NiMH batteries: IEEE AES Systems Magazine, Presented at the 25th International Seminar & Exhibit on Primary and Secondry Batteries. [Online]. pp.17-23. Available: http://ieeexplore.ieee.org/xpls/abs_all.jsp?arnumber=765774

[46] N. Mohan, T. M. Undeland, and W. P. Robbins, *Power Electronics-Converters, Applications, and Design*, 3rd ed. Hoboken, NJ: John Wiley & Sons, 2003.

[47] T. Wildi, *Electrical Machines, Drives, and Power Systems*, 4th ed. New Jersey: Prentice-Hall, 2000.

[48] E. S. Hamdi, *Design of Small Electrical machines*. West Sussex: John Wiley & Sons Ltd., 1994.

[49] S. J. Chapman, *Electric Machinary Fundamentals*, 4th ed. New York: McGraw - Hill, 2005.

[50] M. Peltola. Slip of AC induction Motors and How to Minimize it. Available: www.ieee-kc.org/library/motors/motorslip.htm

[51] T. Kikuchi and T. Kenjo, "A unique desk-top electrical machinery laboratory for the mechatronics age," *IEEE Trans. Education*, vol. 40, p. 18, Nov. 1997.

[52] J. Faiz, M. B. B. Sharifian, M. R. Feyzi, and K. Shaarbafi. "A complete lumped equivalent circuit of three-phase squirrel-cage induction motors using two-dimensional finite-elements technique," IEEE Trans. Enegy conversion, vol. 17, pp. 363-367, Sep. 2002.

[53] I. Boldea and S. A. Nasar, *The Induction Machine Handbook*. Boca Raton,FL: CRC Press LLC, 2002.

[54] H. A. Toliyat, *Handbook of Electric Motors*, 2nd ed. Boca Raton, FL: CRC Press, Taylor & Francis Group, 2004.

[55] G. Madescu, I. Boldea, and T. J. E. Miller, "An analytical iterative model (AIM) for induction motor design," in *IEEE Industry Applications Conference, 31st IAS Annual Meeting*, Oct. 1996, vol. 1, pp. 556-573.

[56] G. Madescu, I. Boldea, and T. J. E. Miller, "The optimal lamination approach (OLA) for induction motor design," *IEEE Trans.*, vol. IA-34, No.2, pp. 1-8, 1998.

[57] K. Vogt, *Electrical Machines. Design of Rotary Electric Machines (in German)*, 4th ed. Berlin: VEB Verlag Technik, 1988.

[58] J. Faiz, M. Ghaneei, A. Keyhani, and A. B. Proca, "Optimum design of induction motors for electric vehicles," *Electric Machines and Power Systems*, vol. 28, pp. 1177-1194, December, 2000.

[59] International Electrotechnical Commission, "Thermal Evaluation and Classification of Electrical Insulation," IEC 85 - 1984, 1984.

[60] P. K. Sattler and G. Balaliemke, "Exprimental and theoretical investigations concerning the design of induction machine especially machines with high power density with respect to the inverter supply and speed regulations," in *2nd IFAC Symposium*. Dusseldrof, West Germany, 1977, pp. 387-398.

[61] I. Boldea, *The Electric Generators Handbook. Variable Speed Generators*, vol. 2. Boca Raton, FL: CRC Press, Taylor & Francis Group, 2006.

[62] P. J. McCleer, J. M. Miller, A. R. Gale, M. W. Denger, and F. Leonardi, "Nonlinear model and momentary performance capability of a cage rotor induction machine used as an automotive combined starter-alternator. ," *IEEE Trans. Industry Applications* 2001, vol. 37, pp. 840-846, May/ June 2001.

[63] J. M. Miller, A. R. Gale, P. J. McCleer, F. Leonardi, and J. H. Lang, "Starter-alternator for hybrid electric vehicle: comparison of induction and variable reluctance machines and drives," in *The 1998 IEEE Industry Applications, 33 rd IAS Annual Meeting*, vol. 1, Oct. 1998, pp. 513-523.

[64] J. M. Miller, A. R. Gale, and V. A. Sankaran, "Electric drive subsystem for a low-storage requirement hybrid electric vehicle," IEEE trans. Vehicular Technology, vol.48, pp. 1788-1796, Nov. 1999.

[65] J. R. Brauer, "Finite element analysis of single-phase and polyphase induction motors," *Conference Record of the IEEE Industry Application Society Annual Meeting*, Oct. 1981.

[66] M. Ravenstahl, J. Brauer, S. Stanton, and P. Zhou, "Maxwell design environment for optimal electric machine design," in *Small Motor Manufacturing Assn. Annual Meeting*, 1998.

[67] P. Zhou, S. Stanton, and Z. J. Cendes, "Dynamic modeling of three phase and single phase induction motors," in *IEEE Int. Electric Machines & Drives*, 1999, pp. 556-558.

[68] P. P. Silvester and M. V. K. Chari, "Finit-element solution of saturable magnetic field problems," *IEEE Trans. Power Apparatus and Systems*, vol. PAS-89, pp. 1642-1651, 1970.

[69] E. S. Hamdi and A. F. Licariao-Nogueira, "Teaching electrical machines CAD: the Cardiff experience," in *AMSE International Conference on Signals and Systems*, vol. 3. New Delhi, India: AMSE Press, 1991, pp. 111-118.

[70] H. Meshgin-Kelk, J. Milimonfared, and H. A. Toliyat, "A comprehensive method for the calculation of inductance coefficients of cage induction machines," *IEEE trans. Energy Conversions*, pp. 187-193, June 2003.

[71] *JMAG-Studio Version 9.0, Motor Template 2.0 Document, JRI Solutions, Ltd.* , 2007.

[72] *JMAG-Studio User's Manual Version 9, JMAG-Studio Group, JRI Solutions, Ltd.*, 2nd ed, August 2007.

[73] *JMAG Application Note - Starting Performance Analysis of a Single Phase Induction Motor, JRI Solutions, Ltd.*, 2007.

[74] *JMAG Application Note - Analysis of a Three Phase Induction Motor, JRI Solutions, Ltd.* , 2006.

[75] B. Brant, *Build Your Own Electric Vehicle*. New York: TAB Books, Division of McGraw-Hill, Inc., 1994.

[76] K. Aoki, S. Kuroda, S. Kajiwara, H. Sato, and Y. Yamamoto. (2000, June). Development of integrated motor assist hybrid system: Development of the 'Insight', a personal hybrid coupe. Presented at Government/Industry Meeting in Washington, D.C., Session: Exploring Efforts to Promote Fuel Efficient Vehicles.[Online].Available: http://www.osti.gov/bridge/purl.cover.jsp;jsessionid=5875A11C7E71C56920149EED0CCE8AFF?purl=/771011-FszVdC/native/

[77] K. B. Wipke, M. R. Cuddy, and S. D. Burch, "ADVISOR 2.1: A user-friendly advanced powertrain simulation using a combined backward/forward approach," *IEEE Trans. Vehicular Technology*, vol. 48, no. 6, pp. 1751-1761, Nov. 1999.

[78] R. D. Senger, M. A. Merkle, and D. J. Nelson, "Validation of ADVISOR as a simulation tool for a series hybrid electric vehicle," in *SAE International Congress & Exposition in Electric Vehicle Technology Session*, Feb. 1998, pp. 95-115.

[79] *Advisor 2004 User's Guid, AVL*, April 2004.

[80] T. Markel, A. Brooker, V. Johnson, K. kelly, B. Kramer, M. O'keefe, S. Sprike, and K. Wipke. (2002, June). ADVISOR: a system analysis tool for advanced vehicle modelling. Journal of Power Sources. [Online]. 110, pp. 255-266. Available: http://www.obitet.gazi.edu.tr/makale/internalcombustionengines/029.pdf

[81] M. Menday and M. Ebrahimi, "The application of dynamic modelling using parametric design methods for an automotive driveline system," in *1st International symposium on Multi-Body Dynamics: Monitoring and Simulation Techniques*. University of Bradford, UK, Mar. 1997.

[82] Dieselnet, "European Union Emission Standards - Cars and Light Trucks," 2009. Available: http://diesel.net/

Appendix A Modelling and Simulation Environment – ADVISOR

The modelling and simulation of the vehicle can be used to determine the performance of the vehicle and its components before manufacturing of a car. This facility can also be utilized to select the best components and optimization of the vehicle design. Therefore it eliminates the cost and time wasting problems extremely in the multiple test procedure.

Many simulation tools have been presented for the hybrid electric vehicles, such as SIMPLEV, OSU-HEVSIM, PSAT, ADVISOR and MARVEL. ADVISOR (Advanced Vehicle Simulator) is one of the most commonly used simulators between them. It was developed at national renewable energy in 1994 to help the hybrid electric vehicle developments program. Most of the main vehicle manufacturers around the world have used this simulator [20 , 77]. It shows the impacts of electric and HEV components on the performance of the vehicle as well as its emissions and fuel economy. ADVISOR is a valid simulator, especially for the series hybrid electric vehicles with enough accuracy of vehicle performance prediction [78]. In this project, the latest version of ADVISOR which is ADVISOR 2004 is used.

A.1 Structure of ADVISOR

ADVISOR which includes some data, script text files and models works in the MATLAB/Simulink environment. It models the vehicle components with the Simulink block diagrams and analyses the performance of the conventional or hybrid vehicles in MATLAB. The Simulink models in ADVISOR are mostly experimental and they present the drivetrain components performance including the efficiency and operating ranges, with a MATLAB file, based on the measured data in the laboratory. The top-

level block diagram for a series HEV in ADVISOR is shown in Figure A.1. Each model of any component includes its Simulink sub-block diagrams which are necessary to process the data and model the component. ADVISOR operates as an analysis simulator originally and it can not be used for the detailed design purposes [79].

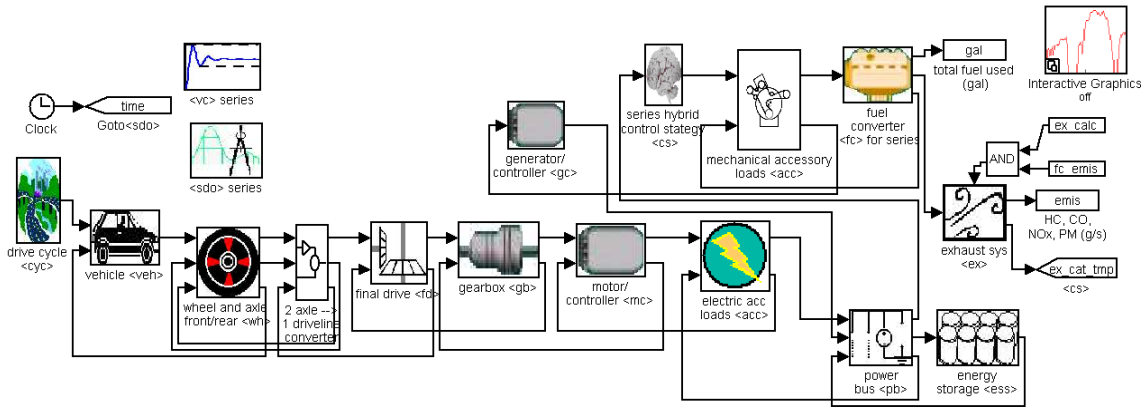

Figure A.1 The series HEV top-level block diagram in ADVISOR [79]

The sub-block diagram of the generator/controller is shown in Figure A.2. The generator/controller Simulink model includes loss data, performance limits and rotational inertia. This is the only completely forward-facing block in ADVISOR, computing the output power from the input torque and speed. The generator map used in the lookup table block is very similar to the input power motor map, with the main difference being that the torque and power sign conventions are opposite. In the generator map torque input to the machine and power output by the machine are positive.

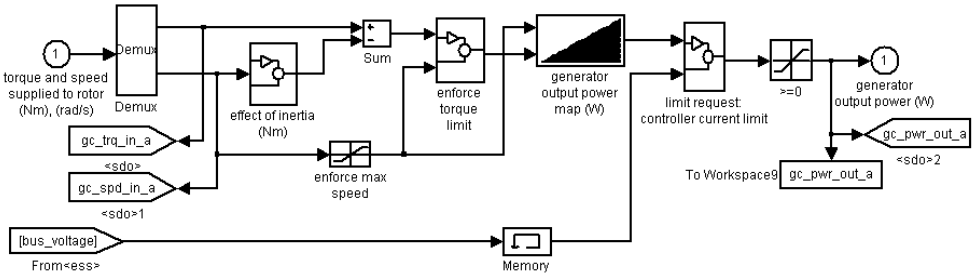

Figure A.2 Generator/controller Simulink block diagram in ADVIDOR [79]

The fuel converter sub-block shown in Figure A.3 models the ICE, and includes performance limits, inertia effects, accessory loads and temperature transient effects on fuel use, engine-out emissions and catalyst efficiency. There are 'leads' to the engine controller shown below, which controller determines whether the engine is on.

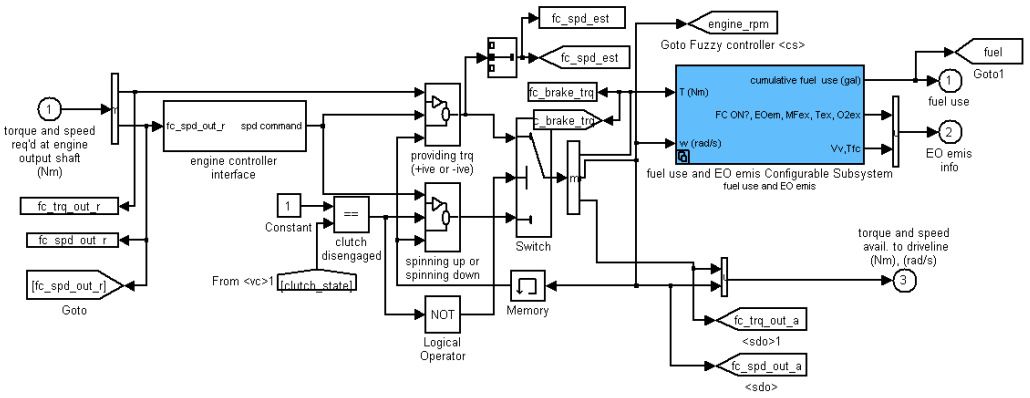

Figure A.3 Fuel converter Simulink block diagrm in ADVIDOR [79]

This modular arrangement gives an opportunity to the user to modify the models and their MATBLAB files and compare the results.

Three graphical user interfaces (GUI) which interacts with the MATLAB workspace data has created in ADVISOR to make it easier for user to assemble a vehicle with desired components, define the simulation parameters and see the results. The provided information about the selections helps the user to choose the required option. Any variable parameter can be altered to the new value by user in the graphical interfaces to see its effect on the performance of the vehicle [80].

A.1.1 ADVISOR Vehicle Input GUI Screen

As shown in Figure A.4, in the vehicle input graphical interface window of ADVISOR, user can define the vehicle configuration (series, parallel, etc) and its drivetrain

components over the available alternatives. If any selected component is mismatched with other components or settings, ADVISOR informs the user and also it suggests an option to resize the component. The user can modify the components size and the scalar variables in input window by only editing its new value in the boxes. The MATLAB file of each component can be also obtained when any component button is clicked. Furthermore, the maps of the components performance, such as efficiency and fuel use maps can be achieved in this window as well as block diagrams of the verified configuration of the vehicle. Once all the desired input variables are selected, the simulation process can be continued by clicking on the continue button.

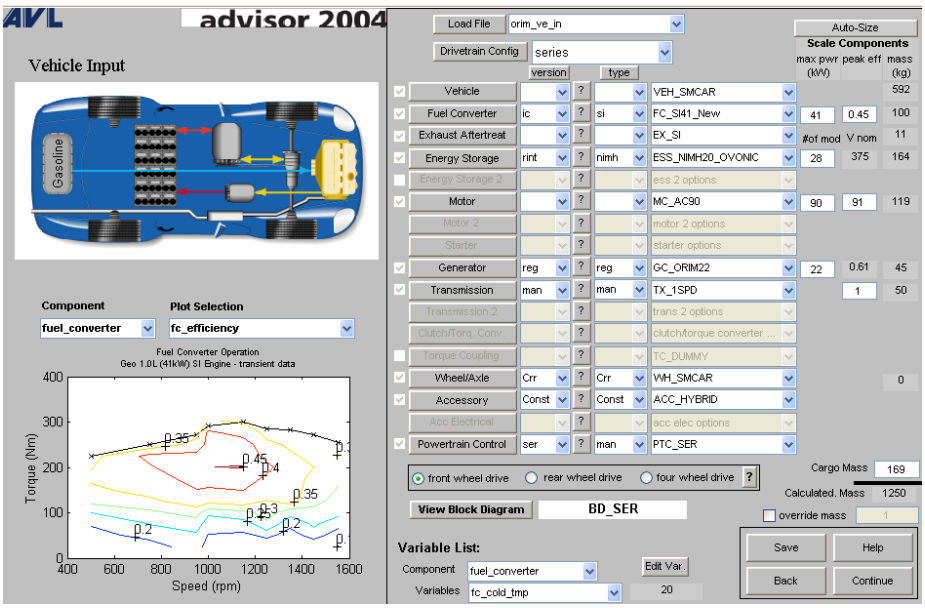

Figure A.4 ADVISOR Vehicle Input screen

A.1.2 ADVISOR Simulation Parameters GUI Screen

In this step, the simulation parameters and required tests are defined. Various drive cycles and particular tests are available in this window, as shown in Figure A.5, and the user can select the suitable one which satisfies the desired simulation requirements. It is possible to choose the multiple drive cycles or even build a trip with combined drive cycles in sequence. The speed trace of the selected drive cycle and its statistical analysis

are shown on the left portion of the screen. If the acceleration and gradeability checkboxes are selected, their values can be shown in the result screen. The gradeability test determines the maximum grade sustainable by the vehicle at the selected drive cycle. In the simulation setup screen, user can perform the parametric study to find out the impacts of the variables on the vehicle. Moreover, the real time simulation can be viewed by running the interactive simulation facility in this window. When the simulation setup for the selected vehicle is completed, the simulation can be performed by clicking on the run button.

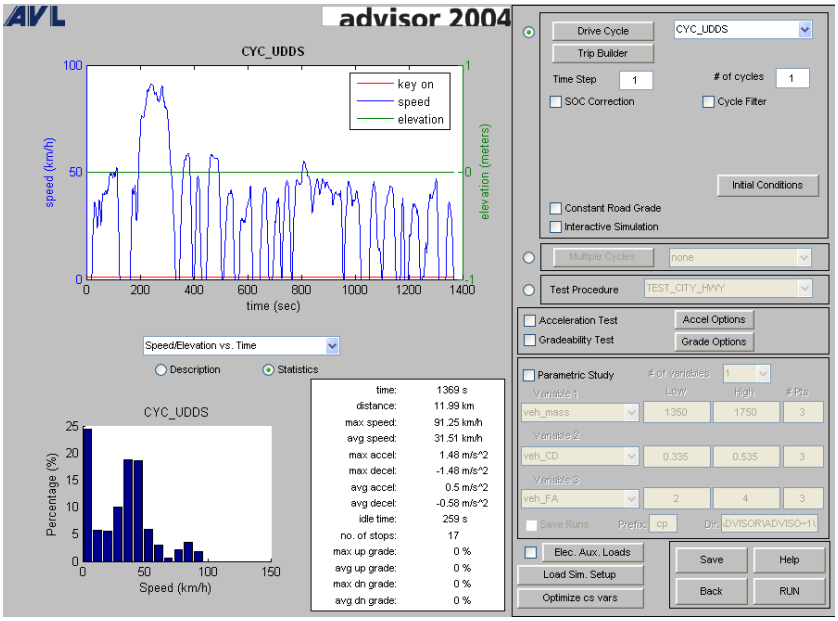

Figure A.5 ADVISOR simulation parameters GUI screen

A.1.3 ADVISOR Results GUI Screen

ADVISOR results screen (Figure A.6) shows the outcome of the selected vehicle simulation. Fuel economy which determines the travelled distance by the vehicle per unit volume of fuel consumed (miles per gallon), exhaust emissions and the vehicle other performance parameters are provided in this window. The plots in the left portion of the screen can be changed to display other required information of the components versus time. In addition, the energy usage tables of the powertrain components and their

efficiencies during power mode or regenerative mode can be obtained by clicking the associated button in the results window. The achieved simulation result can be saved and compared with any new simulation data or any other dependent test data.

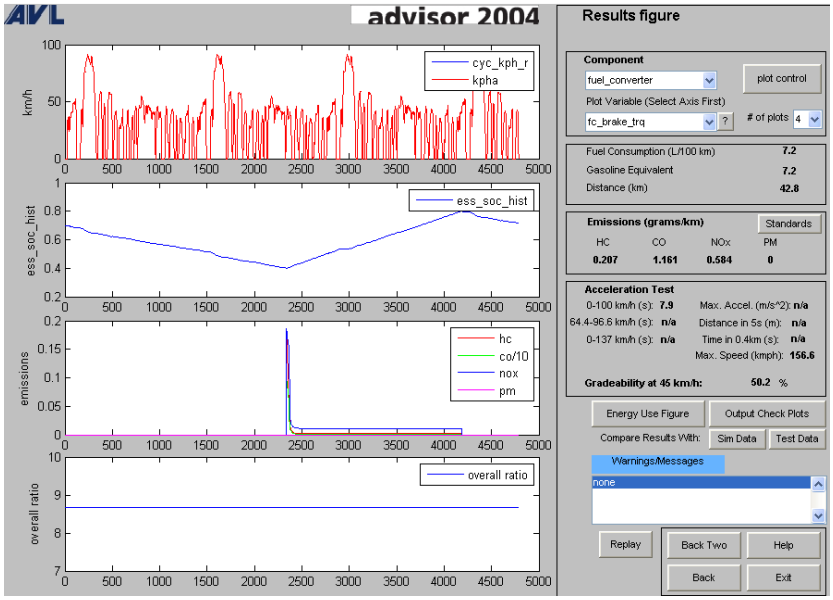

Figure A.6 ADVISOR results screen

A.2 ADVISOR Approach

As Figure A.1 shows the HEV components are modelled in ADVISOR and connected together to present the whole vehicle model. Each component model has some Simulink sub-blocks which are used to model the component and process the data. The data flows within the hybrid vehicle components and finally the vehicle performance parameters such as fuel economy and emissions are calculated.

Two major kinds of calculations, backward and forward – facing are used by vehicle simulation tools. These two techniques are combined in ADVISOR to perform the calculations. The arrows providing data from left to right, shown in Figure A.1, such as the arrow going from the gearbox block to the motor/controller block indicate the backward calculation approach path. These arrows pass the required speed, torque and

power up the powertrain. Whereas, the arrows which go back from right to left in the mentioned figure, such as arrows going from the power bus to the motor/controller block indicate the forward-facing calculation approach path. The forward approach arrows pass the available power, torque and speed within the powertrain.

In the backward simulation process, the driver is not included in the whole model, assuming the components satisfy the requirements. The requested force according to the required speed is calculated and then translated to the requested torque from one component to another one. This approach is performed backward within the powertrain in the opposite direction with the power flow until the fuel consumption is achieved. The backward calculations can be done quickly because in this approach, the performance of the components is tabulated in the model block diagrams according to the measured test data in the laboratories. This increases the calculation progress ability over backward simulation. As the measured data of components such as efficiency maps are measured in the steady-state mode, so the backward approach only simulates the steady- state (not dynamic) performance of the vehicle [77].

Compare to the backward method, in the forward approach, the model of the driver is included in simulation to consider the accelerator and brake pedals commands. These commands are converted into the torque and force in sequence. The acceleration then is computed by the available force divided by mass. This approach is performed in the same direction as power flow within the powertrain. The forward calculation method is useful for development of the hardware because it handles the data which can be measured in a real powertrain such as control commands and real torques (not required torque). Furthermore, this approach can contain the dynamic behaviour of the vehicle

and also can be used for the vehicle acceleration test. The speed of the forward simulation is low and this is the main disadvantage for this approach [80].

In ADVISOR both of the forward and backward calculations are used. However it is closely associated to the backward-facing approach. It contains the limits of the components performance in the backward simulation part combining with the forward simulation approach. It is assumed the efficiency in both calculations are the same and also the powertrain component can not request the power more than it is able to use [77 , 80].

A.3 AVISOR Characteristics

ADVISOR has modular construction and its source code is open for the user. ADVISOR presents the fast and robust simulation of the different configurations of the vehicle. Furthermore, the models in ADVISOR are parameterized and components can be scaled or modified by changing their data file which increases the flexibility of the simulator [77 , 80].

ADVISOR uses experimental data combined with mathematical modelling. This method is a valuable technique for dynamic modelling in the robust engineering design process [81].

ADVISOR has been created as an analysis simulator originally. Because of the quasi-static models of the components in ADVISOR, the dynamic behaviours of the vehicle during the periods of smaller than a tenth of a second cannot be simulated accurately unless it is linked to the other simulators such as Simplorer and Saber. Therefore, ADVISOR cannot be used for the detailed design purposes independently. However,

many of the dynamic behaviour of the components can be simulated if the static-state steps of the events have small enough times. The other limitation for ADVISOR is the requirement for the large number of precise tests for the components [78 , 79].

Appendix B MATLAB Data Files of the ORIM Performance Characteristics

B.1 Torque-speed Characteristics of the ORIM

```
%%%%%%%%%%%%%%%%%%%%%%%%%%%%%%%%%%%%%%%%%%%%%%%%%%%%%%%%%%%%%%%%%%%%%%%%%%%%%%%%
              %Plot the Torque-speed of the designed ORIM
%%%%%%%%%%%%%%%%%%%%%%%%%%%%%%%%%%%%%%%%%%%%%%%%%%%%%%%%%%%%%%%%%%%%%%%%%%%%%%%%

clc, clear all, close all
%%%%%%%%%%%%%%%%%%%%%%%%%%%%%%%%%%%%%%%%%%%%%%%%%%%%%%%%%%%%%%%%%%%%%%%%%%%%%%%%
% Initialise the known values (equivalent circuit elements)
%%%%%%%%%%%%%%%%%%%%%%%%%%%%%%%%%%%%%%%%%%%%%%%%%%%%%%%%%%%%%%%%%%%%%%%%%%%%%%%%
Rs = 0.2207;                                        % stator resistance (ohm)
Xsl = 0.994;                                         % stator reactance (ohm)
Rr = 0.221;                % rotor resistance transfered to stator (ohm)
Xrl =1.2816;                % rotor recatance transfered to stator (ohm)
Xm = 15.7286;                                % magnetisation reactance (ohm)
Rc = 262.91;          % Rc represents the no-load losses (core losses),
Rc=(0.97*V_phase)/Iac_nl [48],=> Rc=(232.41/0.884)=262.91(ohm)

%%%%%%%%%%%%%%%%%%%%%%%%%%%%%
%Power supply specification
%%%%%%%%%%%%%%%%%%%%%%%%%%%%%
V_phase = 415/sqrt(3);                                % phase voltage (volt)
p = 4;                                                     % number of poles
f = 50;                                                     % frequency (Hz)
n_sync = 120*f/p;                                  % synchronous speed (rpm)
w_sync = n_sync*2*pi/60;                          % synchronous speed (rad/s)
s = -1:0.0001:1;                                             % slip
n_m = (1 - s).*n_sync;           % rotor mechanical shaft speed (rad/s)
w_m = (1 - s).*w_sync;           % rotor mechanical shaft speed (rad/s)

%%%%%%%%%%%%%%%%%%%%%%%%%%%%%%%%%%%%%%%%%%%%%%%%%%%%%%%%%%%%%%%%%%%%%%%%%%%%%%%%
%Equivalent circuit elements impedances
%%%%%%%%%%%%%%%%%%%%%%%%%%%%%%%%%%%%%%%%%%%%%%%%%%%%%%%%%%%%%%%%%%%%%%%%%%%%%%%%
Zs = Rs + j*Xsl;                                          % stator impedance
Zm = (Rc*j*Xm)/ (Rc + j*Xm);                       % magnetising impedance
Zr = abs((Rr./s)) + j*Xrl;                                 % rotor impedance
Zeq = Zs + (Zm.*Zr)./(Zm + Zr);                   % equaivalent impedance
I_phase = V_phase./Zeq;                         % Input current to a phase
E1 = V_phase - Zs.* I_phase;                                % induced mmf

%%%%%%%%%%%%%%%%%%%%
%power calculations
%%%%%%%%%%%%%%%%%%%%
PF = cos(angle(I_phase));
P_in = 3*V_phase*abs(I_phase).*PF;                        % input power in W
P_Cu = 3*abs(I_phase).^2*Rs;       % stator winding copper losses in W
P_iron = 3*abs(E1).^2*(1/Rc);                             % core losses in W
P_AG = P_in - P_Cu - P_iron;                                 % airgap power
%OR P_Al = s.*P_AG;                                      % rotor cage losses
P_conv = (1 - s).*P_AG;                                   % converted power
```

```
%%%%%%%%%%%%%%%%%%%%%%%%%%%
%Induced torque calculation
%%%%%%%%%%%%%%%%%%%%%%%%%%%
pos_s = (length(s)-1)/2;                  % position of s in terms of a
centre element of s

t_ind_neg_s = -P_conv./w_m;             % induced torque vector for s<0
t_ind_plus_s = P_conv./w_m;             % induced torque vector for s>0
t_ind_plus_vec = t_ind_plus_s(pos_s+1:end);           % induced torque
vector for s>0

t_ind_neg_vec = t_ind_neg_s(1:pos_s);          % induced torque vector
for s<0

t_ind = [t_ind_neg_vec,t_ind_plus_vec];              % inducced torque
P_conv_1 = (1 -abs(s)).*P_AG;               %converted power regardless
of direction of delivery of the power

figure, plot (n_m,t_ind);
grid on;
```

B.2 ORIM Efficiency Map

```
%%%%%%%%%%%%%%%%%%%%%%%%%%%%%%%%%%%%%%%%%%%%%%%%%%%%%%%%%%%%%%%%%%%%%%%%%%%%
   % calculate the efficiency map of the designed induction machine
%%%%%%%%%%%%%%%%%%%%%%%%%%%%%%%%%%%%%%%%%%%%%%%%%%%%%%%%%%%%%%%%%%%%%%%%%%%%

clc, clear all, close all
%%%%%%%%%%%%%%%%%%%%%%%%%%%%%%%%%%%%%%%%%%%%%%%%%%%%%%%%%%%%%%%%%%%%%%%%%%%%
%Initialise the known values(equivalent circuit elements)
%%%%%%%%%%%%%%%%%%%%%%%%%%%%%%%%%%%%%%%%%%%%%%%%%%%%%%%%%%%%%%%%%%%%%%%%%%%%
Rs = 0.2207;                                    % stator resistance (ohm)
Xsl = 0.994;                                     % stator reactance (ohm)
Rr = 0.221;              % rotor resistance transfered to stator (ohm)
Xrl =1.2816;              % rotor recatance transfered to stator (ohm)
Xm = 15.7286;                           % magnetisation reactance (ohm)
Rc = 262.91;                          % Rc represents the no-load (ohm)
losses, Rc=(0.97*V_phase)/Iac_nl [48],=> Rc=(232.41/0.884)=262.91(ohm)

%%%%%%%%%%%%%%%%%%%%%%%%%%%
%Power supply specification
%%%%%%%%%%%%%%%%%%%%%%%%%%%
V_phase = 415/sqrt(3);                             % phase voltage (volt)
p = 4;                                                  % number of poles
f = 50;                                                  % frequency (Hz)
n_sync = 120*f/p;                                % synchronous speed (rpm)
w_sync = n_sync*2*pi/60;                        % synchronous speed (rad/s)
s = -1:0.0001:1                                        % slip
n_m = (1 - s).*n_sync;          % rotor mechanical shaft speed (rad/s)
w_m = (1 - s).*w_sync;          % rotor mechanical shaft speed (rad/s)

%%%%%%%%%%%%%%%%%%%%%%%%%%%%%%%%%%%%%%%%%%%%%%%%%%%%%%%%%%%%%%%%%%%%%%%%%%%%
%Equivalent circuit elements impedances
%%%%%%%%%%%%%%%%%%%%%%%%%%%%%%%%%%%%%%%%%%%%%%%%%%%%%%%%%%%%%%%%%%%%%%%%%%%%
Zs = Rs + j*Xsl;                                        % stator impedance
Zm = (Rc*j*Xm)/ (Rc + j*Xm);                  % magnetising impedance
Zr = abs((Rr./s)) + j*Xrl;                              % rotor impedance
Zeq = Zs + (Zm.*Zr)./(Zm + Zr);                % equaivalent impedance
I_phase = V_phase./Zeq;                      % Input current to a phase
```

```
E1 = V_phase - Zs.* I_phase;                                % induced mmf
%%%%%%%%%%%%%%%%%%%
%power calculations
%%%%%%%%%%%%%%%%%%%
PF = cos(angle(I_phase));
P_in = 3*V_phase*abs(I_phase).*PF;                    % input power in W
t_in_map = [0:20:200];                                % torque vector
corresponding to columns of efficiency map (t_in>0 =>running as a
generator)

w_m_map = [0:150:1500]* (2*pi)/60;                    % speed vector
corresponding to rows of efficiency map

[T1,W1] = meshgrid(t_in_map,w_m_map);
P_o_map = T1.*W1;                          % output power in motoring mode
coef = [1 1 1 1 1 1 1 1 1 1 1];
P_in1 = [];
for i=20001:-1000:10001
    P_in1 =[P_in1,P_in(i)];
end
[coef1,P_in1] = meshgrid(coef,P_in1);
P_in_map = coef1.*P_in1;
ORIM_eff_map=P_o_map./P_in_map           % eficiency map matrix of ORIM
```

% Efficiency map matrix of ORIM shown in MATLAB Command Window %

ORIM_eff_map =

[

0	0	0	0	0	0	0	0	0	0	0
0	0.0207	0.0415	0.0622	0.0829	0.1037	0.1244	0.1451	0.1659	0.1866	0.2073
0	0.0393	0.0786	0.1180	0.1573	0.1966	0.2359	0.2752	0.3146	0.3539	0.3932
0	0.0554	0.1107	0.1661	0.2215	0.2768	0.3322	0.3876	0.4430	0.4983	0.5537
0	0.0684	0.1368	0.2052	0.2736	0.3420	0.4104	0.4788	0.5472	0.6156	0.6840
0	0.0779	0.1557	0.2336	0.3114	0.3893	0.4671	0.5450	0.6228	0.7007	0.7785
0	0.0831	0.1661	0.2492	0.3322	0.4153	0.4984	0.5814	0.6645	0.7475	0.8306
0	0.0835	0.1669	0.2504	0.3338	0.4173	0.5008	0.5842	0.6677	0.7511	0.8346
0	0.0795	0.1590	0.2384	0.3179	0.3974	0.4769	0.5564	0.6358	0.7153	0.7948
0	0.0797	0.1593	0.2390	0.3187	0.3983	0.4780	0.5577	0.6374	0.7170	0.7967
0	0.0797	0.1593	0.2390	0.3187	0.3983	0.4780	0.5577	0.6374	0.7170	0.7967

]

Appendix C ADVISOR data files of the Genset Components

C.1 Data file of the Outer Rotor Generator

```
%%%%%%%%%%%%%%%%%%%%%%%%%%%%%%%%%%%%%%%%%%%%%%%%%%%%%%%%%%%%%%%%%%%%%%%%%%%%
                    % ADVISOR data file: GC_ORIM22.m
%%%%%%%%%%%%%%%%%%%%%%%%%%%%%%%%%%%%%%%%%%%%%%%%%%%%%%%%%%%%%%%%%%%%%%%%%%%%


%%%%%%%%%%%%%%%
% FILE ID INFO
%%%%%%%%%%%%%%%
gc_description='Outer Rotor 22-kW induction machine/controller';
gc_version=2004;        % version of ADVISOR for which the file was
generated

gc_proprietary=0;       % 0=> non-proprietary, 1=> proprietary, do not
distribute

gc_validation=0;      % 0=> no validation, 1=> data agrees with source
data,
% 2=> data matches source data and data collection methods have been
verified

disp(['Data loaded: GC_PM32 - ',gc_description])


%%%%%%%%%%%%%%%%%%%%%%%%%%%%%%%%%%%%%%%%%%%%%%%%%%%%%%%%%%%%%%%%%%%%%%%%%%%%
% SPEED & TORQUE RANGES over which data is defined
%%%%%%%%%%%%%%%%%%%%%%%%%%%%%%%%%%%%%%%%%%%%%%%%%%%%%%%%%%%%%%%%%%%%%%%%%%%%
% (N*m), torque vector corresponding to columns of efficiency & loss
maps
% this is INPUT torque (>0 => running as a generator)
gc_map_trq=[0 20 40 60 80 100 120 140 160 180 200];

% (rad/s), speed vector corresponding to rows of efficiency & loss
maps
gc_map_spd=[0 150 300 450 600 750 900 1050 1200 1350 1500]*(2*pi)/60;


%%%%%%%%%%%%%%%%%%%%%%%%%%%
% LOSSES AND EFFICIENCIES
%%%%%%%%%%%%%%%%%%%%%%%%%%%
gc_eff_map=[
0   0       0       0       0       0       0       0       0       0
0
0   0.0207  0.0415  0.0622  0.0829  0.1037  0.1244  0.1451  0.1659
0.1866  0.2073
0   0.0393  0.0786  0.118   0.1573  0.1966  0.2359  0.2752  0.3146
0.3539  0.3932
0   0.0554  0.1107  0.1661  0.2215  0.2768  0.3322  0.3876  0.443
0.4983  0.5537
0   0.0684  0.1368  0.2052  0.2736  0.342   0.4104  0.4788  0.5472
0.6156  0.684
0   0.0779  0.1557  0.2336  0.3114  0.3893  0.4671  0.545   0.6228
0.7007  0.7785
```

```
0   0.0831  0.1661  0.2492  0.3322  0.4153  0.4984  0.5814  0.6645
0.7475  0.8306
0   0.0835  0.1669  0.2504  0.3338  0.4173  0.5008  0.5842  0.6677
0.7511  0.8346
0   0.0795  0.159   0.2384  0.3179  0.3974  0.4769  0.5564  0.6358
0.7153  0.7948
0   0.0797  0.1593  0.239   0.3187  0.3983  0.478   0.5577  0.6374
0.717   0.7967
0   0.0797  0.1593  0.239   0.3187  0.3983  0.478   0.5577  0.6374
0.717   0.7967
];    % (--), efficiency of the machine/inverter when run as a motor

%
% convert to losses, assuming losses are symmetric about zero torque
%
[T1,w1]=meshgrid(gc_map_trq,gc_map_spd);
gc_mech_pwr_map=T1.*w1; % (W), output power (when motoring) for each
trq and spd

temp=gc_mech_pwr_map./gc_eff_map;        % input power (when motoring)
gc_loss_map=temp-gc_mech_pwr_map; % (W) loss corresponding to each trq
and spd

%
% assume that losses at zero torque and speed are the same as nearest
  neighbors
%

gc_loss_map(1,:)=gc_loss_map(2,:); % loss at zero spd = loss at lowest
+ive spd

gc_loss_map(:,1)=gc_loss_map(:,2); % loss at zero trq = loss at lowest
+ive trq

%
% convert loss map to output power map for machine running as a
  generator
%
gc_outpwr_map=gc_mech_pwr_map-gc_loss_map;


%%%%%%%%
% LIMITS
%%%%%%%%
gc_max_crrnt=37.5;  % maximum current draw for motor/controller set, A
gc_min_volts=415;   % minimum voltage for motor/controller set, V
% maximum continuous torque corresponding to speeds in gc_map_spd


gc_max_trq=[42 46.43 51.95 58.92 68 80.24 97.5 123 161.7 199.7 1.31];

% factor by which motor torque can exceed maximum continuous torque
for short
% periods of time

gc_overtrq_factor=320/220;  % (--)

 %%%%%%%%%%%%%%%%
% DEFAULT SCALING
%%%%%%%%%%%%%%%%
```

```
% (--), used to scale fc_map_spd to simulate a faster or slower
running engine
gc_spd_scale=1.0;
% (--), used to scale fc_map_trq to simulate a higher or lower torque
engine
gc_trq_scale=1.0;


%%%%%%%%%%%%
% OTHER DATA
%%%%%%%%%%%%
gc_inertia=0.0235;      % (kg*m^2), rotor's rotational inertia same as
22kw IM.
gc_mass=45;   % (kg), mass of machine and controller, same as 25kw IM.


%%%%%%%%%%
% CLEAN UP
%%%%%%%%%%
clear T1 w1 gc_inpwr_map temp gc_loss_map gc_mech_pwr_map


%%%%%%%%%%%%%%%%%%%%%%%%%%%%%%%%%%%%%%%%
% REVISION HISTORY
%%%%%%%%%%%%%%%%%%%%%%%%%%%%%%%%%%%%%%%%
gc_mass_scale_coef=[1 0 1 0];
gc_mass_scale_fun=inline('(x(1)*gc_trq_scale+x(2))*(x(3)*gc_spd_scale+
x(4))*gc_mass','x','gc_spd_scale','gc_trq_scale','gc_mass');
```

C.2 Data File of the Novel Engine

```
%%%%%%%%%%%%%%%%%%%%%%%%%%%%%%%%%%%%%%%%%%%%%%%%%%%%%%%%%%%%%%%%%%%%%%%%%%%%
                    % ADVISOR data file: FC_SI41_New.m
%%%%%%%%%%%%%%%%%%%%%%%%%%%%%%%%%%%%%%%%%%%%%%%%%%%%%%%%%%%%%%%%%%%%%%%%%%%%

% Notes: Novel Engie 41KW SI engine.

%%%%%%%%%%%%%%%
% FILE ID INFO
%%%%%%%%%%%%%%%
fc_description='Geo 1.0L (41kW) SI Engine - transient data';
fc_version=2004; % version of ADVISOR for which the file was generated
fc_proprietary=0; % 0=> non-proprietary, 1=> proprietary, do not
distribute

fc_validation=0; % 1=> no validation, 1=> data agrees with source
data,
% 2=> data matches source data and data collection methods have been
verified

fc_fuel_type='Gasoline';
fc_disp=1.0;                                % (L), engine displacement
fc_emis=1;                          % boolean 0=no emis data; 1=emis data
fc_cold=0;                  % boolean 0=no cold data; 1=cold data exists
disp(['Data loaded: FC_SI41_emis.M - ',fc_description]);
```

```
%%%%%%%%%%%%%%%%%%%%%%%%%%%%%%%%%%%%%%%%%%%%%%%%%%
% SPEED & TORQUE RANGES over which data is defined
%%%%%%%%%%%%%%%%%%%%%%%%%%%%%%%%%%%%%%%%%%%%%%%%%%
% (rad/s), speed range of the engine
fc_map_spd=[500 750 950 1000 1150 1250 1350 1450 1551]*2*pi/60;

% (N*m), torque range of the engine
fc_map_trq=[6.8 13.6 20.4 27.2 33.8 40.6 47.4 54.2 61 67.8 74.6
81.4]*3.7;



%%%%%%%%%%%%%%%%%%%%%%%%%%%%%%
% FUEL USE AND EMISSIONS MAPS
%%%%%%%%%%%%%%%%%%%%%%%%%%%%%%
% (g/s), fuel use map indexed vertically by fc_map_spd and
% horizontally by fc_map_trq
fc_fuel_map_gpkWh =[
635.7   635.7   541.4   447.2   352.9   332.2   311.4   322.4   333.5
333.5   333.5   333.5
678.4   500.1   443.8   387.4   331.1   301.8   297 283.4   269.8
358 358 358
463.4   463.4   407.6   350.1   294.3   280.8   267.3   253.9   269.8
303.2   336.7   336.7
699.1   567.9   500.3   432.7   301.4   283.9   266.3   248.7   258.8
268.8   271.9   317.9
592.9   592.9   494.6   393.4   295.1   279.4   263.6   247.9   255.2
262.5   295 322.6
667.9   524.8   381.6   351.9   322.2   304.9   287.5   270.8   290.8
310.9   330.9   330.9
630.6   630.6   522.5   411.1   303 304.4   305.8   304.2   314.5
324.8   327.7   327.7
698.4   500.5   428.6   392.7   356.8   337.9   328.4   319 328.8
338.6   333.7   333.7
751.1   637.8   521.1   407.8   393.1   378.4   363.3   348.2   318.8
340.2   340.2   340.2];
% fuel map in g/kWh

% (g/s), engine out HC emissions indexed vertically by fc_map_spd and
% horizontally by fc_map_trq
fc_hc_map_gpkWh =[
11.5    11.5    9.8 8.2 6.5 5.8 5.1 5.9 6.8 6.8 6.8 6.8
7.8 7   6.2 5.5 4.7 4.3 4.7 4.6 4.5 4.6 4.6 4.6
5.8 5.8 5.2 4.6 4   4   4   4   4.5 4.6 4.6 4.6
7.1 6   5.4 4.9 3.8 3.7 3.6 3.4 3.2 3   3.4 3.9
5.8 5.8 5   4.3 3.6 3.6 3.6 3.7 3.6 3.6 4   3.9
5.6 4.7 3.7 3.7 3.7 3.4 3.1 3   3.2 3.4 3.5 3.5
8.2 8.2 6.8 5.4 4.1 3.7 3.3 3.1 3.2 3.2 3.3 3.3
5.8 5.2 4.8 4.5 4.3 3.7 3.4 3.2 3.3 3.3 3.3 3.3
5.6 5.8 5.9 6.1 5.7 5.4 5   4.6 3.9 3.9 3.9 3.9];
% engine out HC in g/kWh

% (g/s), engine out CO emissions indexed vertically by fc_map_spd and
% horizontally by fc_map_trq
fc_co_map_gpkWh =[
71.8    71.8    58.8    45.7    32.7    27.5    22.4    82.9    143.3
143.3   143.3   143.3
104.4   68.3    56.8    45.3    33.9    23.3    25.7    24.2    22.8
268.6   268.6   268.6
48.3    48.3    42.9    37.2    31.8    28.6    25.4    22.2    22.8
152.9   283 283
103.1   82.7    72.2    61.8    41.5    36.9    32.3    27.8    31.1
34.4    178.5   279.9
```

```
88.1    88.1    74.2    59.9    46  41.9    37.8    33.7    34.8
35.8    158.8   264.6
96.1    74.5    52.9    51.2    49.5    45.9    42.4    34  117.9
201.8   285.7   285.7
114.6   114.6   92.1    69  46.5    60.7    74.8    129.6   195.5
261.4   277.8   277.8
60.1    63.8    64  64.1    64.3    108.2   130.2   152.2   216.7
281.2   278.1   278.1
51.8    75.2    99.3    122.8   134.9   147.1   159.7   172.2   196.6
286.6   286.6   286.6];
% engine out CO in g/kWh

% (g/s), engine out NOx emissions indexed vertically by fc_map_spd and
% horizontally by fc_map_trq
fc_nox_map_gpkWh =[
5.8 5.8 9.3 12.8    16.3    16.1    15.9    13  10.2    10.2    10.2
10.2
5.2 8.8 9.2 9.7 10.2    8   8.9 13.2    17.5    4.6 4.6 4.6
8.1 8.1 8.8 9.6 10.4    10.8    11.3    11.7    17.5    11.6    5.7
5.7
4.2 5.6 6.3 7   8.4 8.9 9.5 10.1    13.9    17.7    8.1 3.1
5.8 5.8 7.2 8.7 10.1    11  11.8    12.6    15.9    19.2    9.3 6.8
14.9    16.4    17.8    19.4    21  20.6    20.3    19.1    14.6
10.2    5.7 5.7
28.7    28.7    26.8    25  23.1    22.4    21.7    16.5    12.1
7.8 6.5 6.5
31.1    27.9    26.7    26.2    25.6    20.9    18.6    16.3    12.1
7.8 6.8 6.8
35  31.1    27.1    23.2    21.1    19.1    17  14.9    10.9    7.4
7.4 7.4];
% engine out NOx in g/kWh

% (g/s), engine out PM emissions indexed vertically by fc_map_spd and
% horizontally by fc_map_trq
fc_pm_map_gpkWh=zeros(size(fc_fuel_map_gpkWh));

% (g/s), engine out O2 indexed vertically by fc_map_spd and
% horizontally by fc_map_trq
fc_o2_map=zeros(size(fc_fuel_map_gpkWh));


% convert g/kWh maps to g/s maps
[T,w]=meshgrid(fc_map_trq, fc_map_spd);
fc_map_kW=T.*w/1000;
fc_fuel_map=fc_fuel_map_gpkWh.*fc_map_kW/3600;
fc_hc_map=fc_hc_map_gpkWh.*fc_map_kW/3600;
fc_co_map=fc_co_map_gpkWh.*fc_map_kW/3600;
fc_nox_map=fc_nox_map_gpkWh.*fc_map_kW/3600;
fc_pm_map=fc_pm_map_gpkWh.*fc_map_kW/3600;


%%%%%%%%%%%%%%%%%%
% Cold Engine Maps
%%%%%%%%%%%%%%%%%%
fc_cold_tmp=20;                                                 %deg C
fc_fuel_map_cold=zeros(size(fc_fuel_map));
fc_hc_map_cold=zeros(size(fc_fuel_map));
fc_co_map_cold=zeros(size(fc_fuel_map));
fc_nox_map_cold=zeros(size(fc_fuel_map));
fc_pm_map_cold=zeros(size(fc_fuel_map));
%Process Cold Maps to generate Correction Factor Maps
```

```
names={'fc_fuel_map','fc_hc_map','fc_co_map','fc_nox_map','fc_pm_map'}
;
for i=1:length(names)
    %cold to hot raio, e.g. fc_fuel_map_c2h = fc_fuel_map_cold ./
fc_fuel_map
    eval([names{i},'_c2h=',names{i},'_cold./(',names{i},'+eps);'])
end


%%%%%%%%
% LIMITS
%%%%%%%%
% (N*m), max torque curve of the engine indexed by fc_map_spd
fc_max_trq=[61  67.6 73.7 78.5 80.9 77.3 76.2 73.3 68.7]*3.7;

% (N*m), closed throttle torque of the engine (max torque that can be
absorbed)
% indexed by fc_map_spd -- correlation from JDMA
fc_ct_trq=4.448/3.281*(-fc_disp)*61.02/24 * ...
   (9*(fc_map_spd/max(fc_map_spd)).^2 + 14 *
(fc_map_spd/max(fc_map_spd)));


%%%%%%%%%%%%%%%%%%
% DEFAULT SCALING
%%%%%%%%%%%%%%%%%%
% (--), used to scale fc_map_spd to simulate a faster or slower
running engine

fc_spd_scale=1.0;
% (--), used to scale fc_map_trq to simulate a higher or lower torque
engine

fc_trq_scale=1.0;
fc_pwr_scale=fc_spd_scale*fc_trq_scale;           % --  scale fc power
% user definable mass scaling function

fc_mass_scale_fun=inline('(x(1)*fc_trq_scale+x(2))*(x(3)*fc_spd_scale+
x(4))*(fc_base_mass+fc_acc_mass)+fc_fuel_mass','x','fc_spd_scale','fc_
trq_scale','fc_base_mass','fc_acc_mass','fc_fuel_mass');
fc_mass_scale_coef=[1 0 1 0]; % coefficients of mass scaling function


%%%%%%%%%%%%%%%%%%%%%%%%%%%%%%%%%%%%%%%%%%%%%%%%%%%%%%%%%%%%%%%%%%%%
% STUFF THAT SCALES WITH TRQ & SPD SCALES (MASS AND INERTIA)
%%%%%%%%%%%%%%%%%%%%%%%%%%%%%%%%%%%%%%%%%%%%%%%%%%%%%%%%%%%%%%%%%%%%
fc_inertia=0.1*fc_pwr_scale;            % (kg*m^2), rotational inertia
of the engine (unknown)

fc_max_pwr=(max(fc_map_spd.*fc_max_trq)/1000)*fc_pwr_scale; % kW
peak engine power

fc_base_mass=1.8*fc_max_pwr;                % (kg), mass of the engine
block and head (base engine)
                                           % mass penalty of 1.8 kg/kW
from 1994 OTA report, Table 3
fc_acc_mass=0.8*fc_max_pwr;                    % (kg), engine accy's,
electrics, cntrl's - assumes mass penalty of 0.8 kg/kW (from OTA
report)

fc_fuel_mass=0.6*fc_max_pwr;             % (kg), mass of fuel and fuel
tank (from OTA report)
```

```
fc_mass=fc_base_mass+fc_acc_mass+fc_fuel_mass;           % (kg), total
engine/fuel system mass

fc_ext_sarea=0.3*(fc_max_pwr/100)^0.67;              % (m^2), exterior
surface area of engine



%%%%%%%%%%%
% OTHER DATA
%%%%%%%%%%%
fc_fuel_den=0.749*1000;                    % (g/l), density of the fuel
fc_fuel_lhv=42.6*1000;        % (J/g), lower heating value of the fuel
%the following was added for the new thermal modeling of the engine
12/17/98 ss and sb
fc_tstat=96;                        % (C), engine coolant thermostat set
temperature (typically 95 +/- 5 C)

fc_cp=500;                       % (J/kgK), ave cp of engine (iron=500,
Al or Mg = 1000)

fc_h_cp=500;                          % (J/kgK), ave cp of hood & engine
compartment (iron=500, Al or Mg = 1000)

fc_hood_sarea=1.5;              %(m^2), surface area of hood/eng compt.
fc_emisv=0.8;                   % emissivity of engine ext surface/hood
int surface

fc_hood_emisv=0.9;                              % emissivity hood ext
fc_h_air_flow=0.0;                % (kg/s), heater air flow rate (140
cfm=0.07)

fc_cl2h_eff=0.7;      % -- ave cabin heater HX eff (based on air side)
fc_c2i_th_cond=500;          % (W/K), conductance btwn engine cyl & int
fc_i2x_th_cond=500;          % (W/K), conductance btwn engine int & ext
fc_h2x_th_cond=10;           % (W/K), conductance btwn engine & engine
compartment

% calc "predicted" exh gas flow rate and engine-out (EO) temp
fc_ex_pwr_frac=[0.40 0.30];                          % -- frac of waste
heat that goes to exhaust as func of engine speed

fc_exflow_map=fc_fuel_map*(1+14.5);                % (g/s) ex gas flow
map:  for SI engines, exflow=(fuel use)*[1 + (stoic A/F ratio)]

fc_waste_pwr_map=fc_fuel_map*fc_fuel_lhv - T.*w;   % (W), tot FC waste
heat = (fuel pwr) - (mech out pwr)

spd=fc_map_spd;
fc_ex_pwr_map=zeros(size(fc_waste_pwr_map));       % (W), initialize
size of ex pwr map

for i=1:length(spd)
 fc_ex_pwr_map(i,:)=fc_waste_pwr_map(i,:)*interp1([min(spd)
max(spd)],fc_ex_pwr_frac,spd(i));  % (W), trq-spd map of waste heat to
exh

end
fc_extmp_map=fc_ex_pwr_map./(fc_exflow_map*1089/1000) + 20;  % (W), EO
ex gas temp = Q/(MF*cp) + Tamb (assumes engine tested ~20 C)
```

```
%the following variable is not used directly in modelling and should
always be equal to one
%it's used for initialization purposes
fc_eff_scale=1;

% clean up workspace
clear T w fc_waste_pwr_map fc_ex_pwr_map spd fc_map_kW
```

Appendix D ADVISOR Data Files of the Powertrain Components

D.1 Data File of 22KW PM Generator

```
%%%%%%%%%%%%%%%%%%%%%%%%%%%%%%%%%%%%%%%%%%%%%%%%%%%%%%%%%%%%%%%%%%%%%%%%%%%%%%%
                    % ADVISOR data file:  GC_PM22.m
%%%%%%%%%%%%%%%%%%%%%%%%%%%%%%%%%%%%%%%%%%%%%%%%%%%%%%%%%%%%%%%%%%%%%%%%%%%%%%%

% Unique Mobility specification sheet for the SR180p/CR20-300
  motor/controller combination at 195 V.

 %%%%%%%%%%%%%%%%
% FILE ID INFO
%%%%%%%%%%%%%%%%
gc_description='Modified Unique Mobility 32-kW permanent magnet
motor/controller';

gc_version=2004; % version of ADVISOR for which the file was generated
gc_proprietary=0; % 0=> non-proprietary, 1=> proprietary, do not
distribute

gc_validation=0; % 0=> no validation, 1=> data agrees with source
data,
% 2=> data matches source data and data collection methods have been
verified

disp(['Data loaded: GC_PM22 - ',gc_description])


%%%%%%%%%%%%%%%%%%%%%%%%%%%%%%%%%%%%%%%%%%%%%%%%%%%%%%%%%%%%%%%%%%%%%%%%%%%%%%%
% SPEED & TORQUE RANGES over which data is defined
%%%%%%%%%%%%%%%%%%%%%%%%%%%%%%%%%%%%%%%%%%%%%%%%%%%%%%%%%%%%%%%%%%%%%%%%%%%%%%%
% (N*m), torque vector corresponding to columns of efficiency & loss
maps
% this is INPUT torque (>0 => running as a generator)
gc_map_trq=[0 40 80 120 160 200 240 320 400 480 520]*4.448/3.281/12;

% (rad/s), speed vector corresponding to rows of efficiency & loss
maps
gc_map_spd=[0 500 1000 1500 2000 2500 3000 4000 5000 6000
7000]*(2*pi)/60;


%%%%%%%%%%%%%%%%%%%%%%%%%%%
% LOSSES AND EFFICIENCIES
%%%%%%%%%%%%%%%%%%%%%%%%%%%
gc_eff_map=[
0.200   0.200   0.200   0.200   0.200   0.200   0.200   0.200   0.200
0.200   0.200
0.200   0.380   0.490   0.520   0.570   0.600   0.600   0.520   0.450
0.430   0.430
0.200   0.500   0.620   0.670   0.715   0.725   0.730   0.720   0.710
0.700   0.700
```

```
0.200   0.520   0.650   0.710   0.740   0.765   0.770   0.775   0.775
0.767   0.767
0.200   0.540   0.670   0.730   0.770   0.785   0.780   0.800   0.805
0.808   0.808
0.200   0.580   0.700   0.760   0.785   0.810   0.820   0.830   0.835
0.830   0.830
0.200   0.590   0.720   0.770   0.800   0.825   0.835   0.845   0.847
0.846   0.846
0.200   0.600   0.755   0.805   0.830   0.845   0.854   0.865   0.866
0.868   0.868
0.200   0.600   0.770   0.815   0.840   0.860   0.867   0.883   0.888
0.887   0.887
0.200   0.550   0.775   0.830   0.860   0.870   0.884   0.897   0.905
0.910   0.910
0.200   0.500   0.760   0.840   0.870   0.885   0.893   0.905   0.915
0.920   0.920
];% (--), efficiency of the machine/inverter when run as a motor

%
% convert to losses, assuming losses are symmetric about zero torque
%
[T1,w1]=meshgrid(gc_map_trq,gc_map_spd);
gc_mech_pwr_map=T1.*w1; % (W), output power (when motoring) for each
trq and spd

temp=gc_mech_pwr_map./gc_eff_map; % input power (when motoring)
gc_loss_map=temp-gc_mech_pwr_map; % (W) loss corresponding to each trq
and spd

%
% assume that losses at zero torque and speed are the same as nearest
neighbors
%
gc_loss_map(1,:)=gc_loss_map(2,:); % loss at zero spd = loss at lowest
+ive spd
gc_loss_map(:,1)=gc_loss_map(:,2); % loss at zero trq = loss at lowest
+ive trq

%
% convert loss map to output power map for machine running as a
generator
%
gc_outpwr_map=gc_mech_pwr_map-gc_loss_map;


%%%%%%%%
% LIMITS
%%%%%%%%
gc_max_crrnt=300;    % maximum current draw for motor/controller set, A
gc_min_volts=60;     % minimum voltage for motor/controller set, V
% maximum continuous torque corresponding to speeds in gc_map_spd
gc_max_trq=[512 508.1 504.2 500.3 496.3 492.4 488.5 480.7 472.8 465
0]...
   *4.448/3.281/12; % (N*m)
% factor by which motor torque can exceed maximum continuous torque
for short
% periods of time
gc_overtrq_factor=320/220;  % (--)


%%%%%%%%%%%%%%%%%
% DEFAULT SCALING
```

```
%%%%%%%%%%%%%%%%%
% (--), used to scale fc_map_spd to simulate a faster or slower
running engine
gc_spd_scale=1.0;
% (--), used to scale fc_map_trq to simulate a higher or lower torque
engine
gc_trq_scale=1.0;


%%%%%%%%%%%%
% OTHER DATA
%%%%%%%%%%%%
gc_inertia=0.0226; % (kg*m^2), rotor's rotational inertia
gc_mass=25; % (kg), mass of machine and controller


%%%%%%%%%%
% CLEAN UP
%%%%%%%%%%
clear T1 w1 gc_inpwr_map temp gc_loss_map gc_mech_pwr_map


gc_mass_scale_coef=[1 0 1 0];
gc_mass_scale_fun=inline('(x(1)*gc_trq_scale+x(2))*(x(3)*gc_spd_scale+
x(4))*gc_mass','x','gc_spd_scale','gc_trq_scale','gc_mass');
```

D.2 Data File of 22KW IM Generator

```
%%%%%%%%%%%%%%%%%%%%%%%%%%%%%%%%%%%%%%%%%%%%%%%%%%%%%%%%%%%%%%%%%%%%%%%%
                        ADVISOR data file:  GC_IM22.m
%%%%%%%%%%%%%%%%%%%%%%%%%%%%%%%%%%%%%%%%%%%%%%%%%%%%%%%%%%%%%%%%%%%%%%%%

%%%%%%%%%%%%%%%
% FILE ID INFO
%%%%%%%%%%%%%%%
gc_description='Modified Solectria ACgtx20/AC300 25-kW AC Induction
motor/controller';

gc_version=2004; % version of ADVISOR for which the file was generated
gc_proprietary=0; % 0=> non-proprietary, 1=> proprietary, do not
distribute

gc_validation=0; % 0=> no validation, 1=> data agrees with source
data,
% 2=> data matches source data and data collection methods have been
verified

disp(['Data loaded: GC_IM22 - ',gc_description])


%%%%%%%%%%%%%%%%%%%%%%%%%%%%%%%%%%%%%%%%%%%%%%%%%%%%%%%%%%%%%%%%%%%%%%%%
% SPEED & TORQUE RANGES over which data is defined
%%%%%%%%%%%%%%%%%%%%%%%%%%%%%%%%%%%%%%%%%%%%%%%%%%%%%%%%%%%%%%%%%%%%%%%%
% (N*m), torque vector corresponding to columns of efficiency & loss
maps
% this is INPUT torque (>0 => running as a generator)
gc_map_trq=[0 5 10 15 20 25 30 35 40 45 50 55];
```

```
% (rad/s), speed vector corresponding to rows of efficiency & loss
maps
gc_map_spd=[0 1500 3000 4500 6000 7500]*(2*pi)/60;


%%%%%%%%%%%%%%%%%%%%%%%%%
% LOSSES AND EFFICIENCIES
%%%%%%%%%%%%%%%%%%%%%%%%%
gc_eff_map=[
0.72    0.65    0.674   0.691   0.705   0.716   0.722   0.732   0.742
0.737   0.66    0.1

0.72    0.738   0.755   0.768   0.78    0.79    0.796   0.802   0.807
0.8     0.74    0.1

0.72    0.826   0.836   0.845   0.855   0.864   0.87    0.872   0.872
0.863   0.82    0.1

0.72    0.826   0.836   0.845   0.855   0.886   0.899   0.9     0.898
0.89    0.85    0.1

0.72    0.826   0.836   0.845   0.855   0.886   0.899   0.885   0.9
0.899   0.88    0.1

0.72    0.826   0.836   0.845   0.855   0.886   0.899   0.885   0.9
0.897   0.89    0.1
];% (--), efficiency of the machine/inverter when run as a motor

%
% convert to losses, assuming losses are symmetric about zero torque
%

[T1,w1]=meshgrid(gc_map_trq,gc_map_spd);
gc_mech_pwr_map=T1.*w1; % (W), output power (when motoring) for each
trq and spd

temp=gc_mech_pwr_map./gc_eff_map; % input power (when motoring)
gc_loss_map=temp-gc_mech_pwr_map; % (W) loss corresponding to each trq
and spd

%
% assume that losses at zero torque and speed are the same as nearest
  neighbors
%
gc_loss_map(1,:)=gc_loss_map(2,:); % loss at zero spd = loss at lowest
+ive spd
gc_loss_map(:,1)=gc_loss_map(:,2); % loss at zero trq = loss at lowest
+ive trq

%
% convert loss map to output power map for machine running as a
generator
%
gc_outpwr_map=gc_mech_pwr_map-gc_loss_map;

%%%%%%%%
% LIMITS
%%%%%%%%
gc_max_crrnt=210;  % maximum current draw for motor/controller set, A
gc_min_volts=70;   % minimum voltage for motor/controller set, V
% maximum continuous torque corresponding to speeds in gc_map_spd
```

```
gc_max_trq=[55 55 55 39.5 35.9 32.3];

% factor by which motor torque can exceed maximum continuous torque
for short
% periods of time

gc_overtrq_factor=320/220;


%%%%%%%%%%%%%%%%%
% DEFAULT SCALING
%%%%%%%%%%%%%%%%%
% (--), used to scale fc_map_spd to simulate a faster or slower
running engine
gc_spd_scale=1.0;

% (--), used to scale fc_map_trq to simulate a higher or lower torque
engine
gc_trq_scale=1.0;


%%%%%%%%%%%%
% OTHER DATA
%%%%%%%%%%%%
gc_inertia=0.0235; % (kg*m^2), rotor's rotational inertia
gc_mass=45; % (kg), mass of machine and controller.


%%%%%%%%%%
% CLEAN UP
%%%%%%%%%%
clear T1 w1 gc_inpwr_map temp gc_loss_map gc_mech_pwr_map

gc_mass_scale_coef=[1 0 1 0];
gc_mass_scale_fun=inline('(x(1)*gc_trq_scale+x(2))*(x(3)*gc_spd_scale+
x(4))*gc_mass','x','gc_spd_scale','gc_trq_scale','gc_mass');
```

D.3 Data File of UDDS Drive Cycle

```
%%%%%%%%%%%%%%%%%%%%%%%%%%%%%%%%%%%%%%%%%%%%%%%%%%%%%%%%%%%%%%%%%%%%%%%
                    % ADVISOR data file:  CYC_UDDS.m
%%%%%%%%%%%%%%%%%%%%%%%%%%%%%%%%%%%%%%%%%%%%%%%%%%%%%%%%%%%%%%%%%%%%%%%

% Data source: epa website
% Notes:
% Represents the Urban Dynamometer Driving Schedule (UDDS), which is
% equivalent to the first two bags of the Federal Test Procedure (FTP-
  75).
% It is commonly called the "LA4", "FTP 72", "EPA II", or "the city
% test" and represents city driving conditions. It is used for light
% duty vehicle testing.


%%%%%%%%%%%%%%%
% FILE ID INFO
%%%%%%%%%%%%%%%
cyc_description='EPA Urban Dynamometer Driving Schedule';
```

```
cyc_version=2004; % version of ADVISOR for which the file was
generated

cyc_proprietary=0; % 0=> non-proprietary, 1=> proprietary, do not
distribute

cyc_validation=0; % 0=> no validation, 1=> data agrees with source
data,
% 2=> data matches source data and data collection methods have been
verified

disp(['Data loaded: CYC_UDDS - ',cyc_description])


%%%%%%%%%%%%%%%%%%%%%%%%%%%%%%%%
% SPEED AND KEY POSITION vs. time
%%%%%%%%%%%%%%%%%%%%%%%%%%%%%%%%
% load variable 'cyc_mph', 2 column matrix with time in the first
column
load CYC_UDDS.mat
% keep key in 'on' position throughout cycle ('1' in the 2nd column =>
'on')
vc_key_on=[cyc_mph(:,1) ones(size(cyc_mph,1),1)];


%%%%%%%%%%%%
% OTHER DATA
%%%%%%%%%%%%
% Size of 'window' used to filter the trace with centered-in-time
averaging;
% higher numbers mean more smoothing and less rigorous following of
the trace.
% Used when cyc_filter_bool=1
cyc_avg_time=3;  % (s)
cyc_filter_bool=0;  % 0=> no filtering, follow trace exactly; 1=>
smooth trace

cyc_grade=0;    %no grade associated with this cycle
cyc_elevation_init=0; %the initial elevation in meters.

if size(cyc_grade,1)<2
   % convert cyc_grade to a two column matrix, grade vs. dist
   cyc_grade=[0 cyc_grade; 1 cyc_grade]; % use this for a constant
roadway grade
end

% A constant zero delta in cargo-mass:
% First column is distance (m) second column is mass (kg)
cyc_cargo_mass=[0 0
   1 0];

if size(cyc_cargo_mass,1)<2
   % convert cyc_grade to a two column matrix, grade vs. dist
   cyc_cargo_mass=[0 cyc_cargo_mass; 1 cyc_cargo_mass]; % use this for
a constant roadway grade
end

if exist('cyc_coast_gb_shift_delay')
    gb_shift_delay=cyc_coast_gb_shift_delay; % restore the original
gb_shift_delay which may have been changed by cyc_coast
end
```

D.4 Data File of HWFET Drive Cycle

```
%%%%%%%%%%%%%%%%%%%%%%%%%%%%%%%%%%%%%%%%%%%%%%%%%%%%%%%%%%%%%%%%%%%%%%%%%%%%
                    % ADVISOR data file:  CYC_HWFET.m
%%%%%%%%%%%%%%%%%%%%%%%%%%%%%%%%%%%%%%%%%%%%%%%%%%%%%%%%%%%%%%%%%%%%%%%%%%%%

% Data source: epa website
% Notes:
% This data represents the Highway Fuel Economy Test (HFET) driving
% cycle used by the
% US EPA for Corporate Average Fuel Economy (CAFE) certification of
  Passenger vehicles in the US.

%%%%%%%%%%%%%%%%%%%%%%%%%%%%%%%%%%%%%%%%%%%%%%%%%%%%%%%%%%%%%%%%%%%%%%%%%%%%
% FILE ID INFO
%%%%%%%%%%%%%%%%%%%%%%%%%%%%%%%%%%%%%%%%%%%%%%%%%%%%%%%%%%%%%%%%%%%%%%%%%%%%
cyc_description='US EPA highway fuel economy certification test';
cyc_version=2004; % version of ADVISOR for which the file was
generated

cyc_proprietary=0; % 0=> non-proprietary, 1=> proprietary, do not
distribute

cyc_validation=0; % 0=> no validation, 1=> data agrees with source
data,
% 2=> data matches source data and data collection methods have been
verified

disp(['Data loaded: CYC_HWFET - ',cyc_description])


%%%%%%%%%%%%%%%%%%%%%%%%%%%%%%%%%%%%%%%%%%%%%%%%%%%%%%%%%%%%%%%%%%%%%%%%%%%%
% SPEED AND KEY POSITION vs. time
%%%%%%%%%%%%%%%%%%%%%%%%%%%%%%%%%%%%%%%%%%%%%%%%%%%%%%%%%%%%%%%%%%%%%%%%%%%%
% load variable 'cyc_mph', 2 column matrix with time in the first
column

load CYC_HWFET.mat
% keep key in 'on' position throughout cycle ('1' in the 2nd column =>
'on')

vc_key_on=[cyc_mph(:,1) ones(size(cyc_mph,1),1)];


%%%%%%%%%%%%%%%%%%%%%%%%%%%%%%%%%%%%%%%%%%%%%%%%%%%%%%%%%%%%%%%%%%%%%%%%%%%%
% OTHER DATA
%%%%%%%%%%%%%%%%%%%%%%%%%%%%%%%%%%%%%%%%%%%%%%%%%%%%%%%%%%%%%%%%%%%%%%%%%%%%
% Size of 'window' used to filter the trace with centered-in-time
averaging;
% higher numbers mean more smoothing and less rigorous following of
the trace.
% Used when cyc_filter_bool=1
cyc_avg_time=3;  % (s)
cyc_filter_bool=0;  % 0=> no filtering, follow trace exactly; 1=>
smooth trace

cyc_grade=0;    %no grade associated with this cycle
cyc_cargo_mass=0;  % [29-Jun-2001 mpo--] no change in cargo mass over
this cycle
```

```
cyc_elevation_init=0; %the initial elevation in meters.

if size(cyc_grade,1)<2
   % convert cyc_grade to a two column matrix, grade vs. dist
   cyc_grade=[0 cyc_grade; 1 cyc_grade]; % use this for a constant
roadway grade
end

if size(cyc_cargo_mass,1)<2     % added for variable mass vs. distance
functionality
   % convert cyc_cargo_mass to a two column matrix, additional cargo
vs. Dist

   cyc_cargo_mass=[0 cyc_cargo_mass; 1 cyc_cargo_mass]; % use this for
a constant cargo-mass addition
end

if exist('cyc_coast_gb_shift_delay')
    gb_shift_delay=cyc_coast_gb_shift_delay; % restore the original
gb_shift_delay which may have been changed by cyc_coast
end
```

D.5 Data File of Small Car

```
%%%%%%%%%%%%%%%%%%%%%%%%%%%%%%%%%%%%%%%%%%%%%%%%%%%%%%%%%%%%%%%%%%%%%%%
                    % ADVISOR data file:  VEH_SMCAR.m
%%%%%%%%%%%%%%%%%%%%%%%%%%%%%%%%%%%%%%%%%%%%%%%%%%%%%%%%%%%%%%%%%%%%%%%

% Notes:  Defines road load parameters for a hypothetical small car,
          Roughly based on a 1994 Saturn SL1 vehicle.

%%%%%%%%%%%%%%%
% FILE ID INFO
%%%%%%%%%%%%%%%
veh_description='Hypothetical small car';
veh_version=2004; % version of ADVISOR for which the file was
generated

veh_proprietary=0; % 0=> non-proprietary, 1=> proprietary, do not
distribute

veh_validation=0; % 0=> no validation, 1=> data agrees with source
data,
%                          2=> data matches source data and data
collection methods have been verified

disp(['Data loaded: VEH_SMCAR - ',veh_description])


%%%%%%%%%%%%%%%%%%%%
% PHYSICAL CONSTANTS
%%%%%%%%%%%%%%%%%%%%
veh_gravity=9.81;    % m/s^2
veh_air_density=1.2; % kg/m^3
```

```
%%%%%%%%%%%%%%%%%%%%
% VEHICLE PARAMETERS
%%%%%%%%%%%%%%%%%%%%
% Note on vehicle mass:
%       The actual average vehicle mass of a 1994 Saturn SL1 5spd is
        2325 pounds.
%       If you wish to accurately set your totalvehicle mass
%       to this value in the A2 GUI, you should use the mass override
%       checkbox and enter in the value 1191, which is
(2325+300)/2.205 = 1191 kg, which comes from
%       adding on 300 lbs of EPA test mass, and then converting pounds
to kilograms.

%       The glider mass below is just an estimate that gives 2325
pounds for a 95 kW
%       scaled SI95 engine in a conventional vehicle with 5-speed
transmission.
veh_glider_mass=(2325/2.205)-462; % (kg), vehicle mass w/o propulsion
system (fuel converter,
                    % exhaust aftertreatment, drivetrain, motor, ESS,
generator)

veh_CD=0.335;  % (--), coefficient of aerodynamic drag
veh_FA=2.0;    % (m^2), frontal area
% for the eq'n:  rolling_drag=mass*gravity*(veh_1st_rrc+veh_2nd_rrc*v)
%veh_1st_rrc=0.009;  % (--)
%veh_2nd_rrc=0;     % (s/m)

% fraction of vehicle weight on front axle when standing still
veh_front_wt_frac=0.6;  % (--)
% height of vehicle center-of-gravity above the road

veh_cg_height=0.5;  % (m), estimated for 1995 Saturn SL
% vehicle wheelbase, from center of front tire patch to center of rear
patch

veh_wheelbase=2.6;  % (m), 1995 Saturn SL (GM Impact is 2.51 m)
veh_cargo_mass=136; %kg  cargo mass
```

D.6 Data File of Small Engine

```
%%%%%%%%%%%%%%%%%%%%%%%%%%%%%%%%%%%%%%%%%%%%%%%%%%%%%%%%%%%%%%%%%%%%%%%
                % ADVISOR Data file:  FC_SI41_emis.M
%%%%%%%%%%%%%%%%%%%%%%%%%%%%%%%%%%%%%%%%%%%%%%%%%%%%%%%%%%%%%%%%%%%%%%%

% Data source: J. Dill Murrel, JDM & Associates.
% Notes: 1991 Geo Metro 1.0L SI engine.

%%%%%%%%%%%%%%%
% FILE ID INFO
%%%%%%%%%%%%%%%
fc_description='Geo 1.0L (41kW) SI Engine - transient data';
fc_version=2004; % version of ADVISOR for which the file was generated
fc_proprietary=0; % 0=> non-proprietary, 1=> proprietary, do not
distribute

fc_validation=0; % 1=> no validation, 1=> data agrees with source
data,
% 2=> data matches source data and data collection methods have been
verified
```

```
fc_fuel_type='Gasoline';
fc_disp=1.0;    % (L), engine displacement
fc_emis=1;      % boolean 0=no emis data; 1=emis data
fc_cold=0;      % boolean 0=no cold data; 1=cold data exists
disp(['Data loaded: FC_SI41_emis.M - ',fc_description]);


%%%%%%%%%%%%%%%%%%%%%%%%%%%%%%%%%%%%%%%%%%%%%%%%%%%%%%%%
% SPEED & TORQUE RANGES over which data is defined
%%%%%%%%%%%%%%%%%%%%%%%%%%%%%%%%%%%%%%%%%%%%%%%%%%%%%%%%
% (rad/s), speed range of the engine
fc_map_spd=[104.5 149.2 220.9 292.5 364.1 435.7 507.4 552.2 596.9];

% (N*m), torque range of the engine
fc_map_trq=[6.8 13.6 20.4 27.2 33.8 40.6 47.4 54.2 61 67.8 74.6 81.4];


%%%%%%%%%%%%%%%%%%%%%%%%%%%%%%%
% FUEL USE AND EMISSIONS MAPS
%%%%%%%%%%%%%%%%%%%%%%%%%%%%%%%
% (g/s), fuel use map indexed vertically by fc_map_spd and
% horizontally by fc_map_trq
fc_fuel_map_gpkWh =[
635.7   635.7   541.4   447.2   352.9   332.2   311.4   322.4   333.5
333.5   333.5   333.5
678.4   500.1   443.8   387.4   331.1   301.8   297 283.4   269.8
358 358 358
463.4   463.4   407.6   350.1   294.3   280.8   267.3   253.9   269.8
303.2   336.7   336.7
699.1   567.9   500.3   432.7   301.4   283.9   266.3   248.7   258.8
268.8   271.9   317.9
592.9   592.9   494.6   393.4   295.1   279.4   263.6   247.9   255.2
262.5   295 322.6
667.9   524.8   381.6   351.9   322.2   304.9   287.5   270.8   290.8
310.9   330.9   330.9
630.6   630.6   522.5   411.1   303 304.4   305.8   304.2   314.5
324.8   327.7   327.7
698.4   500.5   428.6   392.7   356.8   337.9   328.4   319 328.8
338.6   333.7   333.7
751.1   637.8   521.1   407.8   393.1   378.4   363.3   348.2   318.8
340.2   340.2   340.2];
% fuel map in g/kWh

% (g/s), engine out HC emissions indexed vertically by fc_map_spd and
% horizontally by fc_map_trq
fc_hc_map_gpkWh =[
11.5    11.5    9.8 8.2 6.5 5.8 5.1 5.9 6.8 6.8 6.8 6.8
7.8 7   6.2 5.5 4.7 4.3 4.7 4.6 4.5 4.6 4.6 4.6
5.8 5.8 5.2 4.6 4   4   4   4   4.5 4.6 4.6 4.6
7.1 6   5.4 4.9 3.8 3.7 3.6 3.4 3.2 3   3.4 3.9
5.8 5.8 5   4.3 3.6 3.6 3.6 3.7 3.6 3.6 4   3.9
5.6 4.7 3.7 3.7 3.7 3.4 3.1 3   3.2 3.4 3.5 3.5
8.2 8.2 6.8 5.4 4.1 3.7 3.3 3.1 3.2 3.2 3.3 3.3
5.8 5.2 4.8 4.5 4.3 3.7 3.4 3.2 3.3 3.3 3.3 3.3
5.6 5.8 5.9 6.1 5.7 5.4 5   4.6 3.9 3.9 3.9 3.9];
% engine out HC in g/kWh

% (g/s), engine out CO emissions indexed vertically by fc_map_spd and
% horizontally by fc_map_trq
fc_co_map_gpkWh =[
71.8    71.8    58.8    45.7    32.7    27.5    22.4    82.9    143.3
143.3   143.3   143.3
```

```
104.4   68.3    56.8    45.3    33.9    23.3    25.7    24.2    22.8
268.6   268.6   268.6
48.3    48.3    42.9    37.2    31.8    28.6    25.4    22.2    22.8
152.9   283 283
103.1   82.7    72.2    61.8    41.5    36.9    32.3    27.8    31.1
34.4    178.5   279.9
88.1    88.1    74.2    59.9    46  41.9    37.8    33.7    34.8
35.8    158.8   264.6
96.1    74.5    52.9    51.2    49.5    45.9    42.4    34  117.9
201.8   285.7   285.7
114.6   114.6   92.1    69  46.5    60.7    74.8    129.6   195.5
261.4   277.8   277.8
60.1    63.8    64  64.1    64.3    108.2   130.2   152.2   216.7
281.2   278.1   278.1
51.8    75.2    99.3    122.8   134.9   147.1   159.7   172.2   196.6
286.6   286.6   286.6];
% engine out CO in g/kWh

% (g/s), engine out NOx emissions indexed vertically by fc_map_spd and
% horizontally by fc_map_trq
fc_nox_map_gpkWh =[
5.8 5.8 9.3 12.8    16.3    16.1    15.9    13  10.2    10.2    10.2
10.2
5.2 8.8 9.2 9.7 10.2    8   8.9 13.2    17.5    4.6 4.6 4.6
8.1 8.1 8.8 9.6 10.4    10.8    11.3    11.7    17.5    11.6    5.7
5.7
4.2 5.6 6.3 7   8.4 8.9 9.5 10.1    13.9    17.7    8.1 3.1
5.8 5.8 7.2 8.7 10.1    11  11.8    12.6    15.9    19.2    9.3 6.8
14.9    16.4    17.8    19.4    21  20.6    20.3    19.1    14.6
10.2    5.7 5.7
28.7    28.7    26.8    25  23.1    22.4    21.7    16.5    12.1
7.8 6.5 6.5
31.1    27.9    26.7    26.2    25.6    20.9    18.6    16.3    12.1
7.8 6.8 6.8
35  31.1    27.1    23.2    21.1    19.1    17  14.9    10.9    7.4
7.4 7.4];
% engine out NOx in g/kWh

% (g/s), engine out PM emissions indexed vertically by fc_map_spd and
% horizontally by fc_map_trq
fc_pm_map_gpkWh=zeros(size(fc_fuel_map_gpkWh));

% (g/s), engine out O2 indexed vertically by fc_map_spd and
% horizontally by fc_map_trq
fc_o2_map=zeros(size(fc_fuel_map_gpkWh));


% convert g/kWh maps to g/s maps
[T,w]=meshgrid(fc_map_trq, fc_map_spd);
fc_map_kW=T.*w/1000;
fc_fuel_map=fc_fuel_map_gpkWh.*fc_map_kW/3600;
fc_hc_map=fc_hc_map_gpkWh.*fc_map_kW/3600;
fc_co_map=fc_co_map_gpkWh.*fc_map_kW/3600;
fc_nox_map=fc_nox_map_gpkWh.*fc_map_kW/3600;
fc_pm_map=fc_pm_map_gpkWh.*fc_map_kW/3600;


%%%%%%%%%%%%%%%%%%
% Cold Engine Maps
%%%%%%%%%%%%%%%%%%
fc_cold_tmp=20; %deg C
fc_fuel_map_cold=zeros(size(fc_fuel_map));
```

```
fc_hc_map_cold=zeros(size(fc_fuel_map));
fc_co_map_cold=zeros(size(fc_fuel_map));
fc_nox_map_cold=zeros(size(fc_fuel_map));
fc_pm_map_cold=zeros(size(fc_fuel_map));
%Process Cold Maps to generate Correction Factor Maps
names={'fc_fuel_map','fc_hc_map','fc_co_map','fc_nox_map','fc_pm_map'}
;
for i=1:length(names)
    %cold to hot raio, e.g. fc_fuel_map_c2h = fc_fuel_map_cold ./
fc_fuel_map
    eval([names{i},'_c2h=',names{i},'_cold./(',names{i},'+eps);'])
end


%%%%%%%%
% LIMITS
%%%%%%%%
% (N*m), max torque curve of the engine indexed by fc_map_spd
fc_max_trq=[61  67.6 73.7 78.5 80.9 77.3 76.2 73.3 68.7];

% (N*m), closed throttle torque of the engine (max torque that can be
absorbed)
% indexed by fc_map_spd -- correlation from JDMA
fc_ct_trq=4.448/3.281*(-fc_disp)*61.02/24 * ...
   (9*(fc_map_spd/max(fc_map_spd)).^2 + 14 *
(fc_map_spd/max(fc_map_spd)));


%%%%%%%%%%%%%%%%%%
% DEFAULT SCALING
%%%%%%%%%%%%%%%%%%
% (--), used to scale fc_map_spd to simulate a faster or slower
running engine
fc_spd_scale=1.0;

% (--), used to scale fc_map_trq to simulate a higher or lower torque
engine
fc_trq_scale=1.0;
fc_pwr_scale=fc_spd_scale*fc_trq_scale;   % --  scale fc power
% user definable mass scaling function
fc_mass_scale_fun=inline('(x(1)*fc_trq_scale+x(2))*(x(3)*fc_spd_scale+
x(4))*(fc_base_mass+fc_acc_mass)+fc_fuel_mass','x','fc_spd_scale','fc_
trq_scale','fc_base_mass','fc_acc_mass','fc_fuel_mass');
fc_mass_scale_coef=[1 0 1 0]; % coefficients of mass scaling function



%%%%%%%%%%%%%%%%%%%%%%%%%%%%%%%%%%%%%%%%%%%%%%%%%%%%%%%%%%%%%%%%%%%%%%%
% STUFF THAT SCALES WITH TRQ & SPD SCALES (MASS AND INERTIA)
%%%%%%%%%%%%%%%%%%%%%%%%%%%%%%%%%%%%%%%%%%%%%%%%%%%%%%%%%%%%%%%%%%%%%%%
fc_inertia=0.1*fc_pwr_scale;           % (kg*m^2), rotational inertia
of the engine (unknown)
fc_max_pwr=(max(fc_map_spd.*fc_max_trq)/1000)*fc_pwr_scale; % kW
peak engine power

fc_base_mass=1.8*fc_max_pwr;            % (kg), mass of the engine
block and head (base engine)
                                        %       mass penalty of 1.8
kg/kW from 1994 OTA report, Table 3
fc_acc_mass=0.8*fc_max_pwr;             % kg    engine accy's,
electrics, cntrl's - assumes mass penalty of 0.8 kg/kW (from OTA
report)
```

```
fc_fuel_mass=0.6*fc_max_pwr;            % kg    mass of fuel and fuel
tank (from OTA report)
fc_mass=fc_base_mass+fc_acc_mass+fc_fuel_mass; % kg  total engine/fuel
system mass
fc_ext_sarea=0.3*(fc_max_pwr/100)^0.67;       % m^2    exterior
surface area of engine



%%%%%%%%%%%%%%%%%%%%%%%%%%%%%%%%%%%%%%%%%%%%
% OTHER DATA
%%%%%%%%%%%%%%%%%%%%%%%%%%%%%%%%%%%%%%%%%%%%
fc_fuel_den=0.749*1000; % (g/l), density of the fuel
fc_fuel_lhv=42.6*1000; % (J/g), lower heating value of the fuel

%the following was added for the new thermal modeling of the engine
12/17/98 ss and sb
fc_tstat=96;                    % C      engine coolant thermostat set
temperature (typically 95 +/- 5 C)

fc_cp=500;                      % J/kgK  ave cp of engine (iron=500, Al
or Mg = 1000)

fc_h_cp=500;                    % J/kgK  ave cp of hood & engine
compartment (iron=500, Al or Mg = 1000)

fc_hood_sarea=1.5;              % m^2    surface area of hood/eng compt.
fc_emisv=0.8;                   %        emissivity of engine ext
surface/hood int surface

fc_hood_emisv=0.9;              %        emissivity hood ext
fc_h_air_flow=0.0;              % kg/s   heater air flow rate (140
cfm=0.07)

fc_cl2h_eff=0.7;                % --     ave cabin heater HX eff (based
on air side)

fc_c2i_th_cond=500;             % W/K    conductance btwn engine cyl &
int
fc_i2x_th_cond=500;             % W/K    conductance btwn engine int &
ext

fc_h2x_th_cond=10;              % W/K    conductance btwn engine &
engine compartment

% calc "predicted" exh gas flow rate and engine-out (EO) temp
fc_ex_pwr_frac=[0.40 0.30];                         % --   frac of
waste heat that goes to exhaust as func of engine speed

fc_exflow_map=fc_fuel_map*(1+14.5);                 % g/s  ex gas flow
map:  for SI engines, exflow=(fuel use)*[1 + (stoic A/F ratio)]

fc_waste_pwr_map=fc_fuel_map*fc_fuel_lhv - T.*w;    % W    tot FC waste
heat = (fuel pwr) - (mech out pwr)

spd=fc_map_spd;
fc_ex_pwr_map=zeros(size(fc_waste_pwr_map));        % W   initialize
size of ex pwr map

for i=1:length(spd)
```

```
 fc_ex_pwr_map(i,:)=fc_waste_pwr_map(i,:)*interp1([min(spd)
max(spd)],fc_ex_pwr_frac,spd(i)); % W  trq-spd map of waste heat to
exh
end
fc_extmp_map=fc_ex_pwr_map./(fc_exflow_map*1089/1000) + 20;  % W   EO
ex gas temp = Q/(MF*cp) + Tamb (assumes engine tested ~20 C)

%the following variable is not used directly in modelling and should
always be equal to one
%it's used for initialization purposes
fc_eff_scale=1;

% clean up workspace
clear T w fc_waste_pwr_map fc_ex_pwr_map spd fc_map_kW
```

D.7 Data File of NiMH Battery Pack

```
%%%%%%%%%%%%%%%%%%%%%%%%%%%%%%%%%%%%%%%%%%%%%%%%%%%%%%%%%%%%%%%%%%%%%%%
                % ADVISOR data file:  ESS_NIMH20_OVONIC.m
%%%%%%%%%%%%%%%%%%%%%%%%%%%%%%%%%%%%%%%%%%%%%%%%%%%%%%%%%%%%%%%%%%%%%%%

% Data source:
% Ovonic sales data via UC Davis except VOC (from ESS_NIMH93).
% Notes: These are designed to be a high power, intermediate energy
  battery.
% Cell type = P127
% Nominal Voltage = 12V
% Nominal Capacity (C/3) = 20Ah
% Dimensions (L * W * H) = 340mm X 75mm X 91mm
% Weight = 5.4kg
% Volume (modules only) = 2.3L
% Nominal Energy (C/3) = 250 Wh
% Peak Power (10s pulse @ 50%DOD @ 35 deg. C) = 3kW

%%%%%%%%%%%%%%%
% FILE ID INFO
%%%%%%%%%%%%%%%
ess_description='Modified Ovonic 45Ah NiMH HEV battery';
ess_version=2004; % version of ADVISOR for which the file was
generated

ess_proprietary=0; % 0=> non-proprietary, 1=> proprietary, do not
distribute
ess_validation=0; % 0=> no validation, 1=> data agrees with source
data,
% 2=> data matches source data and data collection methods have been
verified

disp(['Data loaded: ESS_NIMH20_OVONIC - ',ess_description])


%%%%%%%%%%%%%%%%%%%%%%%%%%%%%%%%%%%%%%%%%%%
% SOC RANGE over which data is defined
%%%%%%%%%%%%%%%%%%%%%%%%%%%%%%%%%%%%%%%%%%%
ess_soc=[0:.1:1];  % (--)

%%%%%%%%%%%%%%%%%%%%%%%%%%%%%%%%%%%%%%%%%%%%%%%%%%%%%%%%%%%%%%%%%%%%%%%
% Temperature range over which data is defined
%%%%%%%%%%%%%%%%%%%%%%%%%%%%%%%%%%%%%%%%%%%%%%%%%%%%%%%%%%%%%%%%%%%%%%%
```

```
ess_tmp=[0 22 40];  % (C)


%%%%%%%%%%%%%%%%%%%%%%%%%%%%%%%%
% LOSS AND EFFICIENCY parameters
%%%%%%%%%%%%%%%%%%%%%%%%%%%%%%%%
% Parameters vary by SOC horizontally, and temperature vertically

ess_max_ah_cap=[
   28
   28
   28
];  % (A*h), max. capacity at C/5 rate, indexed by ess_tmp

% average coulombic (a.k.a. amp-hour) efficiency below, indexed by
ess_tmp
ess_coulombic_eff=[
   1
   1
   1
]*0.975;  % (--); unknown

% module's resistance to being discharged, indexed by ess_soc and
ess_tmp
ess_r_dis=[2.135 1.155  1.086   1.011   0.990   0.970   0.958   0.981
1.050   1.125   1.071
          2.135 1.155   1.086   1.011   0.990   0.970   0.958   0.981
1.050   1.125   1.071
           2.135 1.155  1.086   1.011   0.990   0.970   0.958   0.981
1.050   1.125   1.071
        ]*10/1000; % (ohm)

% module's resistance to being charged, indexed by ess_soc and ess_tmp
ess_r_chg=ess_r_dis;% (ohm), no other data available
% module's open-circuit (a.k.a. no-load) voltage, indexed by ess_soc
and ess_tmp
%ess_voc=[11.9 12.3 12.6 12.8 12.9 12.9 13 13.1 13.2 13.4 13.7;
%   11.9 12.3 12.6 12.8 12.9 12.9 13 13.1 13.2 13.4 13.7;
%   11.9 12.3 12.6 12.8 12.9 12.9 13 13.1 13.2 13.4 13.7]; % (V),
Source: Ovonic Charge-decreasing
ess_voc=[12.5 12.8 13.1 13.3 13.4 13.4 13.5 13.6 13.7 13.9 14.2;
   12.5 12.8 13.1 13.3 13.4 13.4 13.5 13.6 13.7 13.9 14.2;
   12.5 12.8 13.1 13.3 13.4 13.4 13.5 13.6 13.7 13.9 14.2]; % (V),
Source: Ovonic Charge-sustaining
%ess_voc=[12.8 13.2 13.5 13.7 13.8 13.8 13.9 14 14.1 14.3 14.6;
%   12.8 13.2 13.5 13.7 13.8 13.8 13.9 14 14.1 14.3 14.6;
%   12.8 13.2 13.5 13.7 13.8 13.8 13.9 14 14.1 14.3 14.6]; % (V),
Source: Ovonic Charge-increasing


%%%%%%%%
% LIMITS
%%%%%%%%
ess_min_volts=0.87*1.05*10; % (V), 0.87*105% safety factor volts time
10 cells
ess_max_volts=1.65*0.95*10;% (V), 1.65*95% safety factor volts times
10 cells


%%%%%%%%%%%%
% OTHER DATA
%%%%%%%%%%%%
```

```
ess_module_mass=5.4;  % (kg), mass of a single ~12 V module
ess_module_volume=0.340*0.075*0.91; % (m^3), length X width X height
ess_module_num=31;  %a default value for number of modules

ess_cap_scale=1; % scale factor for module max ah capacity

% user definable mass scaling relationship
ess_mass_scale_fun=inline('(x(1)*ess_module_num+x(2))*(x(3)*ess_cap_sc
ale+x(4))*(ess_module_mass)','x','ess_module_num','ess_cap_scale','ess
_module_mass');

%ess_mass_scale_coef=[1 0 1 0]; % coefficients in ess_mass_scale_fun
ess_mass_scale_coef=[1 0 0.9832073 0.0160194]; % coefficients in
ess_mass_scale_fun; updated tm:10/22/01 based on Ovonic family

% user definable resistance scaling relationship
ess_res_scale_fun=inline('(x(1)*ess_module_num+x(2))/(x(3)*ess_cap_sca
le+x(4))','x','ess_module_num','ess_cap_scale');

%ess_res_scale_coef=[1 0 1 0]; % coefficients in ess_res_scale_fun
ess_res_scale_coef=[1 0 0.8698015 0.1226830]; % coefficients in
ess_res_scale_fun; updated tm:10/22/01 based on Ovonic family

% battery thermal model
ess_th_calc=1;                              % --     0=no ess thermal
calculations, 1=do calc's

ess_mod_cp=830;                             % J/kgK  ave heat capacity
of module (estimated for NiMH)

ess_set_tmp=35;                             % C      thermostat temp of
module when cooling fan comes on
ess_area_scale=1.6*(ess_module_mass/11)^0.7;   % --     if module
dimensions are unknown, assume rectang shape and scale vs PB25
%tm:3/24/00 ess_mod_sarea=0.2*ess_area_scale;          % m^2    total
module surface area exposed to cooling air (typ rectang module)

ess_mod_sarea=2*(0.340*0.91+0.075*0.91);          % m^2    total
module surface area exposed to cooling air (typ rectang module)

ess_mod_airflow=0.01;                       % kg/s   cooling air mass
flow rate across module (20 cfm=0.01 kg/s at 20 C)
%tm:3/24/00 ess_mod_flow_area=0.005*ess_area_scale;    % m^2    cross-
sec flow area for cooling air per module (assumes 10-mm gap btwn mods)

ess_mod_flow_area=0.005*2*(0.340+0.075);    % m^2    cross-sec flow
area for cooling air per module (assumes 10-mm gap btwn mods)

ess_mod_case_thk=2/1000;                    % m      thickness of
module case (typ from Optima)

ess_mod_case_th_cond=0.20;                  % W/mK   thermal
conductivity of module case material (typ polyprop plastic - Optima)

ess_air_vel=ess_mod_airflow/(1.16*ess_mod_flow_area); % m/s  ave
velocity of cooling air

ess_air_htcoef=30*(ess_air_vel/5)^0.8;      % W/m^2K cooling air heat
transfer coef.
```

```
ess_th_res_on=((1/ess_air_htcoef)+(ess_mod_case_thk/ess_mod_case_th_co
nd))/ess_mod_sarea; % K/W  tot thermal res key on
ess_th_res_off=((1/4)+(ess_mod_case_thk/ess_mod_case_th_cond))/ess_mod
_sarea; % K/W  tot thermal res key off (cold soak)
% set bounds on flow rate and thermal resistance

ess_mod_airflow=max(ess_mod_airflow,0.001);
ess_th_res_on=min(ess_th_res_on,ess_th_res_off);
clear ess_mod_sarea ess_mod_flow_area ess_mod_case_thk
ess_mod_case_th_cond ess_air_vel ess_air_htcoef ess_area_scale
```

D.8 Data File of Electric Drive Motor

```
%%%%%%%%%%%%%%%%%%%%%%%%%%%%%%%%%%%%%%%%%%%%%%%%%%%%%%%%%%%%%%%%%%%%%%%
                        % ADVISOR data file:  MC_AC90
%%%%%%%%%%%%%%%%%%%%%%%%%%%%%%%%%%%%%%%%%%%%%%%%%%%%%%%%%%%%%%%%%%%%%%%

%%%%%%%%%%%%%%%%%%%%%%%%%%%%%%%%%%%%%
% FILE ID INFO
%%%%%%%%%%%%%%%%%%%%%%%%%%%%%%%%%%%%%
mc_version=2004;
mc_description='GE 83-kW AC induction motor/inverter, tested by VA
Tech';
mc_proprietary=0;  % 0=> public data, 1=> restricted access, see
comments above

mc_validation=0; % 0=> no validation, 1=> data agrees with source
data,
% 2=> data matches source data and data collection methods have been
verified

disp(['Data loaded: MC_AC90 - ',mc_description]);


%%%%%%%%%%%%%%%%%%%%%%%%%%%%%%%%%%%%%%%%%%%%%%%%%%%%%%%%%%%%%%%%%%%%%%%
% SPEED & TORQUE RANGES over which data is defined
%%%%%%%%%%%%%%%%%%%%%%%%%%%%%%%%%%%%%%%%%%%%%%%%%%%%%%%%%%%%%%%%%%%%%%%
% (N*m), torque range of the motor
mc_map_trq=[-203.4 -190.0 -176.3 -162.7 -149.2 -135.6   -122.0 -108.5
-94.9 ...
      -81.4 -67.8 -54.2 -40.7   -27.1 -13.6 0.0 ...
      13.6 27.1 40.7 54.2 67.8 81.4 94.9 108.5 122.0 135.6 149.2 162.7
176.3...
      189.8 203.4];

% (rad/s), speed range of the motor
mc_map_spd=[0 105 209 314 419 524 628 733 838 943 1047 1152 1257
1361];


%%%%%%%%%%%%%%%%%%%%%%%%%%
% LOSSES AND EFFICIENCIES
%%%%%%%%%%%%%%%%%%%%%%%%%%
inv_eta=0.01*[
80  80  80  81  81  81  82  82  82  83  83  83  83  83  83  1   83  83
83  83  83  83  82  82  82  81  81  81  80  80  80
80  80  80  81  81  81  82  82  82  83  83  83  83  83  83  1   83  83
83  83  83  83  82  82  82  81  81  81  80  80  80
```

```
84  84  85  86  86  86  86.5    86.5    86.5    87.5    87.5    87.5
87.5    87.5    87.5    1   87.5    87.5    87.5    87.5    87.5
87.5    86.5    86.5    86.5    86  86  86  85  84  84
88  89  89  89  90  90  91  91  91  92  92  92  92  92  92  1   92  92
92  92  92  92  91  91  91  90  90  89  89  89  88
88  94  94  95  95  95  95.5    95.5    95.5    96.5    96.5    96.5
96.5    96.5    96.5    1   96.5    96.5    96.5    96.5    96.5
96.5    95.5    95.5    95.5    95  95  95  94  94  88
88  94  94  94  94  94  94  95  96.6    96.9    97  97.3    98  98
97.7    1   97.7    98  98  97.3    97  96.9    96.6    95  94  94  94
94  94  94  88
88  94  94  94  94  92  93  94  96  96.6    97  97.3    97.5    98.1
97.8    1   97.8    98.1    97.5    97.3    97  96.6    96  94  93  92
94  94  94  94  88
88  94  94  94  94  92  93  93  95  96  96.6    97  97.1    98.2
97.7    1   97.7    98.2    97.1    97  96.6    96  95  93  93  92  94
94  94  94  88
88  94  94  94  94  92  93  93  94  95  96  96.7    97  96.9    97.3
1   97.3    96.9    97  96.7    96  95  94  93  93  92  94  94  94  94
88
88  94  94  94  94  92  93  93  94  94  95  96.4    97.1    98.1
97.9    1   97.9    98.1    97.1    96.4    95  94  94  93  93  92  94
94  94  94  88
88  94  94  94  94  92  93  93  94  94  94  96  97.1    97.3    98.1
1   98.1    97.3    97.1    96  94  94  94  93  93  92  94  94  94  94
88
88  94  94  94  94  92  93  93  94  94  94  95  96  97.1    97.8    1
97.8    97.1    96  95  94  94  94  93  93  92  94  94  94  94  88
88  94  94  94  94  92  93  93  94  94  94  94  96  96.7    97  1   97
96.7    96  94  94  94  94  93  93  92  94  94  94  94  88
88  94  94  94  94  92  93  93  94  94  94  94  95  96  96  1   96  96
95  94  94  94  94  93  93  92  94  94  94  94  88
];

mot_eta=0.01*[
71.1    70  71.6    72  73.5    74.3    76.8    80.1    79.3    80.4
81.2    81.5    82  82.2    81.3    1   81.3    82.2    82  81.5
81.2    80.4    79.3    80.1    76.8    74.3    73.5    72  71.6    70
71.1
71.1    70  71.6    72  73.5    74.3    76.8    80.1    79.3    80.4
81.2    81.5    82  82.2    81.3    1   81.3    82.2    82  81.5
81.2    80.4    79.3    80.1    76.8    74.3    73.5    72  71.6    70
71.1
82.2    81.5    82.4    83.2    85.8    84.9    85.7    88  87.2
87.8    87.9    87.9    87.8    88.3    87.1    1   87.1    88.3
87.8    87.9    87.9    87.8    87.2    88  85.7    84.9    85.8
83.2    82.4    81.5    82.2
85.7    86  86.8    87.4    88.2    88.7    89.3    91  90.3    90.6
90.8    90.5    90.3    90.6    89.3    1   89.3    90.6    90.3
90.5    90.8    90.6    90.3    91  89.3    88.7    88.2    87.4
86.8    86  85.7
85.7    87.8    88.3    88.8    89.3    89.7    91.3    92.5    92.1
92.4    92.5    92.3    91.9    92  90.5    1   90.5    92  91.9
92.3    92.5    92.4    92.1    92.5    91.3    89.7    89.3    88.8
88.3    87.8    85.7
85.7    87.8    88.3    88.2    89.2    90  90.6    91.2    91.6
91.9    91.9    91.6    90.6    93  91.4    1   91.4    93  90.6
91.6    91.9    91.9    91.6    91.2    90.6    90  89.2    88.2
88.3    87.8    85.7
85.7    87.8    88.3    88.2    89.2    87.9    89  91.1    91  91.8
92.4    92.7    92.6    92.1    92.2    1   92.2    92.1    92.6
92.7    92.4    91.8    91  91.1    89  87.9    89.2    88.2    88.3
87.8    85.7
```

```
85.7    87.8    88.3    88.2    89.2    87.9    89  88.4    89.9
91.7    93  94.2    95.1    95.7    94  1   94  95.7    95.1    94.2
93  91.7    89.9    88.4    89  87.9    89.2    88.2    88.3    87.8
85.7
85.7    87.8    88.3    88.2    89.2    87.9    89  88.4    87.2
89.4    91.5    93.2    94.6    95.6    93.7    1   93.7    95.6
94.6    93.2    91.5    89.4    87.2    88.4    89  87.9    89.2
88.2    88.3    87.8    85.7
85.7    87.8    88.3    88.2    89.2    87.9    89  88.4    87.2
86.4    89.2    91.9    93.8    95.3    94.5    1   94.5    95.3
93.8    91.9    89.2    86.4    87.2    88.4    89  87.9    89.2
88.2    88.3    87.8    85.7
85.7    87.8    88.3    88.2    89.2    87.9    89  88.4    87.2
86.4    86.5    89  92.8    94.8    94.1    1   94.1    94.8    92.8
89  86.5    86.4    87.2    88.4    89  87.9    89.2    88.2    88.3
87.8    85.7
85.7    87.8    88.3    88.2    89.2    87.9    89  88.4    87.2
86.4    86.5    87.7    91.5    94.2    94  1   94  94.2    91.5
87.7    86.5    86.4    87.2    88.4    89  87.9    89.2    88.2
88.3    87.8    85.7
85.7    87.8    88.3    88.2    89.2    87.9    89  88.4    87.2
86.4    86.5    83.5    88.8    93.4    93.9    1   93.9    93.4
88.8    83.5    86.5    86.4    87.2    88.4    89  87.9    89.2
88.2    88.3    87.8    85.7
85.7    87.8    88.3    88.2    89.2    87.9    89  88.4    87.2
86.4    86.5    83.5    87.3    92.4    93.8    1   93.8    92.4
87.3    83.5    86.5    86.4    87.2    88.4    89  87.9    89.2
88.2    88.3    87.8    85.7
];

mc_eff_map=inv_eta.*mot_eta;


% CONVERT EFFICIENCY MAP TO INPUT POWER MAP
%% find indices of well-defined efficiencies (where speed and torque >
0)
pos_trqs=find(mc_map_trq>0);
pos_spds=find(mc_map_spd>0);

%% compute losses in well-defined efficiency area
[T1,w1]=meshgrid(mc_map_trq(pos_trqs),mc_map_spd(pos_spds));
mc_outpwr1_map=T1.*w1;
mc_losspwr_map=(1./mc_eff_map(pos_spds,pos_trqs)-1).*mc_outpwr1_map;

%% to compute losses in entire operating range
%% ASSUME that losses are symmetric about zero-torque axis, and
%% ASSUME that losses at zero torque are the same as those at the
lowest positive
%% torque, and
%% ASSUME that losses at zero speed are the same as those at the
lowest positive
%% speed
mc_losspwr_map=[fliplr(mc_losspwr_map) mc_losspwr_map(:,1)
mc_losspwr_map];
mc_losspwr_map=[mc_losspwr_map(1,:);mc_losspwr_map];

%% compute input power (power req'd at electrical side of
motor/inverter set)
[T,w]=meshgrid(mc_map_trq,mc_map_spd);
mc_outpwr_map=T.*w;
mc_inpwr_map=mc_outpwr_map+mc_losspwr_map;
```

```
%%%%%%%%
% LIMITS
%%%%%%%%
% max torque curve of the motor indexed by mc_map_spd
mc_max_trq=[203 203 203 203 193 156 129 111 98 85 79 72 65 60]; %
(N*m)

mc_max_gen_trq=-1*[203 203 203 203 193 156 129 111 98 85 79 72 65 60];
% (N*m), estimate

% maximum overtorque capability (not continuous, because the motor
would overheat)
mc_overtrq_factor=1; % (--), estimated
mc_max_crrnt=385; % (A), maximum current allowed by the controller and
motor

mc_min_volts=200; % (V), minimum voltage allowed by the controller and
motor



%%%%%%%%%%%%%%%%
% DEFAULT SCALING
%%%%%%%%%%%%%%%%
% (--), used to scale mc_map_spd to simulate a faster or slower
running motor
mc_spd_scale=1.0;

% (--), used to scale mc_map_trq to simulate a higher or lower torque
motor
mc_trq_scale=1.0;



%%%%%%%%%%%
% OTHER DATA
%%%%%%%%%%%
mc_inertia=0; % (kg*m^2), rotor's rotational inertia; unknown

mc_mass=110; % (kg), mass of motor and controller

% motor/controller thermal model
mc_th_calc=1;                    % --     0=no mc thermal
calculations, 1=do calc's

mc_cp=430;                       % J/kgK  ave heat capacity of
motor/controller (estimate: ave of SS & Cu)

mc_tstat=45;                     % C  thermostat temp of
motor/controler when cooling pump comes on

mc_area_scale=(mc_mass/91)^0.7;          % --     if motor dimensions
are unknown, assume rectang shape and scale vs AC75

mc_sarea=0.4*mc_area_scale;              % m^2    total module
surface area exposed to cooling fluid (typ rectang module)

%the following variable is not used directly in modelling and should
always be equal to one
%it's used for initialization purposes
mc_eff_scale=1;
```

```
%%%%%%%%%%
% CLEAN UP
%%%%%%%%%%
clear T w mc_outpwr_map mc_outpwr1_map mc_losspwr_map T1 w1 pos_spds
pos_trqs
clear mc_description1 mc_description2 inv_eta mot_eta

mc_mass_scale_coef=[1 0 1 0];

mc_mass_scale_fun=inline('(x(1)*mc_trq_scale+x(2))*(x(3)*mc_spd_scale+
x(4))*mc_mass','x','mc_spd_scale','mc_trq_scale','mc_mass');
```

D.9 Data File of Transmission

```
%%%%%%%%%%%%%%%%%%%%%%%%%%%%%%%%%%%%%%%%%%%%%%%%%%%%%%%%%%%%%%%%%%%%%%%%%%%%
                        % ADVISOR data file:  TX_1SPD.m
%%%%%%%%%%%%%%%%%%%%%%%%%%%%%%%%%%%%%%%%%%%%%%%%%%%%%%%%%%%%%%%%%%%%%%%%%%%%

% Notes:
% This file defines a 1-speed gearbox by defining a gear ratio and
gear number, and calling TX_VW to define loss characteristics.
%Description of type of transmission(important in determining what
 block diagram to run in gui_run_simulation)
tx_type='manual 1 speed';
tx_version=2004;
disp('Data loaded: TX_1SPD - 1-speed transmission')


%%%%%%%%%%%%
% INITIALIZE
%%%%%%%%%%%%
gb_gears_num=1;  % (--), number of gears in gearbox
if exist('mc_map_spd')
   % gear ratio to allow 90 mph given the max. motor speed and 10%
wheel slip

target_ratio=max(mc_map_spd*mc_spd_scale)/(90*0.447/wh_radius*1.10);
else  % using a 1-spd tranny with a piston engine! - let it do 65 mph

target_ratio=max(fc_map_spd*fc_spd_scale)/(65*0.447/wh_radius*1.10);
end
gb_ratio=ones(1,2)*target_ratio;
clear target_ratio


%TX_VW % FILE ID, LOSSES

gb_mass=0; % (kg), mass of the gearbox

%the following variable is not used directly in modelling and should
always be equal to one
%it's used for initialization purposes
gb_eff_scale=1;

%final drive portion
%%%%%%%%%%%%%%%%%%%%%%%%%
% LOSSES AND EFFICIENCIES
%%%%%%%%%%%%%%%%%%%%%%%%%
fd_loss=0;    % (Nm), constant torque loss in final drive, measured at
input
```

```
% below, the loss map for this 1 speed transmission is calculated
gb_vars.gb_loss_input_spd_coeff=0.614307976;  % loss coefficiencts
from old eff equation (TX_VW)

gb_vars.gb_loss_output_spd_coeff=5.530953616; % ""
gb_vars.gb_loss_input_trq_coeff=-0.861652506; % ""
gb_vars.gb_loss_output_trq_coeff=0.229546756; % ""
gb_vars.gb_loss_output_pwr_coeff=0.023981187; % ""
gb_vars.gb_loss_const=-92.07523029;           % ""
w.vals = [0:1:20,25:5:400]; % transmission output speeds to evaluate
efficiency at

T.vals = [-1000:400:-200,-150,-100:10:-40,-36:2:-
2,2:2:36,40:10:100,150,200:400:1000]; % transmission output torque to
evaluate efficiency at
% Note: although a 1-spd gearbox is required to have gb_ratio of
length two (where both elements are the same),
% ...there is no need to make two efficiency maps. Therefore, only one
gb_ratio is fed into the below function.
[tx_eff_map, tx_map_spd, tx_map_trq] =
tx_eff_mapper(gb_vars,w,T,gb_ratio(1)); % create efficiency map and T,
w index

clear w T gb_vars;


%%%%%%%%%%%%
% OTHER DATA
%%%%%%%%%%%%
fd_ratio=1;   % (--), =(final drive input speed)/(f.d. output speed)
fd_inertia=0; % (kg*m^2), rotational inertia of final drive, measured
at input

fd_mass=110/2.205; % (kg), mass of the final drive - 1990 Taurus, OTA
report

tx_mass=gb_mass+fd_mass;% (kg), mass of the gearbox + final
drive=(transmission)

gb_inertia=0;   % (kg*m^2), gearbox rotational inertia measured at
input; unknown

% trq and speed scaling parameters
gb_spd_scale=1;
gb_trq_scale=1;

% user definable mass scaling relationship
tx_mass_scale_fun=inline('(x(1)*gb_trq_scale+x(2))*(x(3)*gb_spd_scale+
x(4))*(fd_mass+gb_mass)','x','gb_spd_scale','gb_trq_scale','fd_mass','
gb_mass');
tx_mass_scale_coef=[1 0 1 0]; % coefficients for mass scaling
relationship
```

D.10 Data File of Wheel

```
%%%%%%%%%%%%%%%%%%%%%%%%%%%%%%%%%%%%%%%%%%%%%%%%%%%%%%%%%%%%%%%%%%%%%%%
% ADVISOR data file:  WH_SMCAR.m
%%%%%%%%%%%%%%%%%%%%%%%%%%%%%%%%%%%%%%%%%%%%%%%%%%%%%%%%%%%%%%%%%%%%%%%
```

```
% Notes:
% Defines tire, wheel, and axle assembly parameters for use with
  ADVISOR 2, for a hypothetical small car.

%%%%%%%%%%%%%%%%%%%%%%%%%%%%%%%%%%%%%%%%%%%%
% FILE ID INFO
%%%%%%%%%%%%%%%%%%%%%%%%%%%%%%%%%%%%%%%%%%%%
wh_description='Wheel/axle assembly for small car';
wh_version=2004; % version of ADVISOR for which the file was generated
wh_proprietary=0; % 0=> non-proprietary, 1=> proprietary, do not
distribute

wh_validation=0; % 0=> no validation, 1=> data agrees with source
data,
% 2=> data matches source data and data collection methods have been
verified

disp(['Data loaded: WH_SMCAR - ',wh_description])


%%%%%%%%%%%%%%%%%%%%%%%%%%%%%%%%%%%%%%%%%%%%%%%%%%%%%%%%%%%%%%%%
% FORCE AND MASS RANGES over which data is defined
%%%%%%%%%%%%%%%%%%%%%%%%%%%%%%%%%%%%%%%%%%%%%%%%%%%%%%%%%%%%%%%%
% vehicle test mass vector used in tandem with "wh_axle_loss_trq" to
estimate
% wheel and axle bearing and brake drag
wh_axle_loss_mass=[0 2000];   % (kg)
% (tractive force on the front tires)/(weight on front axle), used in
tandem

% with "wh_slip" to estimate tire slip at any time
wh_slip_force_coeff=[0 0.3913 0.6715 0.8540 0.9616 1.0212];  % (--)

%%%%%%%%%%%%%%%%%%
% LOSS parameters
%%%%%%%%%%%%%%%%%%
% drag torque applied at the front (drive) axle, used with
"wh_axle_loss_mass"
wh_axle_loss_trq=[4 24]*.4;   % (Nm)
% slip=(omega * r)/v -1; used with "wh_slip_force_coeff"

wh_slip=[0.0 0.025 0.050 0.075 0.10 0.125];


%%%%%%%%%%%%
% OTHER DATA
%%%%%%%%%%%%
wh_radius=0.282;     % (m), rolling radius of 185/70R14 tire from a
                     % ~1990 Mazda 626
% rotational inertia of all wheels, tires, and axles
% below uses OTA's '94 estimate of Taurus wheel, tire & tool mass as
  mass of
% solid cylinders of radius wh_radius, rotating at wheel speed in this
  Vehicle
wh_inertia=181/2.205*wh_radius^2/2;  % (kg*m^2)

% fraction of braking done by driveline, indexed by wh_fa_dl_brake_mph
wh_fa_dl_brake_frac=[0 0 0.5 0.8 0.8];  % (--)
% (--), fraction of braking done by front friction brakes,
% indexed by wh_fa_fric_brake_mph
wh_fa_fric_brake_frac=[0.8 0.8 0.4 0.1 0.1];  % (--)
wh_fa_dl_brake_mph=[-1 0 10 60 1000];   % (mph)
```

```
wh_fa_fric_brake_mph=wh_fa_dl_brake_mph; % (mph)

wh_1st_rrc=0.009; % (--), rolling resistance coefficient
wh_2nd_rrc=0; % (s/m)

wh_mass=0;

% front or rear or both axles driving?
wh_front_active_bool=1; % 0==> inactive; 1==> active
wh_rear_active_bool=0; % 0==> inactive; 1==> active

% braking force limits
wh_max_front_brake_force=-inf;% (N)
wh_max_rear_brake_force=-inf;% (N)


%%%%%%%%%%%%%%%%
% Error checking
%%%%%%%%%%%%%%%%
% dl+fa_fric must add up to <= 1 for all speeds.  Give user warning if
in error
temp_total_braking=wh_fa_dl_brake_frac+wh_fa_fric_brake_frac;
if any(temp_total_braking>1)
    disp('Warning: Driveline and Front Friction Braking need to add to
less than or equal to 1 for')
    disp('         all speeds.  Please edit either wh_fa_dl_brake_frac
or wh_fa_fric_brake_frac');
    disp('         in WH_*.m.  See Chapter 3.2.4, Braking of the
documentation for more info.');
end
clear temp_total_braking
```

D.11 Data File of Accessories

```
%%%%%%%%%%%%%%%%%%%%%%%%%%%%%%%%%%%%%%%%%%%%%%%%%%%%%%%%%%%%%%%%%%%%%%%%
                    % ADVISOR data file:  ACC_HYBRID.m
%%%%%%%%%%%%%%%%%%%%%%%%%%%%%%%%%%%%%%%%%%%%%%%%%%%%%%%%%%%%%%%%%%%%%%%%

% Notes:
% Defines standard accessory load data for use with a hybrid in
  ADVISOR.

%%%%%%%%%%%%%%%
% FILE ID INFO
%%%%%%%%%%%%%%%
acc_description='700-W constant electric load';
acc_version=2004; % version of ADVISOR for which the file was
generated

acc_proprietary=0; % 0=> non-proprietary, 1=> proprietary, do not
distribute

acc_validation=0; % 0=> no validation, 1=> data agrees with source
data,
% 2=> data matches source data and data collection methods have been
verified

disp(['Data loaded: ACC_HYBRID - ',acc_description])
```

```
%%%%%%%%%%%%%%%%%
% LOSS parameters
%%%%%%%%%%%%%%%%%
acc_mech_pwr=0;  % (W), mechanical accessory load, drawn from the
engine

acc_elec_pwr=700; % (W), electrical acc. load, drawn from the
voltage/power bus

acc_mech_eff=1; %efficiency of accessory
acc_elec_eff=1; %
acc_mech_trq=0; % (Nm), constant accessory torque load on engine

vinf.AuxLoads=load('Default_aux.mat');
vinf.AuxLoadsOn=0;

acc_dcdc_eff=1; % dc to dc converter efficiency applied to the 14v
loads
```

D.12 Data File of Series Powertrain Control

```
%%%%%%%%%%%%%%%%%%%%%%%%%%%%%%%%%%%%%%%%%%%%%%%%%%%%%%%%%%%%%%%%%%%%%%%%%%%%
                    % ADVISOR data file:  PTC_SER.m
%%%%%%%%%%%%%%%%%%%%%%%%%%%%%%%%%%%%%%%%%%%%%%%%%%%%%%%%%%%%%%%%%%%%%%%%%%%%

% Notes:
% Defines all powertrain control parameters, including gearbox,
  clutch, hybrid
% and engine controls, for a series hybrid using a thermostat control
  strategy.
% To ensure proper operation, this file must be reloaded every time
  the FC or GC is rescaled.

if ~exist('update_cs_flag')


%%%%%%%%%%%%%%%
% FILE ID INFO
%%%%%%%%%%%%%%%
ptc_description='Powertrain control for series hybrid w/ pure
thermostat cs';
ptc_version=2004; % version of ADVISOR for which the file was
generated

ptc_proprietary=0; % 0=> non-proprietary, 1=> proprietary, do not
distribute

ptc_validation=0; % 1=> no validation, 1=> data agrees with source
data,
% 2=> data matches source data and data collection methods have been
verified

disp(['Data loaded: PTC_SER - ',ptc_description])


%%%%%%%%%%%%%%%%%%%%%%%%%
% CLUTCH & ENGINE CONTROL
%%%%%%%%%%%%%%%%%%%%%%%%%
vc_idle_spd=0;  % (rad/s), engine's idle speed
```

```
%%%%%%%%%%%%%%%%%
% GEARBOX CONTROL
%%%%%%%%%%%%%%%%%
% fractional engine load {=(torque)/(max torque at speed)} above which
a downshift is called for, indexed by gb_gearN_dnshift_spd
gb_gear1_dnshift_load=[2 2];  % (--)
gb_gear2_dnshift_load=[2 2];  % (--)
% fractional engine load {=(torque)/(max torque at speed)} below which
an upshift is called for, indexed by gb_gearN_upshift_spd
gb_gear1_upshift_load=[-1 -1];  % (--)
gb_gear2_upshift_load=[-1 -1];  % (--)
gb_gear1_dnshift_spd=[0 1000];  % (rad/s)
gb_gear2_dnshift_spd=[0 1000];  % (rad/s)
gb_gear1_upshift_spd=[0 1000];  % (rad/s)
gb_gear2_upshift_spd=[0 1000];  % (rad/s)

% convert old shift commands to new shift commands
gb_upshift_spd={gb_gear1_upshift_spd; ...
      gb_gear2_upshift_spd};  % (rad/s)
gb_upshift_load={gb_gear1_upshift_load; ...
      gb_gear2_upshift_load};  % (--)
gb_dnshift_spd={gb_gear1_dnshift_spd; ...
      gb_gear2_dnshift_spd};  % (rad/s)
gb_dnshift_load={gb_gear1_dnshift_load; ...
      gb_gear2_dnshift_load};  % (--)

clear gb_gear*shift* % remove unnecessary data

% fixes the difference between number of shift vectors and gears in
gearbox
if length(gb_upshift_spd)<length(gb_ratio)
   start_pt=length(gb_upshift_spd);
   for x=1:length(gb_ratio)-length(gb_upshift_spd)
      gb_upshift_spd{x+start_pt}=gb_upshift_spd{1};
      gb_upshift_load{x+start_pt}=gb_upshift_load{1};
      gb_dnshift_spd{x+start_pt}=gb_dnshift_spd{1};
      gb_dnshift_load{x+start_pt}=gb_dnshift_load{1};
   end
end

% duration of shift during which no torque can be transmitted
gb_shift_delay=0;  % (s), no delay since no shifts; this is a 1-spd



%%%%%%%%%%%%%%%%%%%%%%%%
% HYBRID CONTROL STRATEGY
%%%%%%%%%%%%%%%%%%%%%%%%
%ess_init_soc=0.7;  % (--), initial battery SOC;  now this is inputed
from the simulation screen

cs_hi_soc=0.8;  % (--), highest desired battery state of charge
cs_lo_soc=0.4;  % (--), lowest desired battery state of charge
cs_fc_init_state=0;  % (--), initial FC state; 1=> on, 0=> off

% (W), minimum operating power for genset
% pure thermostat:set it to operating power
cs_min_pwr=max(fc_max_trq.*fc_map_spd)*.5;

% (W), maximum operating power for genset (exceeded only if
SOC<cs_lo_soc)
% pure thermostat:set it to operating power
cs_max_pwr=max(fc_max_trq.*fc_map_spd)*.5;
```

```
% (W), extra power output by genset when (cs_lo_soc+cs_hi_soc)/2-SOC=1
% pure thermostat:set it to zero to make genset power output
independent of SOC
cs_charge_pwr=0;

% (s), minimum time genset remains off, enforced unless SOC<=cs_lo_soc
% pure thermostat:set it to inf s.t. genset won't come on until
SOC<=cs_lo_soc
cs_min_off_time=inf;

% (W/s), maximum rate of increase of genset power
% pure thermostat:set it to zero s.t. power is constant whenever on
cs_max_pwr_rise_rate=0;

% (W/s), maximum rate of decrease of genset power
% pure thermostat:set it to zero s.t. power is constant whenever on
cs_max_pwr_fall_rate=0;

cs_charge_deplete_bool=0; % boolean 1=> use charge deplete strategy,
0=> use charge sustaining strategy

end


%%%%%%%%%%%%%%%%%%%%%%%%%%%%%%%%%%%%%%%%%%%%%%%
% compute locus of best efficiency points
%%%%%%%%%%%%%%%%%%%%%%%%%%%%%%%%%%%%%%%%%%%%%%%
if ~exist('fc_fuel_map_gpkWh')
   %
   % compute engine efficiency map for use in genset control
   %
   [T,w]=meshgrid(fc_map_trq,fc_map_spd);
   fc_outpwr_map_kW=T.*w/1000;
   fc_fuel_map_gpkWh=fc_fuel_map./(fc_outpwr_map_kW+eps)*3600;
   % if zero speed is in map, replace associated data with nearest
BSFC*4
   if min(fc_map_spd)<eps
      fc_fuel_map_gpkWh(1,:)=fc_fuel_map_gpkWh(2,:)*4;
   end
   % if zero torque is in map, replace associated data with nearest
BSFC*4
   if min(fc_map_trq)<eps
      fc_fuel_map_gpkWh(:,1)=fc_fuel_map_gpkWh(:,2)*4;
   end
end

%
% compute allowable genset torques and speeds
% (these are limited by the max torque envelopes of the FC and GC, and
by the
% extents of their maps)
%
temp1=min([max(fc_map_trq)*fc_trq_scale
max(gc_map_trq)*gc_trq_scale]);
temp2=max([min(fc_map_trq)*fc_trq_scale
min(gc_map_trq)*gc_trq_scale]);
genset_map_trq=[temp2:(temp1-temp2)/10:temp1];

temp1=min([max(fc_map_spd)*fc_spd_scale
max(gc_map_spd)*gc_spd_scale]);
temp2=max([min(fc_map_spd)*fc_spd_scale
min(gc_map_spd)*gc_spd_scale]);
genset_map_spd=[temp2:(temp1-temp2)/10:temp1];
```

```
temp1=interp1(fc_map_spd*fc_spd_scale,fc_max_trq*fc_trq_scale,genset_m
ap_spd);
temp2=interp1(gc_map_spd*gc_spd_scale,gc_max_trq*gc_trq_scale,genset_m
ap_spd);
genset_max_trq=min([temp1;temp2]);

% compute genset BSFC map
temp1=interp2(gc_map_trq*gc_trq_scale,gc_map_spd'*gc_spd_scale,gc_eff_
map,...
   genset_map_trq,genset_map_spd');
temp2=interp2(fc_map_trq*fc_trq_scale,fc_map_spd'*fc_spd_scale,...
   fc_fuel_map_gpkWh,genset_map_trq,genset_map_spd');
genset_BSFC_map=temp2./(temp1+eps);

% Define power vector
genset_max_pwr=max(genset_map_spd.*...

(min([genset_max_trq;ones(size(genset_max_trq))*max(genset_map_trq)]))
);
%genset_max_pwr=min(max(genset_map_spd.*genset_max_trq),...
  % max(genset_map_spd)*max(genset_map_trq));
genset_min_pwr=min(genset_map_spd)*min(genset_map_trq);
cs_pwr=[genset_min_pwr:(genset_max_pwr-
genset_min_pwr)/10:genset_max_pwr];

% Loop on power
for pwr_index=2:length(cs_pwr-1)
   % consider every integer speed in the map
   spds=[ceil(min(genset_map_spd)):floor(max(genset_map_spd))];

   % determine corresponding torque to produce the current power
   trqs1=cs_pwr(pwr_index)./(spds+eps);

   % make sure all torques are on the map
   trqs2=min(trqs1,max(genset_map_trq));
   trqs2=max(trqs2,min(genset_map_trq));

   % compute BSFCs corresponding to spd/trq points

BSFCs=interp2(genset_map_spd,genset_map_trq,genset_BSFC_map',spds,trqs
2);

   % correct BSFCs to disallow points beyond the engine's or
generator's
   % (continuous) operating range
   BSFCs=BSFCs + (trqs1 > interp1(fc_map_spd*fc_spd_scale,...
      fc_max_trq*fc_trq_scale,spds)) * 10000 ...
      + (trqs1 >
interp1(gc_map_spd*gc_spd_scale,gc_max_trq*gc_trq_scale,...
      spds)) * 10000;

   if any(isnan(BSFCs))
      error('Error in PTC_SERFO: couldn''t compute genset eff. map')
   end

   % pick index of best BSFC (choose minimum so that lowest speed will
be
   % chosen for given power, leading to reduced losses in other
components)
   best_index=min(find(min(BSFCs)==BSFCs));

   cs_spd(pwr_index)=spds(best_index);
```

```
end % for pwr_index=...

% make cvt_locus_spd=0 if cvt_locus_pwr=0
zero_indices=find(abs(cs_pwr)<1e-3);
if ~isempty(zero_indices)
   cs_spd(zero_indices)=zeros(size(zero_indices));
end

% insert max power point as last value
cs_pwr(length(cs_pwr))=genset_max_pwr;
if genset_max_pwr==max(genset_map_spd.*genset_max_trq)
   cs_spd(length(cs_pwr))=genset_map_spd(find...
      ((genset_map_spd.*genset_max_trq)==genset_max_pwr));
else
   cs_spd(length(cs_pwr))=max(genset_map_spd);
end

% insert min power point as first value
cs_pwr(1)=min(genset_map_spd)*min(genset_map_trq);
cs_spd(1)=min(genset_map_spd);



%%%%%%%%%%%%%%%%%%%%%%%%%%%%%%%
% PLOT RESULTS OF LOCUS FINDING
%%%%%%%%%%%%%%%%%%%%%%%%%%%%%%%
if 0

c=contour(genset_map_spd*30/pi,genset_map_trq,genset_BSFC_map',[200:20
:400]);
   hold on
   plot(genset_map_spd*30/pi,genset_max_trq,'rx')
   plot(cs_spd*30/pi,cs_pwr./cs_spd,'.')
   plot(fc_map_spd*fc_spd_scale*30/pi,fc_max_trq*fc_trq_scale,'r')
   plot(gc_map_spd*gc_spd_scale*30/pi,gc_max_trq*gc_trq_scale)
   set(gca,'Ylim',[min(genset_map_trq) ...
         max([gc_max_trq*gc_trq_scale fc_max_trq*fc_trq_scale])])
end

%%%%%%%%%%%%%%% START OF SPEED DEPENDENT SHIFTING INFORMATION
%%%%%%%%%%%%%

% Data specific for SPEED DEPENDENT SHIFTING in the (PRE_TX) GEARBOX
CONTROL
% BLOCK in VEHICLE CONTROLS <vc>
% --implemented for all powertrains except CVT versions and Toyota
Prius (JPN)
%
tx_speed_dep=0; % Value for the switch in the gearbox control
%           If tx_speed_dep=1, the speed dependent gearbox is chosen
%           If tx_speed_dep=0, the engine load dependent gearbox is
chosen
%
% Vehicle speed (m/s) where the gearbox has to shift
%tx_1_2_spd=24/3.6; % converting from km/hr to m/s
%tx_2_3_spd=40/3.6;
%tx_3_4_spd=64/3.6;
%tx_4_5_spd=75/3.6;
%tx_5_4_spd=75/3.6;
%tx_4_3_spd=64/3.6;
%tx_3_2_spd=40/3.6;
%tx_2_1_spd=tx_1_2_spd;
```

```
% first column is speed in m/s, second column is gear number
% note: lookup data should be specified as a step function
% ..... this can be done by repeating values of x (first column,
speed)
% ..... for differing values of y (second column, )
% note: division by 3.6 to change from km/hr to m/s

% speeds to use for upshift transition (shifting while accelerating)
tx_spd_dep_upshift = [
   0/3.6, 1
   24/3.6, 1
   24/3.6, 2
   40/3.6, 2
   40/3.6, 3
   64/3.6, 3
   64/3.6, 4
   75/3.6, 4
   75/3.6, 5
   1000/3.6, 5];

% speeds to use for downshift transition (shifting while decelerating)
tx_spd_dep_dnshift = [
   0/3.6, 1
   24/3.6, 1
   24/3.6, 2
   40/3.6, 2
   40/3.6, 3
   64/3.6, 3
   64/3.6, 4
   75/3.6, 4
   75/3.6, 5
   1000/3.6, 5];
%%%%%%%%%%%%%% END OF SPEED DEPENDENT SHIFTING %%%%%%%%%%%%%

%%%%%%%%%%
% CLEAN UP
%%%%%%%%%%
clear T w fc_outpwr_map best_at_each_trq best_trq_index
clear best_at_each_spd best_spd_index
clear genset_max_pwr genset_max_trq genset_map_spd genset_map_trq
clear temp1 temp2 first_index last_index genset_BSFC_map
```

Appendix E European Union (EU) Emission Standards

Directive 70/220/EEC specifies the European emission regulations for cars and light duty vehicles. According to [82] some of the important amendments which have been done to the main directive include:

- Euro 1 standards which refers to passenger cars and light trucks
- Euro 2 standards which also known as EC 96
- Euro 3/4 standards (98/69/EC and 2002/80/EC Directives)
- Euro 5/6 standards that are the draft political legislations (Regulation 715/2007)

Emissions standards for passenger cars and light duty vehicles are summarised in Tables E.1 and E.2 respectively for diesel and petrol engines. In the emission standards, the vehicles categorised as M_1, are designed and built for carrying passengers and comprising no more than nine seats including the driver seat. The N_1 category vehicles are designed for carrying of goods with maximum mass of 3.5 tons.

Table E.1 EU emission standards for passenger cars (category M_1^*), g/km [82]

Tier	Date	CO	HC	HC+NOx	NOx	PM
Diesel						
Euro 1†	1992.07	2.72 (3.16)	-	0.97 (1.13)	-	0.14 (0.18)
Euro 2, IDI	1996.01	1.0	-	0.7	-	0.08
Euro 2, DI	1996.01[a]	1.0	-	0.9	-	0.10
Euro 3	2000.01	0.64	-	0.56	0.50	0.05
Euro 4	2005.01	0.50	-	0.30	0.25	0.025
Euro 5	2009.09[b]	0.50	-	0.23	0.18	0.005[e]
Euro 6	2014.09	0.50	-	0.17	0.08	0.005[e]
Petrol (Gasoline)						
Euro 1†	1992.07	2.72 (3.16)	-	0.97 (1.13)	-	-
Euro 2	1996.01	2.2	-	0.5	-	-
Euro 3	2000.01	2.30	0.20	-	0.15	-

Tier	Date	CO	HC	HC+NOx	NOx	PM
Euro 4	2005.01	1.0	0.10	-	0.08	-
Euro 5	2009.09[b]	1.0	0.10[c]	-	0.06	0.005[d,e]
Euro 6	2014.09	1.0	0.10[c]	-	0.06	0.005[d,e]

* At the Euro 1..4 stages, passenger vehicles > 2,500 kg were type approved as Category N_1 vehicles
† Values in brackets are conformity of production (COP) limits
a - until 1999.09.30 (after that date DI engines must meet the IDI limits)
b - 2011.01 for all models
c - and NMHC = 0.068 g/km
d - applicable only to vehicles using DI engines
e - proposed to be changed to 0.003 g/km using the PMP measurement procedure

Table E.2 EU emission standards for light commercial vehicles, g/km [82]

Category†	Tier	Date	CO	HC	HC+NOx	NOx	PM
Diesel							
N_1, Class I ≤1305 kg	Euro 1	1994.10	2.72	-	0.97	-	0.14
	Euro 2, IDI	1998.01	1.0	-	0.70	-	0.08
	Euro 2, DI	1998.01[a]	1.0	-	0.90	-	0.10
	Euro 3	2000.01	0.64	-	0.56	0.50	0.05
	Euro 4	2005.01	0.50	-	0.30	0.25	0.025
	Euro 5	2009.09[b]	0.50	-	0.23	0.18	0.005[e]
	Euro 6	2014.09	0.50	-	0.17	0.08	0.005[e]
N_1, Class II 1305-1760 kg	Euro 1	1994.10	5.17	-	1.40	-	0.19
	Euro 2, IDI	1998.01	1.25	-	1.0	-	0.12
	Euro 2, DI	1998.01[a]	1.25	-	1.30	-	0.14
	Euro 3	2001.01	0.80	-	0.72	0.65	0.07
	Euro 4	2006.01	0.63	-	0.39	0.33	0.04
	Euro 5	2010.09[c]	0.63	-	0.295	0.235	0.005[e]
	Euro 6	2015.09	0.63	-	0.195	0.105	0.005[e]
N_1, Class III >1760 kg	Euro 1	1994.10	6.90	-	1.70	-	0.25
	Euro 2, IDI	1998.01	1.5	-	1.20	-	0.17
	Euro 2, DI	1998.01[a]	1.5	-	1.60	-	0.20
	Euro 3	2001.01	0.95	-	0.86	0.78	0.10
	Euro 4	2006.01	0.74	-	0.46	0.39	0.06
	Euro 5	2010.09[c]	0.74	-	0.350	0.280	0.005[e]
	Euro 6	2015.09	0.74	-	0.215	0.125	0.005[e]
Petrol (Gasoline)							
N_1, Class I ≤1305 kg	Euro 1	1994.10	2.72	-	0.97	-	-
	Euro 2	1998.01	2.2	-	0.50	-	-
	Euro 3	2000.01	2.3	0.20	-	0.15	-
	Euro 4	2005.01	1.0	0.1	-	0.08	-
	Euro 5	2009.09[b]	1.0	0.10[f]	-	0.06	0.005[d,e]
	Euro 6	2014.09	1.0	0.10[f]	-	0.06	0.005[d,e]
N_1, Class II	Euro 1	1994.10	5.17	-	1.40	-	-

Category†	Tier	Date	CO	HC	HC+NOx	NOx	PM
1305-1760 kg	Euro 2	1998.01	4.0	-	0.65	-	-
	Euro 3	2001.01	4.17	0.25	-	0.18	-
	Euro 4	2006.01	1.81	0.13	-	0.10	-
	Euro 5	2010.09[c]	1.81	0.13[g]	-	0.075	0.005[d,e]
	Euro 6	2015.09	1.81	0.13[g]	-	0.075	0.005[d,e]
N_1, Class III >1760 kg	Euro 1	1994.10	6.90	-	1.70	-	-
	Euro 2	1998.01	5.0	-	0.80	-	-
	Euro 3	2001.01	5.22	0.29	-	0.21	-
	Euro 4	2006.01	2.27	0.16	-	0.11	-
	Euro 5	2010.09[c]	2.27	0.16[h]	-	0.082	0.005[d,e]
	Euro 6	2015.09	2.27	0.16[h]	-	0.082	0.005[d,e]

† For Euro 1/2 the Category N_1 reference mass classes were Class I ≤ 1250 kg, Class II 1250-1700 kg, Class III > 1700 kg.
a - until 1999.09.30 (after that date DI engines must meet the IDI limits)
b - 2011.01 for all models
c - 2012.01 for all models
d - applicable only to vehicles using DI engines
e - proposed to be changed to 0.003 g/km using the PMP measurement procedure
f - and NMHC = 0.068 g/km
g - and NMHC = 0.090 g/km
h - and NMHC = 0.108 g/km

The emission regulations include onboard diagnostic (OBD) requirements for emission systems. According to the OBD provision started the Euro 3 stage, vehicles must be equipped with a diagnostic system in order to notify driver if emissions exceed mandatory values listed in Table E.3.

Table E.3 EU OBD threshold limits, g/km [82]

Category	Class	Tier	Date	CO	HC	NOx	PM
Diesel							
M_1		EU 3	2003	3.20	0.40	1.20	0.18
		EU 4	2005	3.20	0.40	1.20	0.18
N_1	I	EU 3	2005	3.20	0.40	1.20	0.18
		EU 4	2005	3.20	0.40	1.20	0.18
	II	EU 3	2006	4.00	0.50	1.60	0.23
		EU 4	2006	4.00	0.50	1.60	0.23
	III	EU 3	2006	4.80	0.60	1.90	0.28
		EU 4	2006	4.80	0.60	1.90	0.28
Petrol (Gasoline)							
M_1		EU 3	2000	3.20	0.40	0.60	-
		EU 4	2005	1.90	0.30	0.53	-
N_1	I	EU 3	2000	3.20	0.40	0.60	-
		EU 4	2005	1.90	0.30	0.53	-

Category	Class	Tier	Date	CO	HC	NOx	PM
	II	EU 3	2001	5.80	0.50	0.70	-
		EU 4	2005	3.44	0.38	0.62	-
	III	EU 3	2001	7.30	0.60	0.80	-
		EU 4	2005	4.35	0.47	0.70	-

Note: Passenger cars category M_1 > 2,500 kg or with more than 6 seats meet OBD requirements for Category N_1.